U CLASSIFIED

MASTER

ORNL 925

LEGAL NOTICE

This report was prepared as an account of Government sponsored work. Neither the United States, nor the Commission, nor any person acting on behalf of the Commission:

A. Makes any warranty or representation, express or implied, with respect to the accuracy, completeness, or usefulness of the information contained in this report, or that the use of any information, apparatus, method, or process disclosed in this report may not infringe privately owned rights; or

B. Assumes any liabilities with respect to the use of, or for damages resulting from the use of any information, apparatus, method, or process disclosed in this report.

As used in the above, "person acting on behalf of the Commission" includes any employee or contractor of the Commission to the extent that such employee or contractor prepares, handles or distributes, or provides access to, any information pursuant to his employment or contract with the Commission.

Contract No. W-7405, eng 26

HOMOGENEOUS REACTOR EXPERIMENT

QUARTERLY PROGRESS REPORT

for Period Ending November 30, 1950

CLASSIFICATION CANCELLED
DATE MAR 2 1957
For The Atomic Energy Commission
H. B. Carroll
Chief, Declassification Branch

Edited by
C. E. Winters and C. H. Secoy

DATE ISSUED JAN 30 1951

OAK RIDGE NATIONAL LABORATORY
operated by
CARBIDE AND CARBON CHEMICALS DIVISION
Union Carbide and Carbon Corporation
Post Office Box P
Oak Ridge, Tennessee

Photostat Price $ 55.10
Microfilm Price $ 11.10
Available from the
Office of Technical Services
Department of Commerce
Washington 25, D. C.

MASTER

MASTER

DISCLAIMER

This report was prepared as an account of work sponsored by an agency of the United States Government. Neither the United States Government nor any agency thereof, nor any of their employees, makes any warranty, express or implied, or assumes any legal liability or responsibility for the accuracy, completeness, or usefulness of any information, apparatus, product, or process disclosed, or represents that its use would not infringe privately owned rights. Reference herein to any specific commercial product, process, or service by trade name, trademark, manufacturer, or otherwise does not necessarily constitute or imply its endorsement, recommendation, or favoring by the United States Government or any agency thereof. The views and opinions of authors expressed herein do not necessarily state or reflect those of the United States Government or any agency thereof.

DISCLAIMER

Portions of this document may be illegible in electronic image products. Images are produced from the best available original document.

MASTER

TABLE OF CONTENTS

MASTER

UNCLASSIFIED

TABLE OF CONTENTS (Cont'd)

DECLASSIFIED

LIST OF FIGURES

DECLASSIFIED

LIST OF FIGURES (Cont'd)

DECLASSIFIED

LIST OF FIGURES (Cont'd)

DECLASSIFIED

LIST OF FIGURES (Cont'd)

DECLASSIFIED

LIST OF FIGURES (Cont'd)

DECLASSIFIED

LIST OF FIGURES (Cont'd)

DECLASSIFIED

SECRET

FOREWORD

This quarterly report is intended as a detailed progress report on all homogeneous-reactor-motivated work at ORNL, including the work of the Homogeneous Reactor Experiment, the long-range research programs associated with aqueous-fluid fuel systems, and that fraction of the activities of the long-range study group which are associated with aqueous-fluid fuel reactors.

I. SUMMARY

A report, ORNL-830, has been issued covering the prospects for the utilization of homogeneous reactors for plutonium production or breeding with a simultaneous production of useful power. A similar but less detailed report, CF-50-10-114, has been prepared to show the possible application of aqueous homogeneous reactors to mobile propulsion.

The detailed engineering design of the experimental reactor is now about 60% complete, and is expected to be about 90% complete by January 1.

Serious delays have been experienced by the building construction contractor in the procurement of steel and other materials. Receipt of the steel for the building was completed on November 30. The contractor cannot finish on December 21, as originally scheduled, but will be a month or so delayed.

A high-pressure test loop has been added to the full-scale mock-up. Gas holdup and pressure drops have been measured at expected operating temperatures and pressures. The results agree with the predictions of earlier experiments at atmospheric pressures. Bethlehem Steel Company has completed machining on the large forged steel pressure vessel, and is awaiting the receipt of high-tensile strength bolts before pressure-testing it. It is expected that this vessel will be received and installed in the mock-up during this next quarter, at which time dump tests on the core and reflector solution may be performed. The final pressurizer and gas-removal systems will also be completed and tested. It is not certain that the large heat exchanger will be received from

DECLASSIFIED

A. O. Smith in time for complete testing before it is necessary to dismantle the full-scale mock-up for conversion to the final reactor and installation in the new HRE Building.

A high-pressure test loop using a model 30 Westinghouse pump has been operated with limited success. Further work must be done in order that conditions suitable for solution stability may be consistently provided and satisfactory bearing materials for the pump may be developed. The second test loop, utilizing a model 100A pump, is nearly completed. Several thermal siphon loops are also under construction. From these loop experiments the dynamic corrosion results will be obtained. One high-pressure feed pump has been satisfactorily operated at 1000 psi on water and is being converted for a uranyl sulfate test. A soup cooler and a preheater double-pipe type heat exchanger was fabricated but was unsatisfactory because of faulty welding. A new exchanger is under construction. The specially modified pressure-seal ring-joint gaskets and the pressurizer level control have been found to be satisfactory. Neutron fluxes and induced activities have been calculated throughout the shield. The results indicate that all components can be replaced without excessive personnel exposures. Human access to the D_2O compartment should be possible immediately after shutdown. With the incorporation of 1% boron in the concrete shield the induced activity in the concrete itself will be reduced to the point that human access to all compartments should be possible after removal of several of the hotter pieces of equipment.

Nearly all the automatic controls and nuclear instrumentation have either been received, are under construction, or are on order with satisfactory delivery promises. The reactor simulator has been completed to the extent that the transient behavior can be accurately observed for times up to 2 sec after the initiation of the transient. The results match rather closely those obtained by numerical methods, as reported in ORNL-730. Following this check on the simulator accuracy, a large number of additional data were obtained, some of which have been correlated.

Corrosion experiments in the absence of radiation have continued on an extensive scale. Emphasis has been on stainless steels, zirconium, reflector materials, and miscellaneous materials of construction. An exploratory study of corrosion in uranyl fluoride and uranyl nitrate solutions has been started.

DECLASSIFIED

Twenty-two in-pile corrosion and solution stability tests have been made in addition to the 16 previously reported (ORNL-826). Of these, only two gave results considered failures as indicated by precipitation of the uranium and extensive corrosion. There is some reason to believe that the failures may be associated with pile shutdowns.

Corrosion protection is apparently being obtained by means of a chemisorbed film or series of films. With proper preparation the film is completely protective and self-healing. Emphasis during the next quarter will be placed on fundamental studies of this film and factors influencing its reliability.

A demonstration of the feasibility of a combustion type recombiner for the recombination of hydrogen and oxygen has been completed. A satisfactory system for quenching flash backs has been designed and tested. Preliminary testing of catalytic recombination has been completed with encouraging results. The catalyst efficiency at a variety of temperatures and flow rates for various hydrogen-oxygen-steam mixtures has been measured. Temperatures for operation using Product-43 catalyst (platinum on charcoal) should not be allowed to exceed 350°C. Temperature rise in the catalyst bed and pressure drops across the bed have been measured.

Preliminary design for a recombiner and fission-gas-disposal system has been completed.

Studies of the solubilities of fission product sulfates at elevated temperatures has been continued, and data are given for lanthanum, cadmium, and zinc sulfates in water and in uranyl sulfate solution. Tracer technique is being employed to measure low solubilities.

Investigation and development of methods for analytical chemical control of the reactor solution has been continued. Two methods of following uranium concentrations appear most feasible: (1) the use of an electromagnetic densitometer to determine density, and (2) the use of a high-frequency coil linked to an electronic circuit to measure capacitance effects produced by changes in uranium concentration.

Chemical studies now in progress which do not directly apply to the HRE but have a longer range significance in the homogeneous reactor field include a phase study of the thorium nitrate–water system, studies of uranium and

DECLASSIFIED

thorium slurries, and studies on the feasibility of using selective-adsorption methods to effect a continuous and satisfactory processing method for the uranyl sulfate—water reactor solution. Molten thorium nitrate hexahydrate (m.p. 110°C) offers promise as a fluid breeder blanket in so far as chemical stability and thorium density are concerned.

DECLASSIFIED

II. LONG-RANGE REACTOR PROGRAM

DECLASSIFIED

LONG-RANGE REACTOR PROGRAM

A Long-range Reactor Group has been established at ORNL for the purpose of evaluating the possibilities of the many types of reactors capable of producing plutonium and power, breeding U^{233} and producing power, or producing power alone. Their studies are expected to guide the Laboratory and the AEC in establishing a long-range program for developing reactors for mobile power plants and for producing fissionable materials and stationary power economically.

Because at ORNL there is great interest in the future of aqueous homogeneous reactors and the HRE is being built here, the first studies of the group are concerned with the feasibility of aqueous homogeneous reactors in general, the economics of fissionable material and power production in such reactors, and the role of the HRE in obtaining information of importance to the future development of aqueous homogeneous reactors.

From results of the first study reported in ORNL-855, the following statements may be made:

1. It is possible to build a reactor designed to operate at 250°C and 1000 psia pressure with a solution of uranyl sulfate in D_2O. If natural uranium is used as the fuel, the core tank must be 35 ft in diameter and 6 to 8 in. thick. Significant reductions in core size result from enriching the uranium slightly. The feasibility of the engineering design depends upon obtaining stainless steel or a reasonable substitute having satisfactory corrosion resistance.

2. All reactors which produce plutonium by burning U^{235} must eventually be coupled to an isotope-separation plant. It does not appear possible to operate a natural-uranium or a plutonium-seeded reactor to a depletion greater than that achieved economically in a diffusion plant.

3. In a 10^6-kw reactor plutonium and/or power are produced most economically when fuel enriched to 0.75 to 0.8% U^{235} is used. This comes about as a result of a balance between enriching, operating, and chemical-processing costs and fixed charges. The large requirement of expensive D_2O places the natural-uranium reactor in an unfavorable position.

DECLASSIFIED

4. A 0.8% enriched homogeneous reactor operating with a heat output of 10^6 kw and a useful electrical output of 230,000 kw is estimated to produce plutonium at a net cost of $50 per gram while selling the power for 5 mils per kilowatt-hour. If the same reactor produces power only, the power cost (80% load factor) is 7 mils per kilowatt-hour.

5. Homogeneous thermal breeders now appear very attractive. It seems resonable to expect a breeding gain of at least 0.1. No isotope separation plant is required, and the chemical processes are relatively simple. A major problem is that of developing a thorium solution or slurry.

6. Demonstration of satisfactory control and solution stability in an aqueous-solution reactor of high power density and determination of the feasibility of control by solution temperature and concentration, of rates of gas production, and of the resistance of materials of construction to corrosion by the pile solution under operating conditions must be accomplished in the HRE before larger reactors are possible.

A comparison has been made of several 500,000-kw mobile power plants moderated with D_2O and with H_2O. The plants were assumed to contain two reactors, each operating at a power of 250,000 kw. The reactor diameter was limited to a maximum of 9 ft because of space considerations and a minimum of 6 ft by the power density. Because the heat-transfer system outside the reactor is the same in all cases and the pressure vessels do not differ greatly, there are differences which favor one reactor over another because of differences in the fuel solution. Pertinent data leading to the selection of one system as being more desirable than another are given in Table 1.

Although the H_2O-moderated reactors have the advantage of a cheap moderator, this advantage is outweighed by the expense of the more highly enriched uranium required. Also, the D_2O-moderated reactors produce enough plutonium that they can be operated for about 28 days at full power on an initial fuel charge. Fuel must be added to the H_2O-moderated reactors as U^{235} is consumed. Calculations which have been made to date for aqueous homogeneous reactors favor D_2O as a moderator for all types operated at a high total power output.

DECLASSIFIED

TABLE 1

500,000-kw Reactor Specifications

Moderator	H_2O	H_2O	D_2O
Number of reactors	2	2	2
Core diameter (ft)	6.0	6.0	9.0
Isotopic percent U^{235} in fuel	94.3	3.5	1.5
U per liter in solution core (g)	11	400	230
Average thermal flux in core	2.5×10^{14}	1.8×10^{14}	2.1×10^{14}
Power density (kw/liter)	78	78	23
Holdup in cores of two reactors (m^3)	6.4	6.4	20.8
External holdup (m^3)	13.3	13.3	13.3
Reserve (m^3)	1.0	1.0	2.0
Total holdup (m^3)	20.7	20.7	36.1
Total U in system (kg)	228	8300	8300
Total U^{235} in system (kg)	214	290	125
Total cost of fuel solution (dollars)	5,700,000	4,760,000	3,100,000
Total weight of reactors, shielding, and steam production equipment (metric tons)	1600	1600	1600

DECLASSIFIED

III. HRE REACTOR PHYSICS AND ENGINEERING

DECLASSIFIED

DESIGN PROGRESS

Design effort during this period has been concentrated on preparation of a final flow sheet, final design of the shield arrangement, location of equipment within the shield, piping layouts, and preparation of final detailed drawings of equipment. The principal items remaining on which little or no design work has been done are the catalytic recombiners, silica-gel absorbers, charcoal adsorbers, outer dump-tank cooling system, and off-gas condenser.

Flow Diagram. A schematic flow diagram of the reactor process is given in Fig. 1, with instrument lines omitted.

Reactor Tanks. Figure 2 shows the assembly of the core tank and reflector tank with the pressurizer and control-rod housings mounted on top. Detail design of all components shown is complete.

Recombiners. As a result of experimental work with recombiners a flame type recombiner has been designed and is being constructed for use in the HRE. The final design of this unit is shown in Fig. 3.

Air System. It is planned to cool the shield by maintaining a flow of approximately 1000 cfm through it toward the center. A sketch of the duct work and probable flow paths is shown in Fig. 4. The air will be discharged through a 90-ft stack at the southeast corner of the building. Calculations indicate a maximum daily activity output from the stack of 0.56 curie, due to argon activity, and a maximum shield temperature of 249°F. A fan capacity of 3000 cfm is being specified in order to be able to reduce this temperature if necessary. If flow is increased to 3000 cfm the maximum concrete temperature is reduced to 211°F.

Piping. Since location of equipment and general design of the shield has been settled, work has progressed on general layouts of the piping. Estimates of sizes and quantities of pipe and fittings have been made and orders placed for approximately 90% of the large-size pipe required.

Auxiliary Boilers. Two auxiliary high-pressure steam boilers have been designed, one of 10 kw for supplying steam to the pressurizer, and another of 40 kw for heating the entire soup system during passivation treatment. Heat is supplied by electric immersion type heaters in 10-kw units.

DECLASSIFIED

MATERIALS LIST

ITEM NO.	DWG. NO.	QTY.	NAME	SIZE	MATERIAL

Atmos. — Atmos. — SILICA GEL ABSORBERS WITH REHEAT HEATERS — HELIUM CYLINDERS — Atmos.

Vent — C.W. — To Drain — Fin Tubes — To Stack — CHARCOAL TRAP — SPENT HELIUM CYLINDER

SILICA GEL ABSORBERS — C.W. Drain — C.W. — CATALYCAL RECOMBINERS — TWO-PASS CONDENSER

D₂O EVAPORATOR — HEADER — CARRIER — FILTER — D₂O PUMP — D₂O COOLER

CONTROL ROD DRIVES — PRESSURIZED — 10 KW BOILER — REFLECTOR VESSEL — HEAT EXCHANGER

Decontamination Fill — SOUP GAS FLAME RECOMBINER — C.W.D. — C.W. — CATALYCAL RECOMBINER — SOUP OFF GAS CONDENSER — C.W.D. — C.W. — CHARCOAL ABSORBERS — To Vacuum Pump — Bldg. Steam

SOUP GAS CONDENSER — CONDENSATE TANKS — HEAT EXCHANGER — SOUP PUMP — COOLER — STEAM DRUM — TURBINE — Bldg. Cond. Return — 40 KW BOILER

Hot Waste — OIL RESERVOIR — FILTER

HOT WELL — Vent — CONDENSER — Atmos. — Atmos. — C.W. — C.W. Drain — KINNEY VACUUM PUMP — C.W. — Make-Up Water — HOT WELL PUMP — C.W. Drain — PISTON PUMP

EVAPORATOR — FILTER — C.D. — Steam — Decont Waste — PULSAFEEDER — CONDENSER — OUTER DUMP TANK

Bldg. C.W. Steam — COOLER — FILTER — Oil Fill — Drain — OIL RESERVOIR — Drain — PULSAFEEDER — C.W.

LEGEND-STATUS OF PROCUREMENT

- Not Started
- In Design
- In Purchasing
- Ordered or in Shop
- On Hand

NO.	REVISIONS	DATE	APPR.	APPR.

DRAWING NO. D-

DRAWN	DATE	CHECKED	DATE	APPROVED	DATE
CWDay	1-21-50				
DESIGNED	DATE	SUBMITTED	DATE	APPROVED	DATE

HEALTH PHYSICS	MEDICAL	OPERATIONS	SAFETY
FIRE PROTECTION	RESEARCH SHOP	MAINTENANCE	

THIS DRAWING CLASSIFIED

LIMITS ON DIMENSIONS UNLESS OTHERWISE SPECIFIED
FRACTIONS: ±
DECIMALS: ±
ANGLES: ±
SCALE: NONE

HRE EQUIPMENT BLDG. 7500

PROCESS FLOW DIAGRAM

OAK RIDGE NATIONAL LABORATORY
OPERATED BY
CARBIDE AND CARBON CHEMICALS DIVISION
UNION CARBIDE AND CARBON CORPORATION
OAK RIDGE, TENNESSEE

SUBMITTED	ACCEPTED	APPROVED

D-8325

R:

FIG. 1
PAGE 17

REFERENCE DRAWINGS	DWG. NO.

DECLASSIFIED DECLASSIFIED UNCLASSIFIED

D-8301

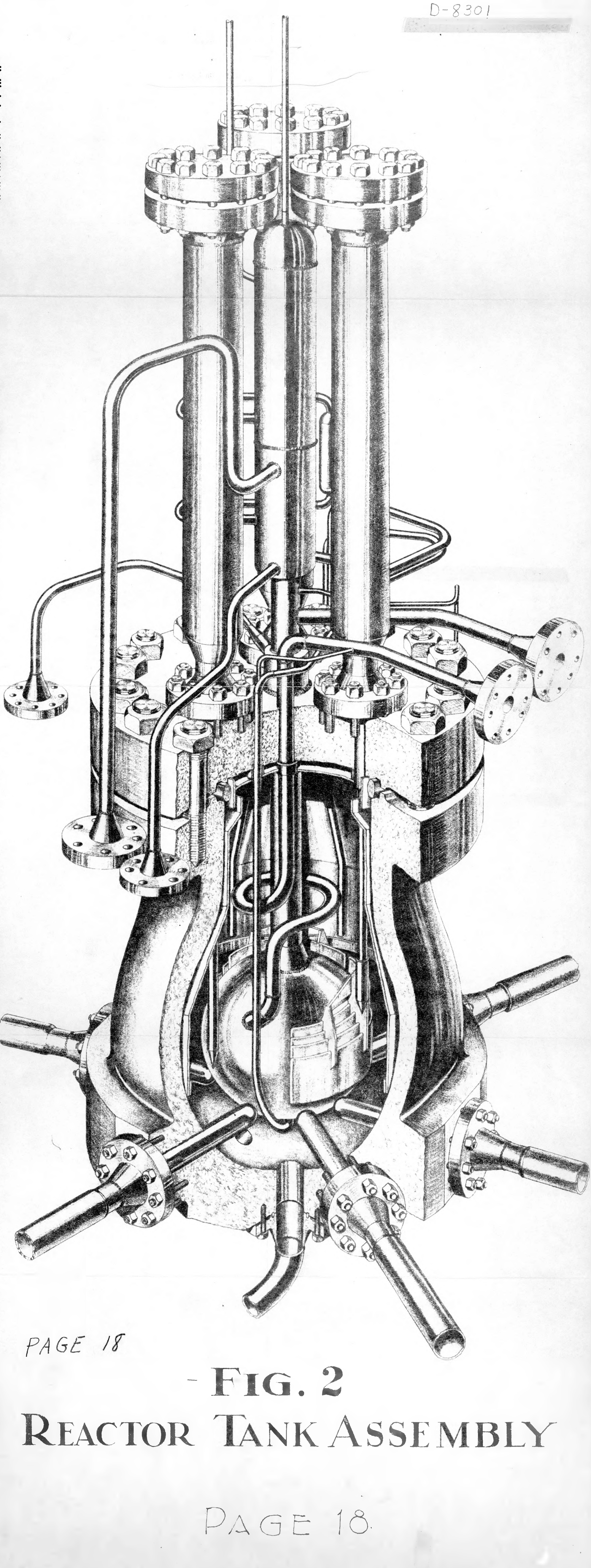

PAGE 18

- FIG. 2

REACTOR TANK ASSEMBLY

D-8318

MATERIALS LIST

ITEM NO.	DWG. NO.	QTY.	NAME	SIZE	MATERIAL
1		2	Sparkplug	18 mm △	
2		1	Pipe Plug	3/8"	347 S.S.
3	D-8319	1	Head Detail	See D-8319	347 S.S.
4		1	Plate	4 1/4" ϕ	SAE 1020
5		1	Jacket	3/16" ϕ	SAE 1020
6		2	Pipe Cap	10"nom. dia. sch. 40	347 S.S.
7		1	Seamless Pipe	10" sch. 40	347 S.S.
8		2	Pipe	1 1/2" IPS	SAE 1020
9		1	Pipe	1" IPS	347 S.S.
12		1	Welding Strip	1/4" x 1/2" x 36"	347 S.S.
13		1	Pipe	1/2" IPS	347 S.S.
14	B-8320	1	Gasket	1/16 thk.	Soft Copper
15	B-8320	1	Burner Nozzle	See Detail	347 S.S.

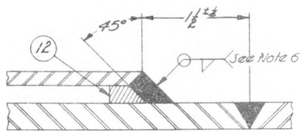

WELDING DETAIL

Scale: Full

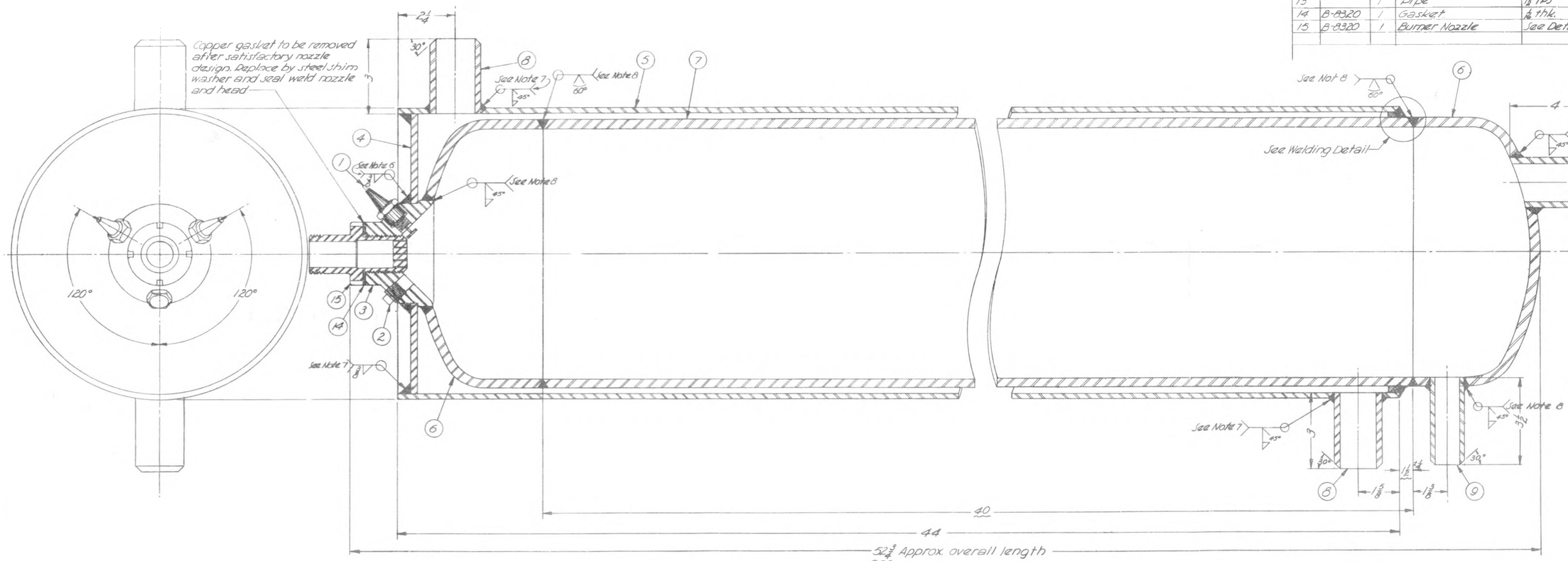

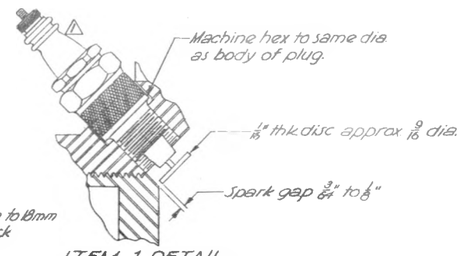

ITEM 1 DETAIL

Showing Spark Gap

Scale-Full

8. Heliarc weld-st. steel to st. steel Oxweld No. 28 welding rod-columbium stabilized, or equivalent.

NOTES:

1. All weld symbols are referred to standard symbols of the American Welding Societ.
2. Design Pressure = 912 psig.
3. Test Pressure = 1375 psig.
4. Fabrication to be in accordance with ASME rules of welded pressure vessels, Rule U-69 of ASME Unfired Pressure Vessels - 1946 Edition.
5. Item 1 - Modified std. 14 mm sparkplug. See Dwg. D-8318.
6. For welding stainless steel to carbon steel, the welding rod shall conform to the following analysis: Chromium 24-26% Manganese 1.25% min. Nickel 19-21% Carbon 0.10% max.
7. Carbon steel welding rod - carbon content not to exceed 0.35%

FIG. 3

PAGE 19

NO.	REVISIONS	DATE	APPR.	APPR.
△	See Note A			

DRAWING NO. D-

DRAWN	DATE	CHECKED	DATE	APPROVED	DATE
C.W. Day	VI-2-50	[illegible]	11-14-50	[illegible]	11-14-50
DESIGNED	DATE	SUBMITTED	DATE	APPROVED	DATE
C.L. Seaman	11-2-50				

HEALTH PHYSICS	MEDICAL	OPERATIONS	SAFETY
FIRE PROTECTION	RESEARCH SHOP	MAINTENANCE	

NOTE A

Changed sparkplug from 14mm to 18mm 18mm was 14mm in main block

THIS DRAWING CLASSIFIED

AS [redacted]

PER [redacted]

LIMITS ON DIMENSIONS UNLESS OTHERWISE SPECIFIED

FRACTIONS: ± 1/64

DECIMALS: ±

ANGLES: ± 0° 30'

SCALE: 1" = 1" EXCEPT AS NOTED

EXPERIMENTAL BUDNER NOZZLE & GASKET	B-8320
HEAD & LEG DETAILS	D-8319
REFERENCE DRAWINGS	DWG. NO.

HRE EQUIPMENT BLDG. 7500

HRE PRIMARY FLAME RECOMBINER ASSEMBLY

OAK RIDGE NATIONAL LABORATORY

OPERATED BY

CARBIDE AND CARBON CHEMICALS DIVISION

UNION CARBIDE AND CARBON CORPORATION

OAK RIDGE, TENNESSEE

SUBMITTED	ACCEPTED	APPROVED
	C.F. Unterwood	

D-8318

R:

DECLASSIFIED 0307823A1330 DECLASSIFIED

DWG. 10139

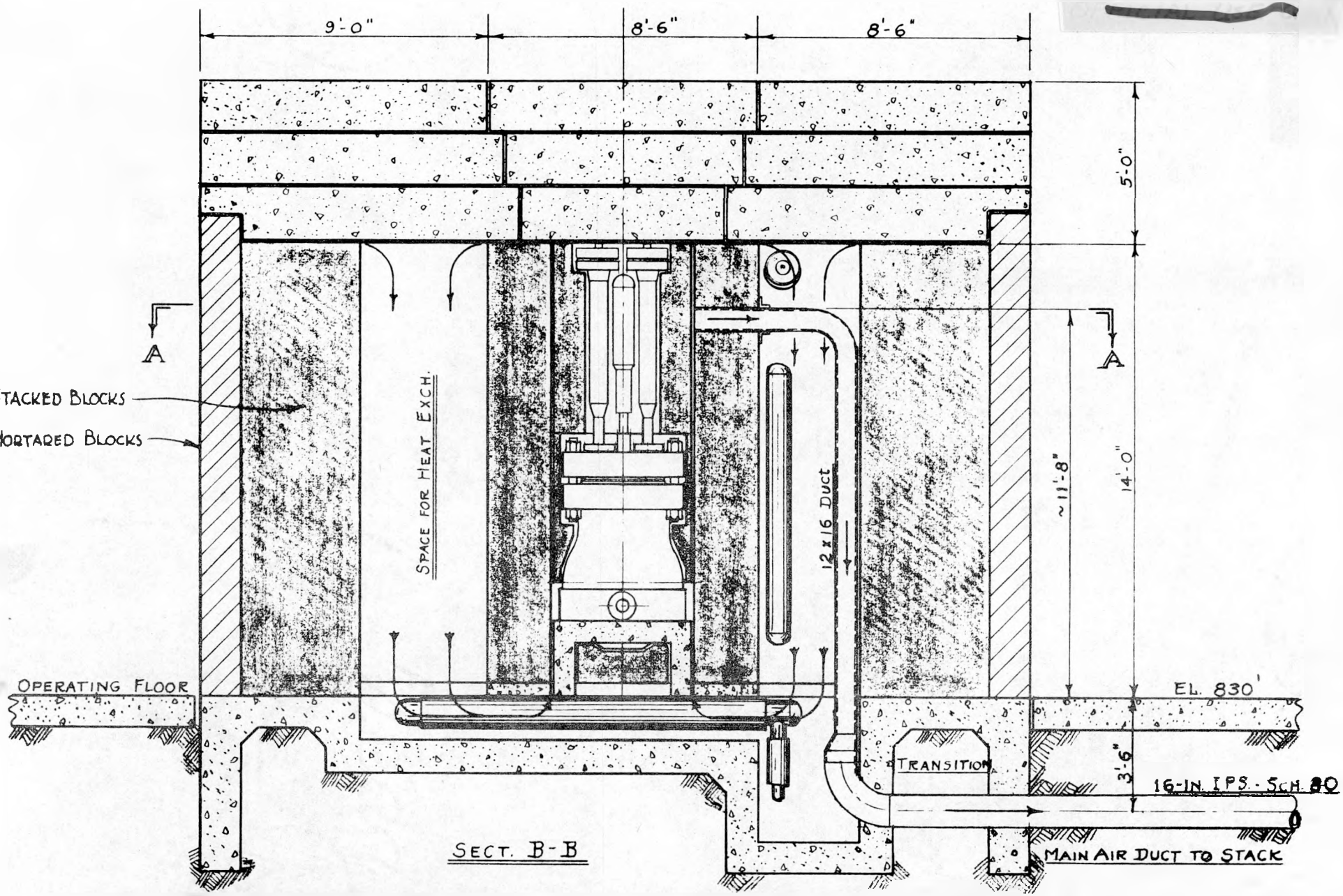

SECTIONAL ELEVATION OF SHIELDING SHOWING LOCATION OF MAIN AIR DUCT

SCALE $\frac{1}{4}$" = 1'-0"

FIG. 4

Oil Systems. A new type of packaged oil system has been designed to cool the two canned-rotor circulating pumps. The oil pump, filter, cooler, and reservoir are all packed inside an 18-in. schedule-40 pipe so that, in event of failure of the rotor cans in either of the circulating pumps, there will be no leakage into the air. Gear type oil-circulating pumps are being used to ensure positive circulation even though radiation may cause thickening of the oil.

Miscellaneous. Bids have been requested for all components of the steam-power system as shown in Fig. 1. Boiler feed pumps and vacuum pumps indicated on the diagram are on hand from available surplus equipment.

The control-rod drives have been detailed according to the design described in a previous report, and a mock rod is being fabricated for dropping tests to determine the amount of shock-absorber capacity required.

Figures 5, 6, and 7 show actual construction details of the reactor steam generator, the soup pressurizer, and the concentric-core draw-off tubes, respectively. In Fig. 7 the outer tube is the pressurizer connection; the next inner one is the soup exit line, and the small inner one is the gas outlet.

Status of Design and Procurement. Design and procurement status of various items of equipment are given in Fig. 1. Tentative scheduling calls for completion of all design and checking work by Jan. 1, 1951, so that by that time all items should be either on hand, on order, or in the shop.

CALCULATIONS AND PRELIMINARY DESIGN

Thermal Stress in Reactor Pressure Shell and Core. Thermal-stress analyses of the various parts of the reactor have been made. It is planned to issue a complete report on the subject in the near future.

Heating of the pressure vessel and cover plate from reactor gammas and neutrons was considered, in addition to normal heat conduction. Three types of cooling were considered: air on the outside, circulating D_2O at reflector temperature in tubes on the outside, and a D_2O jacket on the inside. The reactor operating levels at which the maximum allowable thermal stress of

DECLASSIFIED

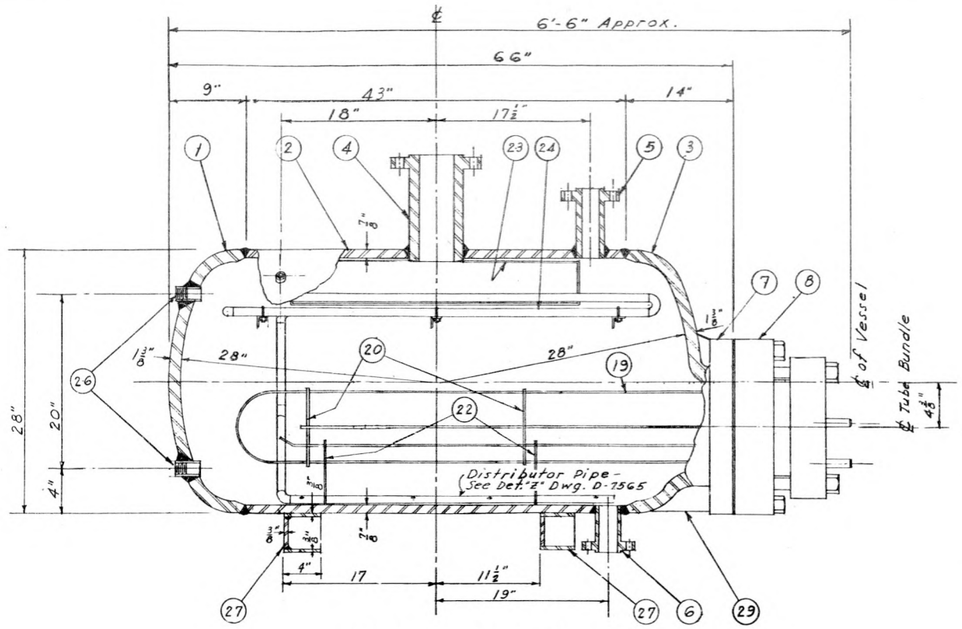

VERTICAL SECTION
Scale: ⅛" = 1"

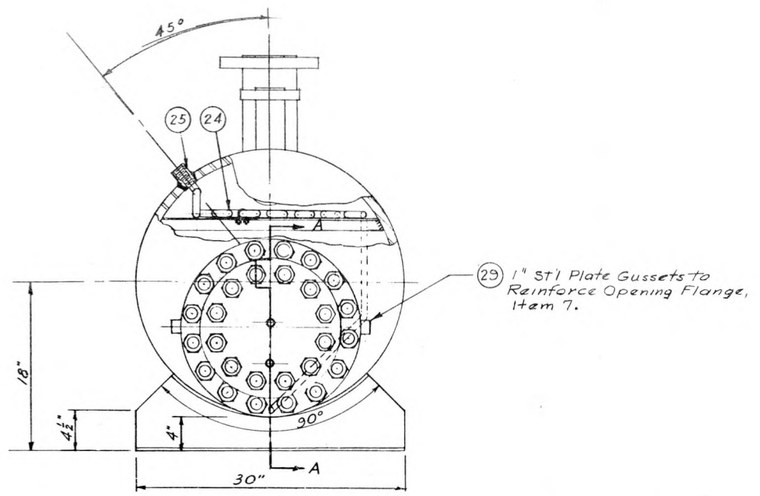

NOZZLE END VIEW
Scale: ⅛" = 1"

MATERIALS LIST

ITEM NO.	DWG. NO.	QTY.	NAME	SIZE	MATERIAL
1	D-7559	1	Rear Flanged &Dished Heads-ASME Code	28" O.D.	ASTM A212B
2	D-7559	1	Shell	28 O.D. x 7/8"	ASTM A212B
3	D-7559	1	Front Flanged&Dished Head; ASME Code	28" O.D.	ASTM A212B
4	D-7559	1	Welding Neck Nozzle	4" ϕ - 600	ASTM A105
5	D-7559	1	Welding Neck Nozzle	2" ϕ - 600	ASTM A105
6	D-7559	1	Welding Neck Nozzle	1½" ϕ - 600	ASTM A105
7	D-7559	1	Flange Ring		ASTM A-212B
8	D-7564	1	Tube Sheet		ASTM A-212B
9	D-7564	1	Tube Sheet	Stainless	Steel 347
10	D-7564	1	Distributor	Stainless	Steel 347
11	D-7559	1	Inlet	1½"Sch 80 x 3" lg.	SS 347
12	D-7559	1	Outlet	1½" Sch 80 x 3" lg.	SS 347
13	D-7559	1	Gasket	R 53 Crane	Type C Octagonal
14	D-7564	1	Gasket	Metalld Gasket Co. New Brunswick N.J.	SS347 Armored
15	D-7559	16	Stud Bolts	1¼"x9"-8 ℓ.:-3	ASTM A193B7
16	D-7559	16	Nuts (Heavy)	1¼"-8tpi-2	ASTM A194-2H
17	D-7559	12	Stud Bolts	1¼"x 10"-8tpi-3	ASTM A193B7
18	D-7559	12	Nuts (Heavy)	1¼"-8tpi-2	ASTM A194-2H
19	D-7559	112	U-Tubes	⅝" O.D.x0.049" Wall	SS-347
20	D-7564	2	Tube Bundle Support Plates	⅜" Plate	Mild Steel
21	D-7564	4	Tube Bundle Support Rails	½" Rounds	Mild Steel
22	D-7564	2	Tube Bundle Support Saddles	⅜" Plate	Mild Steel
23	D-7565	1	Dry Pipe	5"Boiler Tube 0.148"Wall	ASTMAB3
24	D-7565	1	Feed Water Heater Fabricated	50"lg.¾"O.D.x0.035"Wall	SS347 Tubing
25	D-7559	1	Reducer 1"	x ¾"IPS-Crane # 387	Steel
26	D-7559	2	Couplings 1"	IPS-Crane # 386	Steel
27	D-7559	2	Vessel Supports	3/8" Plate	Mild Steel
28	D-7564	1	Tube Bundle Tie Rod	½" Round	Mild Steel
29	D-7559	4	Gussets	1" Plate to fit	ASTM A212B
30	D-7564	2	Spacers	½" IPS Sch. 40	Steel

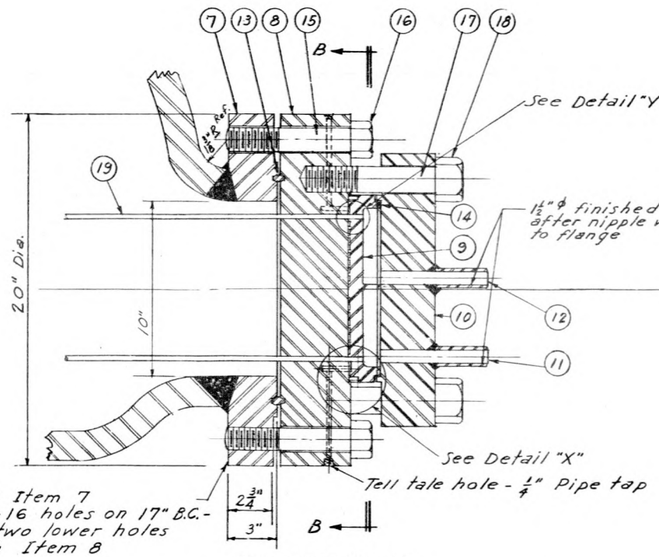

SECTION "A-A"
Scale: ¼" = 1"

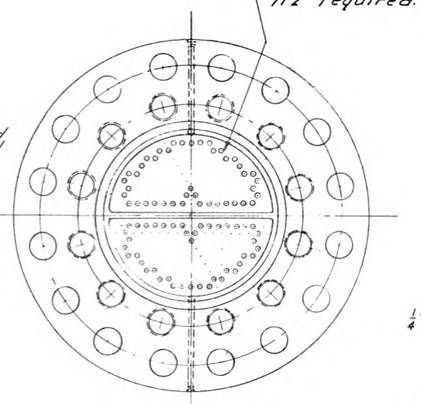

SECTION "B-B"
Scale: ¼" = 1"

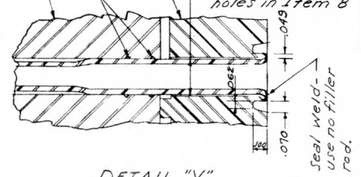

DETAIL "Y"
Tube Joints - Note Clearance
Between Expanded Tube & S.S. Tube Sheet
Scale: 2" = 1"

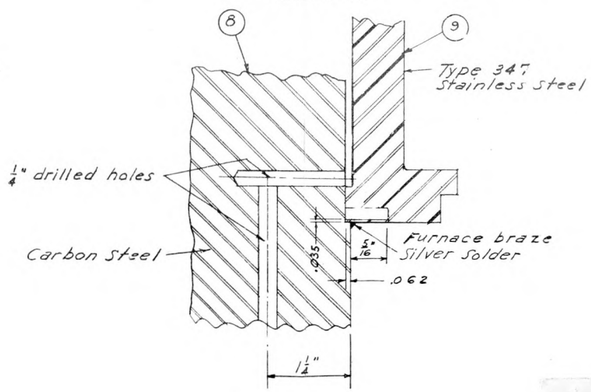

DETAIL "X"
Scale: 1" = 1"

General Notes

1 - Unthreaded portions of stud bolts (Items 15 & 17) must be turned down to Root Dia. of threads.

NO.	REVISIONS	DATE	APPR.	APPR.
DRAWN J.C.B. DATE: 7-12-50	DESIGNED A.H.H. D.T. Jones DATE: 7-11-50	CHECKED H. Terry DATE: 7-21-50	APPROVED J. Mauer Roberton 7/21/50	
HEALTH PHYSICS	MEDICAL	OPERATIONS	SAFETY	
FIRE PROTECTION	RESEARCH SHOP	MAINTENANCE		

FIG. 5
PAGE 22

REFERENCE DRAWINGS	DWG. NO.
EXPERIMENTAL STM. GENERATOR DET. SH. 1	D-7564
" " " " SH. 2	D-7565
H.R.E. EQUIPMENT BLDG. 7500	

EXPERIMENTAL STEAM GENERATOR

OAK RIDGE NATIONAL LABORATORY
OPERATED BY
CARBIDE AND CARBON CHEMICALS DIVISION
UNION CARBIDE AND CARBON CORPORATION
OAK RIDGE, TENN.

LIMITS ON DIM. UNLESS OTHERWISE SPECIFIED ± 1/ FRACTIONS 64, DECIMALS ± .005, ANGLES ± ½°, SCALE: AS NOTED

SUBMITTED	ACCEPTED	APPROVED
W.D. 380638	P. Winters	H.W. Wright

D-7559

DECLASSIFIED DECLASSIFIED DECLASSIFIED

MATERIALS LIST

ITEM NO.	DWG. NO.	QTY.	NAME	SIZE	MATERIAL
1		2	2" PIPE CONNECTION	SHOWN	347 SST
2		2	PIPE CAP	6" SCHED 120	347 SST
3		1	SEAMLESS COLD DRAWN PIPE	6" SCHED 120	347 SST
4		1	WEIGH TANK CONN	SHOWN	347 SST
5		1	1" STEAM CONN	SEE DETAIL "B"	347 SST
6		1	SEAMLESS COLD DRAWN PIPE	6" SCHED 120	347 SST
7		1	SEAMLESS COLD DRAWN PIPE	3" SCHED 160	347 SST
8		1	3/4" DRAIN CONN	SEE DETAIL "A"	347 SST
9		1	PING	SHOWN	347 SST

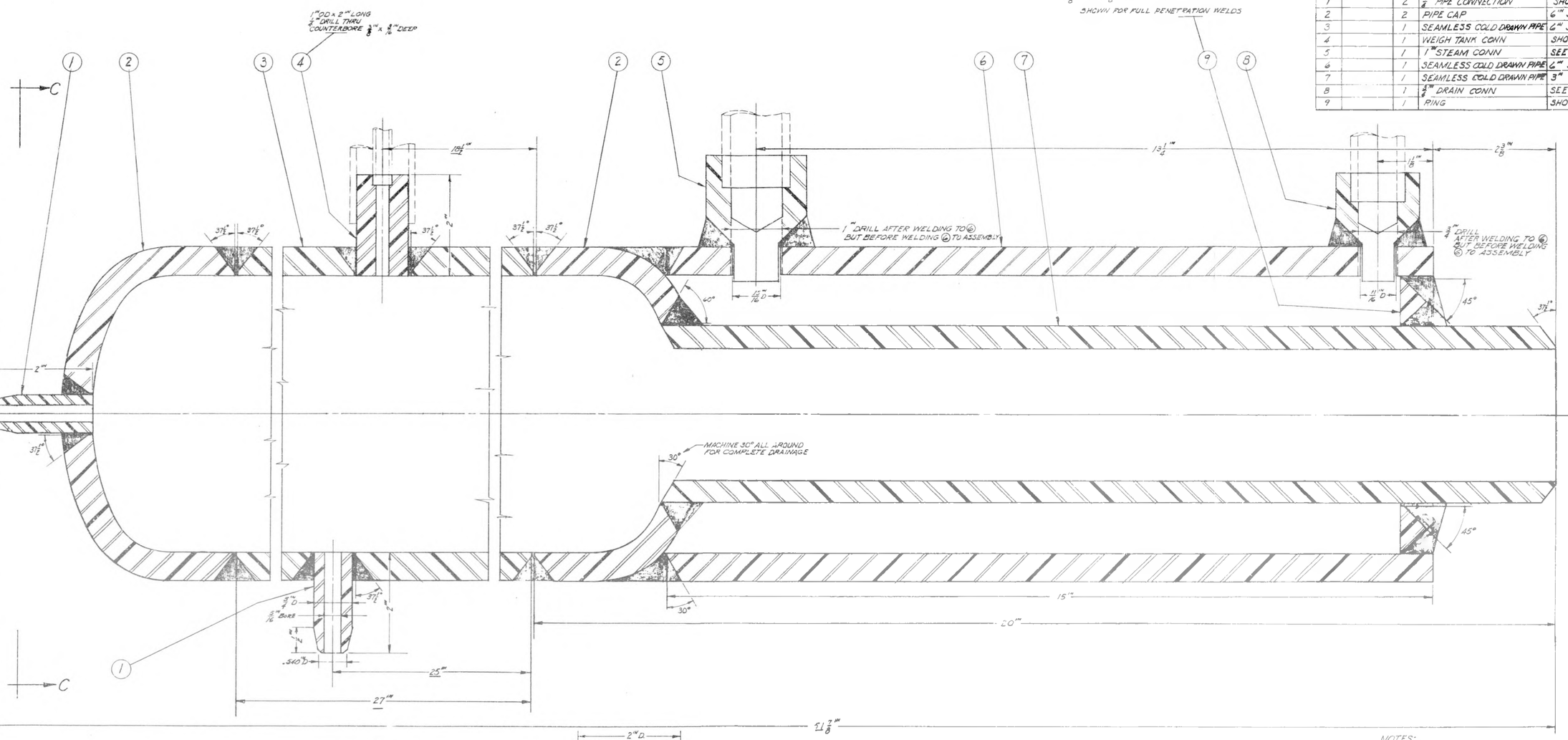

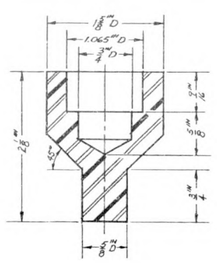

DETAIL "A"
3/4" IPS SOCKET WELD PIPE CONN
MACHINED FROM BAR STOCK

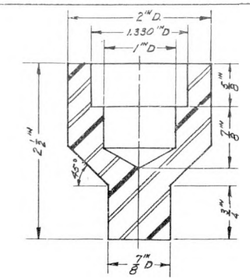

DETAIL "B"
1" IPS SOCKET WELD PIPE CONN
MACHINED FROM BAR STOCK

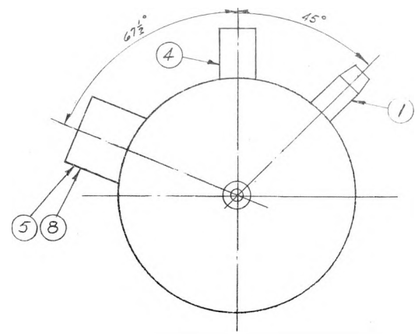

C-C NOZZLE LOCATION
1/2" = 1"

NOTES:
1. ALL WELDS SHALL HAVE FULL PENETRATION AND SHALL BE INERT GAS ARC WELDS WITH INERT GAS FLOW MAINTAINED IN INTERIOR OF VESSEL DURING WELDING.
2. INNER VESSEL WORKING PRESSURE, 2000 PSI, AT 600°F, TEST AT 3000 PSI.
3. STEAM JACKET WORKING PRESSURE, 1500 PSI, AT 600°F, TEST AT 2250 PSI.
5. VESSEL SHALL BE BUILT IN ACCORDANCE WITH 1949 ASME CODE FOR UNFIRED PRESSURE VESSELS, PARAGRAPH U-68.

FIG. 6
PAGE 23

NO.	REVISIONS	DATE	APPR.	APPR.
DRAWN: F.W.L.J.R. DATE: Oct 26 '49	DESIGNED DATE:	CHECKED DATE:	APPROVED	
HEALTH PHYSICS	MEDICAL	OPERATIONS	SAFETY	
FIRE PROTECTION	RESEARCH SHOP	MAINTENANCE		

REFERENCE DRAWINGS	DWG. NO.
HRE EQUIPMENT BLDG 7500	
PRESSURIZER ITEM 2	

THIS DRAWING

LIMITS ON DIM. UNLESS OTHERWISE SPECIFIED
FRACTIONS
DECIMALS
ANGLES
SCALE: FULL SIZE UNLESS AS NOTED

OAK RIDGE NATIONAL LABORATORY
OPERATED BY
CARBIDE AND CARBON CHEMICALS CORP.
FOR THE
ATOMIC ENERGY COMMISSION
OAK RIDGE, TENNESSEE

SUBMITTED	ACCEPTED	APPROVED
		D-7574

DECLASSIFIED
DECLASSIFIED

MATERIALS LIST

ITEM NO.	DWG. NO.	QTY.	NAME	SIZE	MATERIAL
1	Stock	1	Pipe	3" Sched 80	SST 347
* 2	D-7567	1	Elbow	1½" Lg R - E. Strong	SST 347
3	Stock	1	Pipe -	3" Sched. 80	SST 347
4	Stock	1	Pipe	1½" Sched 80	SST 347
* 5	D-7569	1	Concentric Reducer	2" x 1½" E. Strong	SST 347
6	D-7569	1	Supporting Web	As shown	SST 347
7	D-7567	1	Pipe	6" Sched. 40	SST 347
8	D-7569	1	Vaned Nose	2.370 Dia. x 6½ Lg.	SST 347
9	D-7569	1	Adapter	As shown	SST 347
10	D-7569	1	Outlet Tube	As shown	SST 347
11	D-7568	1	Spherical Tank	As shown	SST 347
12	D-7567	1	Weigh Tank Connection	As Shown	SST 347
13	D-7567	1	Weld Nipple (Sched. 40)	½ x 1¼ Lg.	SST 347

* Purchase from Tube-Turn or equivalent.

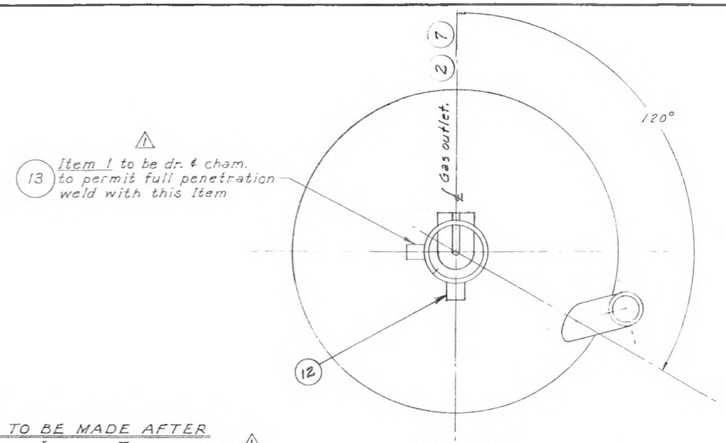

VIEW B-B
Scale ¼"=1"

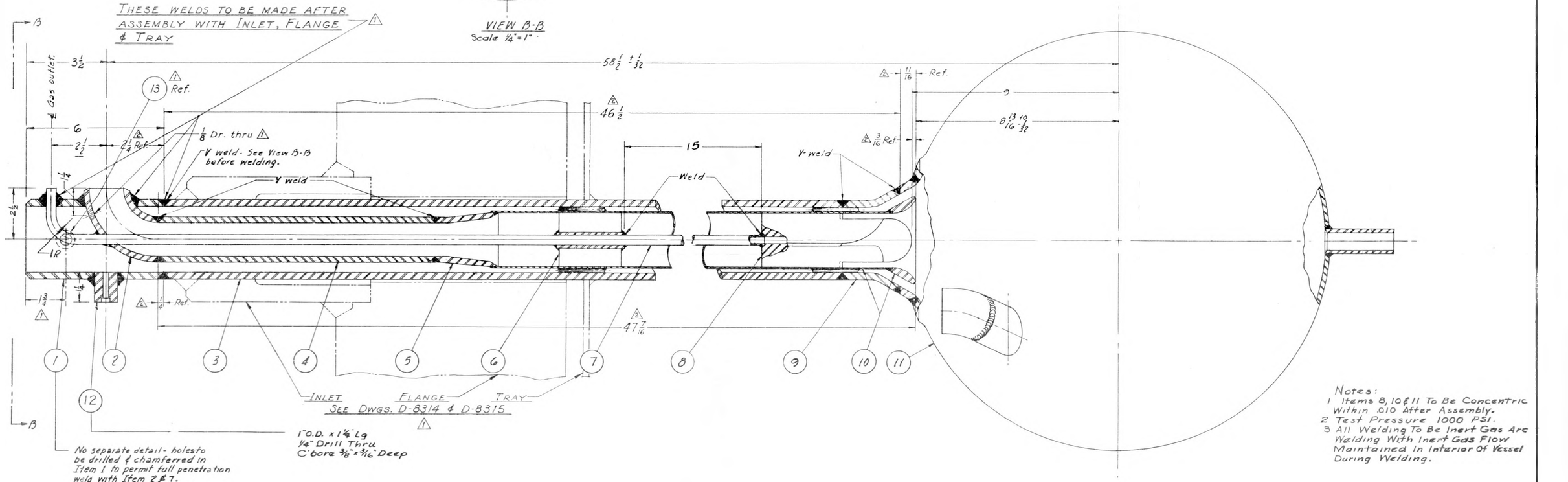

Notes:
1 Items 8, 10 & 11 To Be Concentric Within .010 After Assembly.
2 Test Pressure 1000 PSI
3 All Welding To Be Inert Gas Arc Welding With Inert Gas Flow Maintained In Interior Of Vessel During Welding.

	Reflector Tray & Inlet Details	D-8315
	Core Tank & Flange Assem.	D-8314
	Core Tank Details - Sheet #2	D-7569
	Core Tank Details - Sheet #1	D-7568
	REFERENCE DRAWINGS	DWG. NO.

NO.	REVISIONS	DATE	APPR.	APPR.
2	DIMENSIONS ADDED	12-8-50	WTS	12-8-50
1	ASSEM. PROCEDURE & ITEM 13 ADDED.	11-28-50	WTS.	

DRAWN: ULRICH 8-14-50 DATE:
DESIGNED: W. Terry
CHECKED: WTerry DATE: 5-24-50
APPROVED: [signature]

HEALTH PHYSICS | MEDICAL | OPERATIONS | SAFETY
FIRE PROTECTION | RESEARCH SHOP | MAINTENANCE

EQUIPMENT BLDG 7500

CORE TANK ASSEMBLY

BY: [signature]
LIMITS ON DIM. UNLESS OTHERWISE SPECIFIED
FRACTIONS ±1/64
DECIMALS ±.005
ANGLES ±0°-30'
SCALE: ½"=1"

OAK RIDGE NATIONAL LABORATORY
OPERATED BY
CARBIDE AND CARBON CHEMICALS DIVISION
UNION CARBIDE AND CARBON CORPORATION
OAK RIDGE, TENNESSEE

SUBMITTED: [signature]
ACCEPTED: [signature]
APPROVED: [signature]
W.O. 300630

D-7567

R: 2

FIG. 7

UNCLASSIFIED
UNCLASSIFIED

15,000 psi was reached were 1500, 6700, and 33,000 kw, respectively, for the three types of cooling. These results prompted the selection of internal jacketing for cooling, thus giving a larger factor of safety.

Study of neutron and gamma absorption in the core tank revealed this to be a minor factor in the thermal-stress picture, 15,000 psi stress being reached with no normal heat conduction at 53,000 kw. Calculated normal heat transfer from core to reflector limits the reflector temperature to about 250°F, or higher if excessive thermal stress is not to be encountered. There is considerable uncertainty concerning this temperature owing to the fact that convection effects in the reflector can only be approximated. Measurements in the mock-up will produce more accurate data at a later date.

Reflector Heating. The time required to heat the HRE reflector from room temperature to 200°C by heat transferred from the core has been estimated. Two estimates were made at a 150°C temperature difference (core to reflector), one using a heat-transfer rate of 150 kw and another using one of 50 kw. The high transfer rate gave a required time of 2¾ hr, and the low rate gave a required time of 8 hr. The weight of a full reflector plus pressure shell and plug was assumed to be the mass to be heated.

Investigation of Gas Control by Circulation Through the Reflector. If the reflector feed pump is run continuously, heat and dissolved gases will be removed from the reflector by the D_2O let-down to reflector dump tanks. At a feed-pump rate of 1 gpm and with a 200°C reflector the rate of heat loss is 45 kw. To remove the anticipated gas (H_2 and O_2) production of 1/3 standard cfm (assuming 100 ev per ion pair), it would be necessary to let down 14 gpm from the reflector to prevent the reflector gases from going higher than 10% H_2 plus O_2 in He. Control of gas in the reflector by this means is therefore impractical, and a high-pressure recombiner must be constructed to keep the gas concentration below explosive limits.

Radiation Damage and Gas Formation. *Gas Generation in Pump Armature Compartment.* An estimate of the radiation intensity in the armature compartment of the Westinghouse 100A pump with accompanying water decomposition showed a gas rate of 60.9 cc/hr at standard conditions. A water or soup flow of 60 cc/hr would be adequate to remove the gas by solution.

DECLASSIFIED

Radiation Damage to Pump-cooling Oil. Based on samples exposed in the X-10 pile and an estimate of radiation intensity in the Westinghouse pump, the life of the pump-cooling oil was predicted to be $4.63V$ days, where V is the volume of the oil system in liters. Inasmuch as the volume will be in the neighborhood of 80 liters, the life of the oil will be about a year. Semi-annual oil changes would ensure satisfactory operation. This work is reported more fully in ORNL CF-50-10-145.

Gas Generation in the Pressurizer. Hydrogen and oxygen production in the pressurizer system was estimated at 4.4 standard liters per hour. This amount of gas is very easily soluble in the 1-gpm stream from the pulsafeeder, which is connected to the pressurizer line leading to the core, and gas will diffuse from the pressurizer to this connection. This work is reported in ORNL CF-50-10-133.

There is consequently very little build-up of gas in the pressurizer during operation. However, an equilibrium gas pressure is established in the pressurizer, which produces a pressure gradient that allows the gas to diffuse from the upper part of the pressurizer system to the feed-pump inlet point. This partial pressure has been estimated at 1.75 psi. A vent from the pressurizer to the dump system is provided in case unexpected gas build-up occurs during operation and for venting when the system is being started.

Radiation Damage to the Dump-valve Operator. The soup let-down-valve operator, which contains organic material (neoprene), is exposed to a high continuous radiation level. Assuming the operator to be unshielded and 1 ft from the pipe, this amounts to 7100 r/hr from delayed neutrons and 61,400 r/hr from delayed gammas. With a 10^7-r lifetime, the operator would be good for only 148 hr. Beta dosage is negligible. The data indicate that shielding is required between the line and operator. The operator will be 4 ft from the pipe, and most of the space between it and the pipe will be filled with shielding, resulting in adequate operator life.

Fission-gas Removal. In order to discharge gas accumulated in the soup system with safe release of activity to the atmosphere, it is proposed to install a charcoal column to selectively adsorb krypton and xenon. This column is sized to provide a 100-day holdup of xenon, at which time there is less than 1 curie per day discharged from the bed. Hydrogen (or air) travels

DECLASSIFIED

through the charcoal at a much higher rate, so that this method allows a considerable saving in space as compared to a holdup-tank type of arrangement.

The design of this equipment is not yet complete; a report will be issued in the near future.

Decontamination System. Two auxiliary dump tanks are being installed in the HRE mock-up. They are located at an elevation below that of any other part of the system, and for the actual reactor they would be buried at a remote location outside the building. They are to be used for soup storage during decontamination, and are connected to the regular dump tanks through two valves in series. Provision is made for steam heating to drive soup into the inner dump tanks, and for removing the heat after shutdown. This system has the following advantages over the system of allowing soup to remain in the regular dump tanks as planned previously: (1) Maintenance is possible in the vicinity of the dump tanks; (2) a number of valves have been eliminated from the main reactor system; and (3) there is no longer the necessity of depending on absolutely tight valve shutoff during decontamination.

Steam and water connections for decontamination are provided above the soup condenser and in the line between auxiliary and regular dump tanks. A drain line for decontaminated solutions is connected to the waste-disposal system.

EXPERIMENTAL WORK

Summary. *HRE Component Testing.* 1. A test loop in which uranyl sulfate solution is recirculated at a rate of 30 gpm has been operated for approximately 800 hr. Precipitations have occurred, but in each case a plausible explanation for them has been found. If further precipitations can be prevented, pump operation will probably be reasonably satisfactory. The system is ready for further operation, and longer operation without further precipitation is anticipated.

2. A second 100-gpm pump has been received and will be installed in a second test loop. It will pump uranyl sulfate at 250°C for several thousand hours, or until trouble develops.

DECLASSIFIED

3. The first 100-gpm pump has been operating satisfactorily in a water-filled high-pressure system for measuring gas holdup and core pressure drop. Measurements thus far are in line with those made in the low-pressure apparatus. Data taken in this apparatus have not yet been completely interpreted. This equipment will be converted for an experiment to determine the effect of liquid-flow (to dump tanks) control on the vortex.

4. The high-pressure soup-feed pump has operated satisfactorily with water, and the system has been altered for operation with soup. Erosion and corrosion effects on valves with stainless-steel and stellite trim will be tested in this apparatus.

5. Several additional devices that have been tested or are under construction are the pressurizer level control, the soup let-down heat exchanger, a device for testing corrosion resulting from boiling soup at about 100°C, ring-and-groove seals, and a device for removing gas from a pipe line.

Mock-up Construction. To obtain a test on the important components before final assembly of the reactor, a full-scale mock-up has been constructed which, when testing and development have been completed, will be dismantled and moved into the HRE building and will then serve as the homogeneous reactor.

Soup Recirculating Test Loop. Tests on static solutions have shown that, before being exposed to uranyl sulfate, stainless-steel surfaces must be pretreated in order to prevent precipitation of uranium and excessive corrosion of the steel surfaces at the operating temperature (250°C) used in the HRE. The pretreatment now used consists in (1) etching for 5 to 10 min with a $HgNO_3$-HCl solution (6.5 g of $HgNO_3$, 100 g of HCl, and 100 g of H_2O), rinsing throughly, neutralizing with 1% sodium hydroxide, and rinsing further to remove all traces of HCl; and (2) passivating with 1% HNO_3 at 250°C for a minimum of 4 hr. The etching step appears to be unnecessary on freshly machined or exceptionally clean surfaces.

As reported in ORNL-826 (p. 32), the initial run with soup was made without etching, but the system was passivated with 1% HNO_3 at 250°C for 12 hr. Almost total precipitation of the uranium as the oxide occurred in about 24 hr. Before a second run the system was cleaned, etched, and repassivated. During the etching the Westinghouse pump armature and stator were removed, but the scroll, or housing, remained in the system, and the pump impeller and

DECLASSIFIED

thermal spacer, which are in contact with 250°C soup, were etched separately. The pump was reassembled and run during the passivation with nitric acid. After a total operating time of approximately 700 hr with soup (250°C and 1000 psi), no precipitation or other visible change took place in the solution. There were several shutdowns for pump-bearing checks, repairs were made to the system, and a welded level indicator was added to the system during the time the 700 hr were being accumulated.

At this point the level-indicator tank was removed for necessary changes and replaced. Instead of a second nitric acid passivation to treat the new level-indicator tank, it was decided to try the addition of nitric acid to the soup to prevent corrosion and/or precipitation in the level-indicator tank. This method appeared favorable in the light of static corrosion tests. Therefore 80 cc of concentrated nitric acid was added to 8 liters of soup. After about 20 hr of operation, a precipitate of iron (presumably iron oxide) was picked up by the uranyl sulfate, but there was no precipitation of uranium.

This necessitated recleaning of the system with the etching solution and repassivation with nitric acid. After 150 hr of additional operation (total of 850 hr) with satisfactory results, the system was drained and it stood empty for about four days while changes were made on the level indicator. During the next run of about 140 hr duration the uranyl sulfate precipitated, presumably because of the four-day exposure of the system to air. A series of static tests had indicated that three to four days exposure to air after pretreatment is not harmful. A longer exposure results in precipitation.

From the above results it is apparent that, if solution precipitation is to be avoided, all surfaces must be carefully pretreated and exposure to air for any length of time after pretreatment is undesirable. A question still in doubt is the proper procedure to use when and if precipitation, formation of corrosion products, or prolonged exposure to air occurs in the HRE. Is it necessary to etch before repassivation? Or will cleaning, say, with dilute HNO_3 at lower temperatures, be satisfactory?

Operation of the test loop will continue as soon as repairs to the pump rotor and bearings are made.

Bearings for the Recirculating Pump. The Westinghouse model 100A pump as received is equipped with graphitar No. 14 bearings and titanium carbide

DECLASSIFIED

bushings. These bushings are unsatisfactory for operation in the soup system, and bushings of hardened 410 stainless steel and stellite are now being tested. Bushings of 410 stainless steel hardened to Rockwell C-43 have been used in the model 30 pump in the high-pressure test loop. A check after 150 hr of operation indicated less than 0.001 in. wear on the diameter of the bushings. The uranium precipitation mentioned above has prevented further checks, although it should be noted that after an additional 150 hr of operation, during which the precipitation of soup occurred, wear on the front and rear 410 stainless-steel bushings was 0.0025 in. and 0.0005 in., respectively. Most of this was attributed to the scoring action of the precipitated uranium oxide particles. The graphitar bearings, being much softer, were more severely damaged.

Stellite No. 6 bushings under test in a bearing test device appear to be as satisfactory as type 410 stainless steel. However, the 410 stainless steel is believed to be more desirable because of the necessary nitric acid pretreatment since the action of nitric acid is more severe on stellite. Replacement type 410 bushings are being made for the model 30 pump so that operation of the test loop can be continued.

100A Test Loop. A model 100A pump recently received is being equipped with type 410 stainless-steel bushings and a tantalum labyrinth. This pump will be installed in a second test loop for operation with soup.

The loop will consist of a short length of type 347 stainless-steel pipe connecting the pump suction to the pump discharge. The system will be pressurized by means of helium gas in a small sump tank which is connected to the loop. A cooler will be provided to remove the heat of pumping and will be automatically controlled to maintain the temperature at 250°C in the pump and loop. A circulating-oil system will cool the pump motor. Suitable connections will be provided for sampling the soup for loss of uranium or corrosion products. This system will be etched and passivated in the conventional manner before soup is added.

Gas Holdup and Core Pressure Drop. During this period the heavy steel sphere and its accessory equipment were completed and tested on water. The final flow sheet is shown in Fig. 8.

DECLASSIFIED

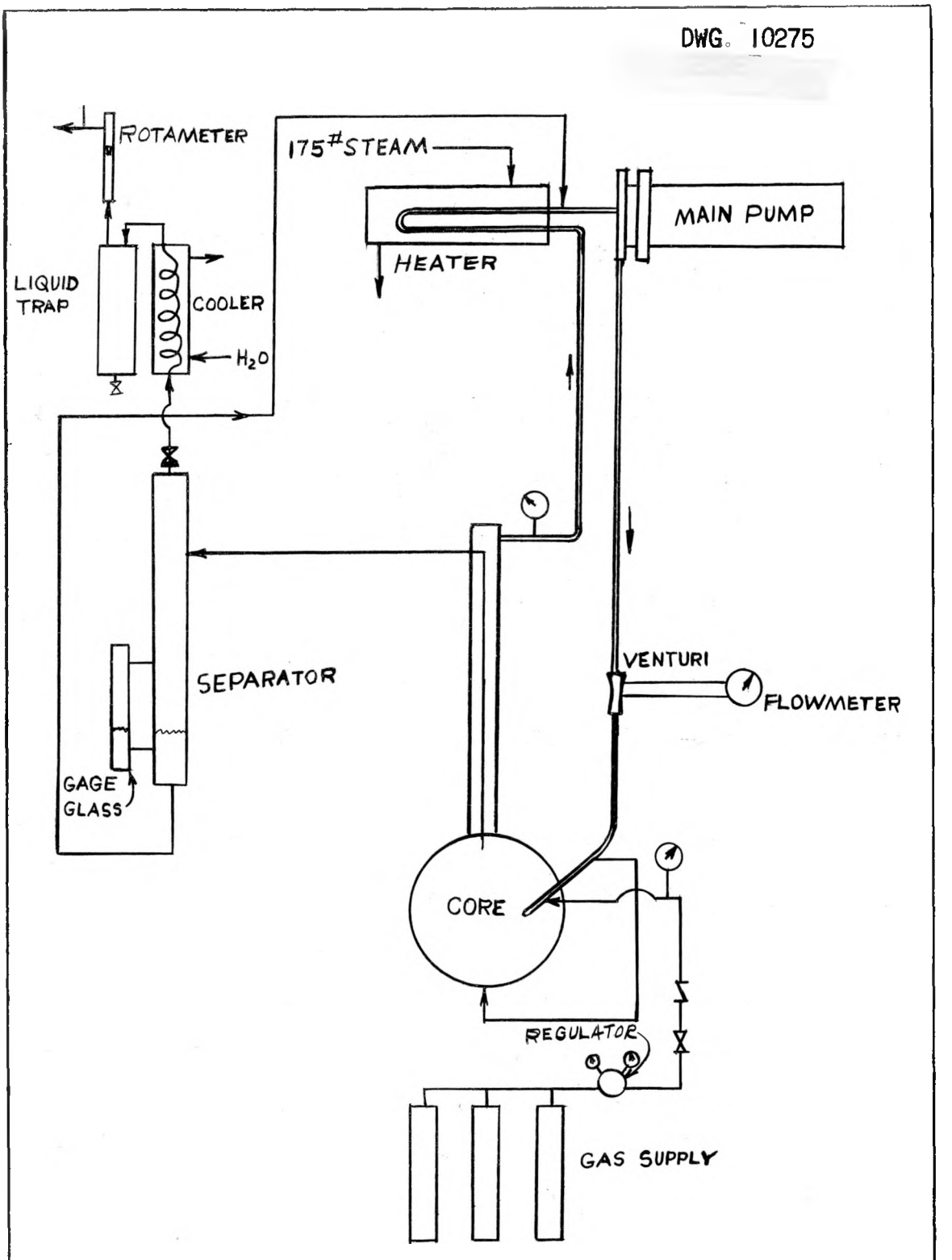

MOCK HIGH-PRESSURE CIRCULATING SYSTEM FIG. 8

DECLASSIFIED

Apparatus. In general, the main circulating system is the same as the proposed reactor circuit described in ORNL-730. Since the final boiler was not available, a small steam heater was inserted in its place to hasten heating and provide additional pressure drop in the external circuit.

No pressurizer was used so that all volume displaced by bubbles would be indicated by increased level in the gas separator. Several vent valves were provided to eliminate errors resulting from trapped gas.

Pressure gauges (0 to 2000 psi) were connected to the inlet and outlet of the sphere to detect any gross changes in pressure drop as a result of reduced viscosity of the solution at high temperatures. A venturi meter in the inlet pipe allowed continuous measurement of flow while the effect of temperature on pump performance was being studied.

The gas separator serves the dual purpose of a separator and holdup measuring device. When operating, the level in the separator is noted before admission of gas and also while gas is flowing. The rise in level then indicates the volume of fluid displaced by bubbles in the system, principally in the sphere itself. The separated liquid is returned to the pump suction. The exhaust gas passes through a throttling valve, a cooler and condenser, a water trap, and a rotameter whose discharge line is equipped with a thermometer and a manometer.

Gas was supplied to the system by a four-tank helium manifold, and the pressure was reduced to 1000 psi by a regulator. During operation this pressure was continually applied to the gas inlet, but gas flows only when the discharge valve is opened, permitting the system to fall slightly below equilibrium pressure. The rotameter was calibrated for helium with a dry-gas meter.

An accessory piece of equipment which proved very convenient was a small high-pressure feed pump, which during start-up maintained any desired pressure up to 1100 psi. It was loaded by means of an air-operated by-pass valve, which accommodated the expanding liquid during heatup but at the same time maintained a constant pressure to protect the Westinghouse pump, which must not be allowed to cavitate. After the desired temperature was reached, the feed system was closed off by means of a valve, and the gas regulator took over, holding the system at 1000 psi.

DECLASSIFIED

Miscellaneous Experiments Conducted to Date. *Sphere Vibration.* Preliminary tests were made to check the vibration characteristics of the sphere. The procedure for determining the magnitude and frequency of vibration for purposes of mechanical clearance and calculation of instrument time constants was as follows:

Two dial gauges were rigidly supported independently of the sphere and so located that their measuring tips contacted the sphere on the top flange, one just above the inlet pipe and the other 90° from it. With 125 gpm of water circulating through the sphere, the indicators were viewed with a strobotac to observe the frequency and maximum amplitude. The maximum deflection was found to be ±0.010 in. parallel to the inlet stream; the frequency varied from 4 to 10 cycles/sec, going through a cycle which took about 5 sec from minimum to maximum. The largest deflection occurred at the lowest frequency.

Heat Transfer from Core to Reflector. A large cubical tank about 30 in. on a side surrounded the sphere and was filled with a weighed amount of water. Thermocouples were spot-welded to the outer wall of the sphere and to the outer surface of the cubical tank, placed in the water in the tank, and one was clamped to a pipe carrying water in the circulating system. All thermocouples were connected to a multipoint recorder.

The pump and steam were allowed to heat the circulating water to 114°C, at which time the system was allowed to cool. From these heating and cooling curves a maximum value of the film coefficient from the sphere to the water in the tank of 957 Btu/hr/sq ft/°F was obtained. Accurate information will be obtained when the mock-up is completed, since uncertainties in the effects of convection in the reflector limit the accuracy of calculations.

Pressure Drop Across the Sphere and Pump Outlet at Various Temperatures. Theoretical investigation of the flow through the sphere predicted an increase in pressure drop across the sphere as the fluid viscosity decreases at higher temperatures. It can also be shown that pressure drop decreases as inlet velocity is reduced.

Since it is desirable to know what might be expected in the HRE, data were taken to observe any gross change between room temperature and 250°C. There was no appreciable change in measured pressure drop across the sphere (about 38 psi) over this temperature range. It may be assumed that both these

DECLASSIFIED

effects are small or tend to nullify each other and will pose no problem in the HRE.

The data presented in Fig. 9 show pump flow vs. the temperature and confirm the curves provided by Westinghouse with the pump.

Gas Holdup. Using the method described earlier to measure gas holdup, numerous runs have been made under varying conditions and the results tabulated. Although runs were made at temperatures up to 250°C, the high-temperature data are not sufficiently well developed to be reported at this time.

Using the outer cubical tank mentioned previously as a cooling vessel with cooling water flowing continuously to remove the approximately 5-kw input of the pump, measurements were made at about 50°C (see Fig. 10). It will be seen that these values of holdup agree with those taken at lower pressures, described in ORNL 826 p. 37. Gas flows recorded were computed for inlet pressure (600 psi), and, since the discharge pressure was only about 38 psi lower, the problem of bubble expansion is now negligible and results can be considered reliable.

Soup Feed Pump (Pulsafeeder). The soup-feed pump with bolted head design has been operated with water for approximately 300 hr and is now pumping at 0.95 ± 0.05 gpm at 1000 psi. The soup-feed pump system now includes a steam heater and two dump valves of different design and trim (type 410 stainless steel and stellite). This system will soon be operated with soup to check corrosion, erosion, and operating properties of the dump valves. After prolonged operation the 0.020-in. stainless-steel diaphragm in the pump and check valves will be removed for inspection.

Equipment and Testing *Pressurizer and Level Control.* Final design of the pressurizer has been completed. Temperature and corresponding pressure will be maintained by a steam jacket. The pressure controller now on the test loop is a prototype of the final instrument and controls at 1000 ± 10 psi. The control will be much better in the mock-up because the on-off electric heaters will be replaced by a continuous steam source.

A level indicator controller, as described in ORNL-826, has been in operation on the test-loop pressurizer. After a few minor modifications, this unit indicated level quite accurately. During steady operation, indicated

DECLASSIFIED

DWG 10153

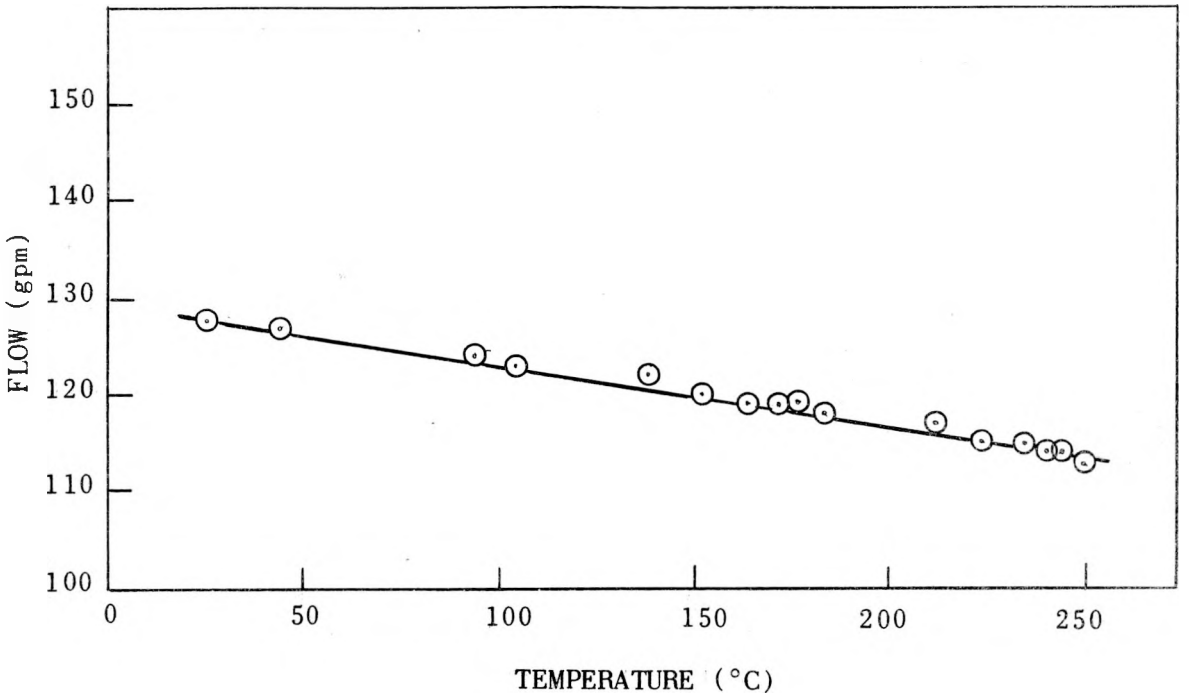

Fig. 9. Effect of Temperature on Water Flow Through Steel Mockup

DECLASSIFIED

DWG 10154

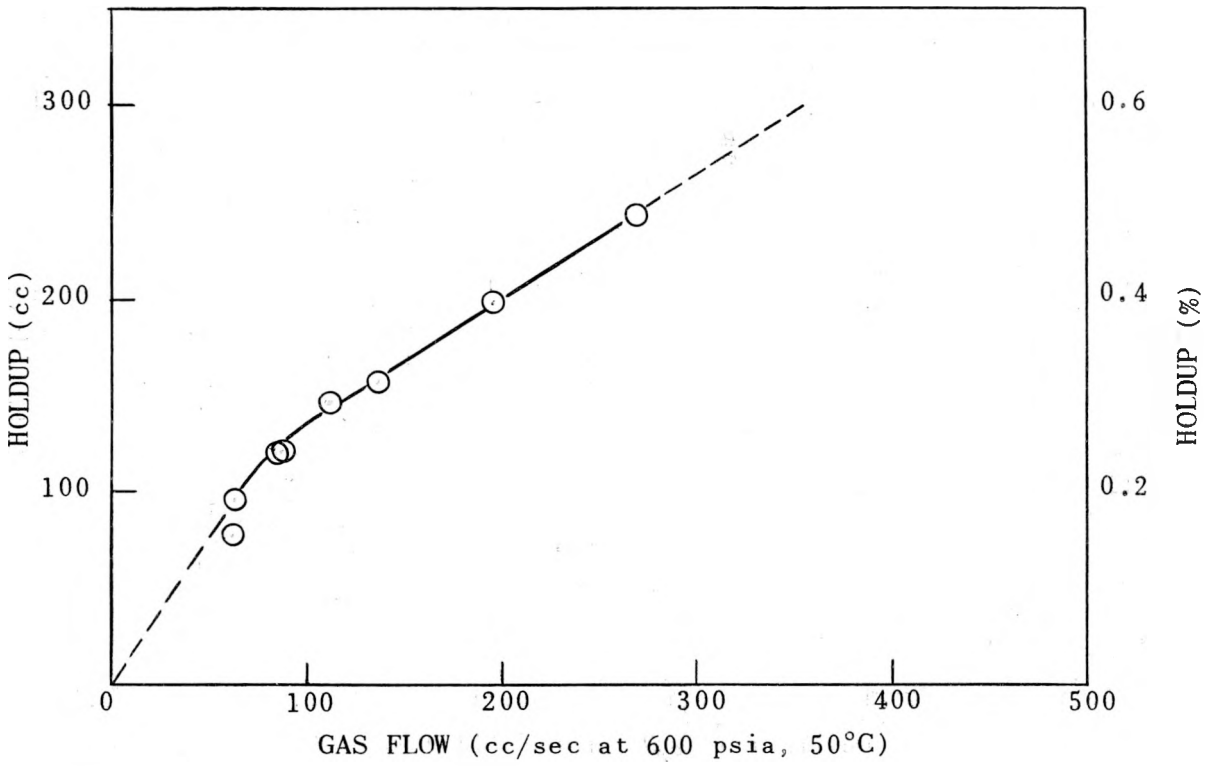

Fig. 10. Gas Holdup

DECLASSIFIED

variations are within ±3% (corresponding to approximately ±0.4 in. of level change in the pressurizer). The control mechanism has not been operated to date, but will be demonstrated in the mock-up.

Soup "Let-down" Heat Exchanger. The soup heat exchanger described in ORNL-826 was installed in the the soup-feed pump system. After the system had been etched, several leaks were found in the heat exchanger between the inner and outer tubes. These leaks were at points where spacers were welded to the inner tube to center it with respect to the outer pipe. This renders the present heat exchanger useless, and a second one essentially of the same design but with a different kind of attachment for spacers will be built.

Boiling Corrosion Test. A miniature prototype of the soup dump tanks and soup evaporator was fabricated of type 347 stainless steel. All joints wetted by uranyl sulfate solution were welded by the heliarc process. The internal surfaces were etched by a solution containing 6½ g of $HgNO_3$ and 100 g of HCl per 100 g of H_2O, which was allowed to remain in the vessel for 15 min at room temperature. This treatment was followed by an alkaline rinse and a thorough rinse with distilled water. The vessel was then filled with 3 liters of a solution of UO_2SO_4 containing 40 g of uranium per liter.

The evaporator was heated with 60-psig steam, and the evaporated water was continuously condensed and returned to the vessel. The system operated for 475 hr with no change in concentration and no observable decomposition of the solution. The boiling-solution temperature varied between 81 and 119°C. The pressure-control system was not functioning properly because of a plugged pressure snubber which was in the line to the pressure gauge and the pressure controller, resulting in temperature fluctuations.

The system was allowed to operate in this way for 824 additional hours before the final sample was taken. During this time water had leaked from the system (as steam) through a threaded connection in the vapor line to the condenser, and the uranium concentration of the solution increased from 40 to 100 g/liter.

The evaporation heater, which is a 6-in. length of 1-in. pipe closed off at one end and containing the heating steam inside, has been cut from the system and examined for corrosion. Its surface was free from pits and other

DECLASSIFIED

evidence of attack by corrosion. The weld at the sealed end was also apparently unattacked.

The heater will be welded back into the system, piping will be rearranged to give better temperature and pressure control, and all joints will be leak-tested. The same procedure as described above will be followed in preparing the surfaces and operating the boiling test. Samples of solution will be taken weekly, and the test will be continued for as many weeks as are required to determine the stability of the solution under continuous boiling in the stainless-steel system.

Ring-and-groove Type Pipe Joints. During the past quarter a second leakage test was run on a 1½-in 1500-lb ring-and-groove type flanged joint of special Taylor Forge design. The test setup was the same as that described in the previous report (ORNL-826).

The joint was disassembled, and the component parts were cleaned prior to the beginning of this test. The hydrostatic pressure applied was such that the pressure inside the gasket ring was about 1300 psi at a furnace temperature of 550°F. The gasket groove was not pressurized. Twenty-seven cycles, alternate heating and cooling to room temperature, were run during a period of 43 days with little or no leakage. The pressure at the completion of the cycling consistently read 1310 ± 20 psi. Calculations show that a pressure decrease of 100 psi represents a leakage of approximately 0.05 cm^3 of water. The data indicate that the leakage, if any, was considerably less than this volume. Including this test, there have been four assemblies of the joint, which indicates that the contact surfaces were not unduly damaged by successive loadings.

A standard ring-and-groove joint will be tested in this apparatus as soon as it is received, and, if successful, will be used in the reactor. The standard joint is essentially the same as the special joint described above, and is expected to be satisfactory.

Device for Removing Gas from a Pipe Line. This device, shown in Fig. 11, an assembly of plastic parts from earlier sphere experiments, was made to test the applications of the vortex separator idea in the pipes of the external circuit. A simple volute with smooth transition curves into the pipe provided

DECLASSIFIED

UNCLASSIFIED

DWG. 10152

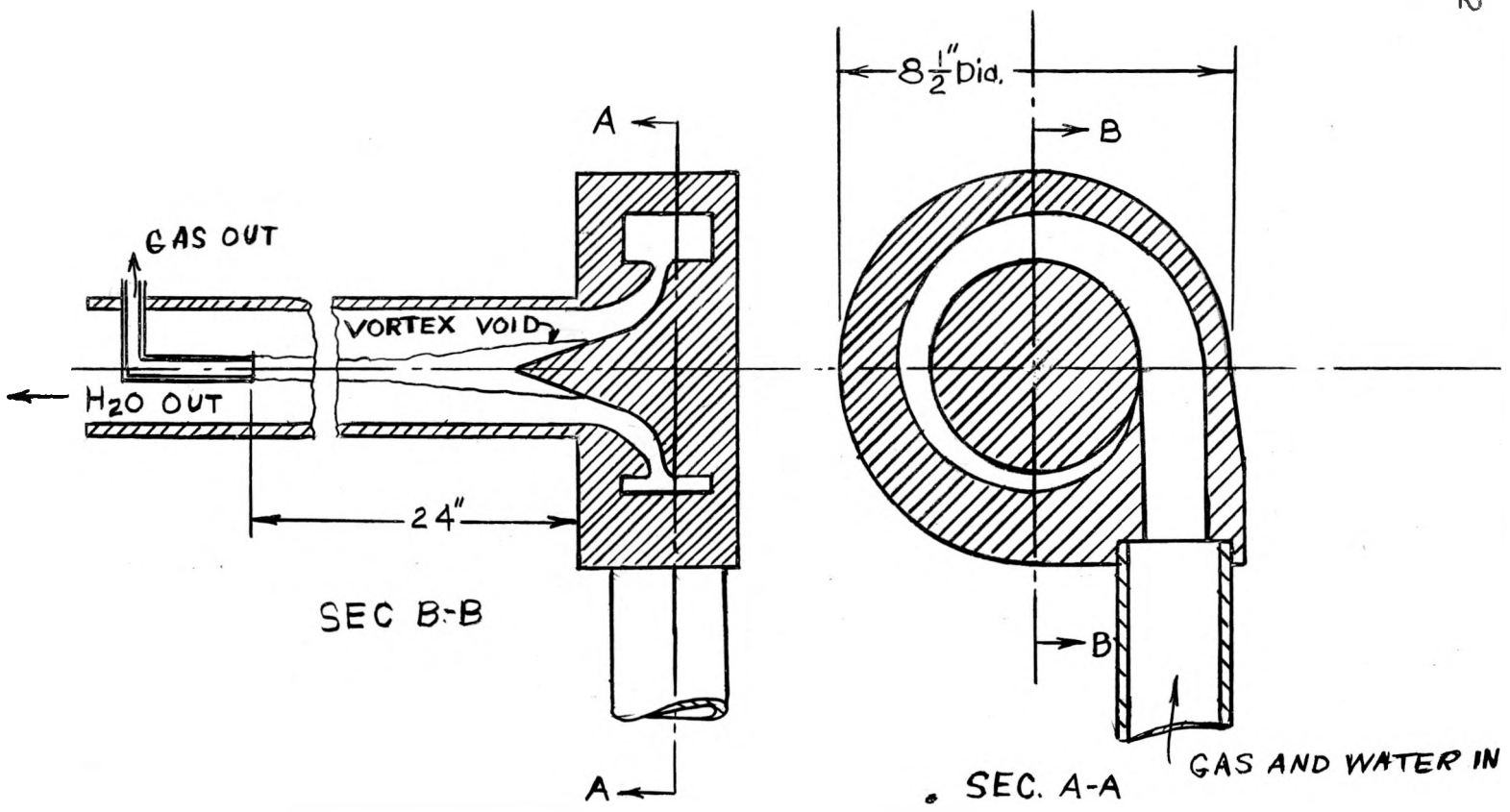

GAS REMOVAL DEVICE FIG. 11

the necessary rotation, and, as the stream emerged, rotating about the axis of the pipe, all visible bubbles moved into the central vortex which terminated at the gas outlet, 18 in. downstream.

Only qualitative tests were made, but they showed the device to be quite insensitive to fluid or gas-flow-rate changes. Visibly, separation was complete and the system was quite stable. No further work is being done on this device until a need for it arises.

CONTROL AND SIMULATOR

Most of the control effort during the quarter has been devoted to acquiring and checking the instrumentation outlined in ORNL-826. Several of the instruments are now on hand and ready for installation.

The instrument panels have been designed and are being fabricated. The design of these allows installation in the Y-12 mock-up and then transfer to the final site with a minimum of dismantling. The instrument placement on these boards and the relation of the boards themselves with respect to the control position are shown in Figs. 12 and 13.

The grouping of various pieces of operating electrical equipment has been altered slightly to permit use of the local generator operating from house-boiler steam for an orderly shutdown in the event of a power failure. The generator will be synchronized on the 120-208-volt system rather than on the 440-volt circuit as previously planned. Essential electrical equipment will be connected to the 120-208-volt circuit so that by a proper operating procedure the load may be removed from the incoming line and supplied from the generator. The house boiler can supply enough steam to give power for an orderly shutdown to stand-by condition without a scram with its attendant longer restarting time.

The simulator has been completed to the point where it simulates the pile behavior without gas evolution for approximately the first 2 sec after a disturbance is introduced. In its present form six delayed neutron groups are simulated with a reduction in the contribution of the longer delayed groups to allow for loss in the external circuit of the actual reactor. Other than this

DECLASSIFIED

DWG 10145

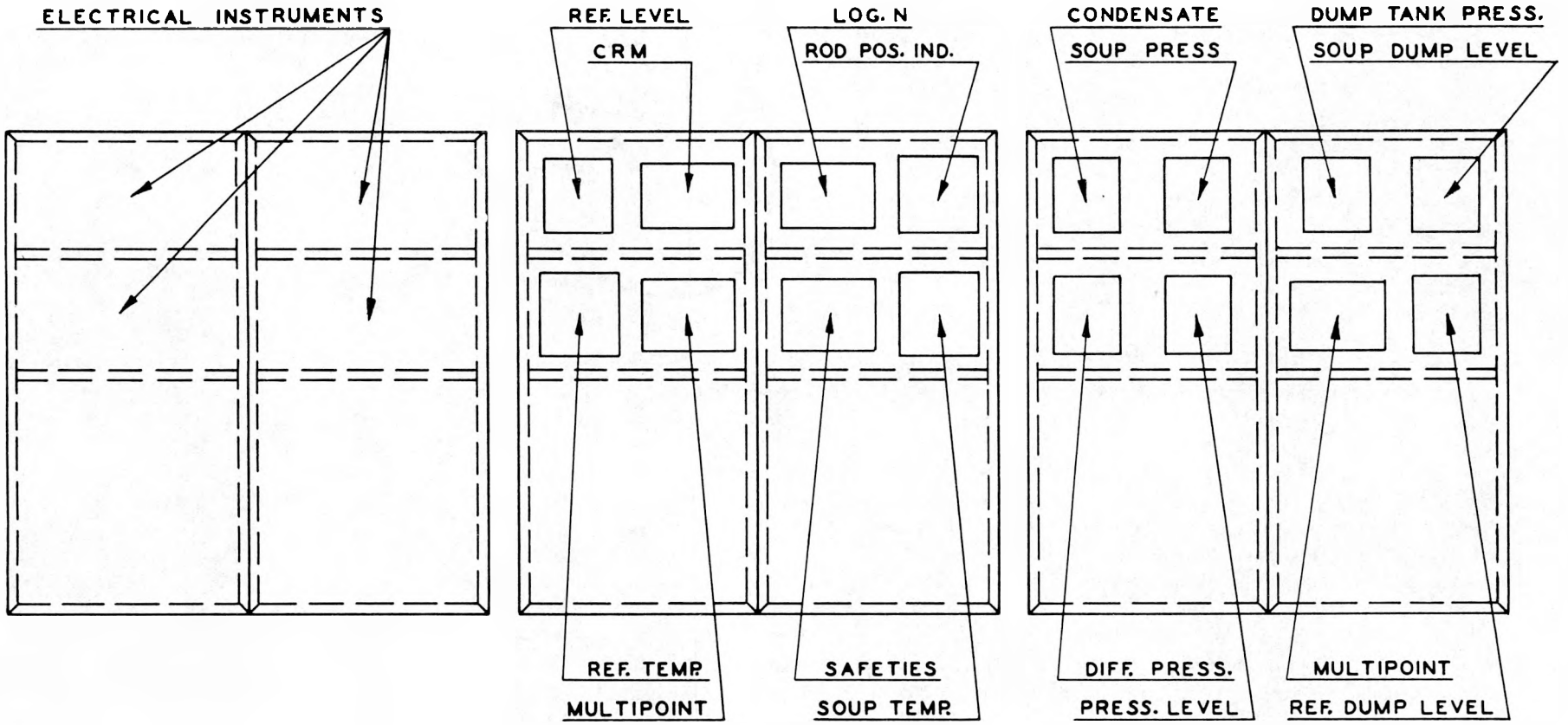

INSTRUMENT PANELS

FIG. 12

DWG. 10146

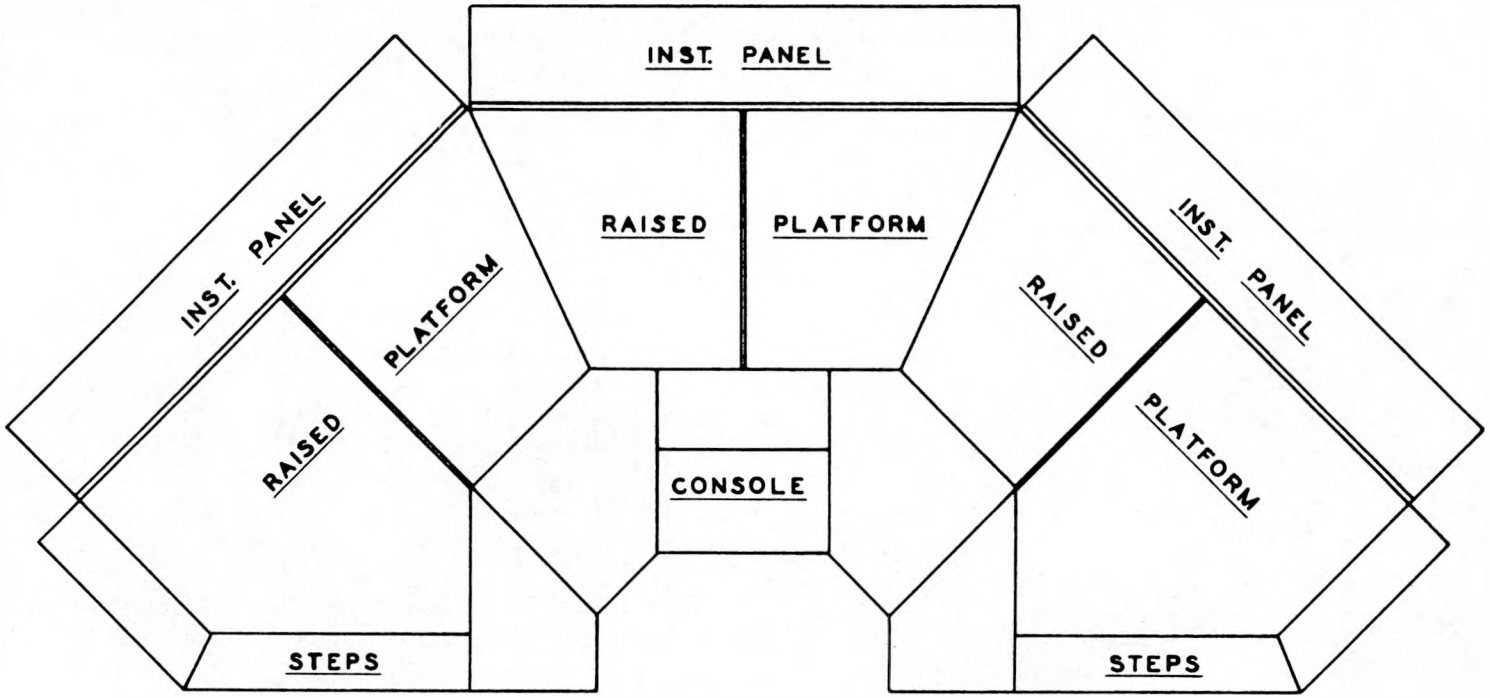

CONTROL POSITION PLAN

FIG. 13

no soup-flow effect is simulated, the temperature circuit representing a turbulent (average) condition with constant dissipation.

Considerable information has already been obtained for step-function changes of k. The experimental procedure of getting these data was, briefly, to set the operating power scale so that the power pulse would not exceed the range of the instrument; then a positive δk step was introduced and neutron level, log n, and temperature were recorded on the oscillograph.

The results of an analysis of a series of these oscillograms are given in Figs. 14 through 18. These results are in agreement with computed check values and a more detailed comparison is presented in the Reactor Physics section of this report (pp. 50 ff.). It should be pointed out that these results cannot be compared with the computed curves in ORNL-730 since the latter neglect delayed neutrons. Furthermore, it should be borne in mind that the curves presented here result from neglect of any gas and a partial neglect of fluid flow.

As an indication of the correct functioning of the simulator, certain characteristics of the curves may be pointed out. The initial period of the simulated reactor is independent of temperature and very closely checks the period computed from the relation

$$T = l/\delta k$$

The final temperature in each case is $\delta k/\alpha$, where α is the temperature coefficient.

In no case were oscillations observed, indicating adequate damping by the delayed neutrons. Additional tests are being made to determine the contribution of each group to this damping and at the same time obtain more data for comparison with computed results to further verify the reliability of the simulator.

Further tests planned for the immediate future will simulate concentration control by varying k at a uniform rate corresponding to various concentration rates. The effect of safety rods will be checked by introducing a positive step function followed by a negative continuous function.

DECLASSIFIED

DWG. 10147

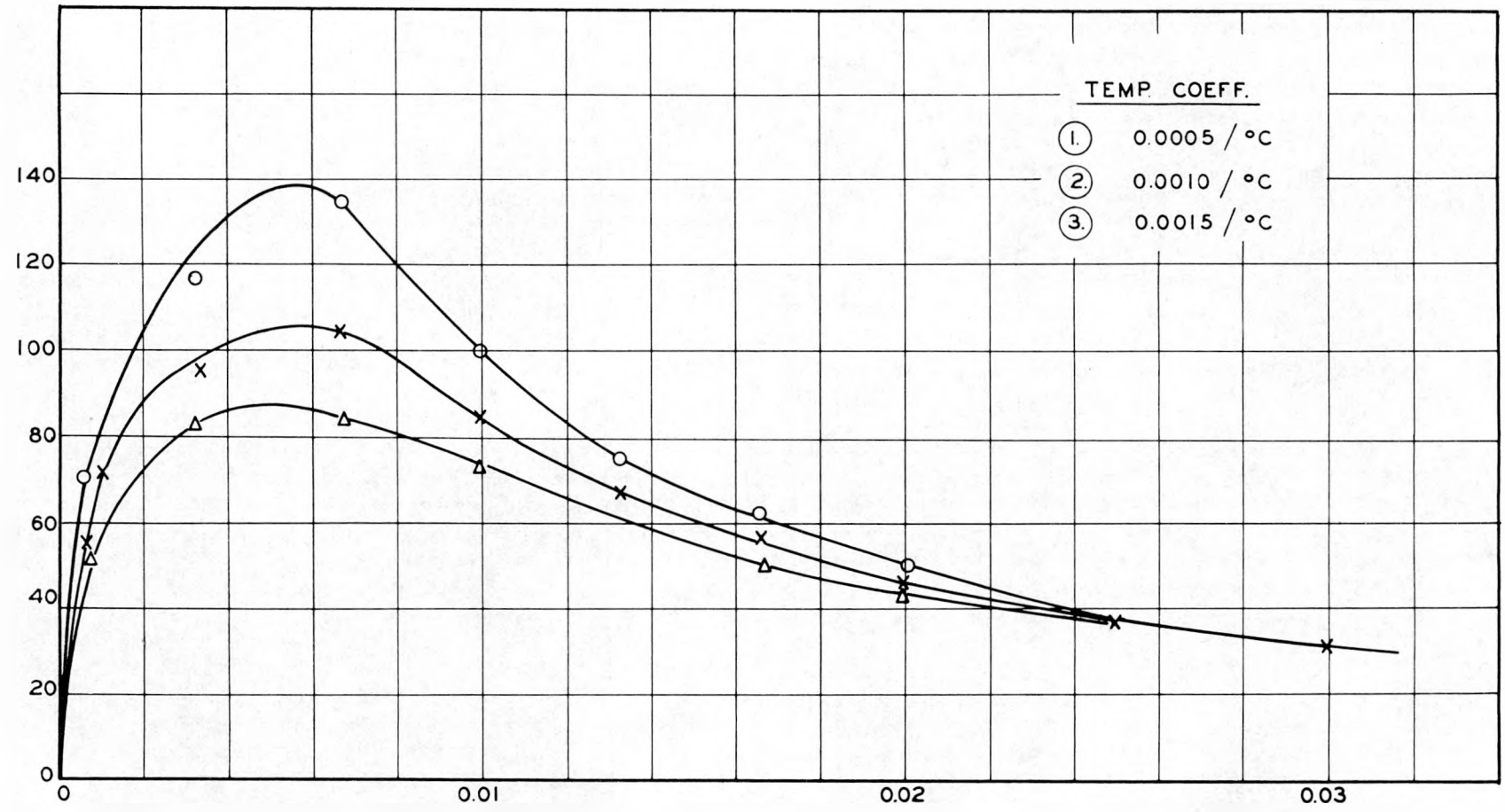

FIG. 14

RISE TIME VS. δK

Approved for Public Release

DWG. 10148

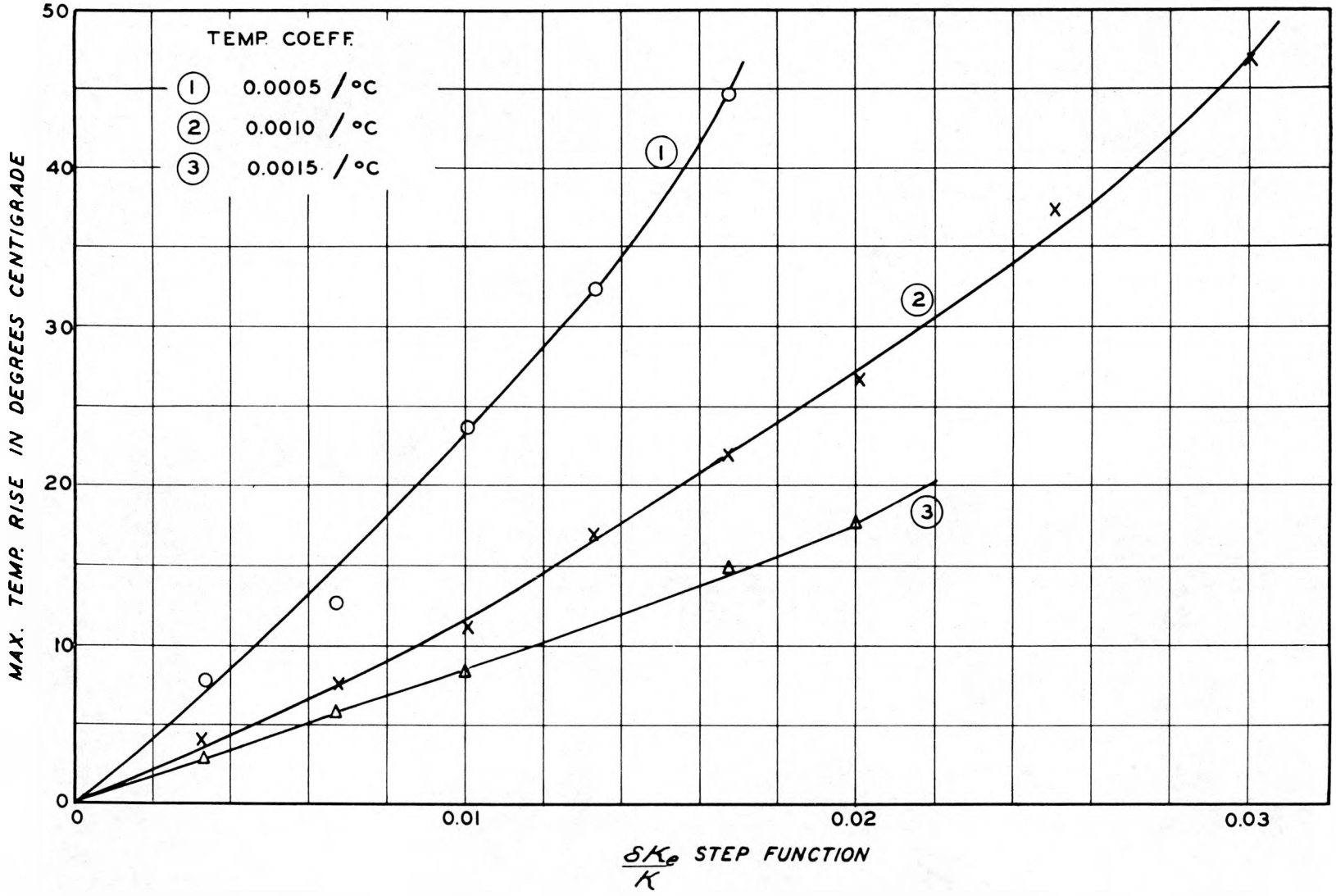

FIG. 15

MAXIMUM TEMPERATURE VS δK

DWG. 10149

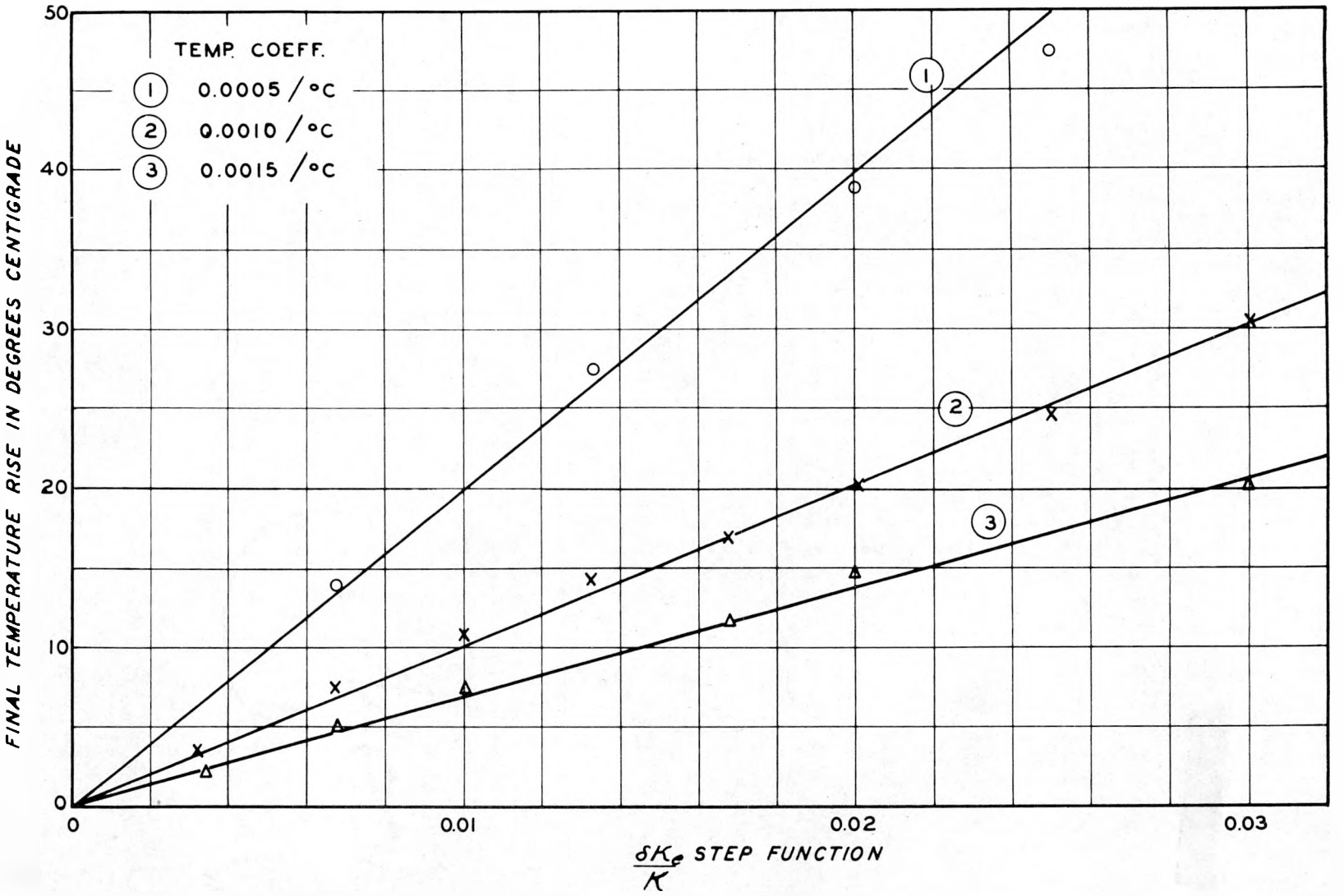

FIG. 16

TEMPERATURE RISE VS δK

DWG. 10150

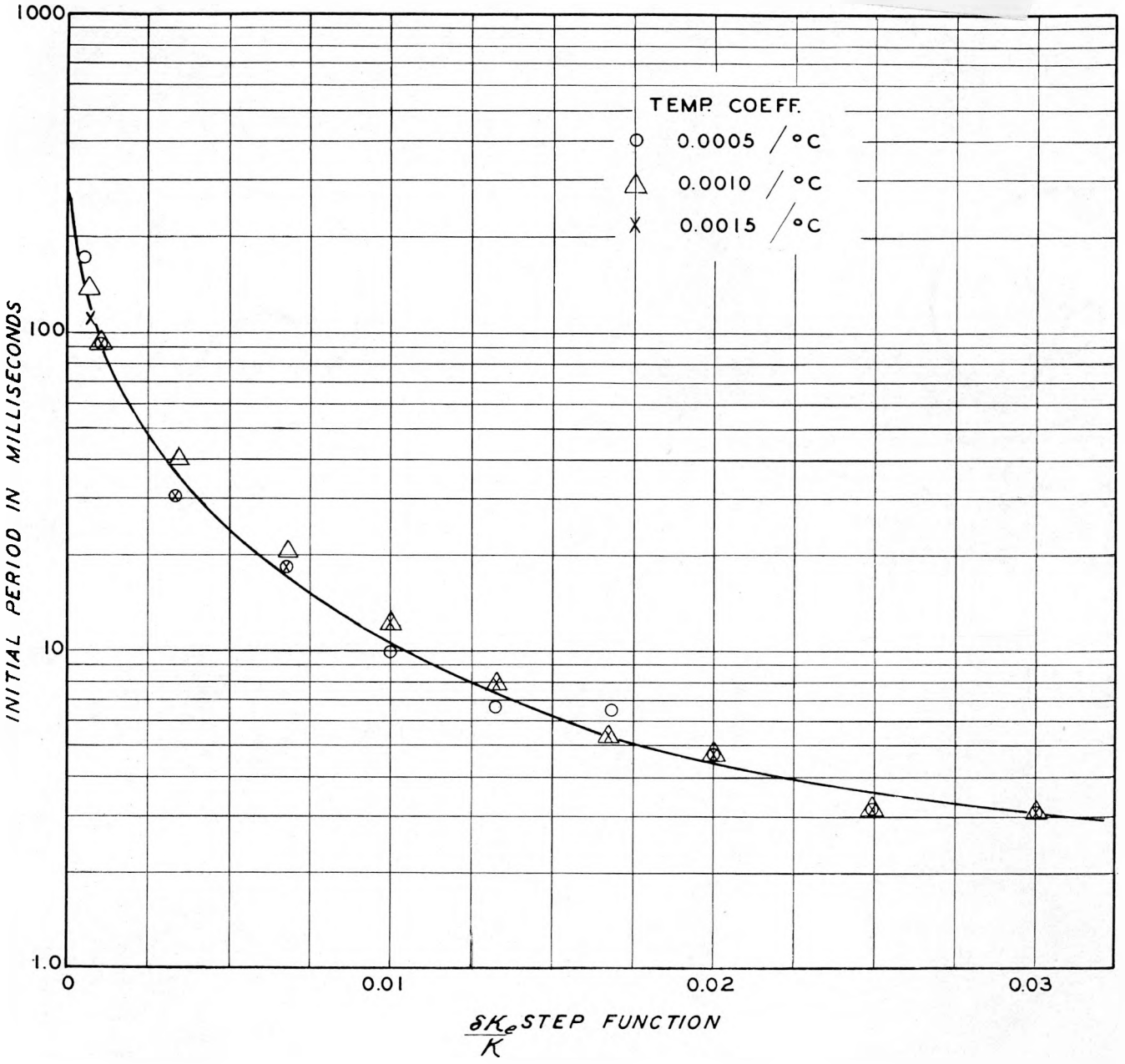

FIG. 17

INITIAL PERIOD VS δK

DECLASSIFIED

DWG. 10151

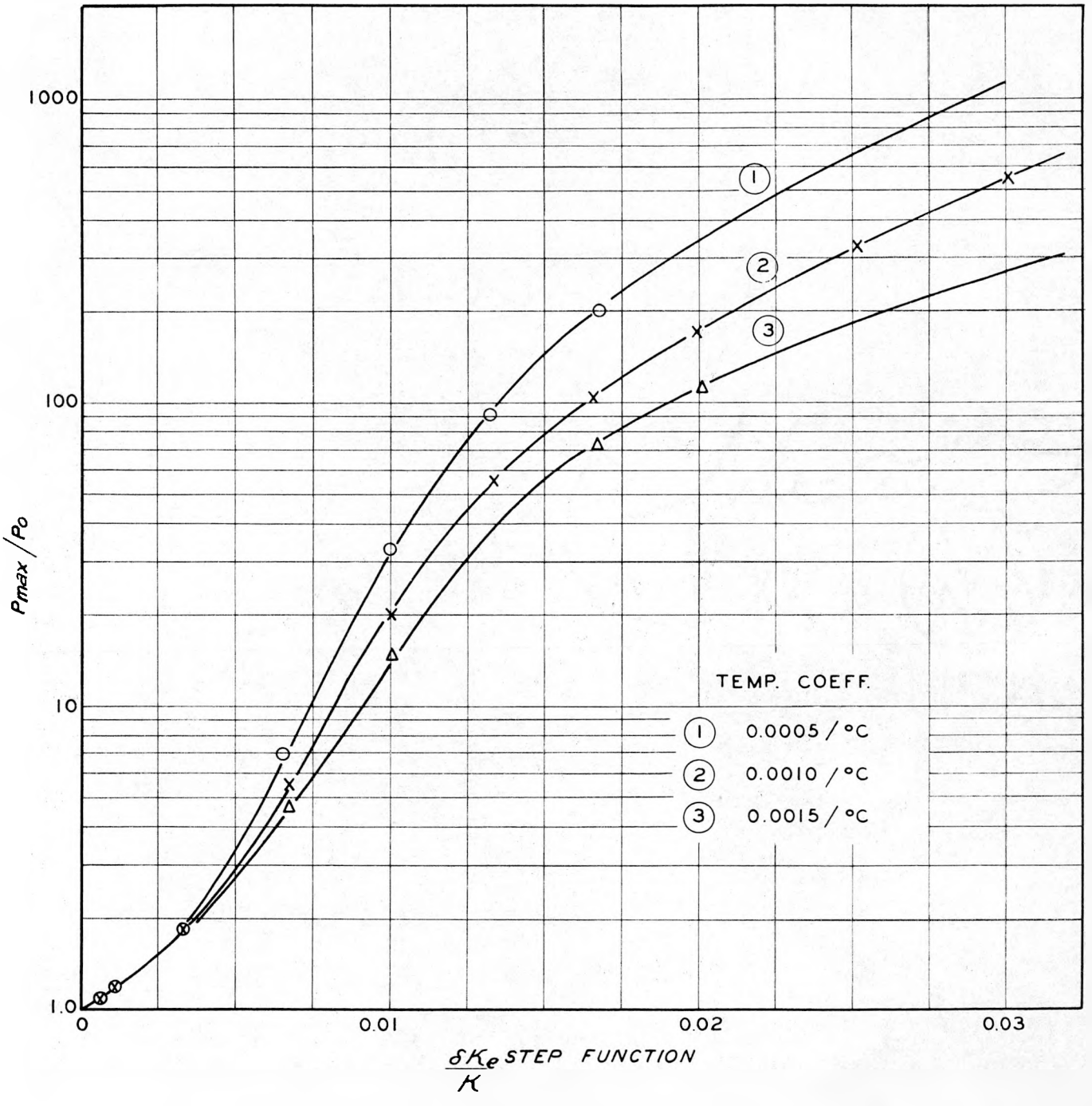

FIG. 18

POWER RISE VS. δK

DECLASSIFIED

The next constructional step will be the addition of a gas simulating unit with adjustable evolution time delay and adjustable gas coefficient. This will be followed by the addition of flow-simulating circuits.

DECLASSIFIED

REACTOR PHYSICS

Induced Activity

Introduction. The HRE being an experimental reactor, accessibility of equipment is a very important factor. The thermal neutrons absorbed in the many components of the reactor and auxiliary equipment result in the formation of radioactive gamma sources (with half-lives ranging from minutes to months). The evaluation of the thermal-neutron absorption, the resulting gamma sources, and the biological effect of these sources is the subject of this section.

Calculation Procedure. A material with macroscopic thermal-neutron absorption cross section Σ_T cm^{-1} and which contains isotopes that are converted to radioactive components by neutron absorption may be labeled in terms of the percentage of the cross section attributable to each of the parent isotopes and the half-lives and gamma energies of the radioactive daughters. The cross sections may be represented by

$$x_1\Sigma_T,\ x_2\Sigma_T,\ x_3\Sigma_T,\ \ldots,\ x_n\Sigma_T,\ \ldots,\ x_N\Sigma_T$$

for the N isotopes of interest. The radioactive daughters will have the corresponding decay constants

$$\lambda_1,\ \lambda_2,\ \lambda_3,\ \ldots,\ \lambda_n,\ \ldots,\ \lambda_N$$

each giving rise to photons of energy

$$E_{11},\ E_{12},\ E_{13}\ \ldots,\ E_{1M1};\ E_{21},\ E_{22},\ E_{23}\ \ldots,\ E_{2M2};\ \ldots;\ E_{n1},\ E_{n2},\ E_{n3}\ \ldots,E_{nMn},\ \text{etc.}$$

When exposed to a thermal flux of ϕ neutrons/cm^2 sec the number of radioactive

DECLASSIFIED

atoms produced per second per cubic centimeter of each kind is

$$P_n = X_n \Sigma_T \phi \tag{1}$$

If the exposure time is t_e seconds, the number of these radioactive atoms present per cubic centimeter at time t_s after shutdown is

$$N_n(t_e, t_s) = \frac{P_n}{\lambda_n}\left[1 - e^{-\lambda_n t_e}\right] e^{-\lambda_n t_s} \tag{2}$$

and the number of disintegrations per cubic centimeter per second is

$$M_n(t_e, t_s) = X_n \Sigma_T \phi \left[1 - e^{-\lambda_n t_e}\right] e^{-\lambda_n t_s} \tag{3}$$

which may be considered sources of $M_n(t_e, t_s)$ photons per cubic centimeter per second of each of the energies $E_{n1}, E_{n2}, \cdots E_{nMn}$.

This source strength multiplied by the appropriate geometric factor $g(r)\,V$, where V is the source volume, will yield a gamma flux (unshielded) at the position r which may be written

$$F_n(t_e, t_s, r) = g(r)\; V\; M_n(t_e, t_s) \qquad \text{photons/cm}^2 \text{ sec} \tag{4}$$

The biological effect of these radiations depends upon the gamma flux and the energy. For a given energy the biological dose rate may be expressed in terms of milliroentgens per hour per unit of gamma flux. (A biological dose rate of 7.5 mr/hr will be considered tolerance for an 8-hr day, 5-day week.) The biological dose rate per unit of gamma flux is shown in Fig. 19. If this

DECLASSIFIED

Dwg. 10169

Not Classified

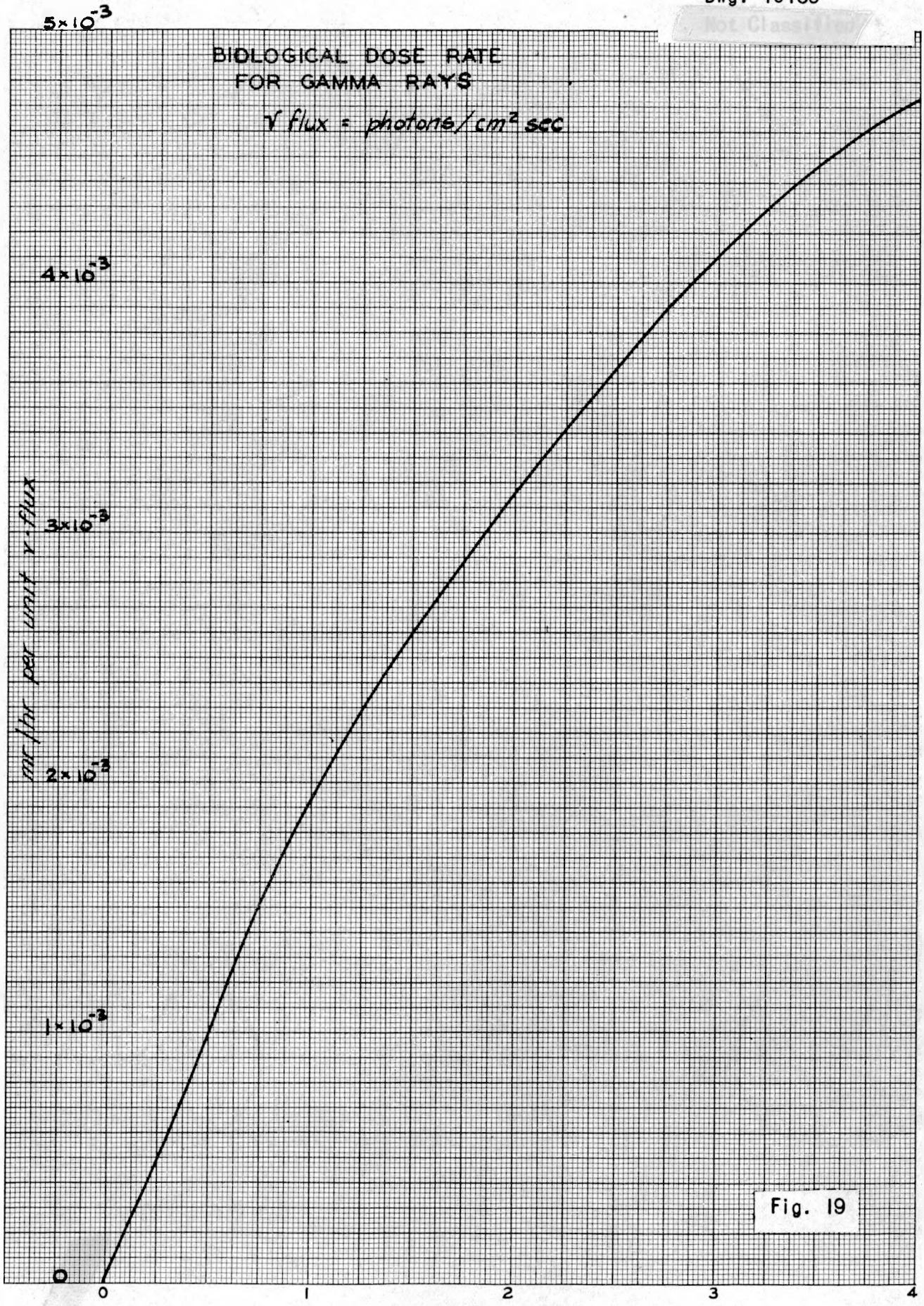

Fig. 19

DECLASSIFIED

value is represented by $B(E_{nk})$ and the shielding is represented by $A(E_{nk})$, the attenuation factor, the biological dose rate due to the radioactive component n is

$$D_n(t_e,\ t_s,\ r) = \sum_k B(E_{nk})\ A(E_{nk})\ F_n(t_e,\ t_s,\ r)$$

and the total biological dose rate is

$$D(t_e,\ t_s,\ r) = \sum_n D_n(t_e,\ t_s,\ r)$$

$$= \sum_{nk}\sum B(E_{nk})\ A(E_{nk}) \left[X_n \left\{ 1 - e^{-\lambda_n t_e} \right\} e^{-\lambda_n t_s} \right] g(r)\ [\Sigma_T \phi V] \quad \text{mr/hr} \qquad (5)$$

which may be written

$$D(t_e,\ t_s,\ r) = \sum_{nk}\sum B(E_{nk})\ A(E_{nk})\ C_n(t_e,\ t_s)\ g(r)\ N \qquad \text{mr/hr} \qquad (6)$$

This expression contains five factors:

$B(E_{nk})$, conversion of gamma flux to biological dose rate

$A(E_{nk})$, attenuation due to shielding

$C_n(t_e,\ t_s)$, conversion of neutrons absorbed per unit time to gamma source strength

$g(r)$, a geometrical factor giving gamma flux due to the gamma source

N, which is the total neutrons absorbed per unit time.

DECLASSIFIED

This subdivision of the calculations was selected to aid visualization and to present data on materials and configurations which will be useful for general induced-activity calculations as well as those of interest here.

The components in which the induced activity has been studied are: (1) core tank, (2) pressure vessel, (3) soup piping, (4) heat exchanger, (5) soup pump, and (6) shield material.

Neutron Sources. The production of neutrons in the reactor when operating at 1000 kw is given in ORNL-730. In this report it was shown that there is a thermal-neutron flux at the core tank of 0.92×10^{13} neutrons/cm^2 sec. The thermal-neutron current into the pressure vessel is 3.5×10^{11} neutrons/cm^2 sec, and the fast-neutron current into the shield is 2×10^{11} neutrons/cm^2 sec. Another source of fast neutrons outside the reactor is the delayed neutrons in the external soup-circulating system. The calculation of this external source is given in ORNL CF-50-10-55 and is plotted in Fig. 20. The thermalization of these two fast sources takes place primarily in the shield material. Figure 21, taken from ORNL CF-50-9-139, shows the fluxes in a borated heavy concrete shield due to the reactor source, and Fig. 22 shows the fluxes due to the delayed neutrons in the piping. On the basis of Fig. 21, the thermal current flowing back into the pressure vessel is 2.5×10^9 neutrons/cm^2 sec. Figures 20 and 22 give a thermal current returning to the piping equal to 0.87×10^8 neutrons/cm^2 sec.

The thermal flux in the heat exchanger is based upon diffusion calculations applied to an equivalent spherical configuration. The source in this configuration is the fast delayed neutrons from the soup in the heat-exchanger tubes. The number of neutrons absorbed per second in the heat exchanger tubes is 6.72×10^{12}, and the thermal current entering the heat exchanger tank from the inside is 10^8 neutrons/cm^2 sec. The soup-circulating pump has a fast-neutron source within it owing to the holdup of soup, but since it is in a rather large compartment there is no effective thermalization of these neutrons near the pump. The slow neutrons absorbed in the pump come primarily from the shield. The evaluation of this flux will be a modification of the pipe calculation illustrated in Fig. 22.

The number of neutrons absorbed in the shield material is based upon Figs. 21 and 22 and varies over an extremely wide range.

CONFIDENTIAL
DECLASSIFIED

Dwg. 9793

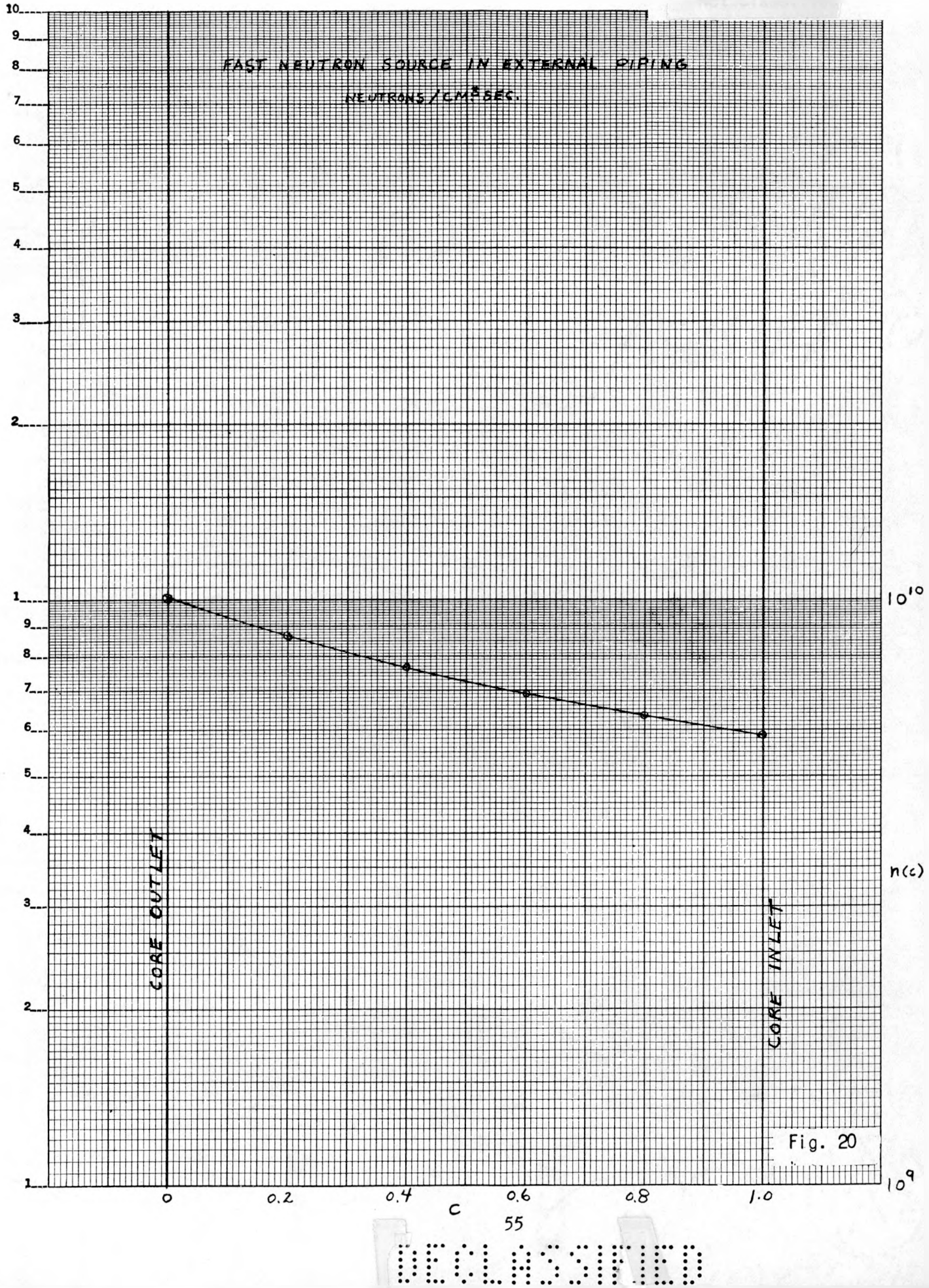

Fig. 20

DECLASSIFIED

Dwg. 9685

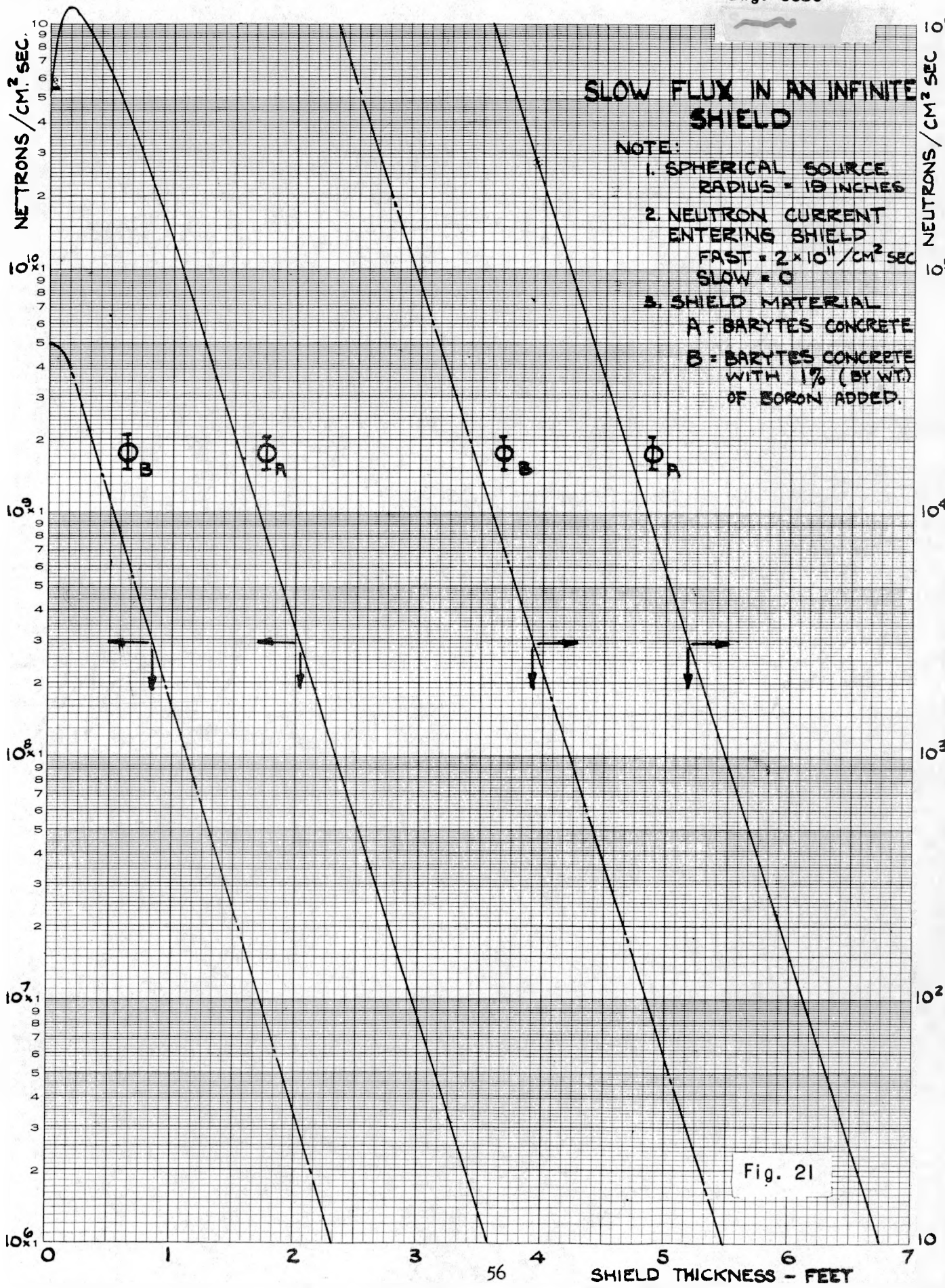

Fig. 21

DECLASSIFIED

Dwg. 10168

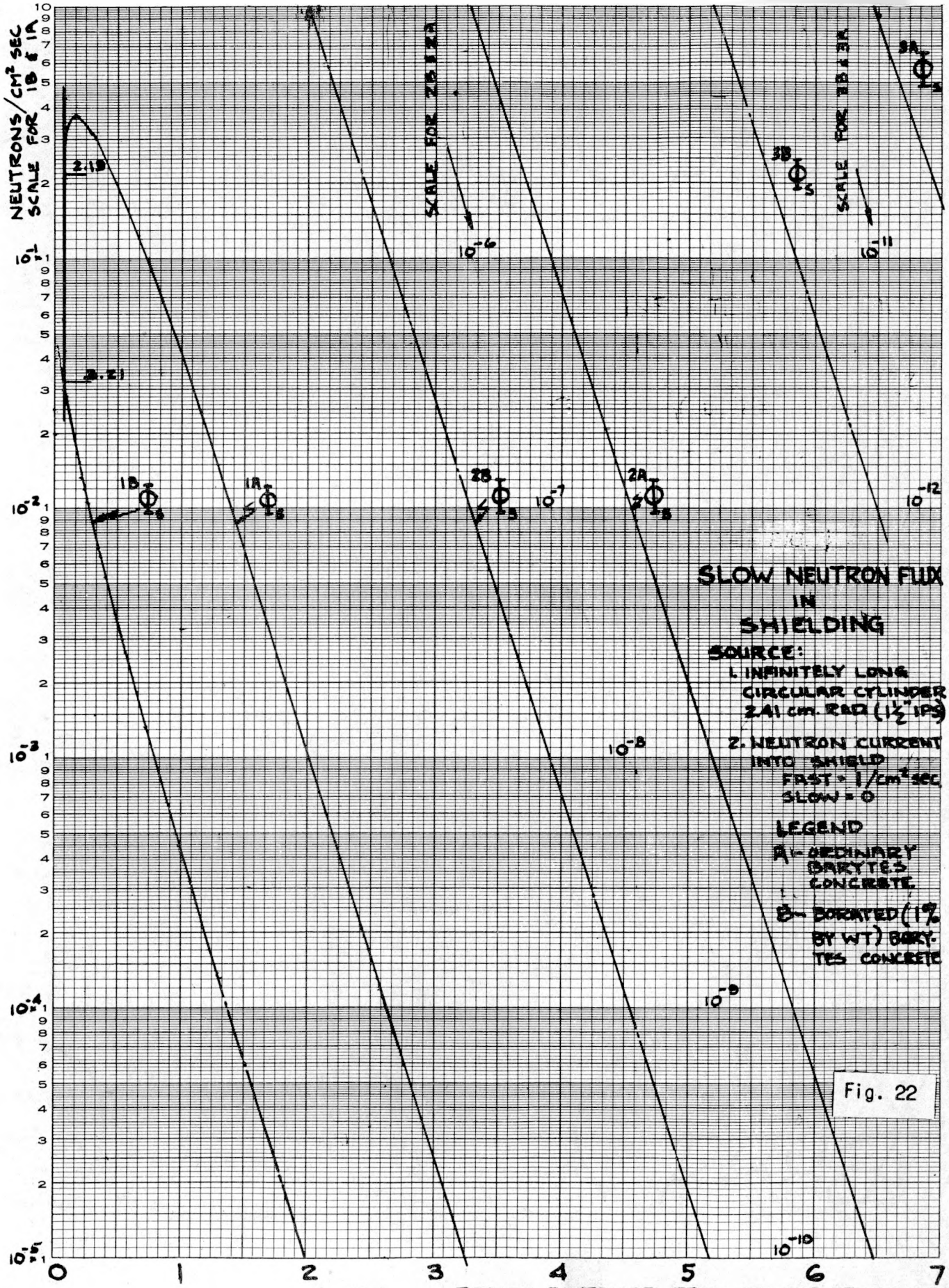

Fig. 22

9/3/50

DECLASSIFIED

Activity Factors in Materials. As outlined under Calculation Procedure (p. 50), the biological dose rate depends on $B(E_{nk})$ which converts gamma flux in photons/cm^2 sec to mr/hr and has the units (mr cm^2 sec)/hr. The factor $C_n(t_e, t_s)$ is nondimensional and contains the time and relative-absorption factors. These two quantities are combined to form a gamma activity factor, $\sum_n B(E_{nk})C_n = \sum_n G_{k3}$ for the material in question. A convenient way to prepare this information for permanent record is illustrated in Fig. 23, which is the chart for 347 stainless steel. The spectrum form with various time levels gives at a glance the relative importance of the various constituents and allows computation of the effect of gamma shielding. On this curve is also shown the sum of all activities for various times after shutdown. The total absorption cross section, Σ_T, is recorded along with other significant data. This form is suggested as a means for preparing data on various materials.

The induced activity in 347 stainless steel has been measured after exposure in the X-10 pile. A comparison between those test values and the calculated values as given in Fig. 23 is shown in Table 2.

TABLE 2

TIME AFTER SHUTDOWN	ACTIVITY (mr cm^2/hr)	
	AFTER EXPOSURE AT PILE TEMPERATURE FOR 49 DAYS	CALCULATED AT 20°C
1 day	1.54×10^5	1.22×10^6
2 days	1.28×10^5	1.13×10^6

The uncertain factors in the calculated values are primarily isotope neutron cross sections, whereas the uncertainties in the measured values are the flux in which exposed, variations in power level of the pile during irradiation, sample temperature, and measurements with an ionization instrument calibrated with a 1.2-Mev cobalt source to give photons per second. Figures 24 and 25 give the activity in SA-105-46I, ASTM-212-B steels, and in barytes concrete.

The induced activity in barytes concrete has been measured, and Table 3 shows a comparison between the experimental and the calculated values.

DECLASSIFIED

Dwg. 10167

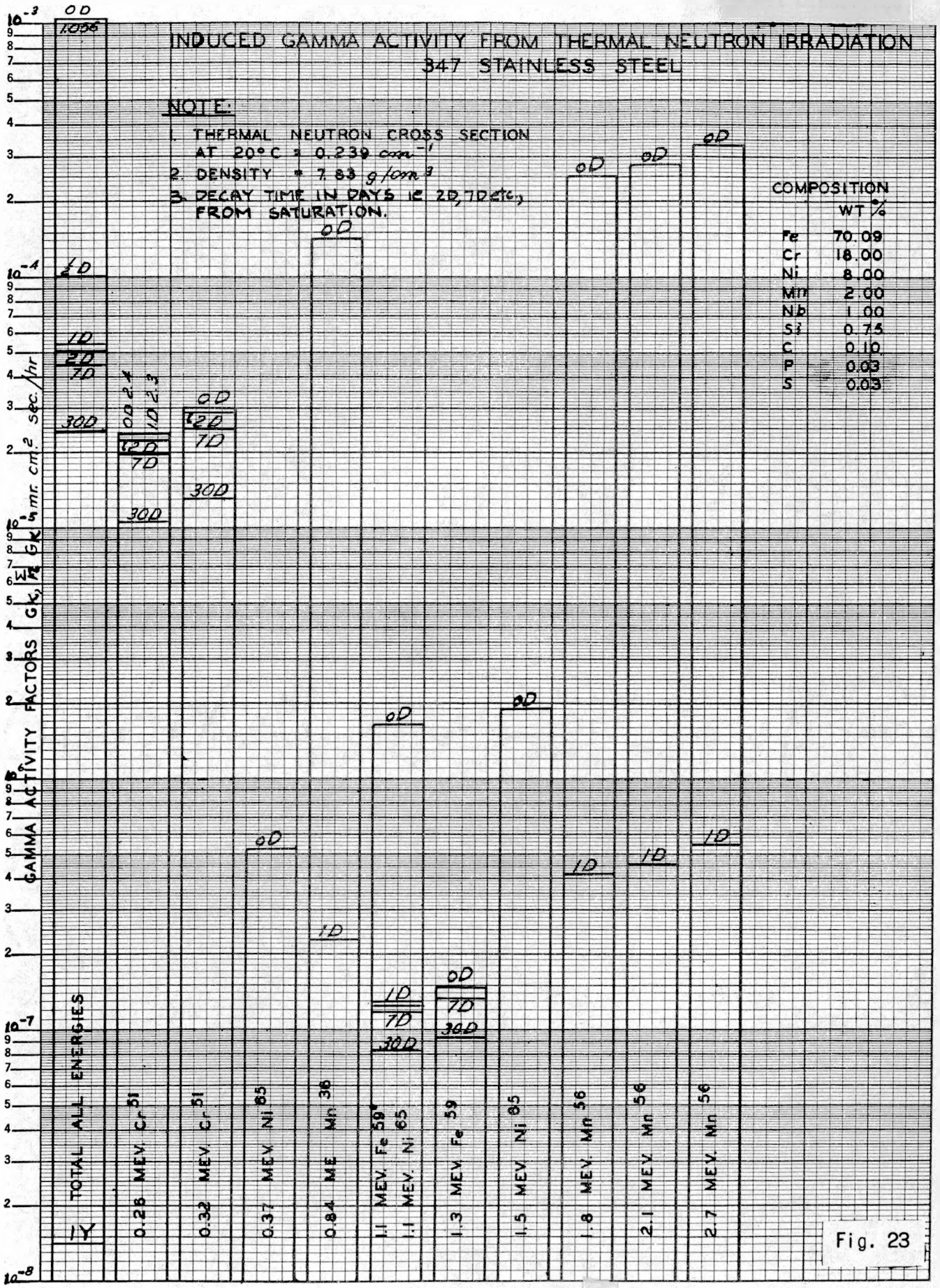

DECLASSIFIED

Dwg. 10166

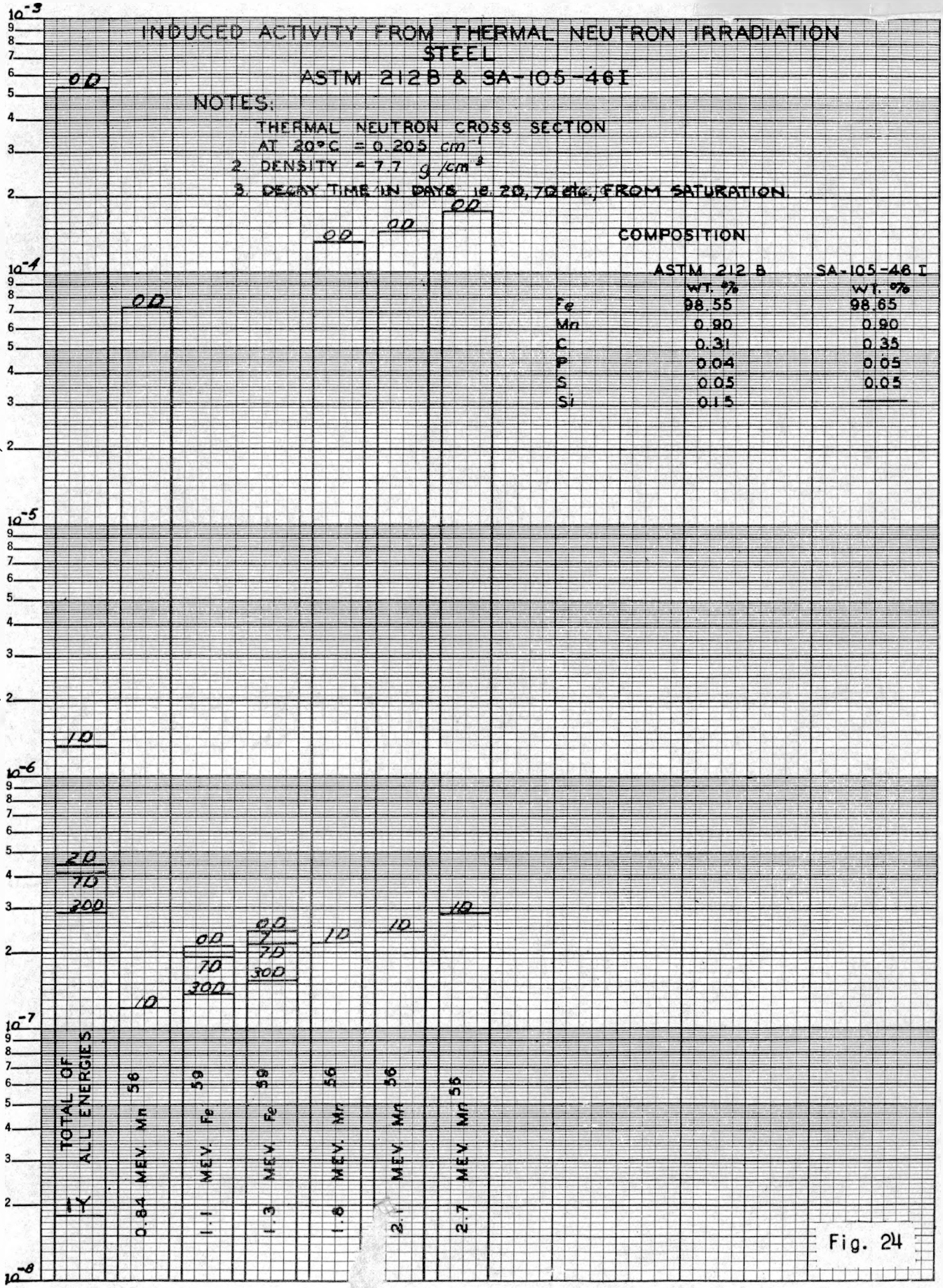

Fig. 24

DECLASSIFIED

Not Classified

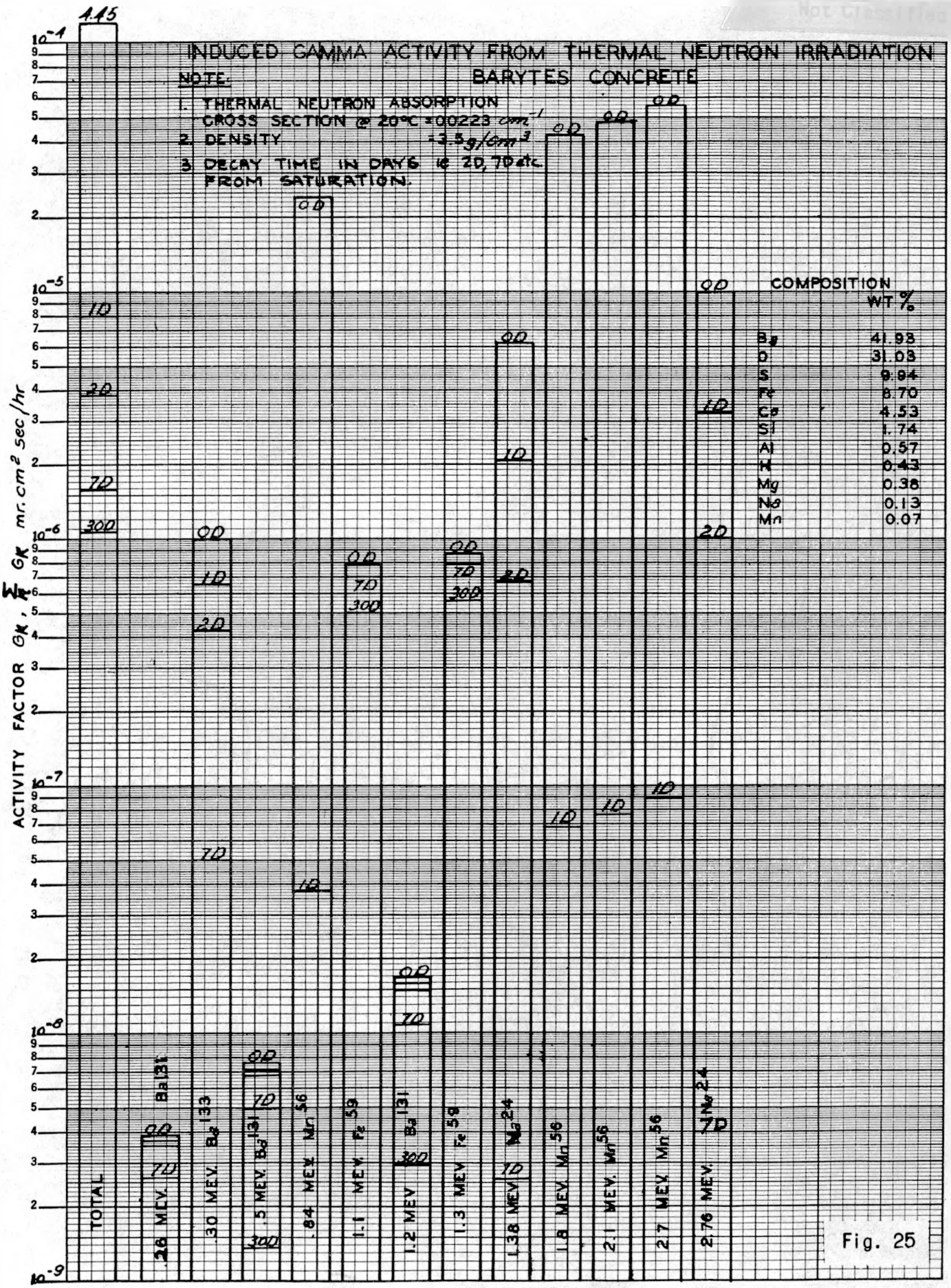

DECLASSIFIED

TABLE 3

TIME AFTER SHUTDOWN	ACTIVITY (mr/hr/cm^2)	
	AFTER EXPOSURE AT PILE TEMPERATURE FOR 28 DAYS	CALCULATED AT 20°C
1 day	2.64×10^4	6.22×10^5
2 days	2.29×10^4	3.60×10^5

The uncertainties again are those given in connection with 347 stainless steel. In any case, if the measured values are correct the calculated values will give conservative estimates of induced activity.

Geometrical Factors. The geometrical factor $g(r)$ referred to above is based on the source configuration and the distance of the point of observation from the source. If the source strength is Q photons/sec and is concentrated at a point, the gamma flux at distance r centimeters is

$$F = Q/4\pi r^2 \qquad \text{photons/cm}^2 \text{ sec}$$

$$= g(r)\, Q$$

the geometrical factor being $g(r) = 1/4\pi r^2$.

When dealing with more complicated distributions, it is desirable to have the geometrical factor in a form for ready reference. This has been done in the case of (1) spherical volume distribution, Fig. 26; (2) spherical surface distribution, Fig. 27; and (3) cylindrical surface distribution, Fig. 28.

Self-shielding. Since most induced activity is due to the absorption of neutrons in heavy materials, it is necessary to consider the shielding of these materials to evaluate the effective source strength. The calculation of self-shielding of a spherical volume source for any point of observation involves difficult integrals. It is fortunate that the effect is of rather small magnitude, as illustrated in Fig. 29 for the cases of (1) observation point on the surface, and (2) observation point at infinity; if the curve for the observation point on the surface is used in all cases, the results will be conservative.

DECLASSIFIED

Not Classified

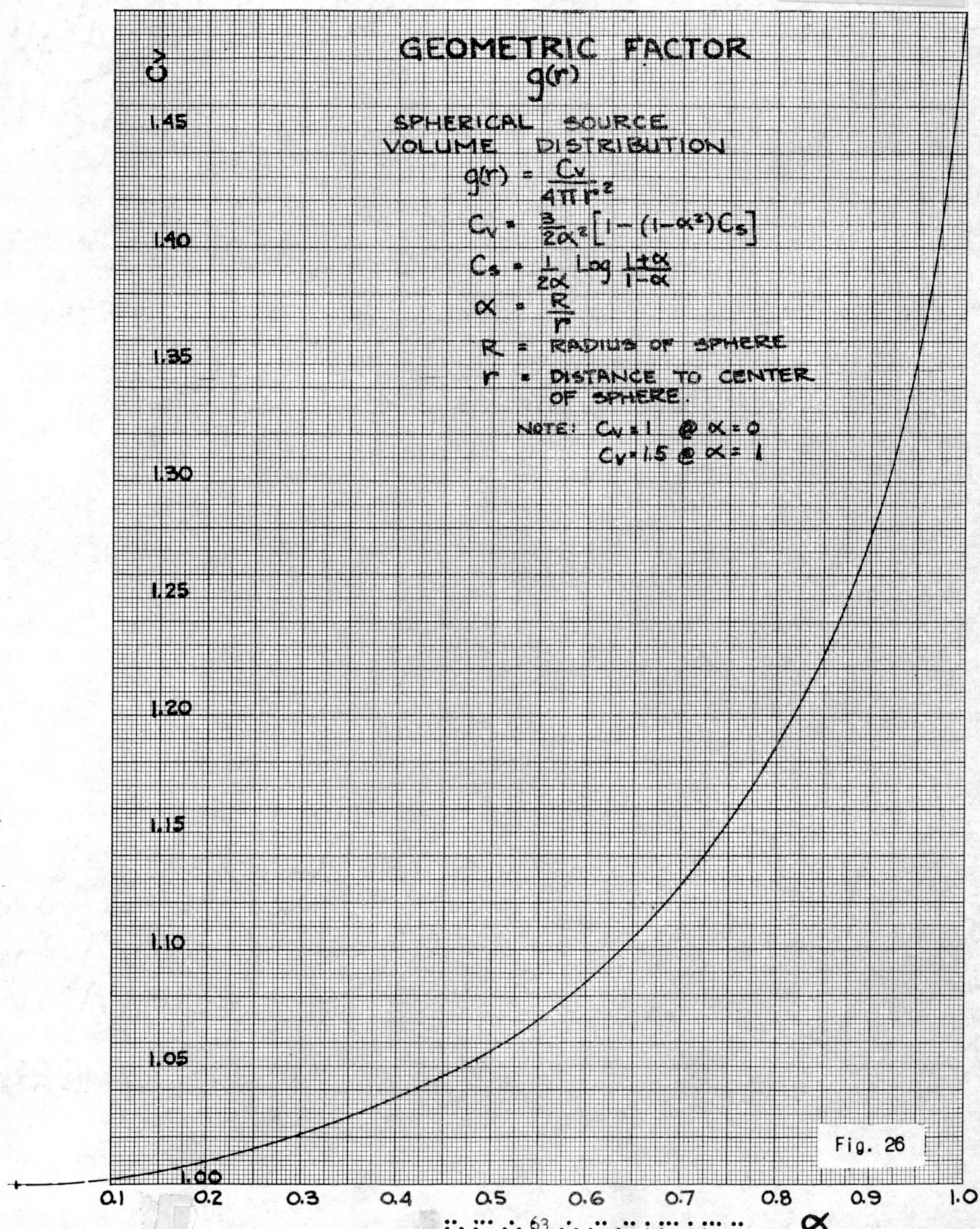

Fig. 26

DECLASSIFIED

Dwg. 10163

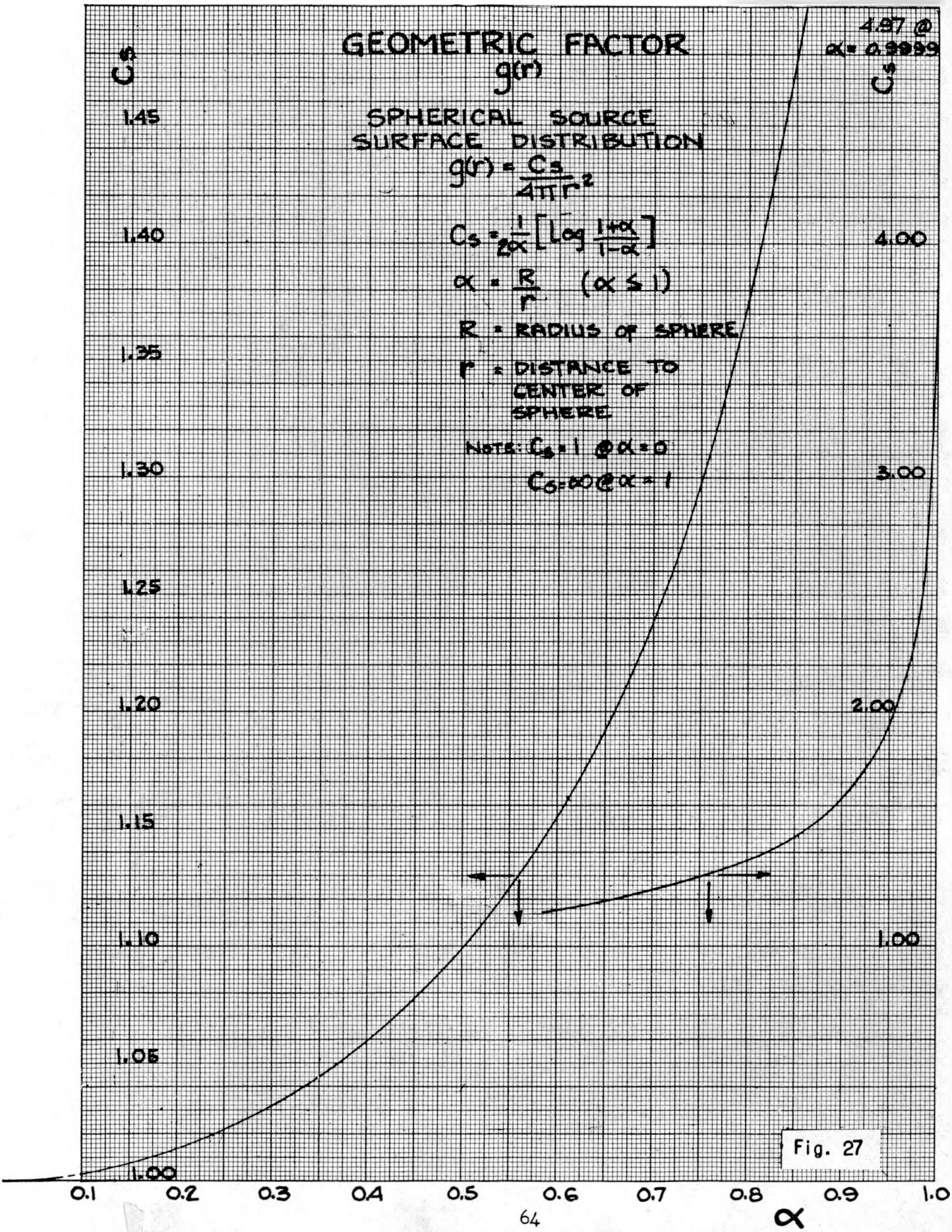

Fig. 27

DECLASSIFIED

Dwg. 10162

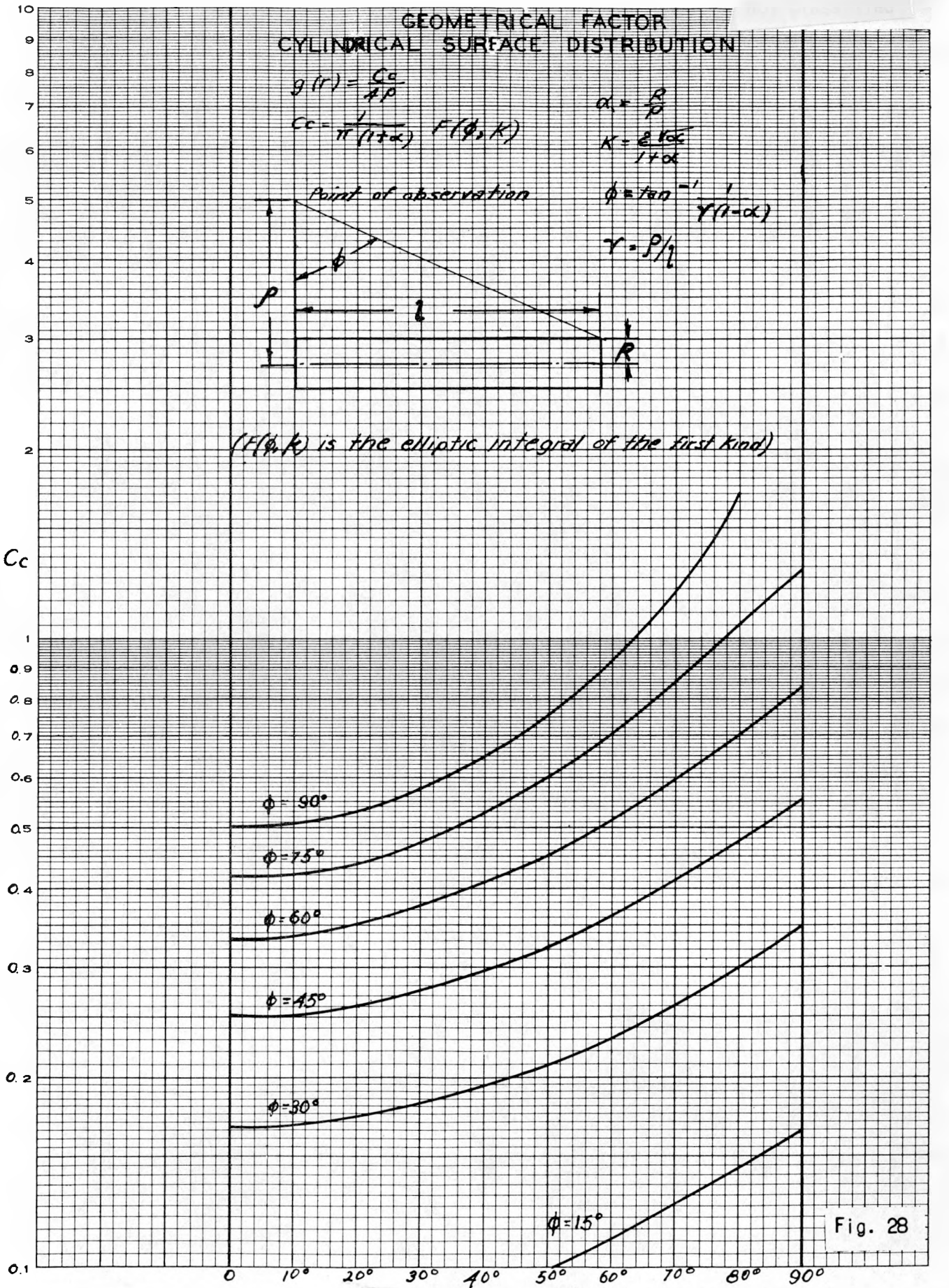

Fig. 28

DECLASSIFIED

Not Classified

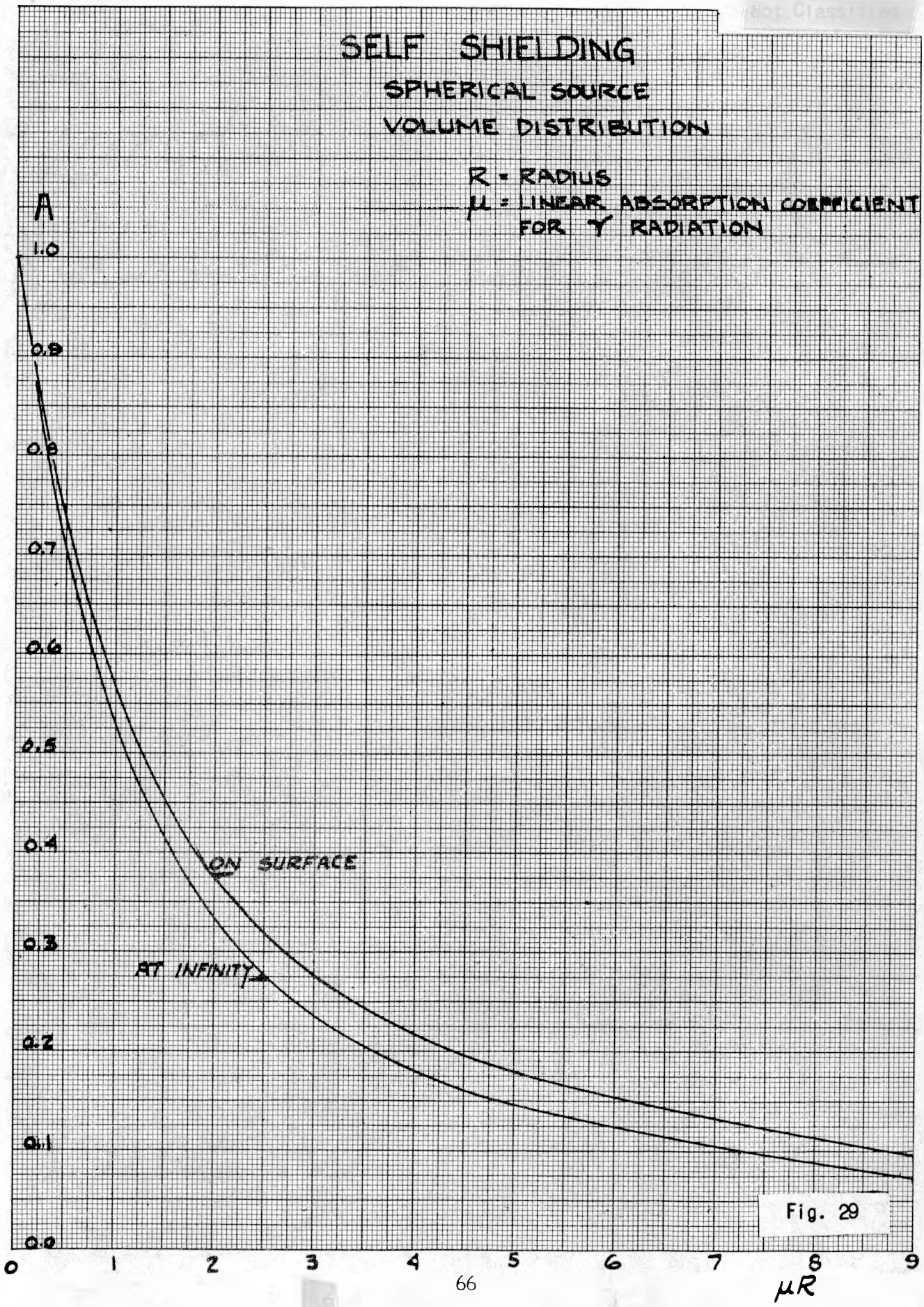

Fig. 29

DECLASSIFIED

The references made above to surface distributions are meant to include volume distributions in thin shells. Since the absorption of thermal neutrons in such shells is not uniform, the self-shielding will depend on both neutron and gamma cross sections. The calculations for such thin shells are made for a slab geometry, and two different cases must be considered, namely, (1) point of observation on the same side of the plate as the neutron source, and (2) point of observation on the opposite side of the plate. The first is illustrated by the activity induced in the piping by a thermal-neutron current coming from the shield, and the second case by the activity induced in the pressure vessel by the pile flux with the obvious point of observation outside the vessel. Figure 30 applies to case (1) and Fig. 31 to case (2).

Induced Activity in Various Components. As pointed out in the section on procedure, the induced activity in any component can be expressed by the relation

$$D(t_e,\ t_s,\ r) = \sum_k G_k(E_k,\ t_e,\ t_s)\ A_k(E_k)\ g(r)\ N \qquad \text{mr/hr} \qquad (8)$$

In a practical problem $G_k(E_k,\ t_e,\ t_s)$ is obtained from Figs. 23 through 25. $A_k(E_k)$ is obtained from Figs. 29 through 31, and $g(r)$ from Figs. 26 through 28.

The factor N is the total neutrons absorbed in the component per second. It is obvious that with a complex arrangement, the induced activity of the components cannot be solved accurately without the expenditure of effort out of proportion to the importance. We can, however, combine some of the simpler geometrical arrangements already discussed to obtain results which are of the correct order of magnitude.

In computing the induced activity we will start with the core tank. The flux in the core tank is 0.92×10^{13} neutrons/cm^2 sec. If this is assumed to be constant throughout the 347-stainless-steel tank, the total number of neutrons absorbed is

$$N = 0.92 \times 10^{13} \times 0.185 \times 3110 = 5.29 \times 10^{15} \qquad \text{neutrons/sec}$$

where 0.185 is the absorption cross section of the steel at 213°C and 3110 cm^3

DECLASSIFIED

Dwg. 10160

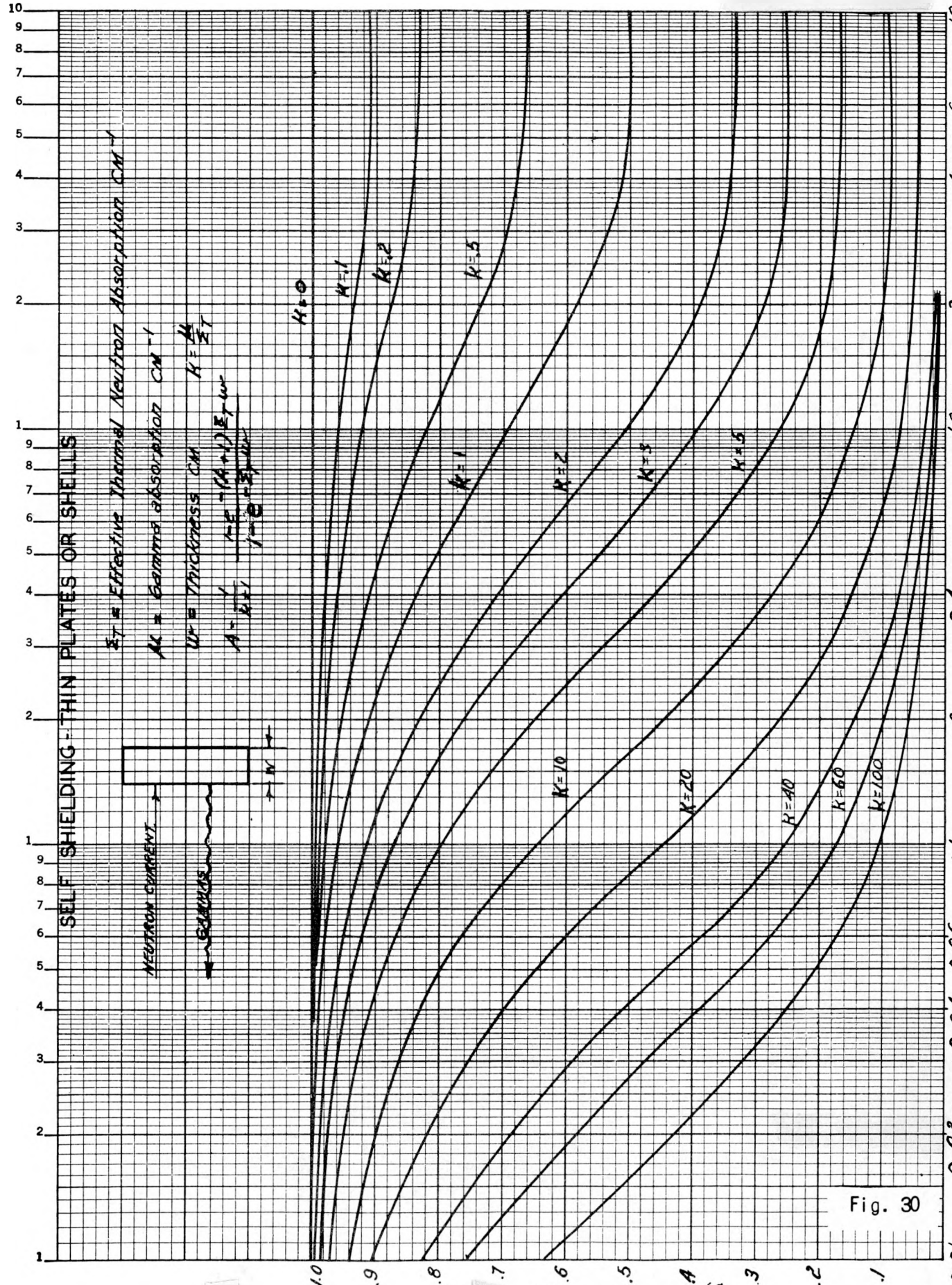

Fig. 30

DECLASSIFIED

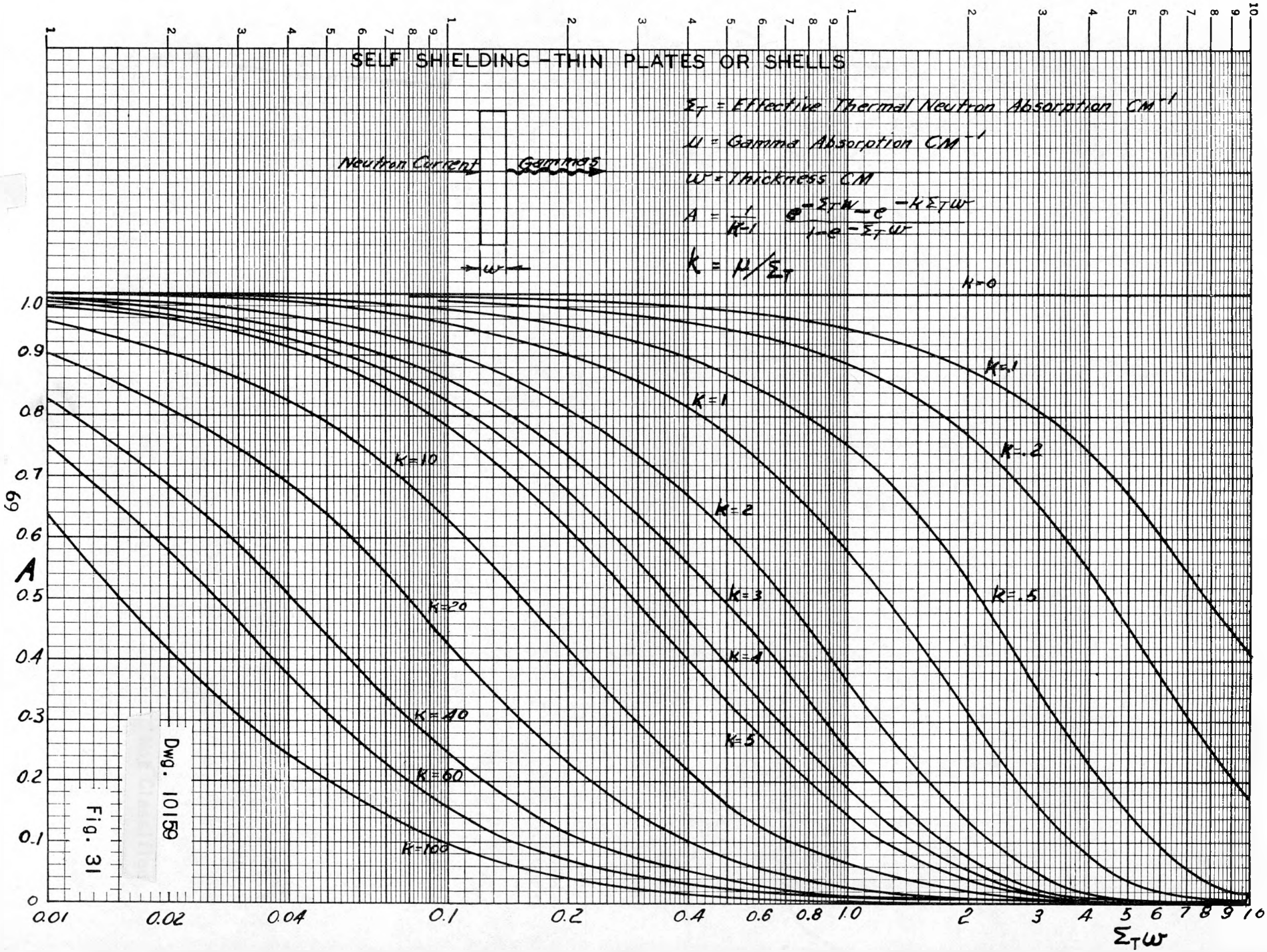
SELF SHIELDING - THIN PLATES OR SHELLS
Σ_T = Effective Thermal Neutron Absorption CM^{-1}
μ = Gamma Absorption CM^{-1}
W = Thickness CM
$A = \frac{1}{K-1}\left[e^{-\Sigma_T W} - e^{-K\Sigma_T W}\right] / \left[1 - e^{-\Sigma_T W}\right]$
$K = \mu/\Sigma_T$
Neutron Current
Gammas
W
K=0
K=.1
K=.2
K=.5
K=1
K=2
K=3
K=4
K=5
K=10
K=20
K=40
K=60
K=100
A
$\Sigma_T W$
0.01
0.02
0.04
0.1
0.2
0.4
0.6
0.8
1.0
2
3
4
5
6
7
8
9
10
0
0.1
0.2
0.3
0.4
0.5
0.6
0.7
0.8
0.9
1.0
Dwg. 10159
Fig. 31

is the volume of the steel. Referring to Fig. 23, it may be seen that the activity factor for all energies of gammas for infinite irradiation time and one day after shutdown is $G_T = \sum_k G_k = 5.4 \times 10^{-5} \frac{\text{mr cm}^2 \text{ sec}}{\text{hr}}$.

The geometrical factor for very large distances is $g(r) = 1/4\pi r^2$, where r is in centimeters. For a distance of 50 ft, which is the greatest distance from the center of the core to some point within the reactor room, the geometrical factor is

$$g(r) = 1/4\pi(30.45 \times 50)^2 = 3.44 \times 10^{-8} \text{ cm}^{-2}$$

Hence the biological dose rate at this point is

$$D = G_T \, g(r) \, N = 9.8 \text{ r/hr}$$

With a tolerance of 7.5 mr/hr for a 40-hr week, a crane operator will receive his permissible daily dose of 60 mr in ½ hr if shielding is provided equivalent to an attenuation by a factor of 82. With the gamma spectrum given in Fig. 23, this would require 7 in. of ordinary concrete, which seems reasonable for a barrier behind which the operator may work. For the operator to work all day and not exceed the dose of 7.5 mr/hr, 13 in. would be required.

Before the core tank is removed from the pressure vessel, the dose rate outside the pressure vessel will depend on the shielding provided by the pressure vessel and the D_2O in the reflector space. This shielding reduces the dose rate to a value of 2.96 r/hr at 1 ft from the surface of the pressure vessel. With 2 ft of concrete around the pressure vessel the effect outside this concrete would be nil. After removal to a dump, it will require 25 months for the core tank to "cool" to tolerance at 1 ft.

The induced activity in the pressure vessel is computed on the basis of an exponential absorption of thermal neutrons. The thermal-neutron current flowing into the vessel from the reflector has been given in a previous section as equal to 3.5×10^{11} neutrons/cm^2 sec. With a surface area of 2.93×10^4 cm^2, the total neutrons entering is 1.03×10^{16} neutrons/sec. From the exponential

DECLASSIFIED

attenuation of the thermal neutrons, we get 79% of these absorbed, or $N = 8.15 \times 10^{15}$ neutrons/sec. The attenuation due to self-shielding is obtained from Fig. 31 and the activity factors from Fig. 24 for SA-105-46I steel. By combining these for each gamma energy and adding, we get

$$\sum_k G_k A_k = 3.03 \times 10^{-7}$$

The geometrical factor for a surface distribution on a sphere is obtained from Fig. 28.

$$g(r) = \frac{C_s}{4\pi r^2} = \frac{1.18}{4\pi r^2} = 1.37 \times 10^{-5} \text{ cm}^2$$

at 1 ft from the surface. The biological dose rate is then

$$D = \sum_k G_k A_k \; g(r) \; N = 33.8 \text{ r/hr}$$

which applies for infinite irradiation time and one day after shutdown. There is also activity induced in the pressure vessel from the absorption of neutrons which come from the shield. From Fig. 21 it may be seen that the returning current should be half of the flux value at the inner face of the shield or 2.5×10^9 neutrons/cm^2 sec. In this case, the shielding is different from that above because the absorbed neutrons have come from the same side of the pressure vessel as the point of observation. This requires the use of Fig. 30 for the self-shielding. The biological dose rate in this case becomes

$$D = 463 \text{ mr/hr}$$

The induced activity in the piping will depend on the extent to which it is embedded in the concrete shielding. There are two sources of the thermal neutrons absorbed in the piping, the neutrons in both cases being thermalized

DECLASSIFIED

in the concrete shield but the initial fast neutrons coming from both the reactor and the soup within the pipe. The neutrons originating in the reactor and thermalized in the shield give, in accordance with Fig. 21 (for a pipe located 2 ft from outside of pressure vessel), an absorption of $N_1 = 1.75 \times 10^8$ neutrons/sec per foot of pipe. The neutrons originating in the pipe and thermalized in the shield (which is assumed in contact with the pipe) give rise, in accordance with Fig. 22, an absorption of $N_2 = 4.6 \times 10^9$ neutrons/sec per foot of pipe. Since these have entered from the same direction they may be added, giving a total of $N = 4.78 \times 10^9$ neutrons/sec per foot of pipe. The pipe is made of 347 stainless steel, whose activity is given in Fig. 23. The self-shielding, given in Fig. 31, results in the value

$$\sum_k G_k A_k = 5.06 \times 10^{-6}$$

The geometrical factor in this case depends upon both the radius and the length of the pipe section in question. From an infinite length at 1 ft,

$$g(r) = 1 \times 10^{-3} \text{ cm}^{-2}$$

The biological dose rate is then

$$D = \sum_k G_k A_k \; g(r) \; N = 24.2 \text{ mr/hr}$$

The activity induced in the heat exchanger may occur in two places: the tube bundle and the tank. In the tube bundle, as shown before, there are 6.72×10^{12} neutrons absorbed per second. The tubes are made of 347 stainless steel and produce the effective values of biological dose rate shown in Table 4. Cases 2 through 5 show how the source is effectively shielded by the surrounding water and tank. Case 6 gives the biological dose rate after the tank has been drained.

DECLASSIFIED

TABLE 4

CONDITIONS	$\sum_k G_k A_k$	$g(r)$	$\sum_k G_k A_k\, g(r)$	D (mr/hr)
1. At 50 ft distance from the removed bundle	5.43×10^{-5}	3.44×10^{-8}	1.87×10^{-10}	12.6
2. At 1 ft from surface of tank; no shielding (r_{eff} = 82.1 cm)	5.43×10^{-5}	1.2×10^{-5}	6.52×10^{-10}	4380
3. At 1 ft from surface of tank; water shielding within bundle volume	1.71×10^{-5}	1.2×10^{-5}	2.05×10^{-10}	1376
4. At 1 ft from surface of tank; shielding as in case 3 plus water layer	4.54×10^{-6}	1.2×10^{-5}	5.45×10^{-11}	366
5. At 1 ft from surface of tank; shielding as in case 4 plus tank wall	8.15×10^{-7}	1.2×10^{-5}	9.78×10^{-12}	65.2
6. At 1 ft from surface of tank; shielding tank wall only	8.64×10^{-6}	1.2×10^{-5}	1.04×10^{-10}	698

The induced activity in the heat-exchanger tank is due to neutrons coming from the tubes inside and to those coming from the shield. Those coming from the inside correspond to a current of 1×10^8 neutrons/cm^2 sec. The tank absorption results in $N_1 = 1.22 \times 10^{12}$ neutrons/sec being actually absorbed. The tank is made of ASTM 212B steel, whose activity is given in Fig. 24. Since the gammas are observed on the outside of the tank, the self-shielding for an inside source is of the form given in Fig. 31. The combination then becomes 8.84×10^{-7}. With a geometric factor of $g(r) = 1.305 \times 10^{-5}$, the biological dose rate is

$$D_1 = \sum_k G_k A_k \; g(r) \; N_1 = 14.1 \text{ mr/hr}$$

The induced activity due to neutrons absorbed from the shield amounts to $D_2 = 0.26$ mr/hr, a negligible amount compared with D_1.

The pump in the soup system is placed in a rather large compartment. The source of fast neutrons within the pump is obtained by multiplying the soup volume of the pump by the source strength from Fig. 20. This gives a total

DECLASSIFIED

fast source of $N_F = 1.435 \times 10^{13}$ neutrons/sec. These are thermalized within the shield, resulting in 3% of them returning to the pump cavity. Not all of these, however, reach the pump since the pump presents an absorption area which is reduced because of the cavity size. If the effective pump radius (considered spherical) is R_1 and the effective cavity radius (considered spherical) is R_2, the fraction absorbed is

$$f = 1 - \sqrt{1 - (R_1/R_2)^2}$$

With an effective R_1/R_2 of 1/3, we have $f = 0.064$ and the number of thermal neutrons reaching the pump as a result of fast neutrons leaving the pump is

$$N = 0.03 \times 0.064 N_F = 1.92 \times 10^{-3} N_F$$

$$= 1.92 \times 10^{-3} \times 1.435 \times 10^{13} = 2.76 \times 10^{10} \text{ neutrons/sec}$$

The pump is constructed of stainless steel, silicon steel, and copper. Using the activity of stainless steel augmented by the 1.35-Mev 12.9-hr activity of Cu^{63}, the biological dose rate at 1 ft, one day after shutdown, is

$$D = 45 \text{ mr/hr}$$

The activity induced in the concrete may be investigated on the basis of absorption of neutrons per unit volume. If the flux is ϕ neutrons/cm^2 sec, with an absorption cross section of 0.022 cm^{-1}, the number of neutrons absorbed per unit volume is

$$n = 0.022\phi \qquad \text{neutrons/cm}^3 \text{ sec}$$

In the case of a cavity in the concrete, the self-shielding and geometrical factors are combined in terms of the gamma absorption coefficient,

UNCLASSIFIED

$$g(r)\ A_k = \frac{1}{\mu_k V}$$

The dose rate at the center of the cavity is given by

$$D = \sum_k G_k A_k\ g(r)\ N = \sum_k \frac{G_k}{\mu_k} \qquad \text{mr/hr}$$

From Fig. 25 and absorption data on barytes concrete we get

$$\sum_k \frac{G_k}{\mu_k} = 4.33 \times 10^{-5}\ \text{mr cm}^3\ \text{sec/hr}$$

resulting in

$$D = 9.5 \times 10^{-7}\phi \qquad \text{mr/hr}$$

For a borated concrete, tolerance is given at a point 22 in. from the reactor pressure vessel. For a non-borated concrete, tolerance is obtained at a point 36 in. from the pressure vessel (Fig. 21).

These induced activity calculations are summarized in Table 5.

Accessibility. By studying Table 5 conclusions may be reached concerning the general accessibility of the system. These conclusions may be expressed in terms of the following list of cautions:

1. The soup system must be thoroughly flushed after shutdown.
2. Piping repairs may be made at 1 ft distance for all piping separated from the pressure vessel by 2 ft of concrete.
3. The pressure vessel must never be uncovered except remotely from behind a 1-ft concrete shield or the equivalent.

DECLASSIFIED

4. The core tank must be removed remotely from 50 ft with the operator behind 1 ft of concrete.

5. When hauling the core tank to the dump, the tank should be 12 ft from the driver and an equivalent of 3 in. of lead-shielding between. This arrangement gives 120 mr/hr, equivalent to ½ hr per day, permissible exposure.

6. Heat-exchanger tubes may be removed from 50 ft without a shield. The header on the heat exchanger may be disengaged manually if not more than ½ hr is required.

7. Shielding blocks which are closer than 2 ft to the pressure vessel should not be handled manually.

TABLE 5

Infinite Irradiation, One Day after Shutdown

COMPONENT	NEUTRON SOURCE	NEUTRONS ABSORBED (n/sec)	BIOLOGICAL DOSE RATE (mr/hr)	REMARKS
Core tank	Core and reflector	5.29×10^{15}	9800	At 50 ft; shielded
			120	At 50 ft; 7 in. concrete
			7.5	At 50 ft; 13 in. concrete
			2960	At 1 ft; outside pressure vessel
Pressure vessel	Reactor	1.03×10^{16}	33,800	At 1 ft
	Shield	5.78×10^{13}	460	At 1 ft
	Total		34,260	At 1 ft
Pressure vessel and core tank	Total		37,220	At 1 ft
			5.4	2-ft barytes concrete shield
Soup pipes	Reactor	1.75×10^{8} per ft		
	Soup in pipe	4.6×10^{9} per ft		
	Total	4.78×10^{9} per ft	24.2	At 1 ft
Heat-exchanger tubes	Soup	6.72×10^{12}	12.6	At 50 ft; no shield
			698	At 1 ft from tank; no water
			65.2	At 1 ft from tank; with water

DECLASSIFIED

TABLE 5 (Cont)

COMPONENT	NEUTRON SOURCE	NEUTRONS ABSORBED (n/sec)	BIOLOGICAL DOSE RATE (mr/hr)	REMARKS
Heat exchanger	Soup	1.22×10^{12}	14.1	At 1 ft
Tank	Shield		0.3	At 1 ft
Heat-exchanger, complete	Total		79.6	At 1 ft
Soup pump	Soup	2.76×10^{10}	45	At 1 ft
Shield	Thermal flux, ϕ	0.022ϕ per cm^3	$9.5 \times 10^{-7}\phi$	In a cavity
(Illustration)	7.9×10^{6}	1.74×10^{5} per cm^3	7.5	In a cavity

The overall accessibility seems to be adequate for changes made one day after shutdown. Some advantage is gained by waiting longer, especially in cases where shielding is involved, since most of the highest energy gammas come from short half-life sources. Probably a schedule should be prepared outlining the procedure to be followed when a particular alteration is undertaken. The preceding material has been prepared in such a way that this scheduling may be made without many detailed calculations.

DECLASSIFIED

Dynamics

Introduction. About a year ago the Instrument Department was called upon to build an electronic simulator for the Homogeneous Reactor. After much preliminary work in selecting components, the first phase of this work has been completed in about the same form as originally proposed. This first phase consists of a conventional simulator augmented by an electronic multiplier to give the effects of a temperature coefficient of reactivity.

It seems timely to attempt a comparison of the data obtained with the simulator and those obtained by numerical and analytical solutions of the equations of motion. It should be borne in mind that the simulation applies to the equations of motion as outlined in ORNL-630 and ORNL-730 and therefore simulates the reactor operation only to the extent of the applicability of these equations.

Analytical Work. The simplified equations of motion which are satisfied by the simulator in its present form may be written

$$\frac{d\phi}{dt} = \lambda_0[(1 - \beta)k - k_c]\phi + \sum_i \lambda_i c_i \tag{1}$$

$$\frac{dc_i}{dt} + \lambda_i c_i = \beta_i \lambda_0 k \phi \tag{2}$$

$$\frac{dT}{dt} = S(P - P_0) \tag{3}$$

$$P = \gamma \lambda_0 k \phi \tag{4}$$

$$k_c = k_{c0} + \alpha(T - T_0) \tag{5}$$

where

ϕ = thermal flux

λ_0 = reciprocal lifetime of prompt neutrons = 10^4 sec^{-1}

DECLASSIFIED

k = material multiplication constant

k_c = multiplication constant required for criticality at temperature T

k_{c0} = multiplication constant required for criticality at temperature T_0

c_i = concentration of delayed neutron emitter

λ_i = time constant of delayed neutron emitter

β_i = fraction of total neutrons from fission having time characteristic λ_i

P = power level of reactor, kw

S = reciprocal heat capacity, °C/kw-sec

α = temperature coefficient of reactivity

T = temperature

T_0 = initial temperature

P_0 = power dissipation

A complete analytical solution of these equations has not been obtained, but the nature of the motion may be studied by various approximations.

The solution of Eq. (2) may be written

$$c_i(t) = c_i(0)\ e^{-\lambda_i t} + \beta_i \lambda_0\ k e^{-\lambda_i t} \int_0^t e^{-\lambda_i \tau}\ \phi(\tau)\ d\tau \qquad (6)$$

The initial value $c_i\ (0)$ is given by

$$c_i(0) = \frac{\beta_i}{\lambda_i} \lambda_0 k_0\ \phi(0) \qquad (7)$$

where k_0 is the initial value of the multiplication constant and $\phi(0)$ the initial flux level.

Using integration by parts, relation (6) may be written

$$c_i(t) = \frac{\beta_i}{\lambda_i} \lambda_0 \left[k_0\ \phi(t) - k \int_{\phi(0)}^{\phi} e^{\lambda_i [t(u) - t(\phi)]}\ du \right] \qquad (8)$$

DECLASSIFIED

Substituting this in Eq. (1) we have

$$\frac{d\phi}{dt} = \lambda_0 [k - \beta(k - k_0) - k_c]\phi - \sum_i \beta_i \lambda_0 k \int_{\phi(0)}^{\phi} e^{\lambda_i [t(u) - t(\phi)]}\, du \qquad (9)$$

In terms of power this may be written

$$\frac{dP}{dt} = \lambda_0 (k - k_c) P - \lambda_0 k \sum_i \beta_i \int_{P_0}^{P} e^{[t(s) - t(P)]}\, ds \qquad (10)$$

where $\beta(k - k_0)$ is neglected as a second-order quantity.

Combining Eq. (10) with Eq. (3) the time derivative is eliminated.

$$\frac{dP}{dT} = \frac{\lambda_0}{S} (k - k_c) \frac{P}{P - P_0} - \frac{\lambda_0 k}{S} \sum_i \beta_i \frac{\int_{P_0}^{P} e^{\lambda_i [t(s) - t(P)]}\, ds}{P - P_0} \qquad (11)$$

The time has not been eliminated from the last term, but it is in the convenient form of an average. If the arithmetic mean is assumed for the time being, we have

$$\frac{dP}{dT} = \frac{\lambda_0}{S} (k - k_c) \frac{P}{P - P_0} - \frac{\lambda_0 k}{S} \sum_i \frac{\beta_i}{2} \left[1 + e^{-\lambda_i t(P)}\right] \qquad (12)$$

The evaluation of

$$\mu(t) = \sum_i \frac{\beta_i}{2} \left[1 + e^{-\lambda_i t(P)}\right]$$

DECLASSIFIED

will be made for various values of time t (see Table 6). The fractions β_i

TABLE 6

t (sec)	$\mu(t)$	REMARKS
0	0.00759	No loss in external system
0	0.00661	100% loss in external system
0.05	0.00650	98.3% loss in external system
0.10	0.00637	96.3% loss in external system

have been modified to take into account the loss of delayed neutrons in the external circulating system. Table 7 shows the values used.

TABLE 7

β_i	λ_i
0.00029	14
0.00084	1.61
0.00217	0.456
0.00172	0.154
0.00138	0.0315
0.00021	0.0125

DECLASSIFIED

On the basis of the arithmetic mean the change in $\mu(t)$ is small for all values of time, including those corresponding to the maximum power surge. Hence we may consider μ as a constant up to the maximum power point. Equation (12) then becomes

$$\frac{dP}{dT} = \frac{\lambda_0}{S}(k - k_c)\frac{P}{P - P_0} - \frac{\lambda_0 k\mu}{S} \tag{13}$$

Adopting new variables given by ($\omega_0^2 = \lambda_0 \alpha S P_0$; $e = k - k_{c0}$),

$$\nu = \frac{\lambda_0}{\omega_0}[e - \alpha(T - T_0)] \tag{14}$$

$$w = \frac{P}{P_0} - 1 \tag{15}$$

$$\epsilon = \frac{\lambda_0}{\omega_0} k\mu \tag{16}$$

Equation (13) becomes

$$\frac{dw}{d\nu} + \frac{\nu}{w} + \nu - \epsilon = 0 \tag{17}$$

On a time basis this corresponds to

$$\frac{d^2\nu}{dt^2} + (\epsilon - \nu)\omega_0 \frac{d\nu}{dt} + \omega_0^2 \nu = 0 \tag{18}$$

DECLASSIFIED

which is a damped oscillation with variable damping. Since this equation is nonlinear and has no known analytical solution it will be discussed in the phase plane.

The similarity with the Van der Pol equation pertaining to relaxation oscillations of a multivibrator circuit may be seen from comparing Eq. (17) with Eq. (19):

$$\frac{dw}{d\nu} + \frac{\nu}{w} - \epsilon(1 - \nu^2) = 0 \qquad \text{(Van der Pol)} \qquad (19)$$

The difference lies in the fact that the damping in our equation is an odd function of ν whereas in the Van der Pol equation it is an even function of ν. A comparison of the damping is shown in Fig. 32.

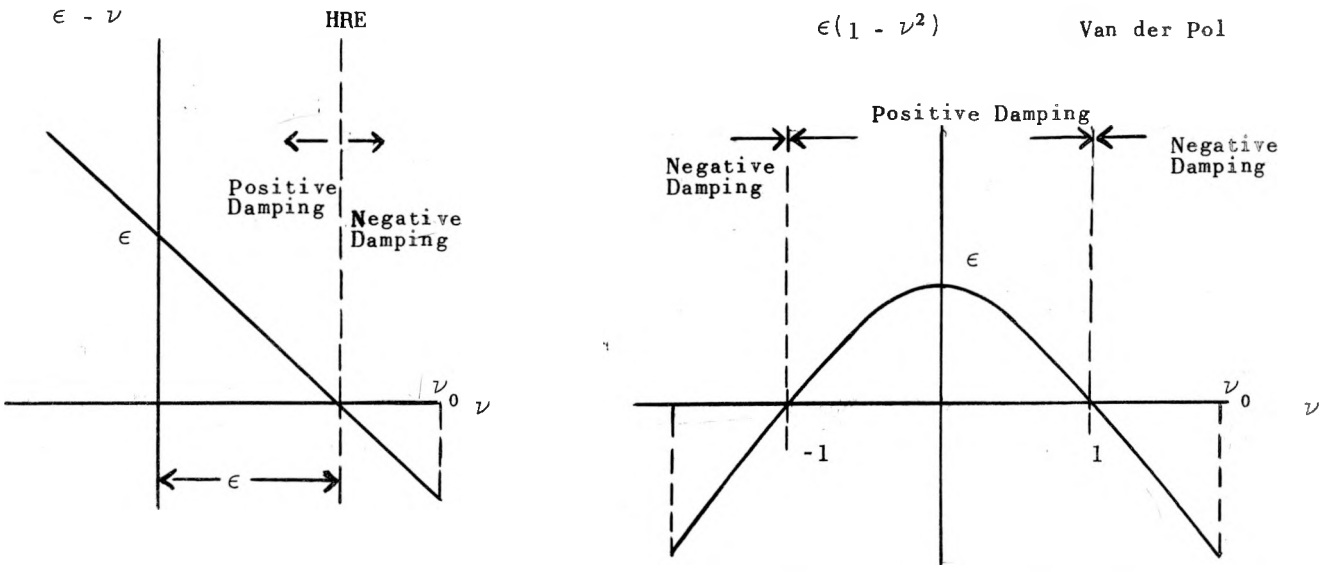

Fig. 32

Plot of Damping, Showing Comparison of HRE with Van der Pol

DECLASSIFIED

The resulting motion is shown in Fig. 33.

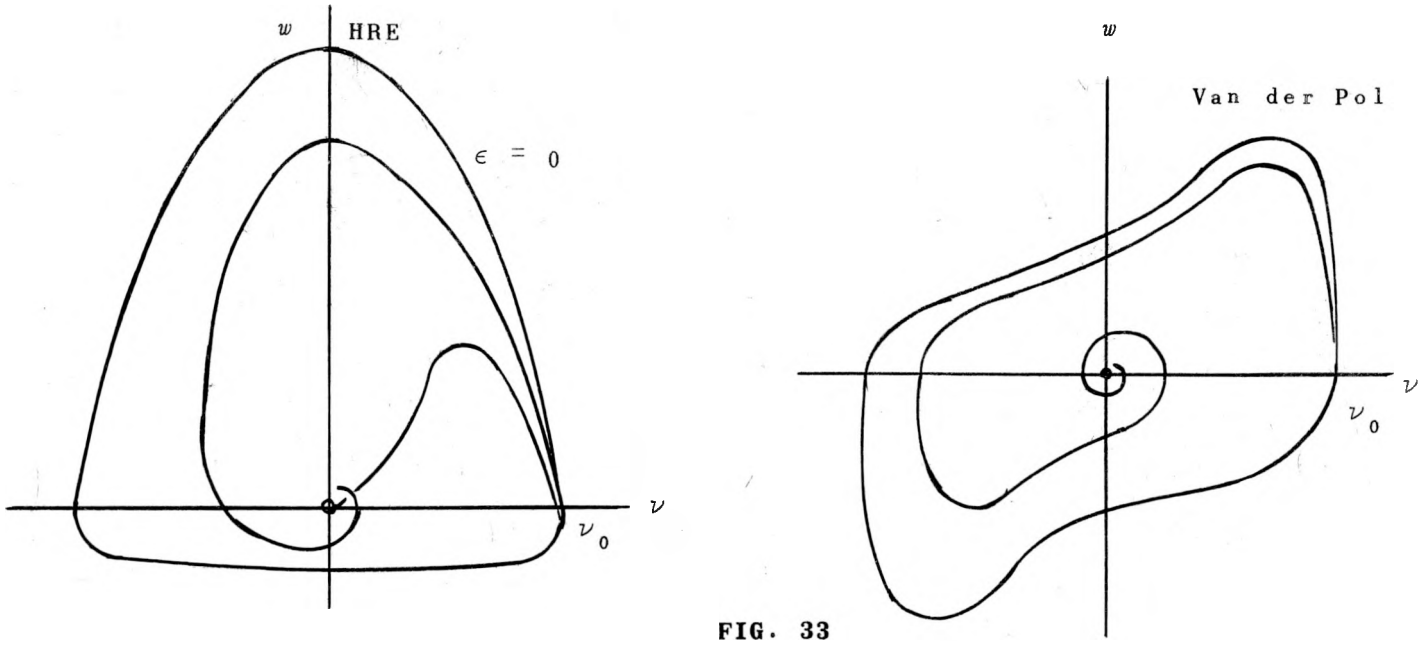

FIG. 33

Plot of Motion Resulting from Damping, Showing Comparison of HRE with Van der Pol

Since Eq. (17) admits no analytical solution we will investigate it by the method of isoclines. The slope of the path being the first derivative, we have

$$\tan \phi = \frac{dw}{d\nu} = \epsilon - \nu - \frac{\nu}{w} \tag{20}$$

Any curve along which tan ϕ is constant is called an "isocline." Some of the simple isoclines of Eq. (20) are as follows:

(1) $\tan \phi = -\infty$ $\quad w = 0$

(2) $\tan \phi = \epsilon$ $\quad \nu = 0$

DECLASSIFIED

(3) $\tan \phi = -\nu/w$ $\quad \nu = \epsilon$ Tangential

(4) $\tan \phi = 0$ $\quad w = \nu/(\epsilon - \nu)$

(5) $\tan \phi = \frac{w}{\nu}$ $\quad w = \nu \left[\frac{\epsilon - \nu}{2} \pm \sqrt{\left[\frac{\epsilon - \nu}{2} \right]^2 - 1} \right]$ Radial

A plot of isoclines ranging from $\tan \phi = -\infty$ to $\tan \phi = \epsilon = 9.1$ is shown in Fig. 34. The arrows on the curves indicate the direction ϕ. A number of loci are plotted on the isoclines, using the arrows as a guide. The motion, at least for initial values ν_0 not much larger than ϵ, is monotonic, rising to a maximum and then dropping to $w = 0$ in infinite time without changing sign.

The petal-shaped curve at the right and above the origin is a plot of the inflection point given by

$$\frac{d^2w}{d\nu^2} = 0; \quad \nu = \frac{w}{w+1} \left[\frac{\epsilon}{2} \pm \sqrt{\left[\frac{\epsilon}{2} \right]^2 - (w+1)^2} \right] \tag{21}$$

When a locus reaches this curve the curvature is zero and the slope begins to decrease, resulting in the locus staying within the region and progressing toward the origin.

Although the criterion has not been established, it seems feasible that, with large enough initial values of ν_0, the locus may cross the $\nu = 0$ axis and actually go negative. By intuition, it seems that the limiting value of ν_0 is 2ϵ and for any value of ν_0 above 2ϵ the locus will not intersect the inflection curve and will cross the $\nu = 0$ axis at a slope equal to ϵ. This, however, should not lead to sustained oscillations, since the damping is high enough that on the second cycle the locus will cross the $w = 0$ axis at a value of ν less than 2ϵ and the subsequent motion will again be monotonic.

UNCLASSIFIED

Dwg. 10170

ISOCLINE TYPE SOLUTION OF EQUATION

$$\frac{dw}{dv} + \frac{v}{w} + v - \epsilon = 0$$

$\epsilon = 9.1$

Fig. 34

DECLASSIFIED

The maximum attained for a given initial value of ν_0 is not easily obtained analytically, but a careful consideration of the equation of motion approximations may be made, at least for large values of ν_0, i.e., above $\nu_0 = \epsilon$.

The motion starts from the $w = 0$ axis with $\nu = \nu_0$ and rises initially vertically with ν not changing much from the initial value ν_0. With this being the case we may make the following approximation:

The accurate equation [Eq. (17)]

$$\frac{dw}{d\nu} = \epsilon - \nu - \frac{\nu}{w} \tag{17'}$$

is approximated by

$$\frac{dw}{d\nu} = \epsilon\frac{\nu}{\nu_0} - \nu - \frac{\nu}{w} \tag{22}$$

when ν is near ν_0. This approximate equation has the solution

$$\frac{\nu_0}{\nu_0 - \epsilon} w - \left[\frac{\nu_0}{\nu_0 - \epsilon}\right]^2 \log\left[\frac{\nu_0 - \epsilon}{\nu_0} w + 1\right] = \frac{\nu_0^2 - \nu^2}{2} \tag{23}$$

Using the values $\nu_0 = 20.65$ and $\epsilon = 9.1$ corresponding to an $e = \delta k$ of 0.014, we have the tabulation given in Table 8.

DECLASSIFIED

TABLE 8

w	ν
0	20.65
5	20.4
10	20.05
15	19.65
20	19.24
25	18.8
30	18.35
35	17.9

Another approximation may be made in the region of the maximum where $w >> 1$. The accurate equation [Eq. (17)]

$$\frac{dw}{d\nu} = \epsilon - \nu - \frac{\nu}{w} \tag{17'}$$

is approximated by

$$\frac{dw}{d\nu} = \epsilon - \nu \tag{24}$$

when $w >> 1$. The solution of this equation may be written

$$w = w_m - \tfrac{1}{2}(\epsilon - \nu)^2 \tag{25}$$

Using the values for w and ν in Table 8 we can tabulate the maximum, as shown in Table 9.

UNCLASSIFIED

TABLE 9

w	w_m	ρ_m
0	67	68
5	69	70
10	70	71
15	71	72
20	71.5	72.5
25	72.2	73.2
30	73	74
35	73.8	74.8

where $\rho_m = w_m + 1 = P_m/P_0$ for comparison with the other data. A comparison of the three sets of data is shown in Table 10.

TABLE 10

$e = \delta k = 0.014$

METHOD	ρ_m
Analytical	68 ($w = 0$ above)
Stepwise numerical	67
Simulator	65

This agreement is more than can be hoped for in general and does contain some adjusting in the case of the damping factor $\epsilon = 9.1$ in the analytic solutions. Also, the closest value in Table 8 was selected corresponding to $w = 0$. Since the agreement is good for this case we will select as a useful approximation:

$$w_m = \tfrac{1}{2}(\epsilon - \nu_0)^2; \qquad \rho_m = 1 + \tfrac{1}{2}(\epsilon - \nu_0)^2 \tag{26}$$

DECLASSIFIED

For comparison with the simulator data the results for various δk values are given in Table 11.

TABLE 11

δk	ρ_m, SIMULATOR	ρ_m, CALCULATED
0.0025	1.5	14.6
0.005	2.9	2.5
0.010	20	17
0.015	80	86
0.020	175	208
0.025	325	435
0.030	550	615

The accuracy at values less than $\delta k = 0.010$ cannot be expected to apply, since the condition $w > 1$ is not satisfied. The agreement for $\delta k = 0.005$ is accidental.

For very low values a third approximation of the maximum may be obtained by examining the plot in phase space. Here we can see that the isocline $dw/d\nu = 0$ is an upper bound for the maximum. The equation then becomes:

$$\text{Upper Bound:} \qquad w_m = \frac{\nu_0}{\epsilon - \nu_0}; \qquad \rho_m = 1 + \frac{\nu_0}{\epsilon - \nu_0} = \frac{\epsilon}{\epsilon - \nu_0} \tag{27}$$

For this equation we have the values in Table 12. This solution loses its usefulness above $\delta k = 0.004$, giving a value $\rho_m = \infty$ somewhere in the range $0.006 < \delta k < 0.007$.

DECLASSIFIED

TABLE 12

δk	ρ_m, SIMULATOR	ρ_m (UPPER BOUND), CALCULATED
0.001	1.15	1.20
0.002	1.38	1.48
0.003	1.69	1.95
0.004	2.17	2.85
0.005	2.9	5.26
0.006	4.0	36.4
0.007	6.0	-7.52

From the above considerations it appears that a reasonable picture of the dynamic behavior can be obtained if reasonable caution is taken in making approximations to the basic equation. This basic equation is itself an approximation of the equations with the separate delayed neutron groups taken into account. The fair success of this treatment gives some justification to lumping the delayed neutrons into a single damping factor. This is true at least for time values up to that corresponding to peak power.

A useful means of visualizing the nature of the motion is afforded by a simple tuned grid vacuum tube oscillator which may have possibilities as a simple simulator. The circuit is shown in Fig. 35.

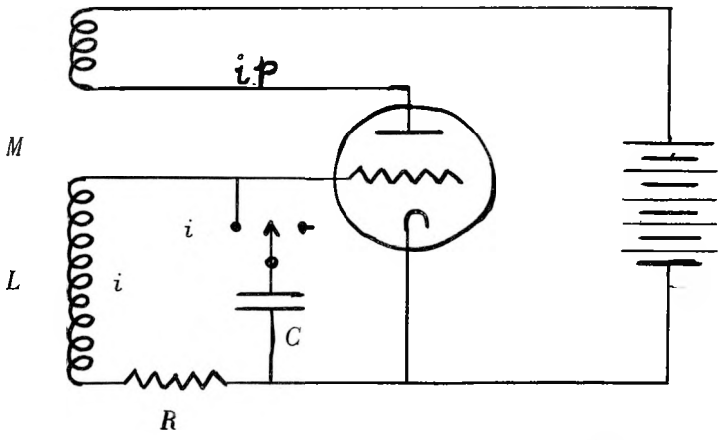

Fig. 35
Simulator Circuit

DECLASSIFIED

If the tube has a quadratic characteristic given by

$$2p = (\alpha v_g + \beta v_g^2) \tag{28}$$

the equation of motion becomes

$$\frac{d^2 v_g}{dt^2} + \omega_0 \left[\left(\frac{R}{\omega_0 L} - \omega_0 M\alpha \right) - 2\beta\omega_0 M v_g \right] \frac{dv_g}{dt} + \omega_0^2 v_g = 0 \tag{29}$$

Comparing this equation with Eq. (18), we see that they are the same if

$$\omega_0 = \frac{1}{\sqrt{LC}}; \qquad \epsilon = \frac{R}{\omega_0 L} - \omega_0 M\alpha; \qquad 2\beta\omega_0 M = 1; \qquad v_g = \nu$$

A step function is introduced by disconnecting the condenser C from the grid, charging it to an initial voltage $v_{g0} = \nu_0$, and then reconnecting it, observing the voltage v_g as a representation of ν or temperature and the current i as a representation of w or power.

Numerical Calculations. The set of Eqs. (1) through (5), along with boundary conditions, values of constants, and corrections for finite circulating time, were submitted to the Mathematics Panel. A typical solution obtained by a stepwise procedure is shown in Figs. 36, 37, and 38, giving the power, temperature, and delayed emitter densities respectively. The motion as shown is monotonic and is as expected from the analysis in the preceding section.

The time consumed in such a calculation may be appreciated when it is considered that the rate for one computer was 0.01 sec per day along the time axis. The accuracy obtained by such a procedure is undoubtedly greater than that of the other methods discussed in this report, but since extreme accuracy is of doubtful value, further expenditure of this kind of effort is not justified.

UNCLASSIFIED

Dwg. 10156

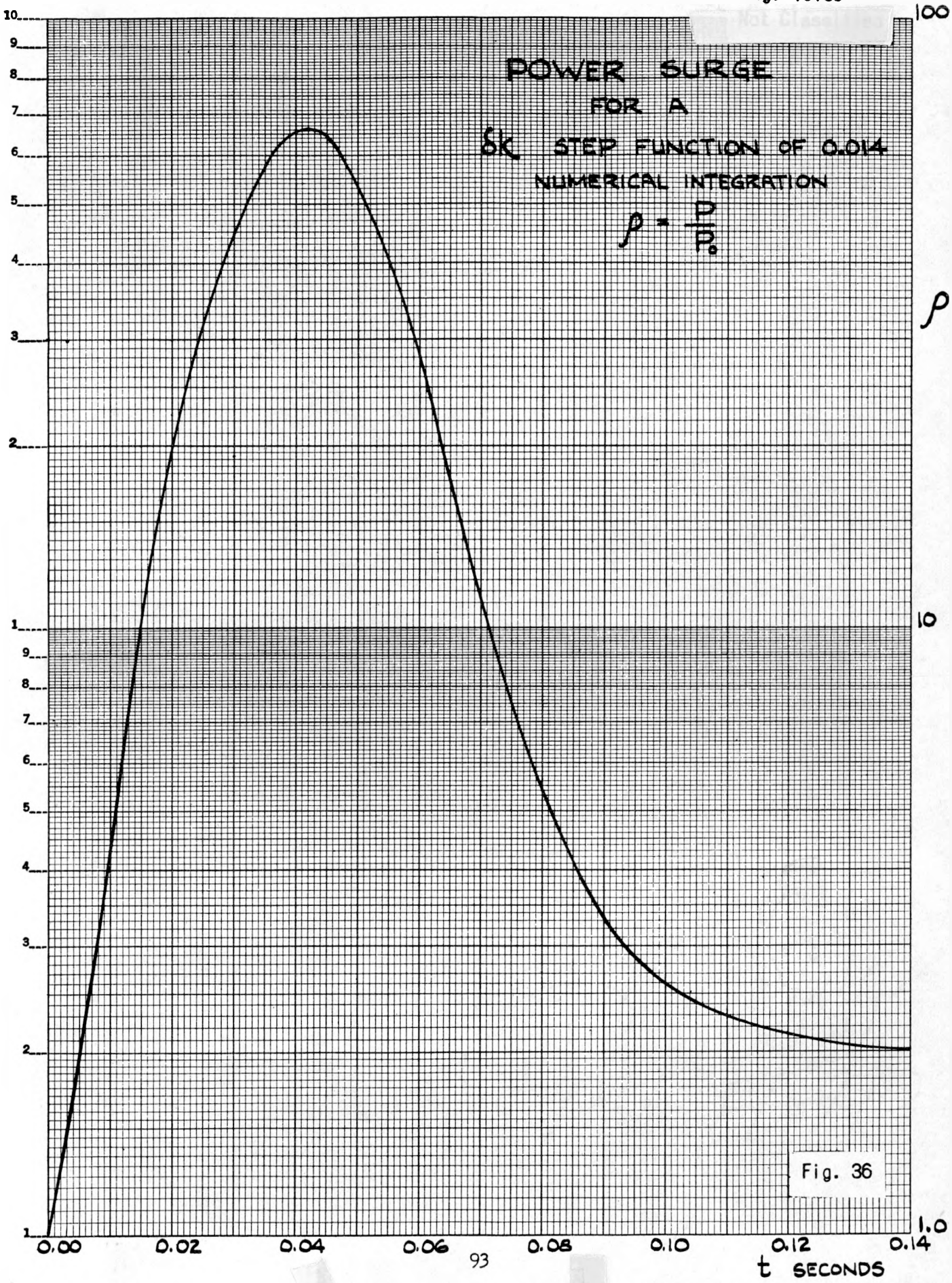

Fig. 36

DECLASSIFIED

Dwg. 10157

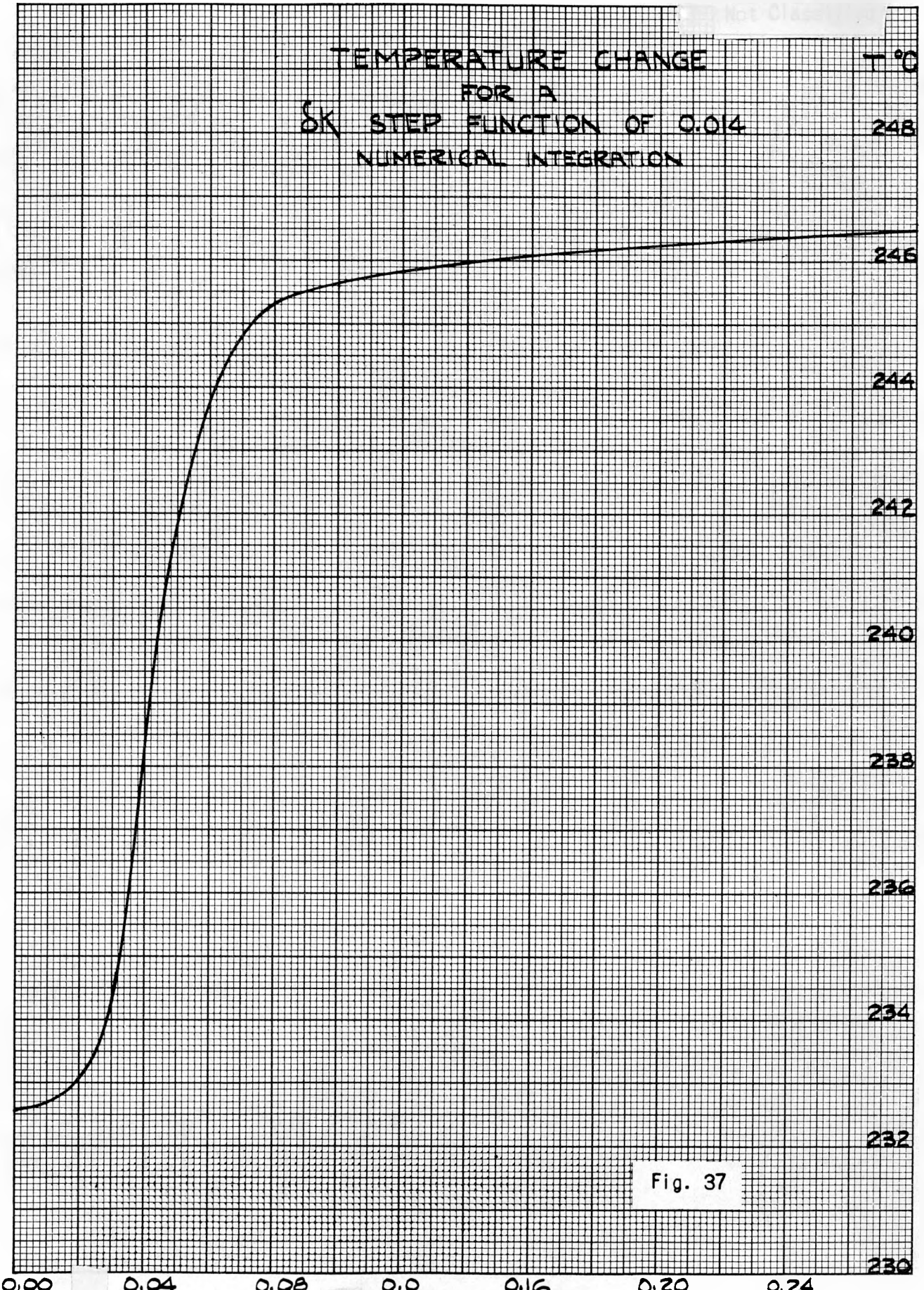

Fig. 37

DECLASSIFIED

Dwg. 10158

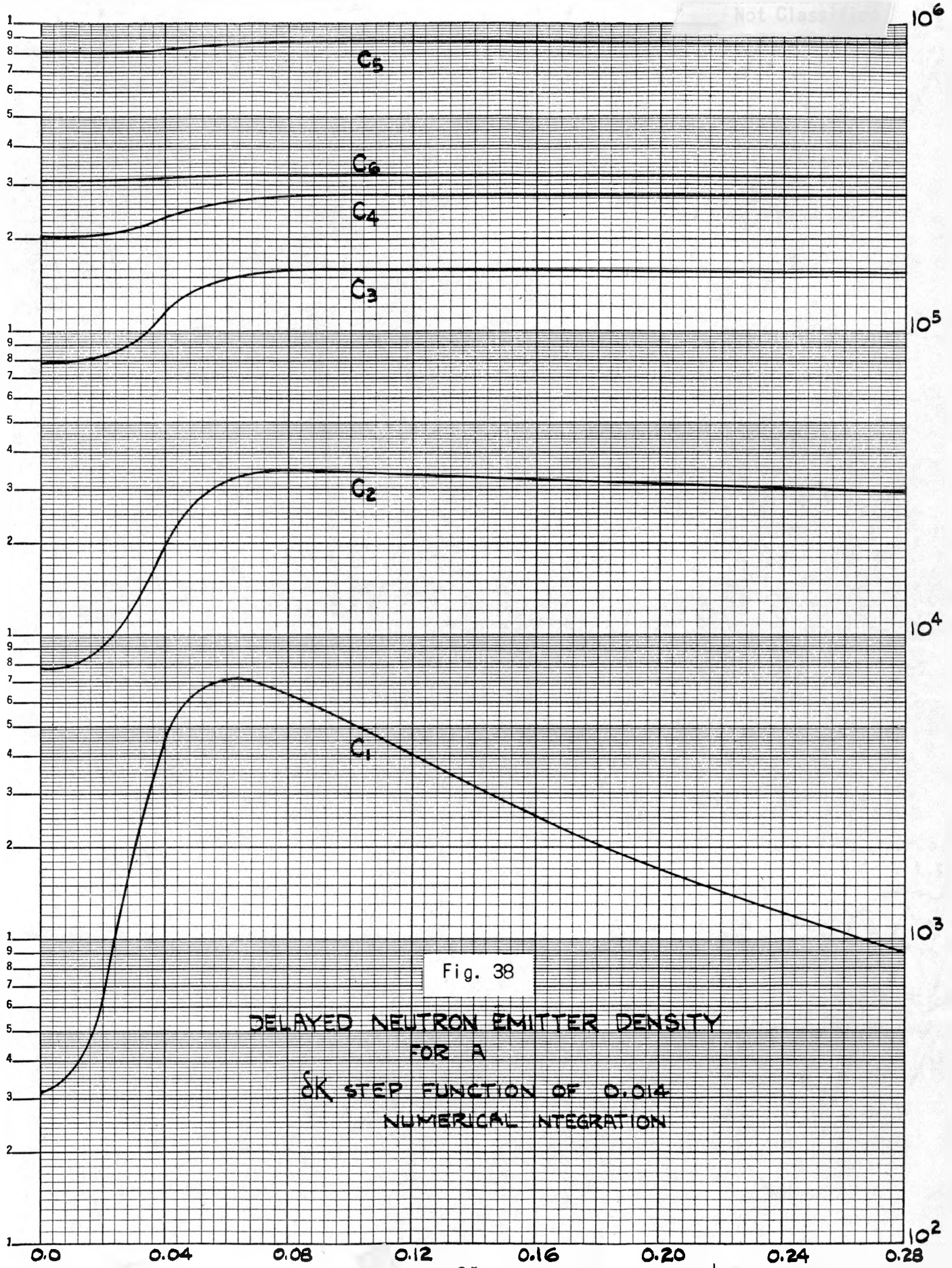

Fig. 38

DELAYED NEUTRON EMITTER DENSITY
FOR A
δK STEP FUNCTION OF 0.014
NUMERICAL INTEGRATION

DECLASSIFIED

Simulation. The simulator as described elsewhere in this report has been used to obtain data on the effect of a step function in reactivity. The motion as measured is monotonic for all values of the step function used, and the agreement with the stepwise calculations is remarkable. There is one discrepancy, however, in the time required to reach maximum power. The numerical calculations indicate 0.04 sec compared with 0.064 sec measured on the simulator.

Additional data were obtained for the case of no delayed neutrons, which agree with the power values obtained by analytical means and reported in ORNL-730. The oscillations which have been predicted have not been obtained because of the presence of resistance in the simulator circuit. The values of peak power, however, are not materially affected by this resistance.

The next step in construction of the simulator will be the inclusion of a time delay in gas generation and a gas coefficient of reactivity. The excess reactivity when gas is taken into account becomes

$$k - k_c = k - k_{c0} - \alpha(T - T_0) - g(v - v_0) \tag{30}$$

where v and v_0 are the volumes of the gas at any time and at equilibrium, respectively, and g is the gas coefficient of reactivity. If the gas takes an appreciable time to cause a change in density, we may write the gas-production equation,

$$\frac{dv(t)}{dt} = r \int_0^\infty \lambda(\tau)\ [P(t - \tau) - P_0]\ d\tau \tag{31}$$

where $\lambda(\tau)$ is a normalized distribution function for the time delay. If the right-hand side is expanded in a Taylor series and only the first two terms are retained, the equation becomes

$$\frac{dv(t)}{dt} = r\left[P(t) - P_0 - \tau_{avg}\frac{dP}{dt}\right] \tag{32}$$

DECLASSIFIED

where

$$\tau_{avg} = \int_0^\infty \lambda(\tau)\tau \, d\tau \tag{33}$$

is the average time delay.

With Eqs. (30) and (32) included in the system, the power equation may be written

$$\frac{d^2 \log P}{dt^2} + \lambda_0 \left[k\mu \frac{P_0}{P} - gr\tau_{avg} P \right] \frac{d \log P}{dt} + \lambda_0 (\alpha S + gr)(P - P_0) = 0 \tag{34}$$

The middle term is the damping, the first part being positive damping due to delayed neutron effect and the second part being negative damping introduced by the gas time delay.

The damping becomes zero when the time delay is of the order of 1 sec. Anything greater than 1 sec will result in a net negative damping with the possibility of a runaway. The simulation to be attempted first will be crude, being effectively an accumulation of energy for a time τ_{avg} and then introducing a negative change in reactivity in proportion to it. This is expressed in the relation

$$c = \frac{dk}{dt} = -\frac{gr}{\tau_{avg}} \int_0^{\tau_{avg}} [P(t) - P_0] \, dt \tag{35}$$

which is the rate at which k is changed, starting at time $t = \tau_{avg}$.

The simulation of the delay described by Eq. (31) requires the aid of a memory device and will be undertaken with other memory requirements for the circulating system at a later date.

The simulator will be modified to provide a variable prompt lifetime to take into account variations in properties from one reactor to another. The

DECLASSIFIED

reciprocal lifetime as it appears in the equations is given by

$$\lambda_0 = \frac{\Sigma_s v_s}{1 + B^2\tau} \tag{36}$$

where Σ_s is the thermal absorption, τ the Fermi age, and B^2 the buckling.

General Equations of Motion. The dynamic behavior of homogeneous reactors in general and the HRE in particular has been analyzed in great detail, but the treatment has been in connection with bulk quantities such as multiplication constant required for criticality, total heat capacity, net flow of coolant, and so on. None of the equations used contained positional coordinates within the system as independent variables. It is obvious that such a treatment can shed no light on such questions as (1) the effects of fluid turbulence; (2) the movement of pressure waves; (3) the growth and movement of bubbles; (4) the local dissipation of heat by conduction, and (5) the effects of local changes in reactivity. These questions are of considerable importance in understanding the behavior and are more fundamental than the previous treatment. The results obtained thus far can be considered as applying to average values of intensity factors and integrated values of capacity factors and should be of value in discriminating between first- and second-order effects.

Nuclear System. The behavior in bulk so far considered is based upon the premise of the permissibility of using a multiplication constant required for criticality, k_c, which has been computed for a static system. For small disturbances a succession of states of equilibrium is reasonable, but for a general treatment of local phenomena the neutron-diffusion equations must be solved for nonstatic conditions. The time-dependent equations to be used are as follows:

DECLASSIFIED

$$\text{Core}\begin{cases} D_{SC}\nabla^2\phi_{SC} - \Sigma_{SC}\phi_{SC} + \Sigma_{FC}\phi_{FC} = \dfrac{1}{v_{SC}}\dfrac{\partial\phi_{SC}}{\partial t} & (1)\\ D_{FC}\nabla^2\phi_{FC} - \Sigma_{FC}\phi_{FC} + (1-\beta)k\Sigma_{SC}\phi_{SC} + \sum_i \lambda_i a_i = \dfrac{1}{v_{FC}}\dfrac{\partial\phi_{FC}}{\partial t} & (2)\\ \dfrac{da_i}{dt} + \lambda_i a_i = \beta_i k\Sigma_{SC}\phi_{SC};\ \beta = \sum_i \beta_i & (3) \end{cases}$$

$$\text{Reflector}\begin{cases} D_{SR}\nabla^2\phi_{SR} - \Sigma_{SR}\phi_{SR} + \Sigma_{FR}\phi_{FR} = \dfrac{1}{v_{SR}}\dfrac{\partial\phi_{SR}}{\partial t} & (4)\\ D_{FR}\nabla^2\phi_{FR} - \Sigma_{FR}\phi_{FR} = \dfrac{1}{v_{FR}}\dfrac{\partial\phi_{FR}}{\partial t} & (5) \end{cases}$$

These equations are to be solved satisfying conditions of continuity between the core and reflector and the condition of no returning current at the outer boundary of the reflector. The boundary condition between core and reflector is to take into account the tank absorption. The total derivative in Eq. (3), as in the rest of this section, will mean a transport derivative,

$$\frac{d}{dt} = \frac{\partial}{\partial t} + \bar{v}\cdot\nabla \qquad (6)$$

It is used in the delayed-neutron-emitter equation to take into account the transport of the fission fragments by the fluid motion.

For the delayed-emitter density outside the reactor, Eq. (3) is to be solved with the right-hand side set equal to zero. Conditions of continuity are to be satisfied at the interfaces,

DECLASSIFIED

Thermal System. The heat removal from a volume element in any region may be written

$$\rho C \frac{dT}{dt} - K\nabla^2 T = P \tag{7}$$

where ρ is the density, C the specific heat, K the thermal conductivity of the fluid, and P the specific power production at the position in question. The first term represents the convection transfer, and with the interpretation of the total time derivative given in Eq. (6) it takes into account both forced and thermal convection. In the cooling system external to the reactor the production can be set equal to zero, and the second term, which represents the conduction, must be considered as satisfying boundary conditions of continuity with thermal solutions in various dissipative elements such as parasitic loss from pipes, intentional cooling in a heat exchanger, etc.

Connection of Nuclear and Thermal Systems. The connections between the nuclear and thermal systems are reciprocal in that the power derived from the fission process is the source function for the thermal equation and because the temperature solutions of Eq. (7) result in changes of cross sections, diffusion constants, and velocities. The conditions are expressed in the relations

$$P = \gamma k \Sigma_{SC} \phi_{SC} \tag{8}$$

$$\Sigma_S = \Sigma_{S0} \frac{\rho}{\rho_0} \left[\frac{T_0}{T}\right]^n \tag{9}$$

$$v_S = v_{S0} \sqrt{T/T_0} \tag{10}$$

In Eq. (9) the exponent for thermal absorption can usually be taken as equal to ½. For scattering cross sections n varies considerably from one substance to another. The thermal diffusion constants may be written

$$D_S = D_{S0} \frac{\rho_0}{\rho} \left[\frac{T}{T_0}\right]^m \tag{11}$$

DECLASSIFIED

The epithermal cross sections and diffusion constants are dependent on temperature also, but only through the density.

$$\Sigma_F = \Sigma_{F0} \frac{\rho}{\rho_0} \tag{12}$$

$$D_F = D_{F0} \frac{\rho_0}{\rho} \tag{13}$$

Thermodynamic System. The dependence on density given in the previous section results in a dependence on temperature and pressure through the equation of state,

$$F_k \ (\rho, \ p, \ T) = 0 \tag{14}$$

The subscript k refers to different phases because the fluid in general is heterogeneous, containing bubbles of gas and steam. Hence, we have a different equation of state in the two phases. The exchange of matter between the different phases will be dependent upon many factors which have meaning only in a state of equilibrium. To make use of these relations it will be necessary to consider any changes as a succession of equilibrium states. The chemical potential of any one component will be considered the same for coexisting phases, and the thermodynamic potential of the complete fluid will be taken as stationary for a fixed temperature and pressure. In general, the relation between variables necessary to determine the state of the fluid will depend on the degrees of freedom dictated by the phase rule. To specify the average density at a particular point in the reactor, it will be necessary to average the concentrations obtained from thermodynamic considerations. Since the phases are separated by curved surfaces (bubbles), the surface tension must be taken into consideration as producing a pressure difference between the phases, given by

$$\Delta p = \sigma \left[\frac{1}{R_1} + \frac{1}{R_2} \right] \tag{15}$$

DECLASSIFIED

where R_1 and R_2 are principal radii of curvature and σ is the surface tension.

Another factor which must be taken into consideration is the change of bubble volume and the consequent motion through the fluid. Both the growth and the motion of the bubbles may be studied by hydrodynamic considerations.

Chemical System. The intimate association of fissionable material and the fluid of a homogeneous reactor results in considerable decomposition of the fluid molecules. It is assumed that the rate of decomposition is proportional to the power density. In the case of water the end decomposition products are hydrogen and oxygen. Since the gas formed may remain in solution or form bubbles it must be considered present in two phases. In the liquid phase the material balance is given by

$$\frac{dC_S}{dt} + k_S\, f(C_S) + Q = P \tag{16}$$

The middle term on the left side is the rate of recombination in solution, P is the power density, and Q is the rate of formation of gas. The rate of formation of gas may be written

$$Q(t) = \int_0^\infty \lambda(\tau)\, C_S(t - \tau)\, d\tau \tag{17}$$

where $\lambda(\tau)$ is a distribution function of the time delay involved.

The kinetic equation in the gas phase may be written

$$\frac{dC_g}{dt} + k_g\, f(C_g) = Q \tag{18}$$

where the second term on the right is again a recombination rate in the gas phase.

There is no apparent removal of gas shown in Eqs. (17) and (18), but it is present and contained in the total derivatives as given in Eq. (6). In the case of dissolved gas the velocity in Eq. (6) is the velocity of the liquid

DECLASSIFIED

which carries the gas with it. In the case of the gas itself the velocity is a vectorial sum of the liquid velocity and the gas diffusion through the liquid. In a reactor with rotation imparted to the liquid, centrifugal forces play a prominent part in this diffusion.

Hydrodynamic System. The equation of state [Eq. (14)] shows that the density is a function of pressure. The pressure under conditions of motion is velocity-dependent. To obtain the pressure and velocity dependence it is necessary to consider the hydrodynamic equations. The first of these is the equation of continuity,

$$\frac{d\rho}{dt} + \rho\nabla\cdot\bar{v} = 0 \tag{19}$$

The second hydrodynamic equation is the force equation,

$$\rho\frac{d\bar{v}}{dt} = F - \nabla p + \mu\nabla^2\bar{v} \tag{20}$$

where the terms on the right are (1) body forces (gravitation), (2) pressure gradient, and (3) viscous forces. The total time derivative contains the shock forces. The solution of these equations gives relations between $\bar{v}$, ρ, and p such that the propagation of pressure waves may be determined.

Connections Between All Systems. It has been mentioned that there is a connection between the nuclear and thermal systems which involves the temperature T and the power density P. This combination is not completely determined because of the variations of density ρ with pressure p and temperature T. The density and pressure are related by the equation of state and the hydrodynamic equations. The density is dependent upon the presence of gas as given under the chemical system.

In general, the systems of equations outlined are sufficient to discuss all first-order effects. The simultaneous solution of these equations appears to be practically unattainable, but with a careful selection of approximations it is hoped that a more refined dynamic theory of operation may be developed.

DECLASSIFIED

Conclusion. The analytical or numerical solution of these equations is very important if consideration is given to the problems involved in large expensive reactors, small scale models of which would not give useful information unless the effect of scaling down can be evaluated. The application of electrical analogs is not very promising unless relaxation methods are used containing a vast network of components.

With the increasing interest in large-scale fluid fuel reactors, both boiling and nonboiling, the answers to many questions which may determine feasibility are likely to be found in such an analysis.

CONSTRUCTION

Figure 39 is a picture of the construction taken on December 1, 1950. The construction contractor experienced serious delays in procurement of steel and copper products. However, as of December 1, most of these materials were either on hand or their receipt was momentarily expected. It is expected that the contractor will be approximately one month behind the scheduled completion date of December 21.

DECLASSIFIED

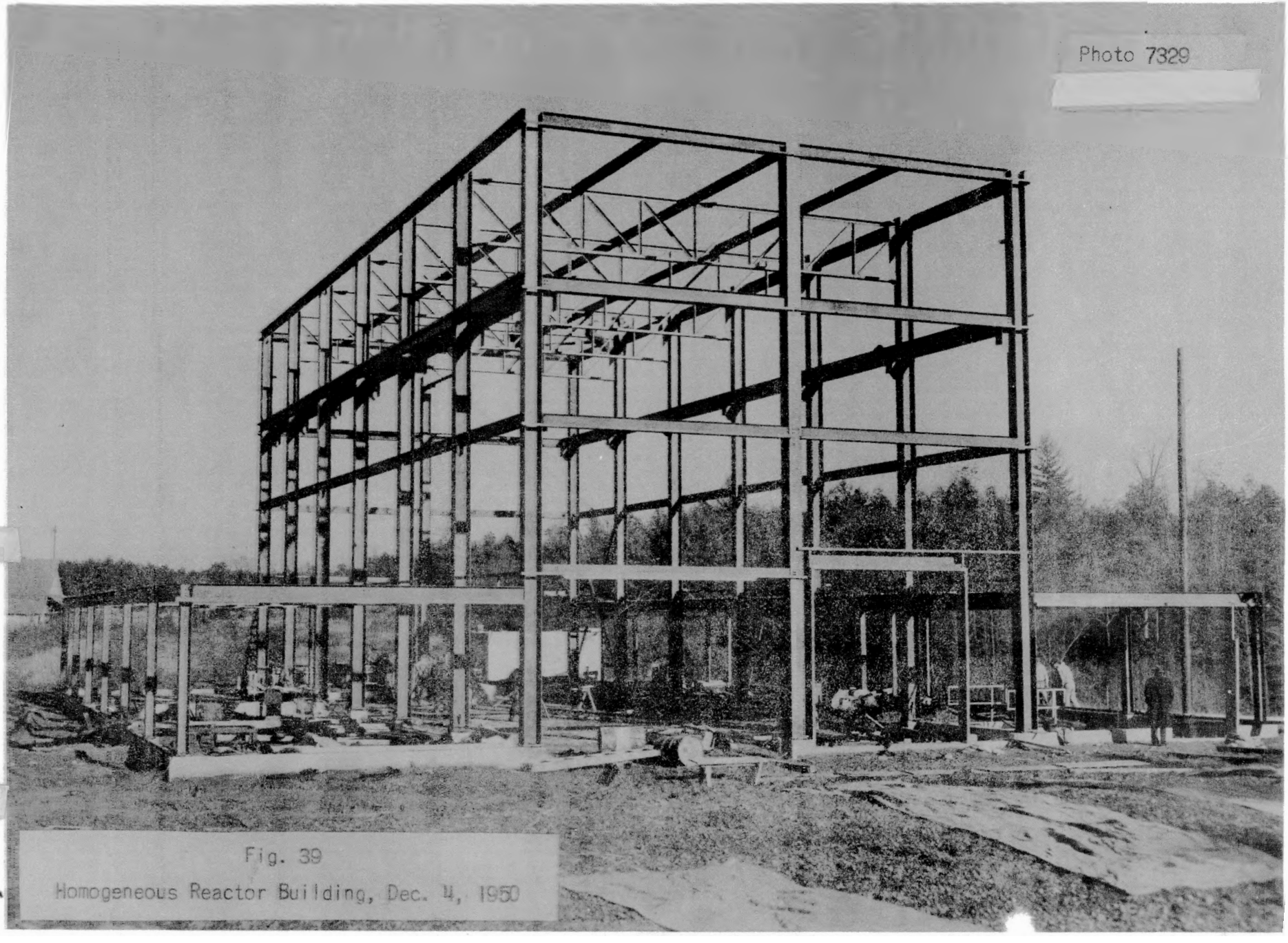

Fig. 39
Homogeneous Reactor Building, Dec. 4, 1950

DECLASSIFIED
105

ORNL-925 (delete)

IV. CORROSION AND RADIATION STABILITY

DECLASSIFIED

X-29-1

OUT-OF-PILE CORROSION

J. L. English L. L. Fairchild
A. R. Olsen J. W. Brown
S. H. Wheeler H. Barker
E. Bonifaceous*

Summary

Continued success has marked the use of either nitric or chromic acid pretreatment on stainless-steel surfaces prior to their exposure in 0.17 *M* uranyl sulfate at 250°C in the absence of irradiation. Corrosion attack on these steels has been reduced to negligible magnitudes as compared to intensified attack on untreated surfaces, and evidences of mass reduction of the sulfate medium are nearly nonexistent. Numerous tests, operated for 18 to 22 weeks to date, have substantiated the preceding observations. Film studies on pretreated and sulfate-exposed films have been made; the identification of the nitric acid pretreatment surface has not been completed. Three layers, 3 to 7 μ in total thickness, have been found on exposed stainless-steel surfaces. A general mechanism for the formation of these films in uranyl sulfate at elevated temperatures has been suggested. Surface pretreatments, with either nitric or chromic acid, must be performed at 250°C to be effective in reducing corrosion attack and greatly minimizing reduction of the uranyl sulfate. A minimum pretreatment time for nitric acid has been established tentatively as 4 hr. The protective influence of nitric and chromic acid pretreatments was destroyed by heating in air at 115 to 120°C for periods of 1 hr. Similar results were obtained on permitting nitric acid–pretreated surfaces to stand exposed to air at room temperature for a period of seven days; intensified corrosion attack and solution reduction were evident on subsequent exposure to uranyl sulfate at 250°C. Complete immersion of treated surfaces in uranyl sulfate at room temperature for a period of seven days prevented any loss in the effectiveness of the pretreatment film at elevated temperatures.

Low concentrations of chloride, bromide, and iodide ions destroyed the protective nature of nitric acid–pretreated surfaces in uranyl sulfate at 250°C. Severely scratching a nitric acid–pretreated stainless-steel surface did not impair the quality of the unscratched film when exposed to elevated temperatures in uranyl sulfate. No signs of increased corrosion attack on the scratched area were observed, and there was no indication of solution reduction at this area. This behavior indicates that the protective film may be self-healing or that solution volume–surface area ratio is a critical factor in controlling solution stability.

* Full time, on loan from Analytical Chemistry Division.

DECLASSIFIED

Corrosion rates of type 347 stainless steel, pretreated with 1% nitric acid, have averaged 0.01 to 0.05 mil/year after 18 to 20 weeks in 0.17 *M* uranyl sulfate at 250°C. Corrosion rates for types 309, 316ELC, and 410 stainless steel and Carpenter 20, exposed to similar conditions, have averaged 0.02 to 0.11 mil/year after 20 to 24 weeks in uranyl sulfate containing 1% nitric acid. Heliarc welded stainless steels, pretreated in nitric or chromic acid, have shown comparable corrosion resistance after four to six weeks in sulfate at 250°C.

Zirconium corrosion studies have continued on an expanded scale with excellent results. Recent Bureau of Mines zirconium having no initial pretreatment has shown corrosion rates of 0.05 to 0.07 mil/year after 23 weeks in 0.17 *M* uranyl sulfate at 250°C. These rates are comparable to the rates obtained on pretreated stainless steel surfaces. The corrosion resistance of Bureau of Mines zirconium containing 0.86% niobium has been very good in uranyl sulfate at 250°C.

The corrosion resistance of reflector materials has been studied at 200°C in distilled water with and without small amounts of hydrogen peroxide to simulate irradiation effects. In the absence of hydrogen peroxide, increasing the water *p*H to 11.0 to 11.5 greatly reduced corrosion attack on 1030 carbon steel. At a *p*H of 5.1 to 5.5, with no peroxide present, corrosion rates averaged 1.4 mils/year, at a *p*H of 10.2, with no peroxide present, corrosion rates averaged 0.8 to 1.4 mils/year. When the *p*H was increased to 11.7 the corrosion rate of the 1030 carbon steel dropped to 0.08 mil/year. In the presence of 0.005 *M* hydrogen peroxide, initial corrosion attack on carbon steel was high, 7.2 mils/year, but it decreased to 1.4 mils/year after 13 weeks at 200°C. No bulky rust deposits were observed on these samples. The galvanic corrosion behavior of 1030 carbon steel—2S aluminum and zirconium—2S aluminum samples in distilled water at 200°C have been studied also.

Corrosion studies have continued with materials that could be substituted for stainless steels in component reactor parts. Titanium and tantalum are two metals which show excellent promise. The corrosion resistance of both materials in 0.17 *M* uranyl sulfate at 250°C has been excellent after 19 weeks.

A preliminary study of the corrosion resistance of various metals and alloys in uranyl fluoride and uranyl nitrate systems at 100°C has been begun.

UNCLASSIFIED X-29-3

Introduction

Corrosion studies for the Homogeneous Reactor Experiment have continued with increased emphasis during the past quarterly work period. The major portion of these studies are concerned with the uranyl sulfate system containing 40 g of uranium per liter at 250°C. Preliminary work has started on an investigation of the corrosion resistance of various metals and alloys in uranyl fluoride and uranyl nitrate systems at 100°C. Corrosion studies with the uranyl sulfate system at 150 to 200°C will be conducted also.

Additional stainless steel autoclaves, 225 ml capacity, are being procured and will increase the number of these test facilities to 76. In addition, plans have been made for the installation of 10 dynamic test loops for corrosion studies under slow flow conditions. These loops will employ electrical heating to obtain thermal cycling of the sulfate medium, and solution velocities will probably not exceed several feet per second or so. A 35-gal-capacity autoclave, previously used for high-temperature beryllium corrosion testing, is being converted for use as a dynamic system at 250°C. Flow velocities of 2 to 4 ft/sec will be obtained with this apparatus.

The bulk of the corrosion program for the Homogeneous Reactor Experiment has been conducted under stagnant-test conditions. There are two reasons for using this type of test:

1. Procurement of corrosion data on approximately one hundred types of metals and alloys in a relatively short time was essential.
2. Obtaining of these data was not feasible when the necessarily large dynamic systems were used to obtain high flow velocities.

The use of stagnant-test conditions has permitted the acquisition of voluminous corrosion data on many materials many times faster than they could be obtained with cumbersome and expensive, and oftentimes completely impractical, flow systems. The need for dynamic corrosion data has always been realized, and efforts are being made to fulfill this need. Since laboratory corrosion tests can only hope to simulate actual operating conditions, the true evaluation of corrosion resistance of materials can be obtained only in a full-scale working model of the Homogeneous Reactor Experiment. To construct a suitable apparatus for determining the dynamic corrosion behavior of materials would mean essentially an expensive duplication of portions of the reactor itself.

DECLASSIFIED

It is believed, with good reason, that stagnant-test results presented in this investigation are indicative of results to be expected in a large-scale dynamic system. This opinion is substantiated by good experimental evidence, namely

1. The films involved in pretreatments and in subsequent exposures to uranyl sulfate at 250°C have been found to be very thin (3 to 7 μ total film thickness), extremely adherent, uniform, and hard and, for all purposes, impervious. Velocity ranges contemplated in actual reactor operation are 15 to 18 ft/sec. The film characteristics indicate that negligible disturbance of the film itself will occur with these rates in regions of unrestricted flow. Excluded from this statement are mechanical damage effects that can be produced by erosion cavitation at high velocities which create pockets or low-pressure areas by irregularities in the flow. Such effects are apt to occur on the suction side of pump impellers and on the discharge end of regulating valves.

2. The fact that no bulky or voluminous corrosion products are produced on the metal surfaces during exposure gives additional support to the belief that velocity effects in the operational range will not materially affect the corrosion behavior of the stainless steels. In cases where the corrosion reaction produces loosely adherent and voluminous corrosion products, the velocity effects are very pronounced and generally tend to increase corrosion rates by removing the loose films, thus permitting the continual exposure of the unprotected metal surfaces to fresh corrosion medium. By this mechanism there is no chance for protective films to be permanently oriented on the metal surfaces.

3. The operation of a large-scale dynamic test loop containing 8 liters of uranyl sulfate solution at 250°C has been demonstrated successfully for a period of approximately 700 hr. This system was pretreated initially with 1% nitric acid at 250°C. Inspection of internal surfaces, wherever possible, showed no indications of increased corrosion attack as a result of fluid flow. Solution velocities averaged 10 to 15 ft/sec. The only indication of corrosion damage as a result of mechanical effects due to cavitation was observed on the suction side of the pump impeller in the Westinghouse totally enclosed induction pump. This attack was manifested by a small concentric area of depleted metal surface, pitted in appearance. This type of metal removal is generally attributed to the impingement and collapse of large low-pressure bubbles on the metal surfaces. The collapse of the bubbles actually tears away metal particles, resulting in a pitted-appearing surface.

DECLASSIFIED

X-29-5

The evaluation of corrosion data in the investigation is based not only on physical measurements from test specimens, but also on chemical and spectrographic analyses of the corrosion test solutions. The present scope of the corrosion study necessitates the analysis of hundreds of solutions. During the next quarter the results of these chemical analyses will be analyzed and evaluated to obtain a more complete presentation of the corrosion data. The chemical and spectrographic analyses are concerned with *p*H measurements, uranium(VI) and uranium(IV) concentrations, and the determination of all metallic constituents of the material undergoing test.

A general observation on the correlation of solution analyses with corresponding weight-change measurements on test specimens has been made. When there is no indication of solution reduction, the concentrations of chromium, nickel, iron, and manganese in the test solution, as constituents of stainless steels, are extremely low, 100 ppm or less, individually. When solution decomposition occurs, very high concentrations of these ions are found in the test solutions. Uranium analyses, conducted on all solutions before and after test, check within the ±2% accuracy permitted by the colorimetric method when solution reduction does not occur. In the cases in which the solution is reduced, the uranium content of the liquid phase is almost negligible, indicating that reduction is practically complete when it occurs.

This report is divided into six sections:

1. Protective Treatments for Stainless Steels
2. Corrosion Resistance of Stainless Steels
3. Corrosion Resistance of Zirconium
4. Corrosion Resistance of Reflector Materials
5. Miscellaneous Corrosion Studies
6. Uranyl Fluoride and Uranyl Nitrate Corrosion Studies

Protective Treatments for Stainless Steels

A summary of 25 different pretreatments used on stainless-steel surfaces to overcome the reduction of the uranyl ion in uranyl sulfate systems operating at 250°C was presented in the *Homogeneous Reactor Experiment Quarterly Progress Report for Period Ending August 31, 1950* (ORNL-826). Of the treatments attempted, only two were found to be effective in eliminating the reduction phenomenon; these were the use of either 1% nitric acid or 2% chromic acid

UNCLASSIFIED X-29-6

anhydride. It was found by experiment, that the temperature of application of both these solutions was the same as the proposed operating temperature of the reactor experiment, namely 250°C. Much effort has been expended on studying the nature and characteristics of the films formed on stainless steel using either nitric acid or chromic acid anhydride for pretreatment at 250°C prior to the introduction of uranyl sulfate into the stainless steel system.

Numerous experiments conducted to date have shown conclusively that, under controlled conditions, uranyl sulfate solution may be operated in a pretreated stainless steel system at 250°C successfully and with almost negligible corrosion. These results, of necessity, are based on stagnant corrosion tests made in the absence of irradiation. The feasibility of using nitric acid for pretreatment of a large scale dynamic test loop has been successfully demonstrated also, although again in the absence of irradiation. The controlled conditions previously mentioned are very important to the success or failure of the pretreatment. One of these effects, surface condition, was described in the Homogeneous Reactor Feasibility Report, July 6, 1950 (ORNL-730) and is discussed again here. The presence of heavy layers of oxide film or scale, such as that formed during welding operations, renders the protective film useless for preventing reduction of the uranyl ion at operating temperatures. This effect has been verified by repeated experimentation. In every case where heavy welding-scale formation was permitted, the uranyl sulfate solution was reduced, with the weld area acting as a focal point for the reduction. In the absence of the welding scale, accomplished by machining or etching, there was no difficulty encountered with solution reduction. Therefore these data stress clearly the need for cleanliness in a stainless-steel system designed to handle uranyl sulfate at 250°C. Several measures must be undertaken to eliminate unclean surfaces as a cause of solution reduction. Welding scale may be removed by chemically etching with suitable reagents. If it is not feasible to etch the entire reactor-experiment assembly, thought must be given to etching component parts prior to installation in the system. If welding is required for the installation of these parts, it should be done using a backing of inert gas to eliminate or at least minimize welding-scale formation. It may be possible in some cases to remove welding scale by mechanical means such as grinding or buffing. Corrosion studies have shown that a machined stainless steel surface, even after exposure to air for four to six months, will successfully contain uranyl sulfate solution after the steel has been

DECLASSIFIED

X-29-7

pretreated. These data indicate the magnitude of the consideration that must be given to the fabrication and assembly of the reactor experiment. The importance of metal surface cleanliness cannot be overemphasized since the successful operation of the experiment hinges greatly on this one factor.

Another controlling factor in the effectiveness of a pretreatment, and which has been demonstrated by experiment, is that any extended heating in normal atmospheres at temperatures above 100°C will destroy the protective nature of the pretreatment film. This would mean that after a stainless-steel system has been pretreated, it would not be possible to perform any welding operation on or near any part of the system which contacts uranyl sulfate solution at 250°C without incurring the danger of destroying the inactive nature of the pretreatment film.

A discussion of test results with the nitric acid and chromic acid anhydride pretreatments appears in the following paragraphs.

Effect of Nitric Acid Pretreatment Time on Film Stability. It has been reported previously that the effect of pretreating with 1% nitric acid at 250°C has been to cause either a slight weight increase or decrease on type 347 stainless-steel samples, dependent upon the time of the pretreatment. The amount of time generally employed for pretreatment in the laboratory corrosion tests was 24 hr. For this period of time a corrosion rate of 0.7 mil/year and less was obtained. Tests were then undertaken to determine the minimum pretreatment time required to obtain surfaces on stainless steels which would not promote solution deterioration. It was found that a pretreatment time of 1 hr in 1% nitric acid at 250°C did not prevent precipitation of uranium oxides from the uranyl sulfate. Pretreatment times of 4, 8, and 12 hr were successful, however, and these tests have been in operation for a period of 16 weeks without any indication of solution reduction. The tests are inspected weekly, and the old uranyl sulfate is replaced with fresh sulfate solution. Corrosion rates of type 347 stainless steel specimens, treated in the same manner as the test bombs, are extremely low; they are summarized below for 15 weeks in 0.17 *M* uranyl sulfate at 250°C.

PRETREATMENT TIME (hr)	CORROSION RATE (mils/year)
4	0.010
8	0.030
12	0.005

DECLASSIFIED

X-29-8

Thus, under the test conditions, the minimum time required for pretreating stainless steel surfaces in 1% nitric acid at 250°C is 4 hr. A pretreating time of 8 hr resulted in a slightly greater corrosion rate on subsequent exposure to uranyl sulfate, while a pretreating time of 12 hr resulted in an overall corrosion rate slightly less than that obtained with the 4-hr pretreatment. However, the magnitude of all results is so low that there appears to be no particular advantage in pretreating a system for 12 hr rather than 4 hr.

Figure 40 shows cumulative weight changes as a function of exposure time for type 347 stainless steel specimens, pretreated for various intervals in 1% nitric acid at 250°C and then exposed to 0.17 *M* uranyl sulfate solution at 250°C. The pattern of the weight change–time curves is very similar for all three cases; the sample pretreated for 8 hr showed the greatest weight losses. During the first week of the test in uranyl sulfate, all samples exhibited a weight gain. Points of maximum weight loss during the ensuing 15 weeks occurred at periods of 3, 7, and 13 weeks; points of lowest weight loss occurred at periods of 1, 4, 9, and 14 weeks. No measurable solution reduction has taken place during the course of these tests, and there is no reasonable explanation to be made at this time for the apparent cyclic behavior of weight loss.

Effect of Cyclic Nitric Acid Pretreatments on Film Stability. A series of tests was operated for 16 weeks in which stainless steel bombs were pretreated with 1% nitric acid for 12 to 24 hr at 250°C. One set of bombs was given a single initial treatment, one set was pretreated initially and thereafter once every two weeks, one set was pretreated initially and once every three weeks thereafter, and the last set was given an initial pretreatment and then pretreated once every four weeks during the course of the test. All tests were inspected weekly, and the uranyl sulfate was replaced with fresh solution weekly. The tests were operated with 0.17 *M* uranyl sulfate at 250°C for 16 weeks, after which time they were stopped. During the entire test period no signs of solution reduction were seen. Inasmuch as one initial pretreatment on a bomb did last as long as the cyclic treatments without solution decomposition being incurred, no particular advantage is obtained by pretreating stainless steel periodically every two, three, or four weeks, unless under actual operating conditions such a pretreatment should be required after a reactor was shut down for an extended time interval.

DECLASSIFIED X-29-9

DWG. 10118

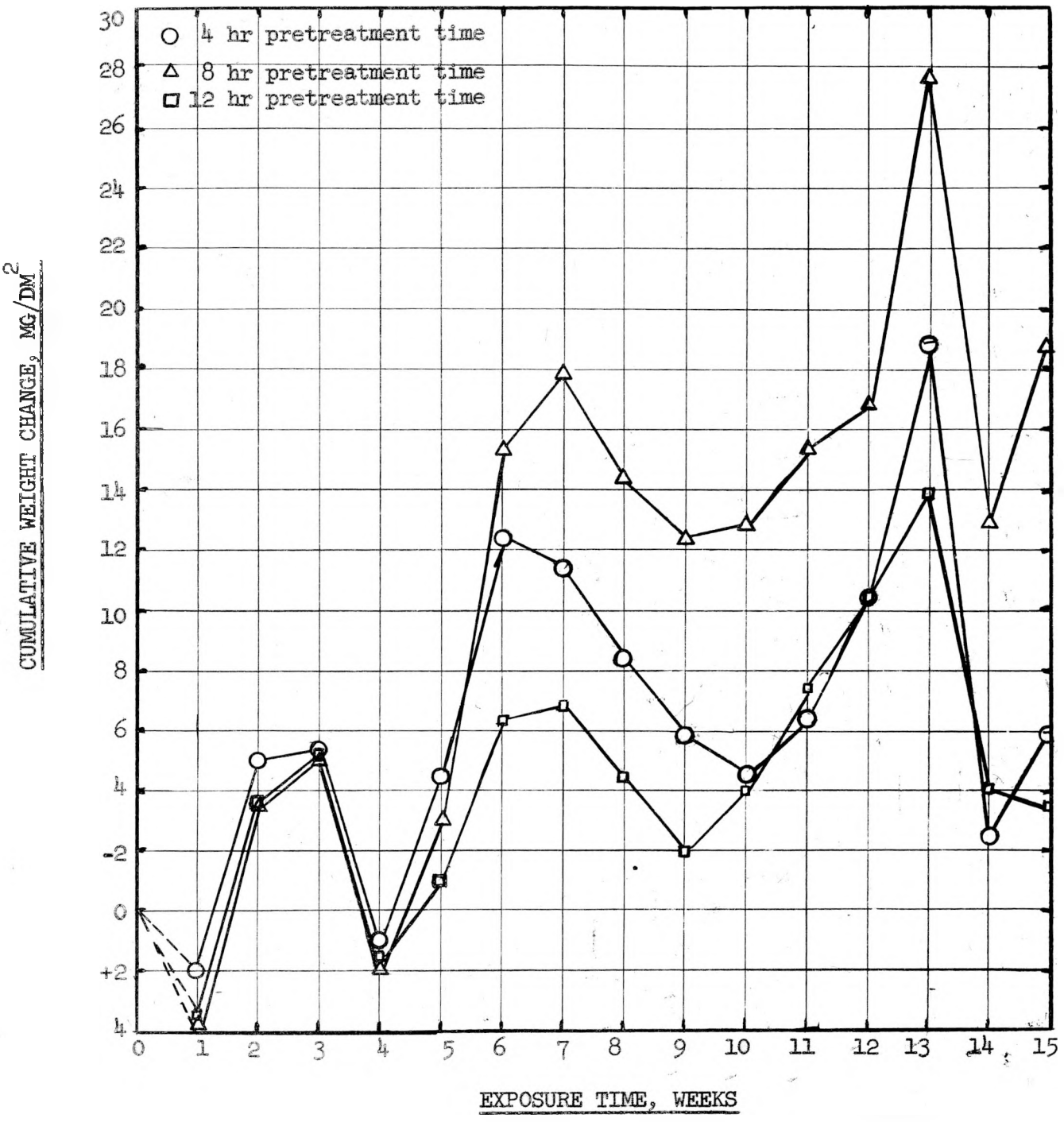

Figure 40. Cumulative Weight Changes on Type 347 Stainless Steel Specimens (Pretreated for Various Times in 1% Nitric Acid at 250°C) in 0.17M Uranyl Sulfate at 250°C

DECLASSIFIED X-29-10

A stainless steel autoclave was initially pretreated in 1% nitric acid for 24 hr at 250°C. Thus far it has operated in 0.17 *M* uranyl sulfate, replaced weekly, at 250°C for a period of 22 weeks without failure of the original protective film. Chemical analyses for uranium, made on the sulfate solution used each week, have shown negligible variation from the original uranium content.

Effect of Nitric Oxide Removal on Film Stability. Since the formation of a protective film on stainless steel surfaces is a direct result of contact with the thermal decomposition products of nitric acid at 250°C, a test was carried out to determine the effect of early removal of these decomposition products from a solution of uranyl sulfate at 250°C. Uranyl sulfate, 0.17 *M*, containing 1% nitric acid was placed in a stainless-steel bomb and heated to 250°C. The gases were bled from the system after a period of 20 hr at this temperature. The test was then carried out for 17 weeks with weekly inspections. No failure of the protective film occurred during this time, and corrosion samples of 347 stainless steel exhibited a shiny, dark appearance. Figure 41 shows a graph of weight losses vs. time for duplicate samples of 347 stainless steel. The average corrosion rate of the stainless steel was 0.01 mil/year at the end of 17 weeks. The maximum corrosion attack occurred at the end of 10 weeks; the corrosion rate at this point was 0.05 mil/year. The graph in Fig. 41 shows two peaks of increased corrosion attack, both followed by a gradual decline in the intensity of attack. These results indicate that the protective film is required initially to prevent reduction of the sulfate medium at 250°C, but, after an extended period of time, when the sample actually shows a weight loss the original protective film must be removed or displaced. Therefore, if continued protection of the stainless steel is to exist, a new type of film must be formed. The initial film, which is obtained by treatment in nitric acid, must be of such nature that it acts as an effective barrier to prevent exchange or molecular rearrangement of electrons for sufficient time until the new film or films are formed. Work is in progress to determine the mechanism of this film formation.

Effect of Extended Nitric Acid Pretreatments on Film Stability. A group of tests is being conducted in which stainless steel autoclaves were pretreated in 1% nitric acid for a period of 96 hr at 250°C. These autoclaves have been operated for 18 weeks with 0.17 *M* uranyl sulfate at 250°C. No evidences of solution reduction have been observed during this time, and the

DECLASSIFIED X-29-11

DWG. 10119

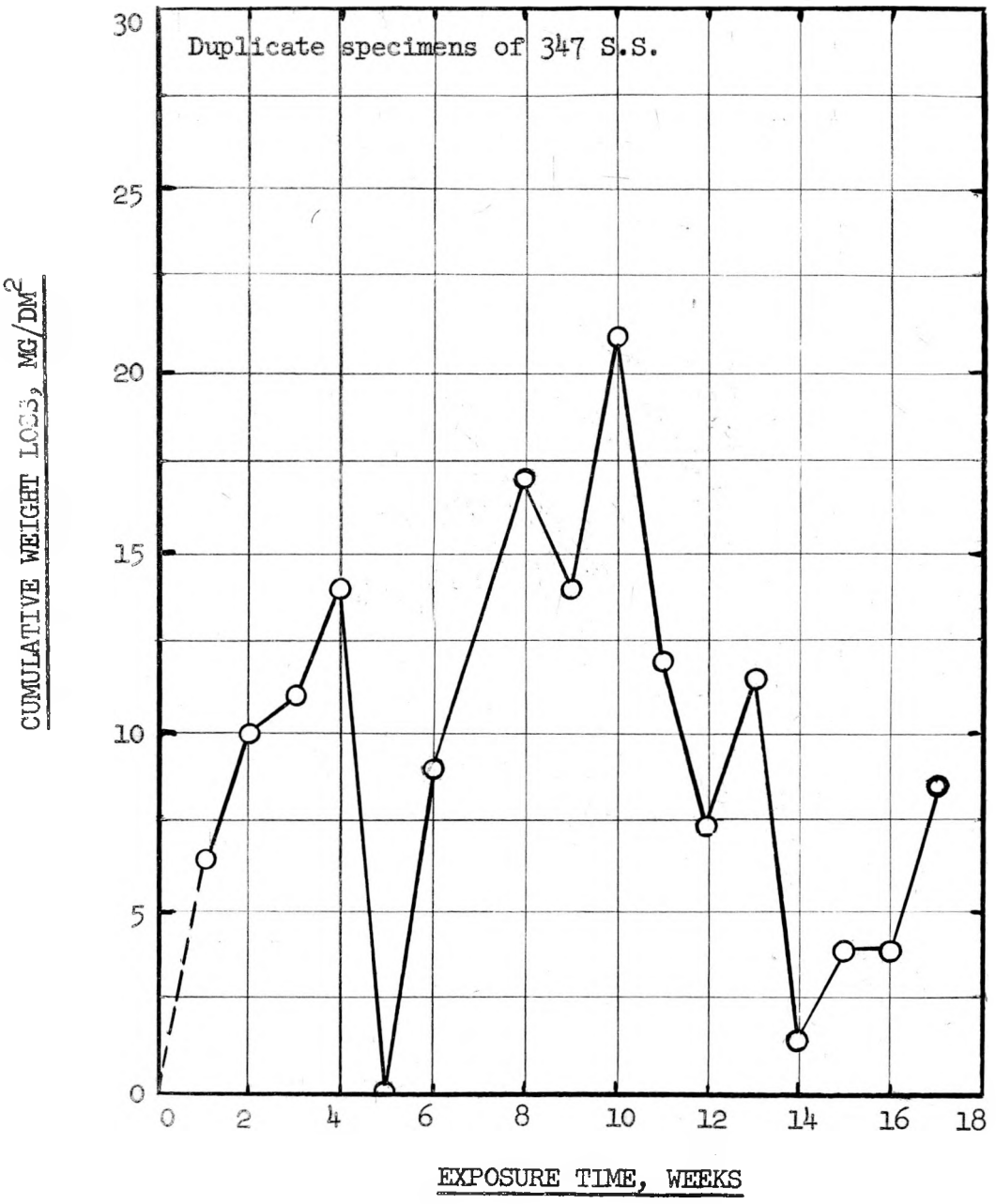

Figure 41. Cumulative Weight Losses on 347 Stainless Steel Exposed to 0.17M Uranyl Sulfate at 250°C (Nitric Acid Decomposition Products Removed after 20 Hours at 250°C)

DECLASSIFIED X-29-12

tests are being continued. The value of the tests lies in the effort to show whether or not a long exposure to 1% nitric acid at 250°C is of greater advantage than a short (4 to 12 hr) exposure. At this point in the testing program there does not appear to be any advantage in a long pretreating time as compared to one of 4 to 12 hr in length.

Effect of Heating Nitric Acid—pretreated Stainless-steel Surfaces. An unknown factor in the stability of uranyl sulfate solution in contact with a pretreated stainless steel system was the effect of heating the stainless-steel system prior to the introduction of the uranyl sulfate. A stainless-steel autoclave was pretreated with 1% nitric acid for 24 hr at 250°C. After this treatment the entire assembly, including corrosion samples, was heated in air for 1 hr at 115 to 120°C. Uranyl sulfate, 0.17 *M*, was introduced into the bomb and the apparatus was operated at 250°C. At the end of three days the test was stopped. Examination of the test solution showed that reduction of the sulfate had occurred and that the stainless-steel sample was corroded to the extent of 5.4 mils/year. These data indicate that the application of heat to a nitric acid—pretreated stainless-steel surface destroys the protective nature of the film, thus putting it in such a condition that it reacts with uranyl sulfate at 250°C and causes reduction of the uranyl ion. Study of this type of test is continuing.

Effect of Air Exposure on Nitric Acid—pretreated Films. A group of tests is in progress to determine the effective life of a nitric acid—treated surface film as a function of subsequent exposure time to ordinary atmospheres. Three stainless steel autoclaves were treated with 1% nitric acid solution at 250°C for 24 hr and were then allowed to stand open in air for periods of 48, 72, and 168 hr. At the end of these periods 0.17 *M* uranyl sulfate was placed in the bombs, which were then operated at 250°C. The bombs exposed for 48 and 72 hr, respectively, have operated thus far for 672 hr without any indication of solution reduction; the bomb exposed to air for 168 hr showed nearly complete reduction of the sulfate medium after a run of 168 hr at 250°C. The following results on type 347 stainless steel corrosion specimens were obtained from these tests.

AIR-EXPOSURE TIME (hr)	TESTING TIME (hr)	WEIGHT CHANGE (mg/dm^2/day)	CORROSION RATE (mils/year)	SAMPLE APPEARANCE
48	672	-0.07	0.013	Shiny brown-red color
72	672	-0.15	0.03	Dull black color
168	168	+10.40		Heavy black scale

DECLASSIFIED X-29-13

Thus it appears that a stainless-steel system that has been pretreated with 1% nitric acid may be safely exposed to ordinary atmospheres for a period of three days without disrupting the stability or protective nature of the film. However, in a period between three and seven days, the protective value of the pretreatment film is lost. These tests are being repeated to determine the time that a pretreated system may remain exposed to air without causing reduction of uranyl sulfate during subsequent operation.

The above series of tests was repeated with the exception that all pretreated parts were submerged in uranyl sulfate solution at room temperature for periods of 48, 72, and 168 hr. The bombs were then operated with uranyl sulfate solution at 250°C. After 672 hr of test (four weeks) no indication of solution reduction has been observed. Corrosion data for type 347 stainless steel specimens appear below.

SULFATE PRE-EXPOSURE TIME (hr)	TESTING TIME (hr)	WEIGHT CHANGE ($mg/dm^2/day$)	CORROSION RATE (mils/year)	SAMPLE APPEARANCE
48	672	-0.26	0.05	Shiny brown-red film
72	672	-0.15	0.03	Shiny brown film
168	672	-0.34	0.06	Shiny blue film

If uranyl sulfate solution is used to "wet" nitric acid—pretreated stainless-steel surfaces, there is no apparent deterioration of the protective film. The above tests will be continued until solution decomposition occurs to ascertain the effect of pre-exposure in uranyl sulfate at room temperature on the life expectancy of the pretreatment film.

A rather significant observation made on this group of tests was that when a specimen was allowed to stand exposed to air for a period of 72 hr, the resulting appearance of the sample after exposure to uranyl sulfate was different from that of the sample pre-exposed for 48 hr in air. In the case of the former the sample showed a very dull black, uniform film; in the case of the specimen exposed to air for 48 hr the sample had a shiny reddish-brown color, very similar to the appearance of the sample after the nitric acid pretreatment. This indicates that the extended exposure to air results in some physical or chemical change in the characteristics of the pretreatment film.

DECLASSIFIED X-29-14

Effect of Halide Ions on Pretreated Nitric Acid Films. The effect of chloride ions present in the uranyl sulfate solution as a contaminant, possibly from brazing, welding, or etching operations, on the life of a nitric acid–pretreatment film was determined. This study also included the determination of the effect of bromides and iodides, formed as fission products during the operation of the reactor. For the chloride tests stainless-steel bombs were pretreated with 1% nitric acid for 24 hr at 250°C. Uranyl sulfate, 0.17 *M* containing 12.5 and 25 ppm, respectively, of chloride ion as sodium chloride was introduced into two bombs. The tests were operated for 168 to 336 hr at 250°C. The solution containing 25 ppm of chloride ion showed heavy precipitation of uranium oxides; the solution containing 12.5 ppm of chloride showed no signs of solution reduction. Corrosion data for type 347 stainless-steel test samples appear below. The test with uranyl sulfate containing 12.5 ppm of choride ion will be continued until solution decomposition takes place.

TEST TIME (hr)	CHLORIDE (ppm)	WEIGHT CHANGE ($mg/dm^2/day$)	CORROSION RATE (mils/year)	SAMPLE APPEARANCE
336	12.5	+0.1		Shiny black film
168	25.0	-29.0	5.3	Heavy black scale

Chloride concentrations of 25 ppm act to destroy the protective nature of the pretreatment film; the phenomenon of the destruction of the passivity of stainless steel by halogen ions, particularly chlorides, is well known.

Calculations by J. O. Bradfute, based on reactor operation at rated capacity with 75 liters of uranyl sulfate, have shown that the fission-product concentration build-up of bromine and iodine can be approximately 0.8 and 13.2 ppm, respectively, after 100 days of operation. Corrosion tests were conducted at 250°C with 0.17 *M* uranyl sulfate to which was added 25 ppm of potassium iodide or 25 ppm of potassium bromide. Both tests showed solution decomposition at the end of 168 hr. The test bombs were pretreated with 1% nitric acid at 250°C for 24 hr before the tests. A 347 stainless-steel specimen, pretreated similarly to the test bombs, showed a corrosion rate of 11.4 mils/year in the solution containing the 25 ppm of potassium iodide. This sample was

DECLASSIFIED X-29-15

unique in that it exhibited numerous pits, 10 to 20 mils in depth, over all the surface. This pitting phenomenon has been encountered rarely in the entire corrosion investigation. A pretreated 347 stainless-steel specimen exposed to the sulfate solution containing 25 ppm of potassium bromide showed a weight gain rate of 115.2 mg/dm^2/day. This specimen was irregularly coated with a heavy black scale.

These tests have shown that the nitric acid pretreatment is of no value in the presence of 25 ppm of chloride ion or of 17 ppm of bromide ion and 19 ppm of iodide ion.

Effect of Damaging a Nitric Acid—pretreatment Film. A test was conducted using a 347 stainless-steel specimen pretreated in 1% nitric acid for 24 hr at 250°C. After the pretreatment an approximately 1/8-in.-wide area across the face of the specimen was scratched with a file to a depth of at least several mils. The sample was then placed in 0.17 *M* uranyl sulfate for 168 hr at 250°C. At the end of this exposure, there was only slight change in the appearance of the scratched area. It was light gray in color as compared to the shiny brown-black color of the surrounding pretreated areas. There were no signs of increased corrosion attack or adhering black deposits of reduced uranium sulfate. The test solution remained yellow in color throughout, and chemical analyses for uranium before and after the test gave no evidence of solution reduction. The overall corrosion rate of the specimen at the end of the testing time was 0.5 mil/year.

These preliminary data suggest that the nitric acid pretreatment film may be self-healing in nature, similar to the behavior of scratched surfaces on aluminum. The other possibility exists of the effect of solution volume—surface area ratio. The existence of small areas devoid of a pretreatment film may be relatively insignificant when in contact with fairly large volumes of uranyl sulfate. Not much conclusive evidence along these lines can be presented until additional studies have been completed.

Chromic Acid Anhydride Pretreatments of Stainless Steels. The fact has been discussed previously that the use of 2% chromic acid anhydride in water at 250°C for 24 hr will successfully prepare stainless-steel surfaces to prevent reduction of uranyl sulfate solution at 250°C. Numerous tests using this method have proved satisfactory. The chromic acid treatment results in a heavier protective film on surfaces than is obtained with nitric acid pretreatments.

DECLASSIFIED X-29-16

A stainless-steel autoclave pretreated with chromic acid, has operated for 22 weeks without indications of solution reduction. The autoclave is inspected weekly, and fresh uranyl sulfate solution is used weekly. The test is operated at 250°C.

Other stainless-steel autoclaves, initially pretreated with chromic acid at 250°C, were subjected to cyclic chromic acid pretreatments at intervals of two and three weeks, respectively. These tests have operated at 250°C with 0.17 *M* uranyl sulfate for a period of 22 weeks without solution breakdown occurring. More emphasis will be placed on the use of chromic acid pretreatments during the next quarter.

In order to determine the effect of heating a chromate-treated stainless-steel surface, a sample of 347 stainless steel was pretreated in 2% chromic acid anhydride at 250°C for 24 hr in a stainless-steel bomb. After the pretreatment, the sample and test bomb were heated in air for 1 hr at 115 to 120°C. Uranyl sulfate was introduced into the bomb, and the assembly was heated to 250°C for 168 hr. Solution decomposition occurred during this period, and the corrosion rate of the sample was 3.2 mils/year. From these data it may be seen that the protective influence of the chromate pretreatment is destroyed by heating in air at 115 to 120°C for a period of 1 hr. The nitric acid–pretreated film reacted in a fashion similar to that described previously.

General Discussion of Pretreatment Films. A program was initiated by the Corrosion Group in September, 1950, with T. E. Willmarth of the Optical Microscopy Section of the Analytical Chemistry Division to study pretreatment films and films formed during exposure of pretreated stainless-steel specimens to uranyl sulfate at 250°C. These studies were made on types 410 and 347 stainless-steel specimens which had been exposed approximately 3000 hr. The results of Willmarth's work have made possible the formulation of a general theory on the mechanism of the film propagation and characteristics.

Three films or strata were observed on the sulfate-exposed specimens. The outer film was identified as containing uranium oxide, U_3O_8; this film thickness was 75 to 100 angstrom units. The film was extremely adherent and homogeneous. Beneath the outer film there was another thin layer, as yet not completely identified but found to contain iron, which constitutes essentially the nitric acid–pretreatment film. The substrate film, very thin, appeared to be the film normally found on stainless steels exposed to air.

CONFIDENTIAL UNCLASSIFIED X-29-17

This information coupled with observations and results from numerous corrosion tests, suggests a possible mechanism for the formation of film on stainless steels in uranyl sulfate at 250°C. Previous corrosion studies have shown conclusively that an untreated stainless-steel surface in contact with uranyl sulfate at 250°C causes nearly complete reduction of the uranyl ion throughout the solution. This effect is apparently a direct result of a corrosion reaction between the acidic sulfate medium, *p*H 2.1 to 2.6, and the untreated stainless steel, involving the liberation of hydrogen and subsequent reduction of the uranyl ion throughout the solution to oxides of uranium. It has been shown experimentally that uranyl sulfate contained in a nitric acid—pretreated stainless-steel system at 250°C under partial pressure of hydrogen also undergoes nearly complete reduction.

The presence of a film formed by treatment with dilute (1%) nitric acid at 250°C acts to greatly restrict the reduction phenomenon, and from outward appearances, eliminates it completely. However, from a study of existing information on the films, it appears that, essentially, the same type of solution reduction is taking place, but it is now confined to a purely metal-solution interface region. The fact that iron has been observed in the middle layer of the films formed on pretreated and sulfate-exposed stainless steels suggests that the metallic iron atoms migrate through the pretreated layer to contact the sulfate solution. At this point of contact, reduction of the uranyl sulfate by the iron atoms to uranium oxide occurs and the oxide is deposited very tightly on the metal surface. This reaction must continue until a thin and uniform layer of uranium oxide is deposited over the entire stainless-steel surface. When the film attains an optimum thickness, seemingly 75 to 100 A, the diffusion of iron atoms through the oxide layer is greatly slowed and the build up of uranium oxide discontinues. The reduction of uranyl sulfate by an atom of iron may be explained by two mechanisms. (1) It has been determined experimentally that metallic iron will cause some reduction of uranyl sulfate at 250°C, and (2) the reduction may occur by the simple process of a chemical action on the iron atoms by the acidic sulfate solution; this causes hydrogen to be liberated, which reduces the solution.

Thus, the protective film formed by pretreatment seems to act as a barrier to greatly restrict the mass migration of metallic iron atoms to contact the sulfate solution. The fact that iron atoms eventually do migrate through the initial protective film indicates that this film is not completely nonporous.

DECLASSIFIED X-29-18

These suppositions as to the mechanism of the protective film formation are based on preliminary observations and may not represent what is actually taking place. Additional experimental evidence is needed to verify or disprove them.

The actual role of the initial nitric acid pretreatment at 250°C is not well defined at this point. The mechanism appears undoubtedly to be one of physical adsorption or chemisorption or a combination of the two. Test data indicate that the nitric acid film, considered completely independently of the natural thin layer of oxide always present on stainless steels exposed to air, is physically adsorbed, although little or no adsorption of gases would be expected to take place on stainless steel at temperatures of 250°C. One of the major differences between physically adsorbed and chemisorbed films is the reversibility of the former. The results of two tests indicate the reversibility of the nitric acid pretreatment. First, it was determined that the protective influence of the nitric acid pretreatment was destroyed by heating for 1 hr at 115 to 125°C, and, secondly, it was shown that a pretreated surface loses its protective nature after exposure to air at room temperature for a period of one week.

The passivity of stainless steels is believed generally to be the result of a chemisorption process with oxygen or other substances which have a high affinity for chromium. By this mechanism oxygen is adsorbed on the surfaces of the metal, causing a reduction in its chemical activity by a satisfaction of surface valence forces. The chemisorbed film is not sufficient in itself to prevent reduction of uranyl sulfate from occurring at 250°C. Only when such a surface is first pretreated with nitric acid at 250°C is the reduction phenomenon greatly minimized. Therefore at least the initial corrosion behavior of pretreated stainless steel surfaces appears to be primarily the result of the presence of a physically adsorbed film with or without the presence of the already existent chemisorbed film found to exist normally on stainless steels. It is fully realized that these assumptions are based on very little preliminary information, but, nevertheless, the results do emphasize the need for additional studies along similar lines.

Another line of reasoning, more sound perhaps than the consideration of a physically adsorbed film, suggests the possibility that the initial nitric acid pretreatment results in a reaction-product type of film. Subsequent failure of this type of film by heating at 115 to 120°C on long exposure to

DECLASSIFIED X-29-19

air could be explained by the loss of water of crystallization from the film. This water of crystallization, formed at high temperatures as an inherent part of the film, may become unstable at ordinary temperatures and may attempt to reach a state of equilibrium. The loss of water of crystallization may tend to make the film more pervious and therefore more susceptible to conditions promoting solution reduction.

Corrosion Resistance of Stainless Steels

Corrosion studies on stainless steels in uranyl sulfate systems at 250°C have advanced sufficiently to demonstrate their successful behavior under controlled laboratory conditions for use as component parts in a homogeneous reactor. These studies have been concerned almost entirely with pretreated stainless steels since the use of untreated steels is not feasible. Lack of facilities and equipment have made it necessary to conduct the majority of these tests in the absence of irradiation and under stagnant conditions. An intense effort on this phase of the program is being expended in cooperation with members of the Chemistry Division. Plans are also in progress to expand stainless steel corrosion studies to dynamic systems in order that the effect of velocity on the protective films may be investigated.

Average corrosion rates for 347 stainless steel, pretreated for 24 hr or less in 1% nitric acid at 250°C and then exposed to 0.17 *M* uranyl sulfate solution at 250°C for periods of 16 to 18 weeks, have ranged from 0.01 to 0.05 mil/year, an extremely small rate. No reduction of uranyl sulfate solution occurred during the operation of these tests.

A series of tests has been in process for 20 to 24 weeks with various stainless steels exposed at 250°C to 0.17 *M* uranyl sulfate containing 1% nitric acid. These samples were run in duplicate and did not receive any pretreatment with nitric acid initially. The tests were dismantled weekly for sample inspection and fresh uranyl sulfate–nitric acid solution was used weekly. Results of the tests appear in Table 13.

With the exception of 410 stainless steel, all other materials exhibited very minor corrosion rates at the end of the test periods. Type 410 stainless steel showed a slight weight gain, 0.44 mg/dm^2/day. Figures 42 through 44

DECLASSIFIED X-29-20

DWG. 10120

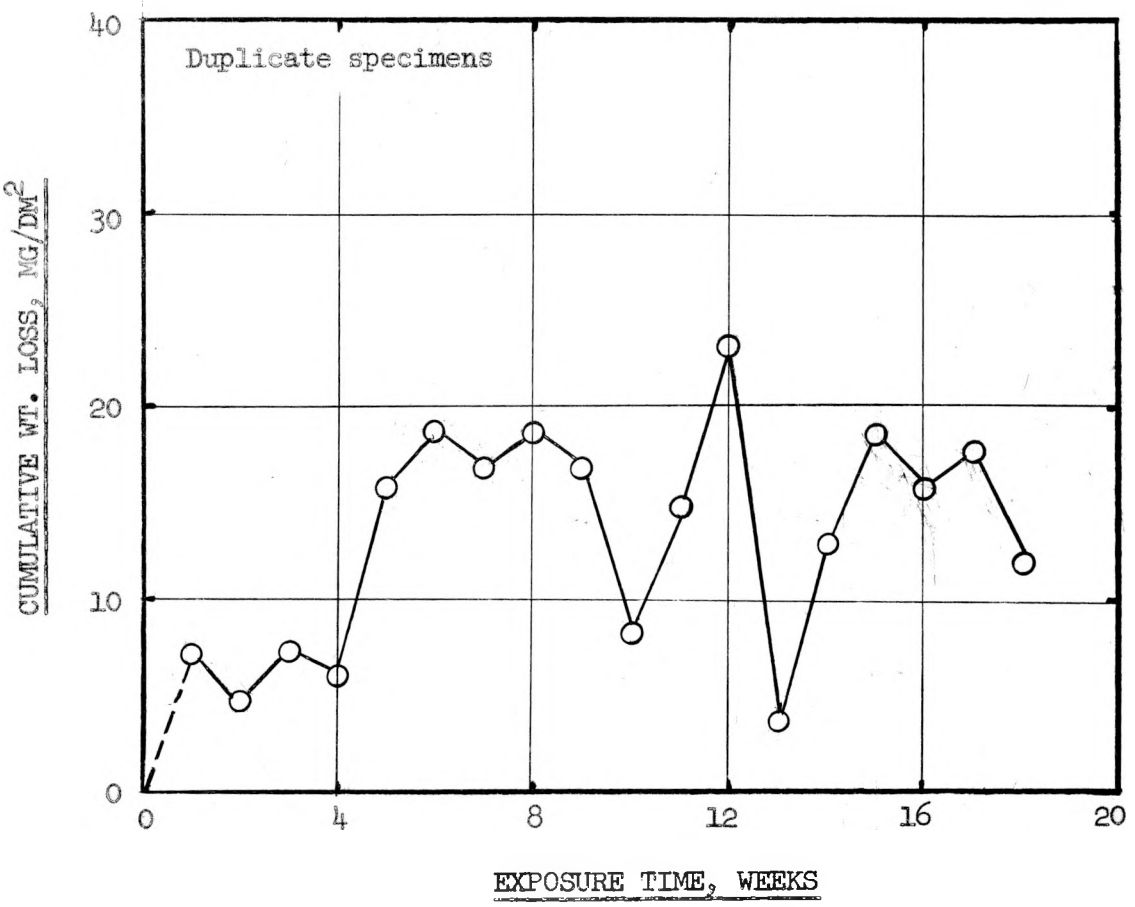

Figure 42. Cumulative Weight Loss on Type 316 Extra Low Carbon Stainless Steel Exposed to 0.17M Uranyl Sulfate Containing 1% Nitric Acid at 250°C

DECLASSIFIED

X-29-21

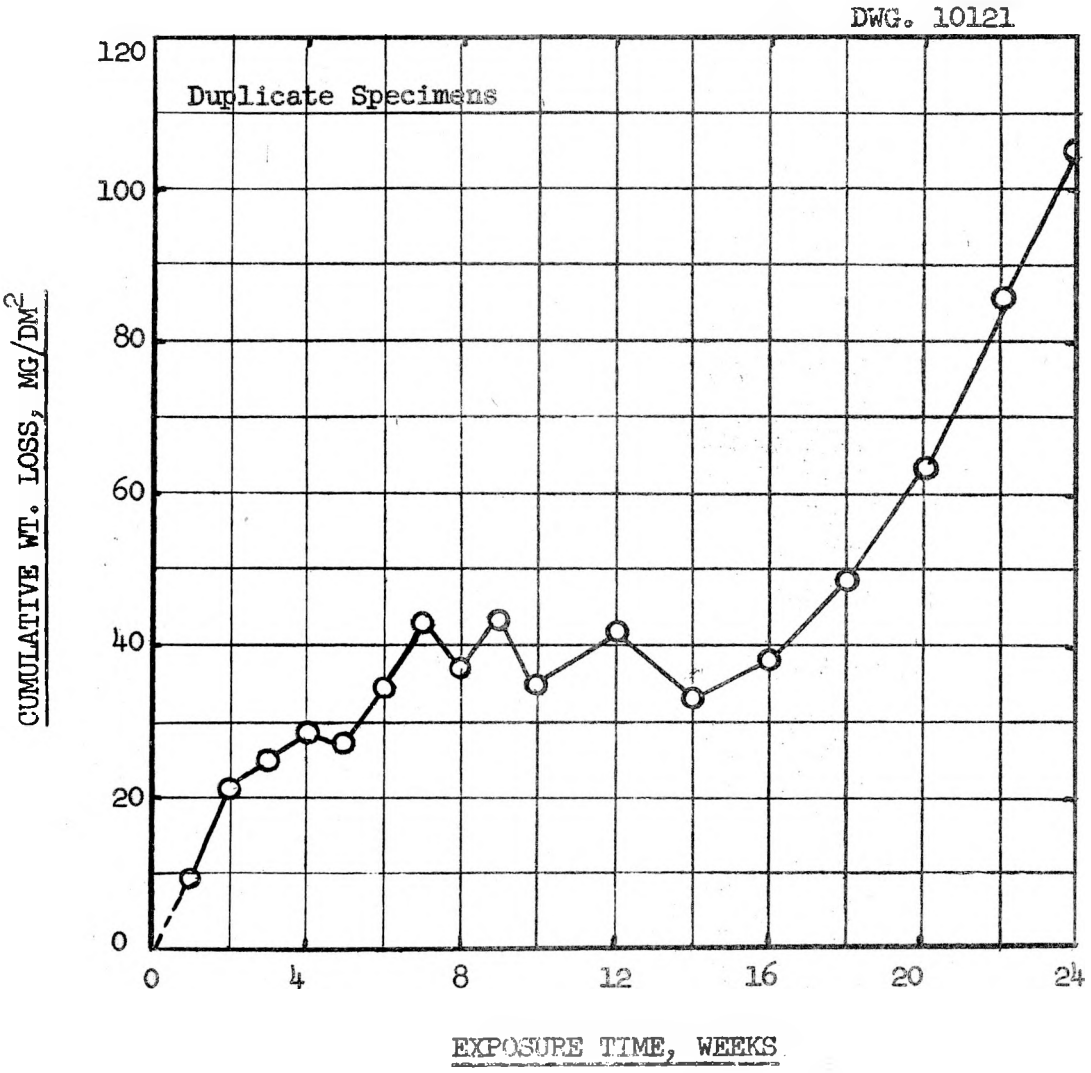

Figure 43. Cumulative Weight Loss on Type 347 Stainless Steel Exposed to 0.17M Uranyl Sulfate Containing 1% Nitric Acid at 250°C

DECLASSIFIED
X-29-22

DWG. 10122

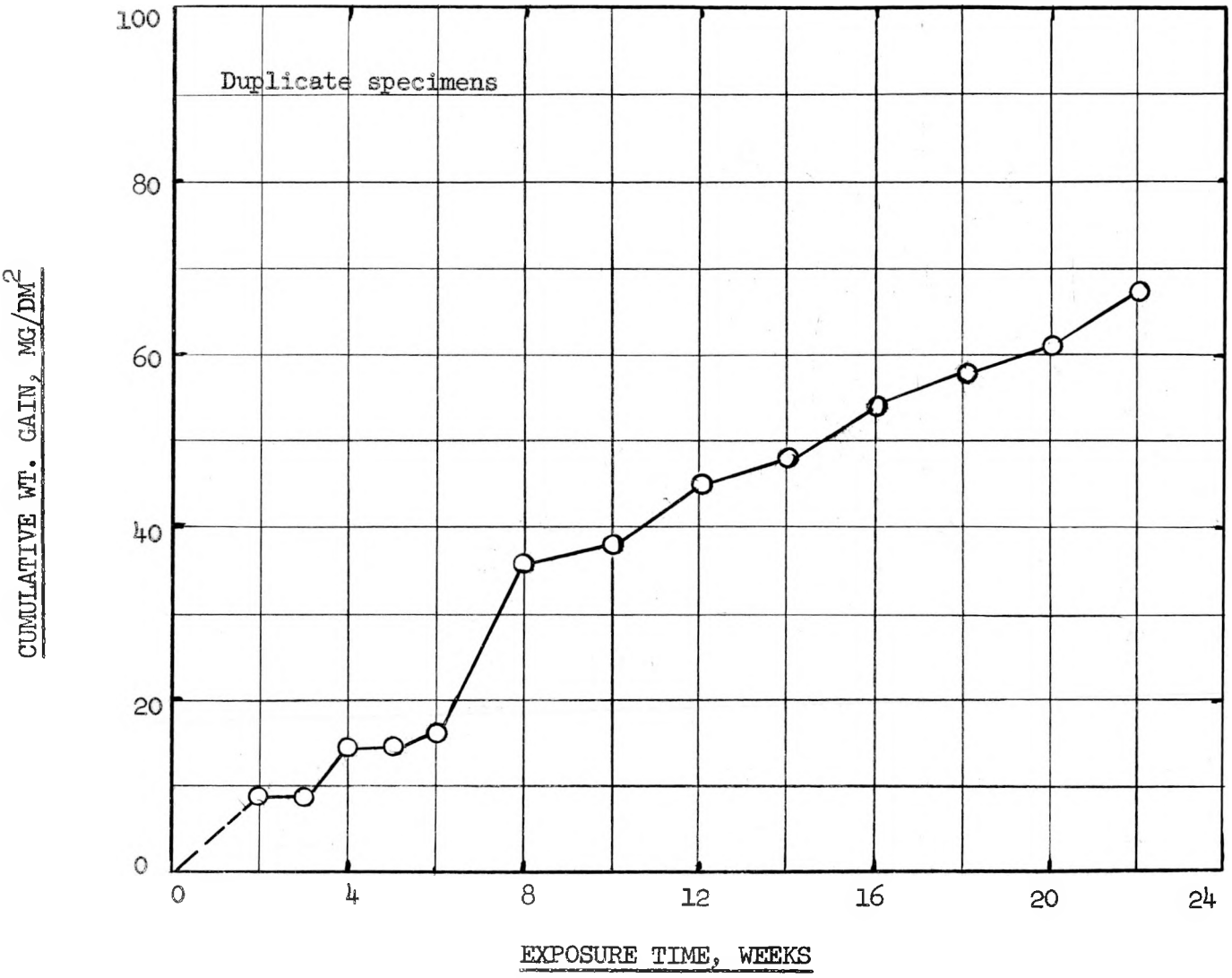

Figure 44. Cumulative Weight Gain on Type 410 Stainless Steel Exposed to 0.17M Uranyl Sulfate Containing 1% Nitric Acid at 250°C

DECLASSIFIED

X-29-23

TABLE 13

The Corrosion of Stainless Steels in 0.17 *M* Uranyl Sulfate Containing 1% Nitric Acid at 250°C

MATERIAL	EXPOSURE (weeks)	WEIGHT CHANGE ($mg/dm^2/day$)	CORROSION RATE (mils/year)	SAMPLE APPEARANCE
309 SS	18	-0.59	0.11	Shiny black uniform film
316ELC SS	18	-0.09	0.02	Shiny black uniform film
347 SS	24	-0.62	0.11	Dull black uniform film
410 SS	22	+0.44		Dull gray uniform film
Carpenter 20	19	-0.32	0.06	Dull black film

illustrate the behavior of types 316ELC, 347, and 410 stainless steels. The curve for 316ELC stainless steel shows a gradually increasing weight loss for a period of six weeks. From this time to the end of the test a fairly constant rate of weight change was maintained with only a few fluctuations in the curve. The corrosion rate at the time of maximum weight loss, 12 weeks, was 0.05 mil/year; the corrosion rate at the end of 18 weeks was 0.02 mil/year.

The corrosion behavior of 347 stainless steel is shown in Fig. 43. The trend was a gradual increase in weight loss for a period of seven weeks, after which time the rate remained fairly constant for nine weeks. At the end of 16 weeks, an increase in weight loss occurred which has continued almost linearly with time for an additional eight weeks. The corrosion rate at the end of 24 weeks was small, 0.11 mil/year.

Figure 44 shows the cumulative weight gains recorded for 410 stainless steel in uranyl sulfate—nitric acid solutions. This curve approaches an exponential function of weight gain vs. exposure time. The fact that the specimens exhibited weight gains rather than weight losses as in the case of the other stainless steels indicates a distinct difference in behavior attributable to either a difference in the mechanism of film formation or to the inherent characteristics of the alloy. The weight gain at the end of 22 weeks was 0.0044 mg/cm^2.

CONFIDENTIAL

DECLASSIFIED

X-29-24

The corrosion resistance and behavior of welded stainless-steel specimens exposed to uranyl sulfate at 250°C is being investigated. Samples were initially pretreated in either 1% nitric acid or 2% chromic acid at 250°C for 24 hr. Previous work had shown that these pretreatments were completely ineffective in preventing reduction of uranyl sulfate when applied over heavy welding scale. For this reason it is absolutely necessary to remove this scale by mechanical or chemical means. The samples for these tests were heliarc-welded; no additional heat treatment was performed after the welding operation. The samples were then machined to remove welding scale and pretreated in nitric or chromic acid at 250°C. Test results are given in Table 14.

TABLE 14

The Corrosion of Pretreated Heliarc-Welded Stainless Steels in 0.17 *M* Uranyl Sulfate at 250°C

MATERIAL	EXPOSURE (weeks)	PRETREATMENT	WEIGHT CHANGE		SAMPLE APPEARANCE
			(mg/dm^2)	($mg/dm^2/day$)	
309 SS	3	HNO_3	+1.3	+0.06	Shiny brown film
316 SS	3	CrO_3	-6.2	-0.30	Uniform black film
316 SS	5	HNO_3	+0.2	+0.01	Shiny blue film
347 SS	3	HNO_3	-8.0	-0.38	Shiny brown film

The condition of these samples at the end of the test periods was excellent. The weight gains exhibited were very slight, and in no instance were any signs of solution deterioration observed. The tests are being continued.

Several tests were conducted with type 410 stainless steel at a temperature of 150°C in 0.17 *M* uranyl sulfate. One set of cold-rolled and polished specimens was exposed without any pretreatment in silica tubes at this temperature. Corrosion attack was severe and amounted to 27.3 mils/year at the end of three weeks. Chemical analyses indicated that solution reduction had occurred also at this temperature.

A test was made with 410 stainless steel which had been heated at 1850°F for 15 min, cooled in air, and pickled to remove heat-treating scale. The

DECLASSIFIED X-29-25

samples were then pretreated in 1% nitric acid for 24 hr at 250°C and exposed to 0.17 *M* uranyl sulfate at 150°C. Figure 45 shows the cumulative weight gains as a function of exposure time at this temperature. Film formation was rapid during the first three weeks of the test but remained constant during the following nine weeks. These data indicate that very little film growth occurred during the last nine weeks after the initial film was formed. The samples retained a shiny green-blue color throughout the entire test period.

Corrosion Resistance of Zirconium

Emphasis has continued on the corrosion testing of zirconium metal in uranyl sulfate at 250°C since zirconium remains of great interest as a construction material for a homogeneous reactor. Both crystal bar zirconium and Bureau of Mines zirconium have been considered in this investigation although the use of the latter is preferred because of its lower cost and availability in the necessary shapes and sizes required for component parts of a reactor.

Crystal Bar Zirconium. Crystal bar zirconium, made by the iodide reduction process, was obtained from MIT and has been in test for considerable time. Since the purity of this material has been generally better than that of Bureau of Mines zirconium, the corrosion results from these samples were intended to be used as relative standards to obtain a basis of comparison for Bureau of Mines corrosion test results. In order to operate the corrosion tests without incurring precipitation of the uranyl sulfate in untreated stainless-steel systems, it was decided to contain the sulfate medium in fused silica tubes, open at one end, in stainless-steel bombs. This method has proved satisfactory except that the tubes do require replacement after several runs owing to the pickup of silica in the test solutions.

Corrosion results for the various crystal bar zirconium samples are given in Table 15. Chemical analyses of the material have been reported previously (ORNL 826). The tests were inspected weekly, and fresh uranyl sulfate solution was used weekly.

It may be readily seen that the weight gains and corrosion rates, where corrosion attack occurred, are extremely small. All samples remained in excellent condition throughout the tests except CB-6, which became coated with

DECLASSIFIED X-29-26

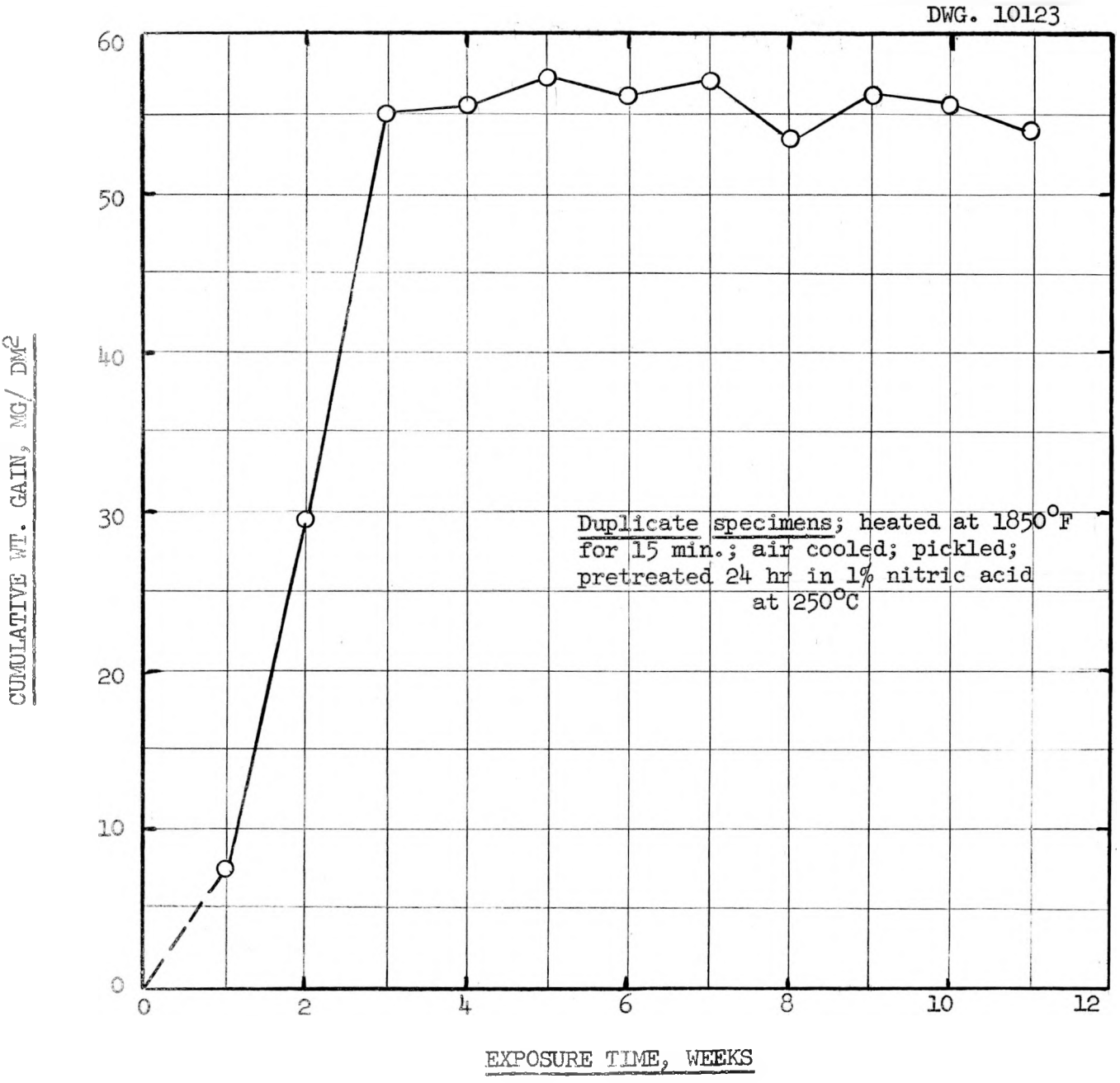

Figure 45. Cumulative Weight Gain on Pretreated 410 Stainless Steel Exposed to 0.17M Uranyl Sulfate at 150°C

DECLASSIFIED

X-29-27

TABLE 15

Corrosion of Crystal Bar Zirconium in 0.17 *M* Uranyl Sulfate at 250°C

MATERIAL	EXPOSURE (weeks)	WEIGHT CHANGE ($mg/dm^2/day$)	CORROSION RATE (mils/year)	SAMPLE APPEARANCE
CB-1	19	-0.11	0.03	Shiny gray film
CB-3	18	-0.26	0.06	Dark gray shiny film
CB-4	24	+0.09		Dull gray film
CB-5	23	+0.21		Light gray shiny film
CB-6	23	+0.30		Red colored film
CB-7	18	+0.17		Dull gray film
CB-109	23	-0.04	0.01	Shiny light gray film

an as yet unidentified red-colored film near the end of the test. Figure 46 shows the cumulative weight changes for samples CB-1, CB-4, and CB-5 as a function of exposure time. Sample CB-1 exhibited a general increase in corrosion attact for a period of 11 weeks; there followed a gradual decrease in corrosion attack for the ensuing eight weeks of the test. The increase period during the first 11 weeks was accompanied by several peaks of decreased weight loss, suggesting the repeated formation and deterioration of a protective film. The second phase of the curve seemed to indicate a more stable type of film formation, as evidenced by decreased weight losses. Sample CB-4 exhibited the same general type of behavior on a slightly more pronounced scale. The behavior of sample CB-5 was characterized throughout the major portion of the test by changing weight gains rather than losses. Initially film formed rapidly, but the rate of formation was gradually decreased by corrosion reactions. After a period of 11 weeks this film started to grow again.

A sample of crystal bar zirconium, cold-rolled sheet, was obtained from Battelle Memorial Institute and exposed to 0.17 *M* uranyl sulfate at 250°C in a silica tube for 10 weeks. The sample at the end of this period showed a slight weight gain, 0.13 $mg/dm^2/day$, and exhibited a shiny gray uniform film on all surfaces. Initial sample preparation consisted of a degreasing treatment only. The test is being continued.

DECLASSIFIED X-29-28

DWG. 10124

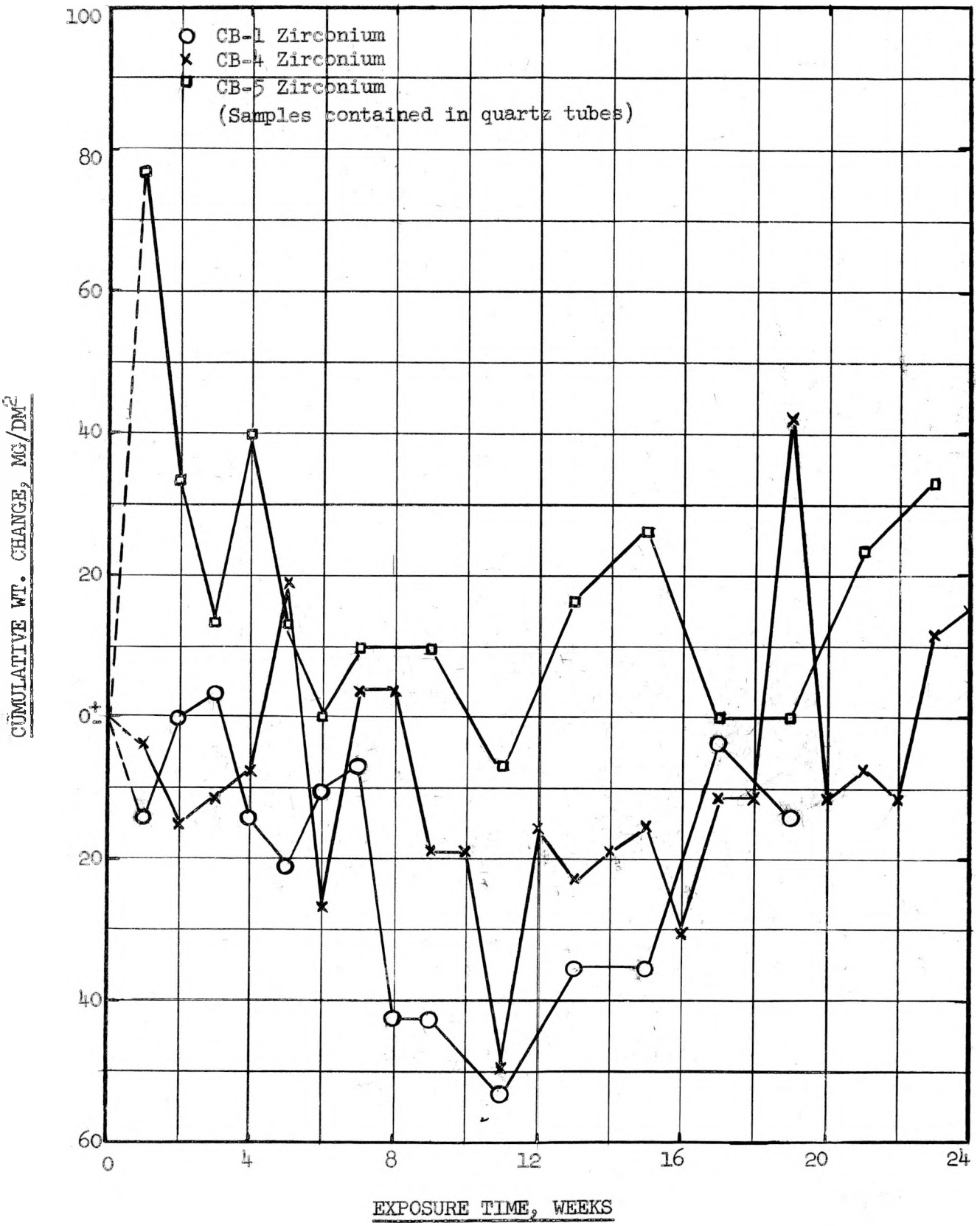

Figure 46. Cumulative Weight Changes on Crystal Bar Zirconium Samples Exposed to 0.17M Uranyl Sulfate at 250°C

DECLASSIFIED
X-29-29

Crystal bar zirconium samples, designated VI-A, were procured from the Foote Mineral Company. This metal was produced from Y-12 oxide, prepared by salicylic acid treatment. The chemical analysis of the zirconium was:

Aluminum	<0.01%	Titanium	0.042%
Calcium	0.004	Carbon	0.01
Iron	0.15	Nitrogen	0.002
Magnesium	<0.001	Chloride	0.0028

One sample was degreased just prior to exposure in uranyl sulfate; another sample was etched for 5 min at room temperature in 5% hydrofluoric acid prior to exposure. The samples were run in 0.17 *M* uranyl sulfate, contained in silica tubes at 250°C for 10 weeks. The results were:

EXPOSURE (weeks)	WEIGHT CHANGE (mg/dm^2) Nonetched	Etched
2	-2.5	+4.3
4	0.0	+10.8
6	+4.9	+15.0
8	+4.9	+19.4
10	0.0	+17.2

The etched specimen exhibited slight weight gains throughout the test, suggesting a tight, protective film. This sample was shiny gray in color with a few interference colors. The sample which was not etched showed a weight-loss period, a period of weight gain, and finally another period of weight loss. These data indicate cyclic film formation and degenerations. The sample retained a very shiny blue-purple cast during the test. Both tests are being continued.

Crystal bar zirconium designated VI-B, having a slightly different chemical analysis from VI-A, was obtained from Foote Mineral Company. This material was produced in a similar manner to VI-A. The chemical analysis was:

Aluminum	0.02%	Titanium	0.061%
Calcium	0.033	Carbon	0.07
Iron	0.036	Nitrogen	0.009
Magnesium	0.002	Chloride	0.0025

DECLASSIFIED

X-29-30

These samples, one not etched and the other etched for 5 min in 5% hydrofluoric acid, were exposed to 0.17 *M* uranyl sulfate at 250°C for 10 weeks. The uranyl sulfate, in silica tubes, was changed weekly. Test results appear below.

EXPOSURE (weeks)	WEIGHT CHANGE (mg/dm^2/day) Nonetched	Etched
2	0.0	+6.3
4	-12.5	+7.8
6	-14.1	+7.8
8	-17.2	+14.0
10	-28.1	+7.8

The nonetched specimen showed a continuous loss in weight, more severe than that exhibited by the nonetched VI-A sample. The corrosion rate at the end of 10 weeks was 0.09 mil/year; the sample was dull gray in color. The etched VI-B specimen showed a very slight increase in weight, less than that of the etched VI-A specimen, and exhibited a shiny gray surface spotted with interference colors. The difference in corrosion behavior of the VI-A and VI-B samples, assuming all variables constant in both series of the test, may be attributed to the difference in the chemical analysis of the two materials.

Crystal bar zirconium tubing, ¼ in. O.D. and 0.040 in. wall thickness, was procured from MIT for corrosion studies. The tubing was made from previously extruded crystal bar metal. No chemical analysis is available at this time. Samples, nonetched and etched 5 min in 5% hydrofluoric acid, were exposed to 0.17 *M* uranyl sulfate in silica tubes at 250°C. Both specimens showed weight gains during the test; the nonetched sample was removed from the test at the end of three weeks owing to the formation of heavy black specks, presumed to be uranium oxide, on the interior walls of the tubing. The weight gain at this time was 214.9 mg/dm^2, a rate equal to 10.2 mg/dm^2/day. The etched specimen showed an initially high rate of weight pickup, 225.7 mg/dm^2 during the first 168 hr. This weight increase gradually decreased over a period of seven weeks, so that by the end of the seventh week the weight gain was 49.9 mg/dm^2, a weight-gain rate of 1.02 mg/dm^2/day for the entire time of the test. The decreasing weight-gain trend indicated that the initially formed film was gradually being removed by the corrosive action of the solution.

DECLASSIFIED

The major emphasis on the zirconium-corrosion program has been placed on Bureau of Mines material. The history and chemical analysis of the materials undergoing test, with the exception of recently received samples, have been reported previously in ORNL-826. These data are discussed in the following paragraphs.

BM: I-H-7 (Vacuum resistance-melted sponge metal in graphite crucible; tested in cast condition). This sample was exposed for 10 weeks in 0.17 *M* uranyl sulfate containing 1% nitric acid at 250°C. The specimen showed a cumulative weight gain of 17.3 mg/dm^2 at the end of the test. This figure is equivalent to a weight-gain rate of 0.24 mg/dm^2/day. The sample remained light gray in color during the test.

BM: I-I-7 (Graphite-melted sponge metal; forged and rolled in mild-steel sheath at 850°C; sheath removed and metal hot-rolled in air at 650°C). A sample was run 13 weeks in 0.17 *M* uranyl sulfate contained in a silica tube at 250°C. At the end of 10 weeks a corrosion rate of 2.1 mils/year was observed; during the following week of exposure, however, a very black film deposition was noted. The sample increased in weight by 1603.6 mg/dm^2, the bulk of which was due to adhering deposits of uranium oxide. The sudden reduction of the uranyl sulfate by these samples after 10 weeks of quiet corrosion behavior is unexplained at the present time.

BM: I-K-7 (Graphite-melted sponge metal; forged and hot-rolled in mild-steel sheath at 850°C; sheath removed and zirconium swaged in air at 650°C; cold-swaged with annealing to 0.210 in.). A set of samples, one nonetched and one etched in 5% hydrofluoric acid, were run in 0.17 *M* uranyl sulfate in silica tubes at 250°C. Cumulative-weight-change data for both samples are reported in the following table.

EXPOSURE (weeks)	CUMULATIVE WEIGHT CHANGE (mg/dm^2) Nonetched	Etched
2	+310.1	-17.0
4	-104.4	-74.9
6	-199.3	-315.2
8	-362.3	-482.2
10	-446.1	-579.4
12	-612.3	-770.3
14	+797.3	-1233.7
16		-1269.5
18		-1905.1

DECLASSIFIED

X-29-32

The sudden weight gain exhibited by the nonetched specimens at the end of 14 weeks is attributed to uranium oxides produced from the uranyl sulfate solution which adhered to the sample. The etched sample showed a steady weight loss during the entire test. This sample remained light gray in color. The corrosion rate after 18 weeks was 3.4 mils/year. The effect of etching the specimen was pronounced during the early stages of the test. The nonetched sample showed a weight increase after two weeks, which was followed by a gradual increase in weight loss until reduction of the sulfate occurred. The etched specimen exhibited a weight loss after two weeks. These data indicate that the initial film on the nonetched specimen tended to retard corrosion attack for several weeks, but then the two samples followed nearly identical trends in weight losses until precipitation occurred on the nonetched sample.

A sample of the same material, I-K-7, was exposed to 0.17 *M* uranyl sulfate containing 1% nitric acid at 250°C for 16 weeks. The sample was not etched prior to the test. The corrosion data below again indicate the formation of an original film on the metal which was rapidly removed during the course of the test by the corrosive action of the solution. A light gray uniform film remained on the specimen throughout the test.

EXPOSURE (weeks)	CUMULATIVE WEIGHT CHANGE (mg/dm^2)	CORROSION RATE (mils/year)
2	+61.6	
4	-10.3	0.1
6	-79.9	0.4
8	-176.0	0.7
10	-263.2	0.9
12	-478.5	1.1
14	-991.2	1.8
16	-1621.8	2.4

BM: S948 (Arc-melted with consumable electrode in inert atmosphere; hot-rolled at 650°C). The test specimen was etched for 5 min in 5% hydrofluoric acid prior to exposure to 0.17 *M* uranyl sulfate (silica tube) at 250°C. Corrosion data on this specimen were very interesting; cumulative weight changes are plotted in Fig. 47. The corrosion pattern was divided into two

DECLASSIFIED

X-29-33

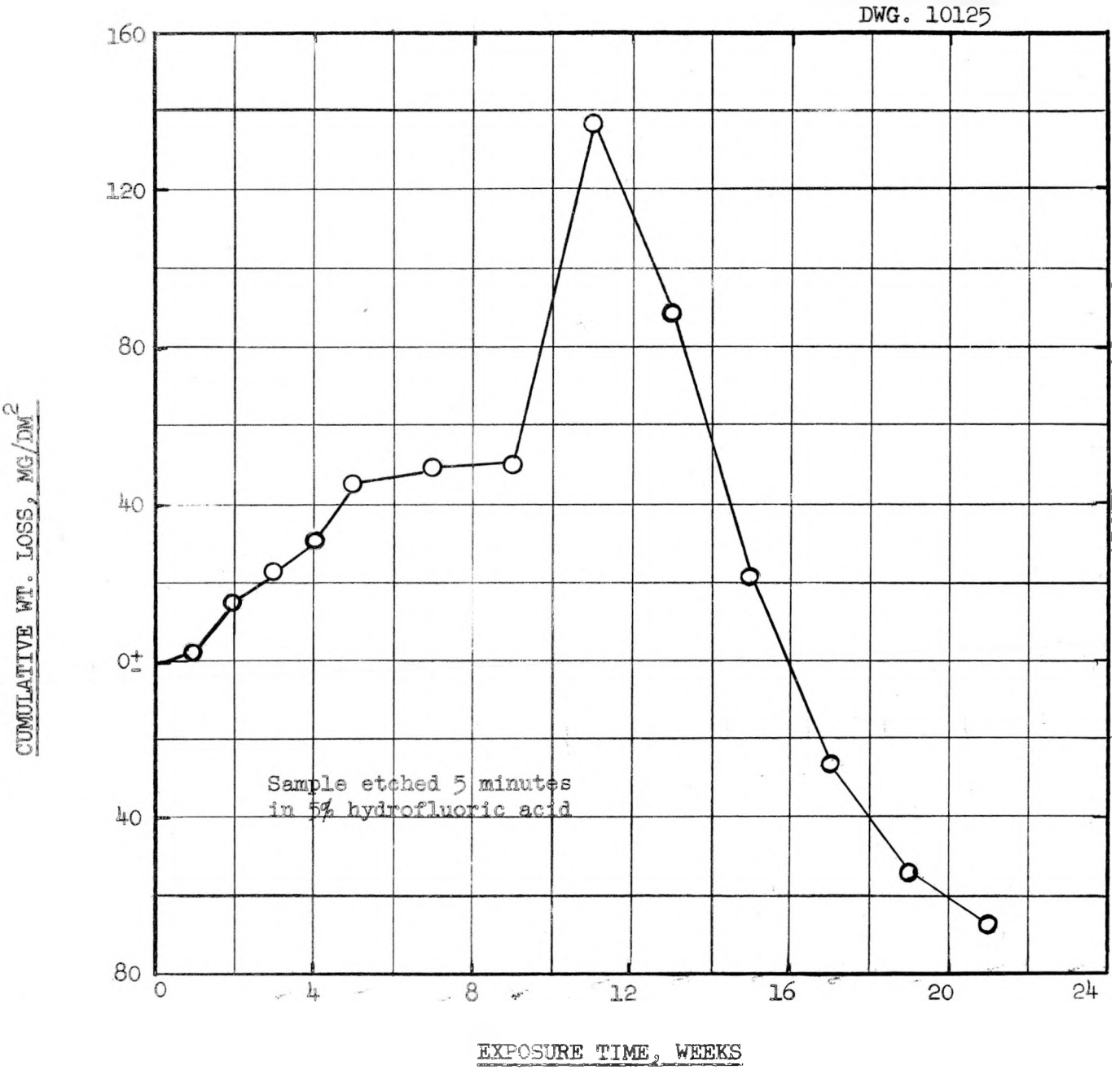

Figure 47. Cumulative Weight Changes on Bureau of Mines Zirconium (S948) Exposed to 0.17M Uranyl Sulfate at 250°C

DECLASSIFIED

X-29-34

distinct phases over the 21 weeks of the test. The first phase, 11 weeks duration, consisted of a gradual film formation and weight increase until a maximum increase of 137.3 mg/dm^2 was obtained. From this point corrosion attack on the film started and continued until the end of the test, at which time the corrosion rate was 0.1 mil/year. The initial corrosion behavior of this specimen was different from that of zirconium specimens mentioned previously. These specimens, also etched, exhibited weight losses after only one to two weeks of exposure. The S948 specimen, even though etched, showed a good rate of film formation for as long as 11 weeks in uranyl sulfate at 250°C.

BM: S980, S982, and S983 (Arc-melted with consumable electrode containing tantalum; hot- and cold-rolled to 0.062 in. thickness; containing 0.80, 0.30, and 0.095% tantalum, respectively). Samples of these zirconium-tantalum alloys were exposed to 0.17 *M* uranyl sulfate at 250°C for 23 weeks in order to determine the effect of the tantalum addition on corrosion resistance. Cumulative weight-change data are plotted in Fig. 48. Addition of tantalum in the range 0.3 to 0.8% afforded the best corrosion resistance; the addition of 0.095% resulted in increased weight gains for a period of 15 weeks, after which very rapid loss in weight occurred. The corrosion rate of this specimen at the end of 21 weeks was 0.7 mil/year. The corrosion rate of S980 (0.8% tantalum) at the end of 23 weeks was 0.01 mil/year; sample S982 (0.3% tantalum) showed a weight-gain rate of 0.35 mg/dm^2/day at the end of 23 weeks.

BM Zirconium-Titanium Welded Samples (Sheet zirconium butt-welded to titanium sheet). Samples of these welded specimens have been exposed to 0.17 *M* uranyl sulfate at 250°C for 19 weeks thus far. One specimen, *A*, was polished on all sides prior to testing; the other sample, *B*, was polished on one side only before exposure. Cumulative weight changes are tabulated below.

EXPOSURE (weeks)	CUMULATIVE WEIGHT CHANGE (mg/dm^2) Sample *A*	Sample *B*
1	-5.2	-7.5
2	-8.7	-25.1
3	-17.4	-50.2
4	-25.2	-56.9
5	-42.6	-41.1
7	+36.5	-4,2
9	-192.9	-281.7
11	-283.3	-369.5
13	-326.7	-464.0
15	-344.1	-539.2
17	-470.1	-602.8
19	-524.9	-671.2

DECLASSIFIED X-29-35

DWG. 10126

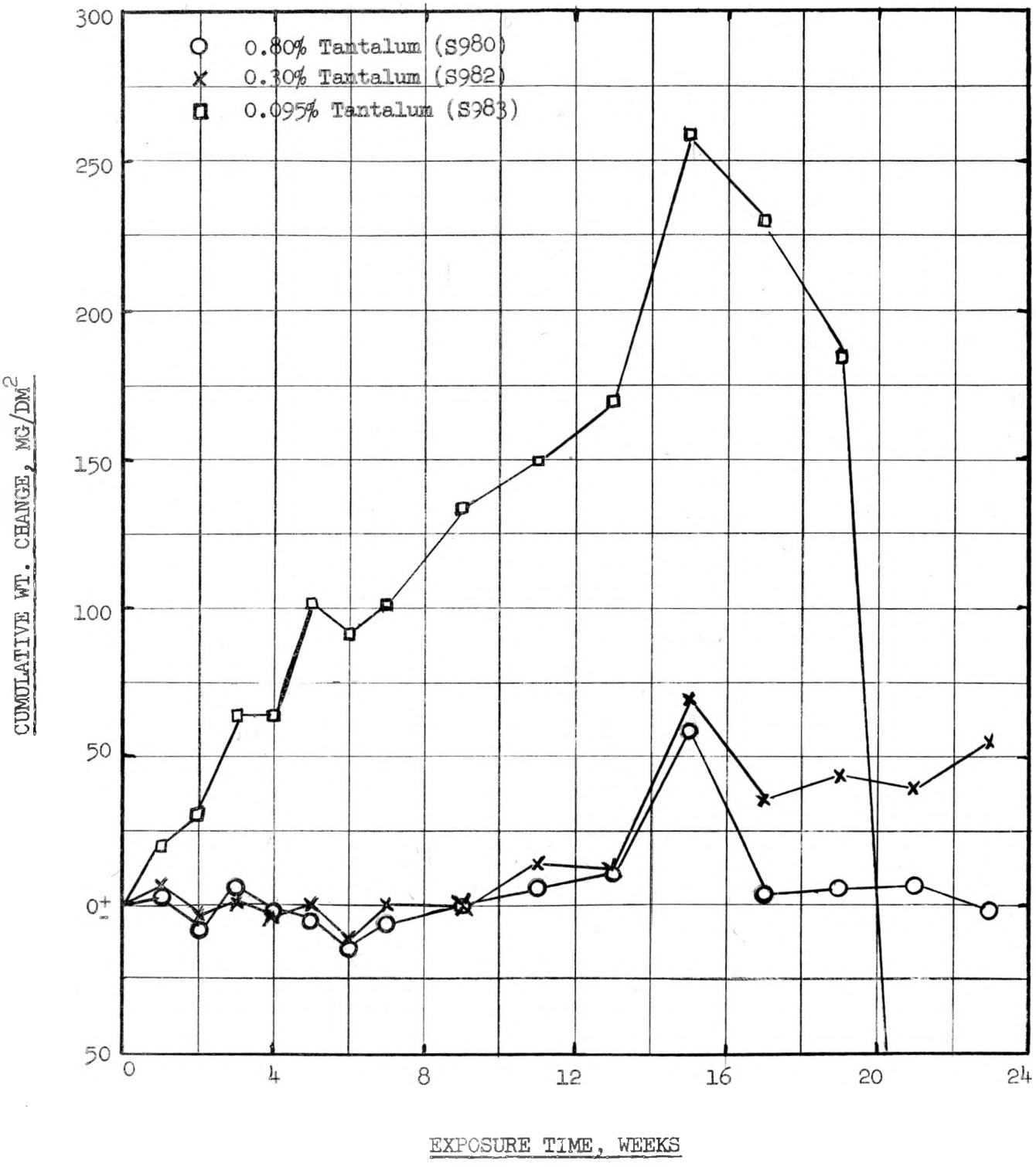

Figure 48. The Effect of Tantalum Additions to Bureau of Mines Zirconium on Corrosion Resistance to 0.17M Uranyl Sulfate at 250°C

UNCLASSIFIED X-29-36

At the end of seven weeks it was observed that both samples, run independently, showed a sudden increase in weight. After this period weight losses increased fairly rapidly for the remainder of the test. The physical appearance of both specimens indicated that the bulk of the corrosion attack was taking place on the zirconium portion of the specimen. The titanium, in both cases, was shiny brown, while the zirconium was pink-white. The immediate area of the weld was black on the titanium side and white-streaked on the zirconium side. The weld area showed no other signs of increased corrosion attack. The tests are being continued.

BM: **VI-D** (Recent Bureau of Mines zirconium prepared from zirconium oxide purified by salicylic acid treatment at Y-12; oxide converted to sponge and resistance-melted in graphite crucible). This zirconium represents recent Bureau of Mines production material, and therefore much emphasis has been placed on the determination of its corrosion resistance in uranyl sulfate at elevated temperatures.

One sample was tested in an as-machined condition in 0.17 *M* uranyl sulfate at 250°C; at the end of two weeks, black specks, apparently uranium oxides, were observed on the samples and the test was discontinued. The sample increased in weight from 21.2 mg/dm^2 at the end of the first week to 269.6 mg/dm^2 at the end of the second week. The great increase in weight was due obviously to the heavy deposits of adhering uranium oxides.

Another set of duplicate specimens, run independently, were polished on all sides using Nos. 80 and 120 paper, and exposed to 0.17 *M* uranyl sulfate contained in silica tubes at 250°C. The samples were inspected weekly, and fresh sulfate solution was used each week. The results are shown in Fig. 49. The samples reacted similarly for 21 weeks of the test, but after the following two weeks one showed an abrupt weight increase while the other showed a pronounced weight decrease. The corrosion rate of the latter, after 23 weeks, was 0.17 mil/week; the weight-gain rate for the other specimen was 0.75 mg/dm^2/day. Both samples remained light gray in color throughout the tests, which are being continued.

A sample of VI-D zirconium was etched in 5% hydrofluoric acid at room temperature for 5 min and then exposed to 0.17 *M* uranyl sulfate (in a silica tube) at 250°C for 23 weeks. The solution was changed weekly. The cumulative weight change data are shown in the following table:

DECLASSIFIED X-29-37

DWG. 10127

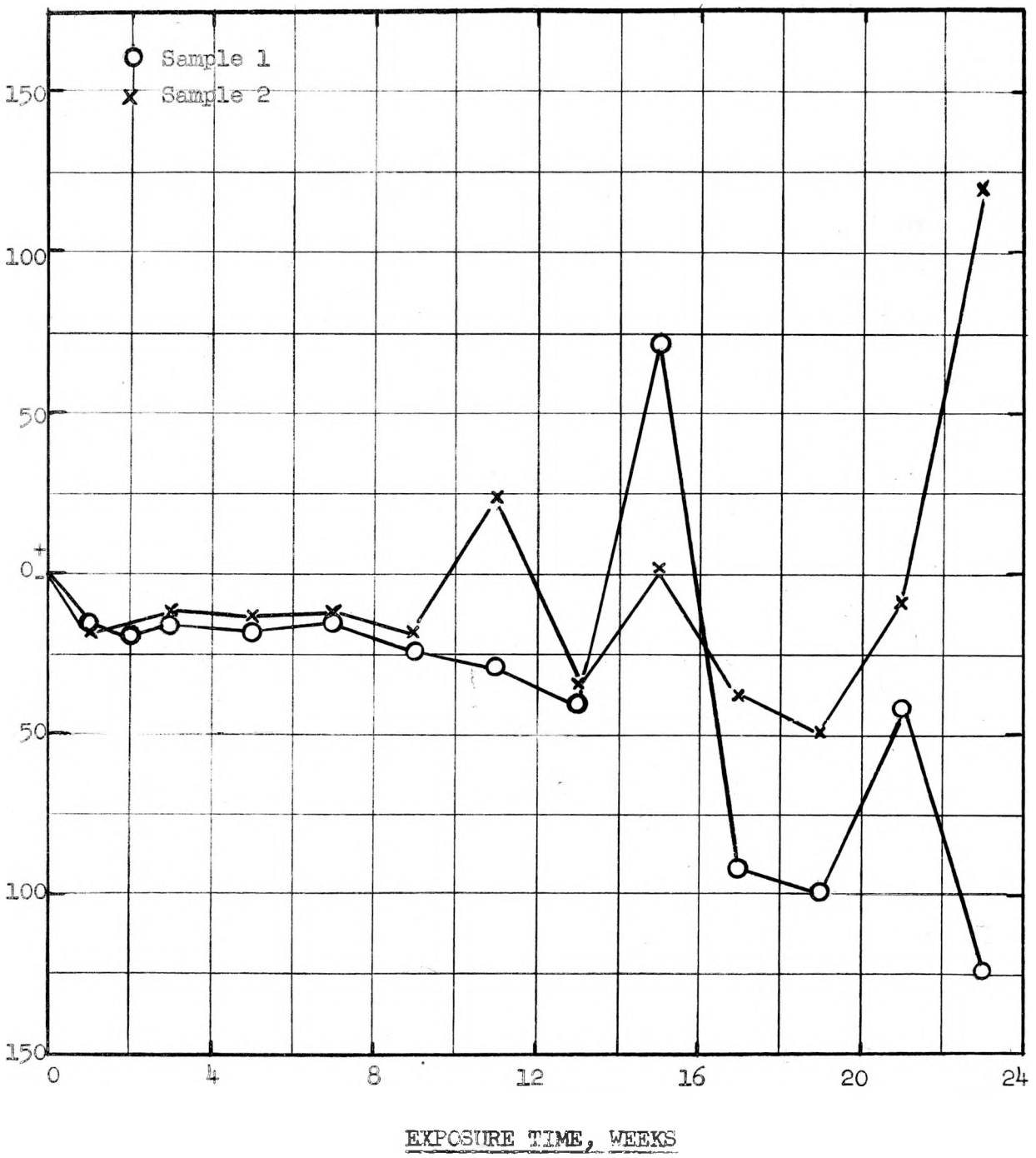

Figure 49. The Corrosion Resistance of Bureau of Mines Zirconium (VT-D) in 0.17M Uranyl Sulfate at 250°C

DECLASSIFIED X-29-38

EXPOSURE (weeks)	WEIGHT CHANGE (mg/dm^2)
1	0.0
2	-2.6
3	-6.5
5	+9.1
7	+18.1
9	-11.7
11	+141.8
13	+133.4
15	+296.6
17	-129.5
19	-147.6
21	+15.5
23	-47.9

These data were quite erratic, and no definite trends or patterns were established. Again, the corrosion behavior appears to be a function of cyclic film formation and dissolution. There appeared to be no particular advantage in etching the specimen as compared to corrosion results on polished and non-etched samples. The corrosion rate of this etched specimen was 0.07 mil/year after 23 weeks. There was a soft-gray-colored film on the sample.

Another sample of VI-D zirconium was polished and pretreated in 1% nitric acid at 250°C for 24 hr. This treatment of the zirconium was more severe than that encountered in pretreating stainless steels; the weight loss was 0.10 mg/cm^2, equivalent to a corrosion rate of 4.7 mils/year, or a metal thickness of 0.008 mil in 24 hr. The cumulative weight changes are plotted below for 15 weeks in 0.17 *M* uranyl sulfate at 250°C.

EXPOSURE (weeks)	WEIGHT CHANGE (mg/dm^2)
1	-10.4
2	-13.8
3	-6.9
5	-2.6
7	+13.0
9	+18.1
11	+18.1
13	+20.7
15	+15.6

SECRET
UNCLASSIFIED X-29-39

The sample had a uniform light-gray-colored film throughout the entire test. There were no indications of any reduction of the uranyl sulfate solution. The test is being continued.

Figure 50 shows a comparison of the corrosion resistance of Bureau of Mines zirconium samples, VI-D, which were treated by different procedures before being exposed to 0.17 *M* uranyl sulfate at 250°C. Sample *A* was polished only, using Nos. 80 and 120 emery paper; sample *B* was etched for 5 min in 5% hydrofluoric acid at room temperature; and sample *C* was polished and pretreated for 24 hr in 1% nitric acid at 250°C. It is readily seen that sample *C* shows by far the best corrosion resistance in the sulfate medium. The weight change—time curve is very regular and consists of an initial period of slight weight loss followed by a period of slight weight gain. The other two samples exhibited very erratic behavior after a period of nine weeks. The behavior of all three specimens was somewhat similar during the first nine weeks of testing, but then samples *A* and *B* differed widely in their corrosion characteristics as compared to sample *C*. Sample *B* showed a very large weight increase during the 9- to 15-week period, which was followed by a drastic loss in weight during the 15- to 17-week period. This phenomenon indicates that a complete breakdown of the surface-layer film may have occurred, resulting in severe weight losses by corrosion attack.

A series of tests was conducted with Bureau of Mines zirconium IC-235, containing 0.86% niobium. The metal was prepared by arc-melting, using a zirconium electrode low in hafnium content and impregnated with niobium. The metal was tested in a cold-rolled condition, 0.050 in. thick. The chemical analysis of the material was as follows:

Aluminum	<0.01%	Carbon	0.012%
Iron	>0.60	Nitrogen	0.011
Magnesium	0.001	Chloride	0.002
Titanium	0.04	Columbium	0.86

The samples were treated by different methods prior to exposure in 0.17 *M* uranyl sulfate at 250°C. The surface preparations were:

Sample *A*: degreased only

Sample *B*: degreased and etched 5 min in 5% hydrofluoric acid at room temperature

DECLASSIFIED X-29-40

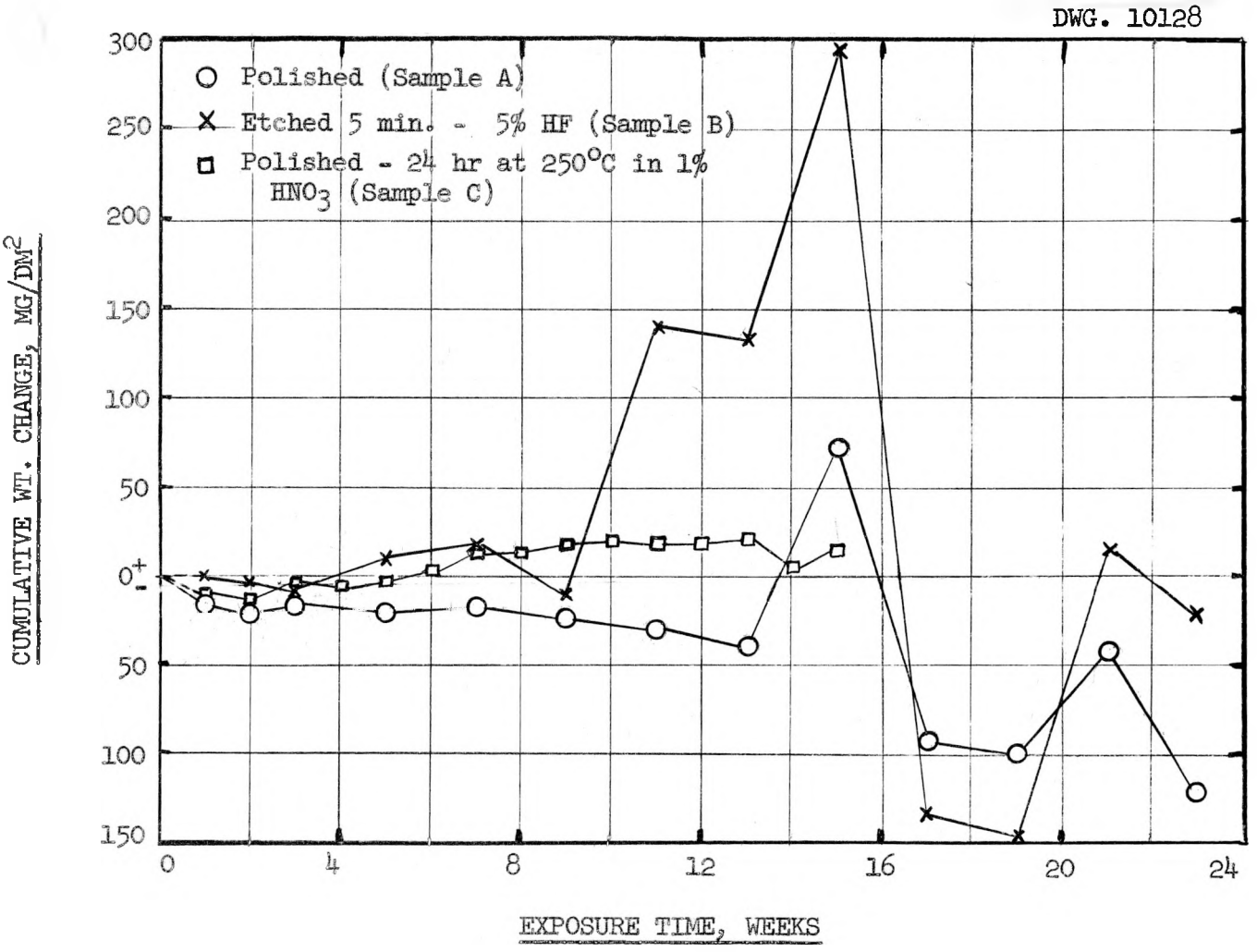

Figure 50. The Effect of Initial Preparation on the Corrosion Resistance of Bureau of Mines Zirconium (VI-D) in 0.17M Uranyl Sulfate at 250°C

DECLASSIFIED X-29-41

Sample *C*: degreased and pretreated for 24 hr in 1% nitric acid at 250°C (weight gain, 1.1 mg/dm^2)

Sample *D*: degreased, etched 5 min in 5% hydrofluoric acid at room temperature, and pretreated 24 hr in 1% nitric acid at 250°C (weight loss, 1.2 mg/dm^2 in nitric acid pretreatment)

Sample *E*: degreased and pretreated 24 hr in 2% chromic acid anhydride at 250°C (weight gain, 3.0 mg/dm^2)

Figure 51 is a graph of the cumulative weight changes as a function of exposure time for the five specimens. The tests have not been in operation long enough to permit any conclusive statements as to the merits of the various pretreatments. Samples *D* and *E*, nitrate and chromate pretreatments, respectively, did show substantial weight increases during the first two weeks of the test, which were followed by rather abrupt weight losses. Sample *B*, etched with hydrofluoric acid, also showed a steady weight increase during the course of the test. Samples *A* and *C* showed slight initial weight increases which were followed by fast-increasing weight losses. All samples exhibited a pinkish-white color during the tests except the chromate-treated specimen, which was dark gray in color. The weight changes for the five specimens are given below.

EXPOSURE (Weeks)	WEIGHT CHANGE (mg/dm^2/day)				
	A	*B*	*C*	*D*	*E*
1	+1.0	+1.5	+0.5	+1.5	+1.2
2	+1.1	+1.2	+0.8	+3.5	+6.9
3	+1.2	+1.4	+0.3	+1.1	+0.7
4	+1.0	+1.4	-0.4	+1.3	-0.4
5	+0.1	+1.6	-1.0		
6	-0.4	+1.5			
7	-0.8				

Corrosion Resistance of Reflector Materials

Corrosion studies have continued with materials to be used in the D_2O-cooled reflector. The reflector shell is a forged carbon steel, ASTM A-105-46, grade 1.

DECLASSIFIED X-29-42

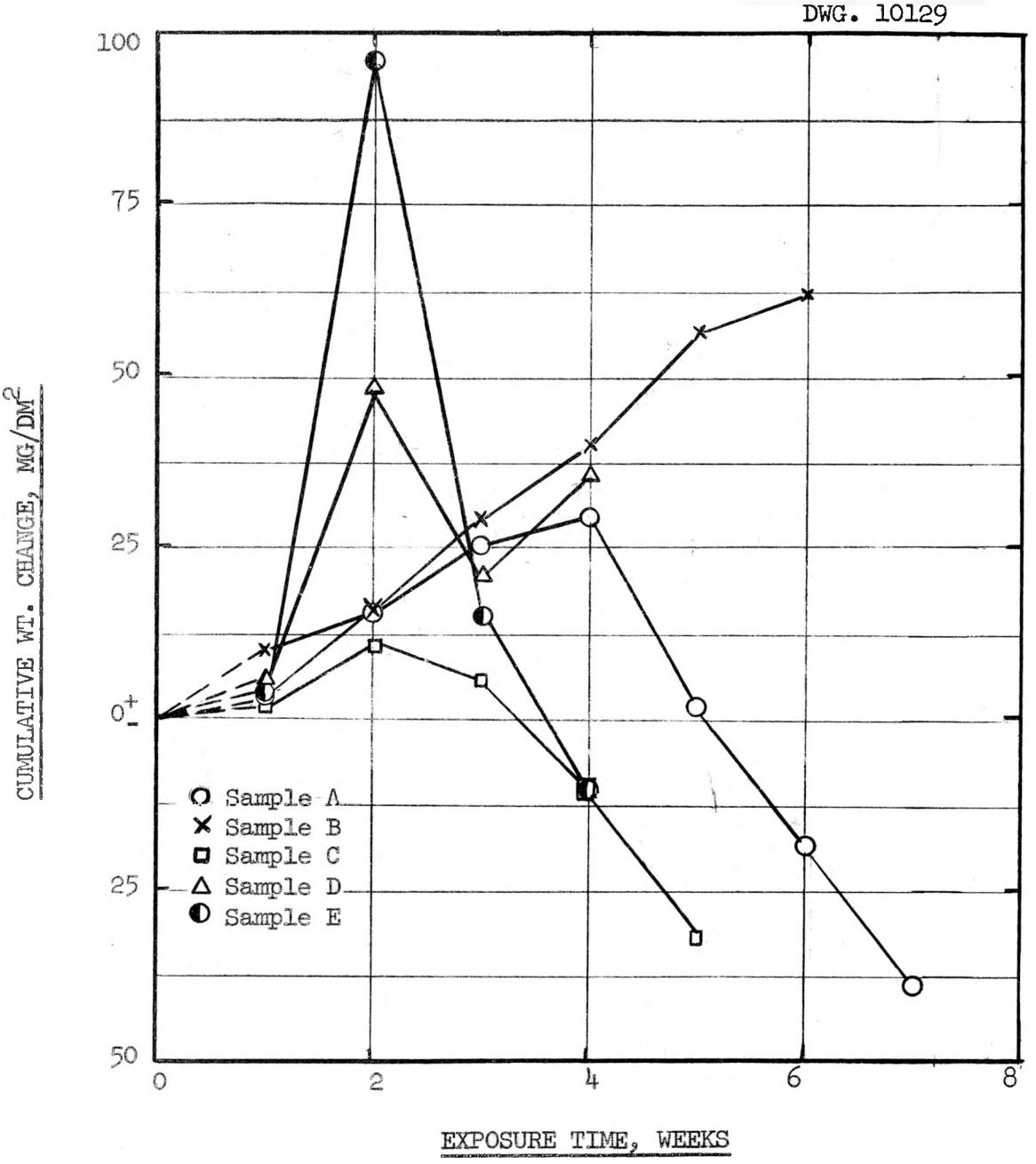

Figure 51. The Effect of Surface Preparation on the Corrosion Resistance of Bureau of Mines Zirconium (IC-235) Exposed to 0.17M Uranyl Sulfate at 250°C

DECLASSIFIED X-29-43

The corrosion problem in the reflector system will be largely dependent upon the D_2O_2 formation by irradiation and the subsequent presence of oxygen, free and dissolved, from the decomposition of the peroxide. High concentrations of either or both of these constituents will promote corrosion attack on carbon steel to a great extent. The general practice in the operation of industrial steam boilers is a combination of low oxygen concentration and high water *p*H to minimize corrosion.

The use of highly alkaline water for a homogeneous reactor reflector system is not practical as long as the system contains aluminum, such as Boral, (aluminum-boron carbide) in the neutron-absorbing plates in the shim controls.

Corrosion data on type 1030 carbon steel at 100°C were presented in the *Homogeneous Reactor Experiment Quarterly Progress Report for Period Ending August 31, 1950* (ORNL-826). Tests at 200°C, the probable maximum temperature in the reflector system, are summarized in this report.

A set of specimens was etched in 6 *N* hydrochloric acid containing 3% Rodine-60 as a corrosion inhibitor. After washing and weighing, the samples were exposed to distilled water at 200°C for 12 weeks. The samples were inspected weekly, and the test water was replaced with new at each inspection period. The initial water *p*H ranged from 5.1 to 5.5; the final water *p*H, at the end of the weekly runs, averaged 6.3 to 6.8. The specimen areas were 20.3 cm^2. Average weight losses vs. time are shown in Fig. 52, as is the corrosion rate, as a function of time. These tests were conducted under stagnant conditions. Corrosion attack progressed in a rapid fashion and followed an exponential type of curve when plotted on semilogarithmic paper. During the test, the specimens remained shiny black in color and did not appear badly corroded. A maximum corrosion rate of 2.4 mils/year was observed after 8.6 weeks; the corrosion rate at the end of the test, 12.6 weeks, was 1.4 mils/year. It should be mentioned that no attempt was made to de-gas the test water prior to the start of each weekly run.

In an effort to determine the effect of increasing the water *p*H on the corrosion resistance of 1030 carbon steel, tests were run in which the initial water *p*H was adjusted to 10.0 to 10.5 with sodium hydroxide. The tests were operated at 200°C, were inspected weekly, and had the test water replaced with new at each inspection period. Stagnant conditions were employed. The initial water *p*H averaged 10.2; the final water *p*H at the end of each week's

DECLASSIFIED X-29-44

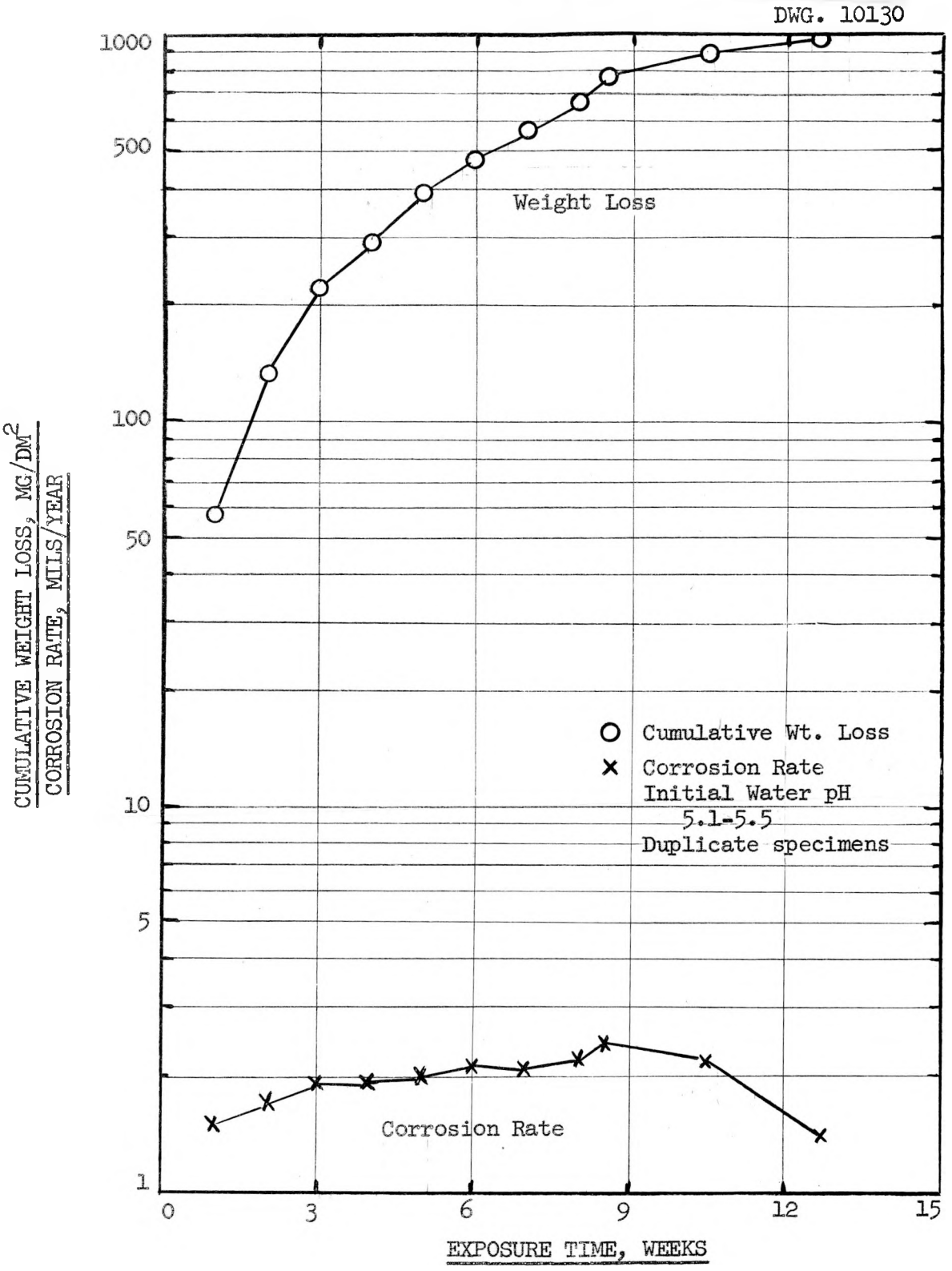

Figure 52. The Corrosion Behavior of 1030 Carbon Steel in Distilled Water at 200°C

DECLASSIFIED X-29-45

test was 7.8 to 8.2. One specimen, sample 1, was polished with No. 80 and with No. 120 emery paper before testing; sample 2 was etched 5 min in 6 *N* HCl–Rodine solution at room temperature and rinsed in alkaline solution. Both specimens were degreased before weighing. A comparison of the corrosion resistance of the samples is shown in Fig. 53. Initial corrosion attack on the etched specimen was greater than that on the nonetched sample, but, as the test proceeded, this situation was reversed. The cumulative weight loss on the etched sample was 234.0 mg/dm^2 as compared to 393.1 mg/dm^2 on the nonetched sample. These results are based on 7.6 weeks of exposure. Corrosion rates of the carbon steel were 1.36 and 0.87 mils/year for the nonetched and etched specimens, respectively. The sample condition in both cases was fairly good. There were no bulky, rust-colored corrosion products visible, but instead the surfaces were shiny with a few rough black-brown streaks.

The effect of increased water *p*H was investigated still further by exposing carbon-steel specimens at 200°C distilled water made 0.01 *N* in sodium hydroxide. The initial water *p*H was 11.7; the water *p*H at the end of each week's test dropped to 10.1 to 10.2. Fresh test water was used weekly and stagnant test conditions were maintained. Initial corrosion data with type 1030 carbon-steel specimens have been excellent for a period of approximately five weeks with these test conditions. The data are tabulated below.

EXPOSURE (hr)	WEIGHT CHANGE (mg/dm^2)	CORROSION RATE (mils/year)
96	+13.1	
264	+9.0	
432	-1.6	0.09
600	-2.5	0.10
768	-2.5	0.08

The sample condition was excellent at the end of the test period. All surfaces were covered with a glossy blue-colored film. No evidences of corrosion attack were detected. A slight weight gain was observed during the first 264 hr, after which very slight corrosion attack occurred. Although the corrosion resistance of the carbon steel is greatly minimized by employing water of *p*H 11.5 to 11.7, the use of highly alkaline water would not be practical if other metals or alloys such as aluminum were present in the system.

DECLASSIFIED X-29-46

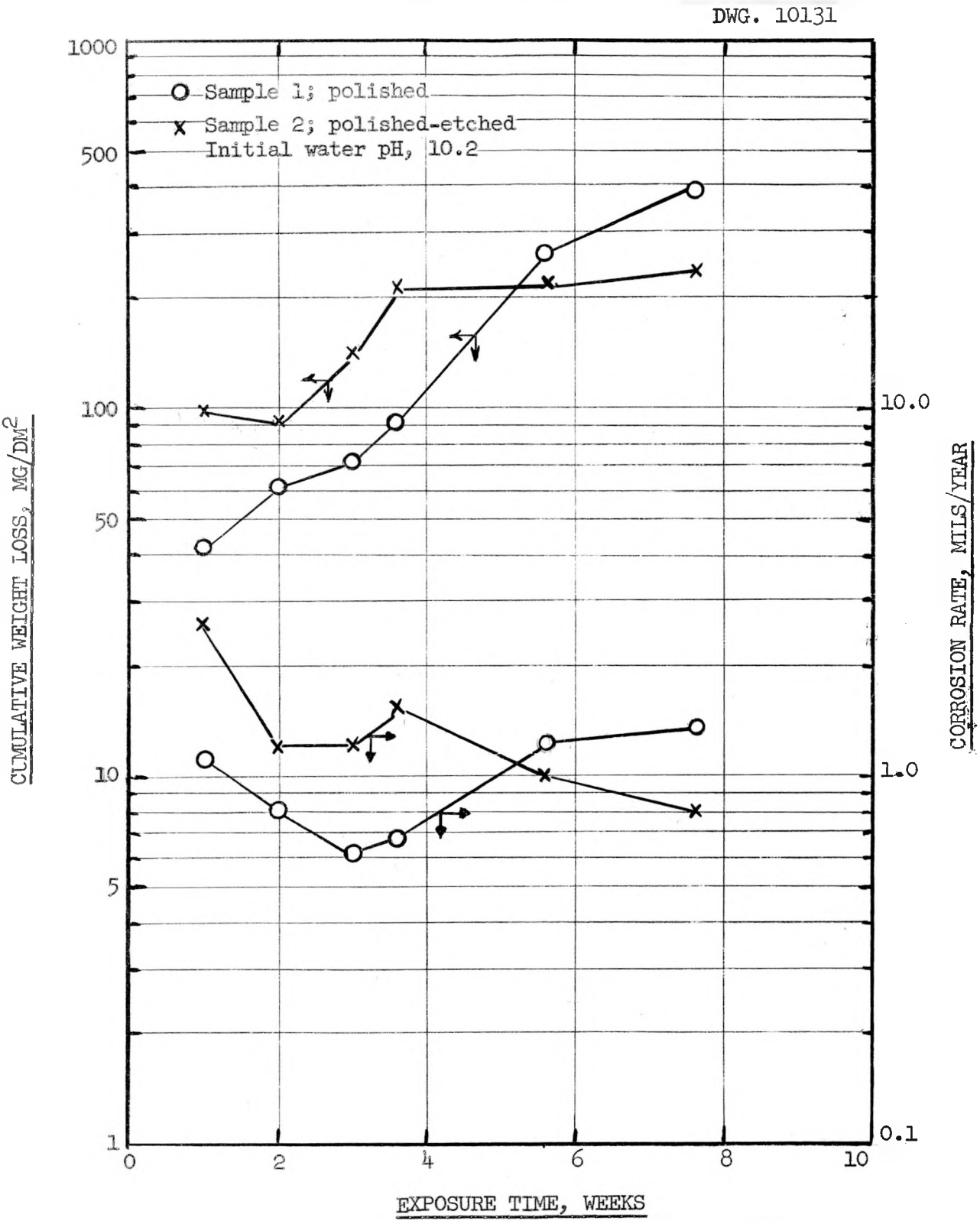

Figure 53. The Corrosion Behavior of 1030 Carbon Steel in Distilled Water at 200°C

DECLASSIFIED X-29-47

Several tests have been in operation to determine the corrosion resistance of 1030 carbon steel in distilled water at 200°C containing a small concentration of hydrogen peroxide. Samples were run in distilled water containing 0.005 *M* hydrogen peroxide and at two ranges of *p*H, 5.5 to 6.5 and 10.0 to 10.5. Duplicate specimens were used which were first etched in HCl-Rodine solution for 5 min followed by an alkaline rinse. Care was taken to assemble the test bombs rapidly after adjusting the peroxide solution to the higher *p*H since alkalinity acts to accelerate hydrogen peroxide decomposition. The tests were run under stagnant conditions. The data are plotted in Fig. 54. For the two ranges of *p*H there was not any great difference in the corrosion behavior of the specimens. However, after eight weeks the high *p*H test specimen was being corroded at a slower rate than the low *p*H sample. The corrosion rate curve for the *p*H 5.5 to 6.5 water test sample was very regular and dropped off exponentially with increasing time; at the end of 13 weeks the rate had decreased from 7.2 to 1.4 mils/year. The corrosion rate of the *p*H 10.0 to 10.5 specimen was 1.6 mils/year after eight weeks. The surfaces of this specimen were dull, stained, and black streaked in appearance. The *p*H 5.5 to 6.5 specimen was streaked and dull black in appearance. There were no bulky deposits of corrosion products visible.

Galvanic-couple tests with 2S aluminum and 1030 carbon steel were run at 200°C in distilled water with and without 0.005 *M* hydrogen peroxide under stagnant conditions. Samples were bolted together by means of a 2S-aluminum nut and bolt. The initial water *p*H was 5.5 to 6.5; fresh water was used weekly. The carbon-steel specimens were etched 5 min in HCl-Rodine solution before exposure to the test solution. Weight losses and corrosion rates are plotted as a function of the exposure time in Fig. 55. The corrosion resistance of the carbon steel decreased with 0.005 *M* hydrogen peroxide present in the water, as shown in Fig. 55. In both tests, with and without hydrogen peroxide, weight losses increased rapidly for a period of seven weeks, after which time a general decrease in the intensity of corrosion attack was observed. The 1030 carbon steel was attacked preferentially in both cases, with more severe attack occurring in the peroxide water. The 2S aluminum, with no peroxide present, showed slightly increasing weight gain throughout the course of the test, which lasted eight weeks. This specimen was black in color on the area contacting the carbon steel and dull gray on all other surfaces. There were no indications of localized corrosion attack on any of the surfaces.

DECLASSIFIED X-29-48

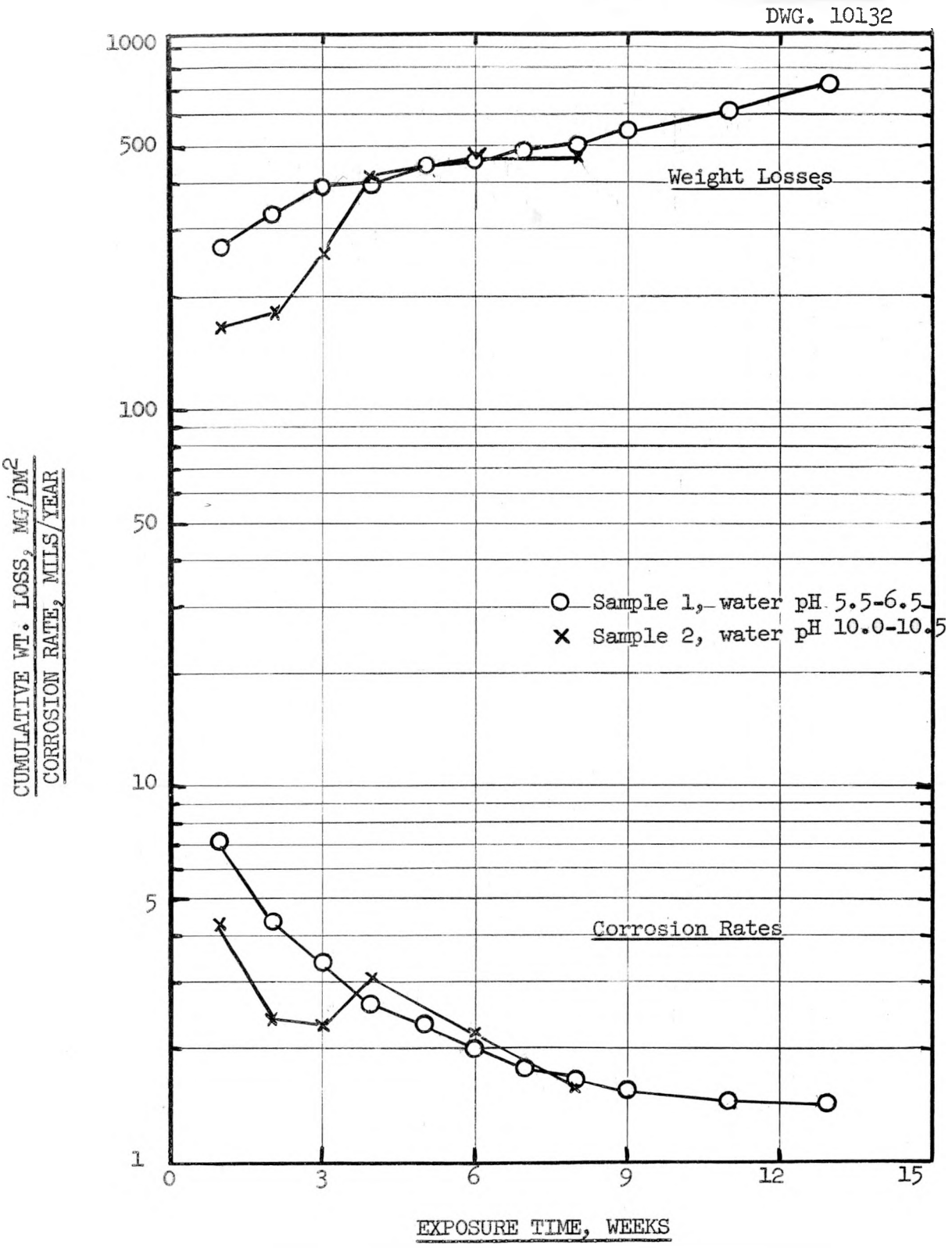

Figure 54. The Effect of Water pH on the Corrosion Resistance of 1030 Carbon Steel at 200°C in Distilled Water Containing 0.005M Hydrogen Peroxide

DECLASSIFIED X-29-49

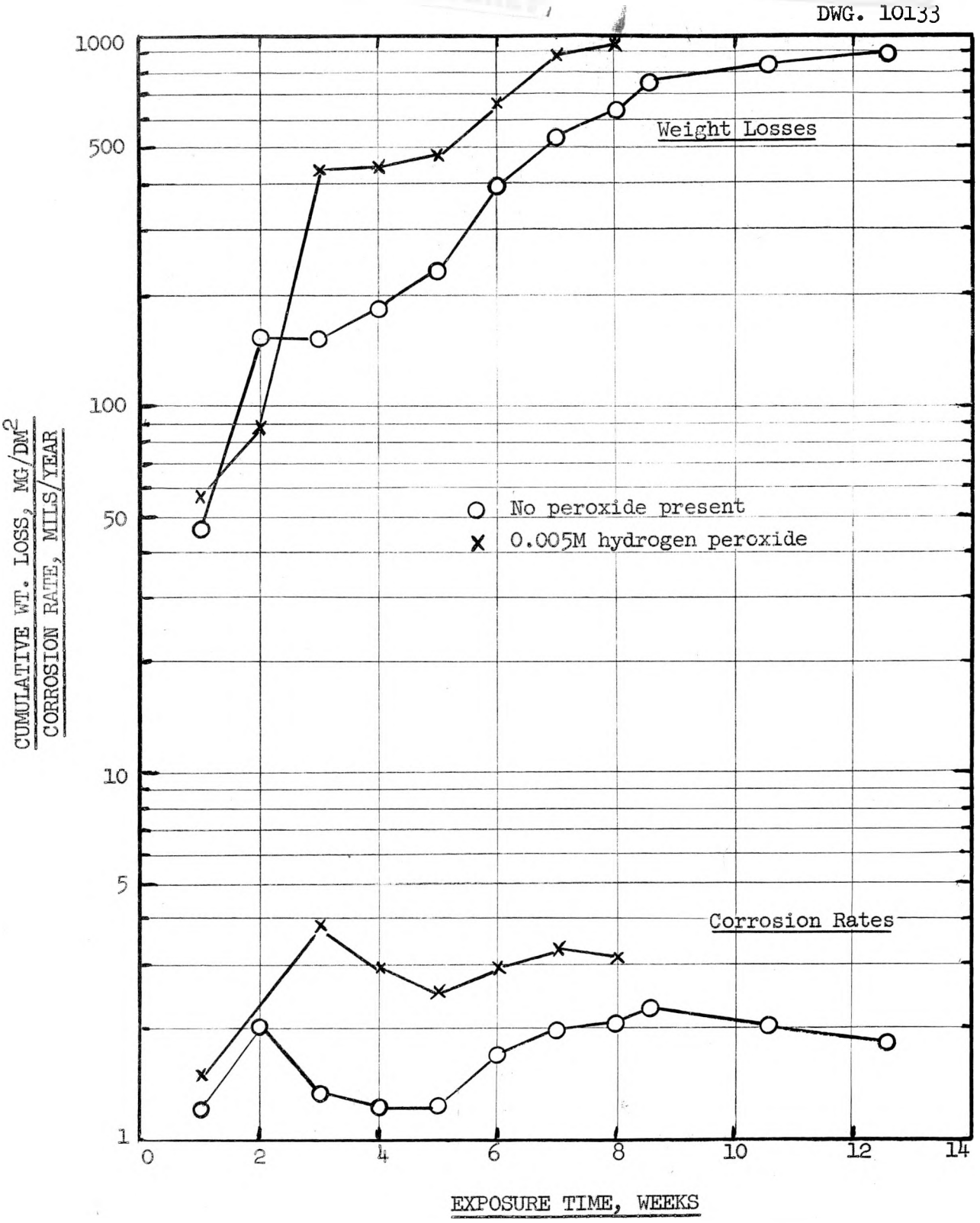

Figure 55. The Effect of Hydrogen Peroxide in Distilled Water on the Galvanic Corrosion Behavior of 1030 Carbon Steel in Contact With 2S Aluminum at 200°C

DECLASSIFIED X-29-50

The aluminum specimen contacting the carbon steel in the 0.005 *M* peroxide water was badly pitted on all surfaces except the contact area. The carbon steel sample with no peroxide present was discolored black and showed a shiny film on all surfaces; the specimen exposed to the peroxide water was coated with a black film and had numerous rusted areas. Data from the aluminum and carbon steel specimens are given in Table 16.

TABLE 16

The Corrosion of 1030 Carbon Steel—2S Aluminum Galvanic Couples in Distilled Water at 200°C

EXPOSURE (weeks)	NO PEROXIDE				0.005 *M* HYDROGEN PEROXIDE			
	2S ALUMINUM		1030 CARBON STEEL		2S ALUMINUM		1030 CARBON STEEL	
	($mg/dm^2/day$)	(mils/year)	($mg/dm^2/day$)	(mils/year)	($mg/dm^2/day$)	(mils/year)	($mg/dm^2/day$)	(mils/year)
1	+7.5		-6.7	1.2	+1.3		-8.1	1.5
2	+4.4		-11.1	2.0	-9.3	4.9	-6.2	1.1
3	+2.9		-7.3	1.3	-5.3	2.8	-20.7	3.8
4	+2.5		-6.7	1.2	-2.3	1.2	-15.7	2.9
5	+2.1		-6.6	1.2	-1.4	0.7	-13.4	2.5
6	+1.9		-9.3	1.7	-1.2	0.6	-15.7	2.9
7	+1.7		-10.8	2.0	-1.0	0.5	-17.9	3.3
8	+1.6		-11.4	2.1	-1.1	0.6	-17.0	3.1
8.6	+1.5		-12.6	2.3				
10.6	+1.2		-11.3	2.1				
12.6	+1.0		-10.1	1.9				

Although it has long been established that the dichromates and chromates undergo reduction to trivalent chromium compounds under irradiation, a group of tests was run with 1030 carbon steel—2S aluminum couples in distilled water, with and without 0.005 *M* hydrogen peroxide, at 200°C, and containing sodium chromate. Previous tests at 100°C with aluminum-steel couples in distilled water, with and without peroxide, had established that a minimum concentration of sodium chromate to reduce corrosion attack was 125 ppm. This concentration was used in the 200°C tests. The test solutions were replaced with new solutions every time the tests were stopped for sample inspection. Figure 56 shows the corrosion data for both the carbon steel and the aluminum alloy under both conditions of testing. In the absence of hydrogen peroxide the 2S-aluminum alloy was attacked preferentially and the 1030 carbon steel

DECLASSIFIED X-29-51

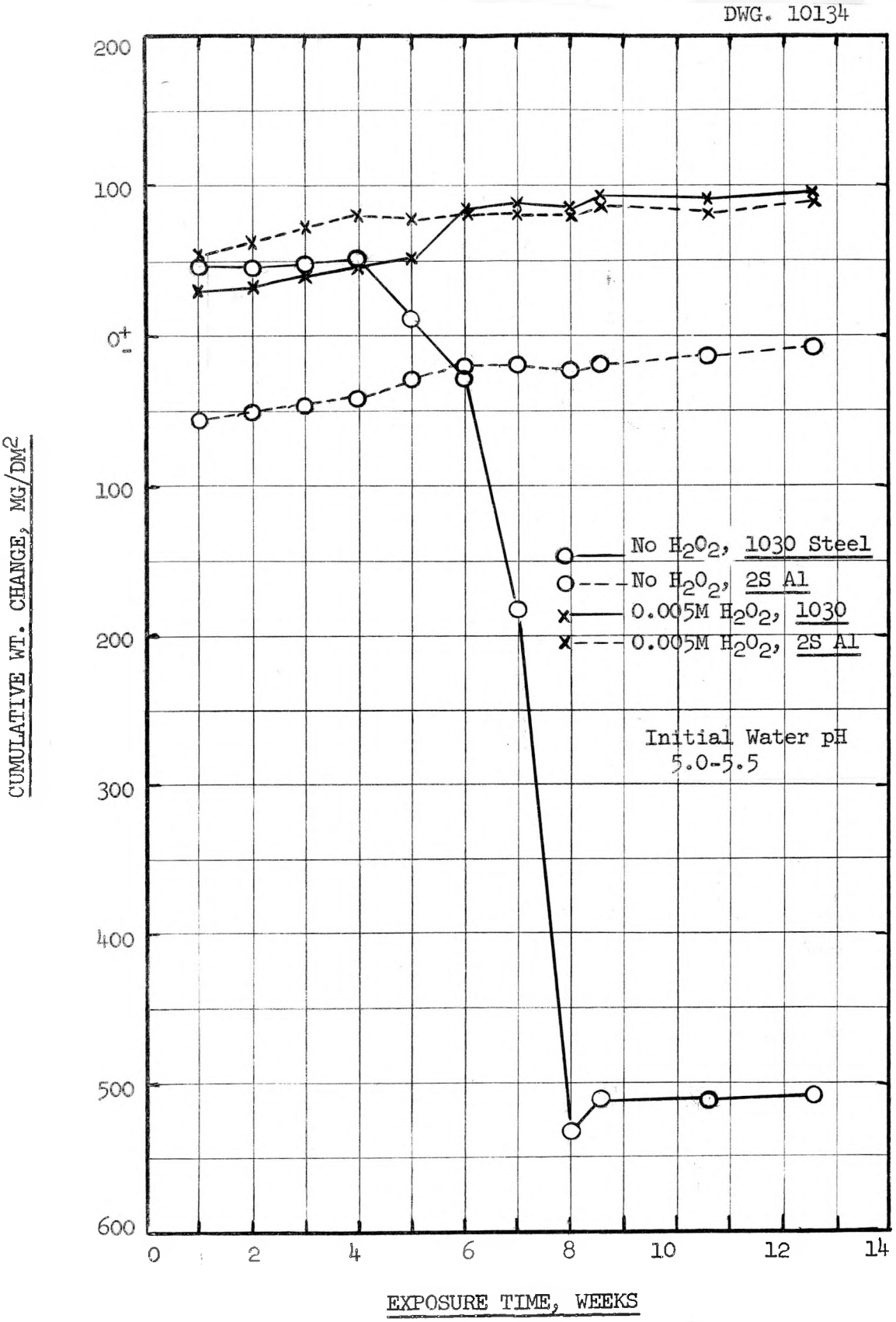

Figure 56. The Effect of Hydrogen Peroxide in Distilled Water Containing 125 ppm Sodium Chromate on the Galvanic Corrosion Behavior of 1030 Carbon Steel in Contact with 2S Aluminum at 200°C

DECLASSIFIED
X-29-52

exhibited weight gains. This relation continued for six weeks, and then a direct reversal of behavior was observed. The carbon steel became the anodic member of the couple while the aluminum continued to show very slight weight losses as in the first six weeks of the test. With 0.005 *M* hydrogen peroxide present in the test solutions, the corrosion resistance of both the aluminum and carbon steel was greatly enhanced by the presence of 125 ppm of sodium chromate. Both specimens exhibited slight, fairly constant weight increases during the 13 weeks of exposure. In this test the carbon steel surfaces were shiny black in color; the aluminum surfaces were gray on the outside and brown-black on the contact surface. There were no signs of localized corrosion attack on either specimen. Thus, from these data, the presence of 125 ppm of sodium chromate was effective as a corrosion inhibitor only when hydrogen peroxide was present in the solution. Without hydrogen peroxide present, the carbon steel was attacked preferentially and there was also corrosion attack on the 2S aluminum. For these specimens, corrosion rates, at the end of 13 weeks were 1.1 mils/year for the 1030 carbon steel, and 0.04 mil/year for the 2S aluminum.

The galvanic corrosion behavior of Bureau of Mines zirconium and 2S aluminum was also determined in distilled water at 200°C. Tests were run for 21 weeks under stagnant conditions; fresh water was used each time the tests were stopped for sample inspection (every two weeks). The initial water *p*H was 5.0 to 6.0. A summation of the data is presented in Fig. 57. Both samples exhibited weight increases during the entire time of the test. The increase of the aluminum sample was always greater than that of the zirconium specimen. The weight-gain rates after 21 weeks were 0.36 mg/dm^2/day for the zirconium and 0.61 mg/dm^2/day for the 2S aluminum. Both specimens were in excellent condition at this time; the aluminum was gray in color and the zirconium was dark gray in appearance. There were no evidences of pitting corrosion attack on the contact areas or the outer surfaces.

Miscellaneous Corrosion Studies Involving Uranyl Sulfate Systems

Titanium and Tantalum. Much consideration has been given to the corrosion resistance of materials which could be used as possible substitutes for stainless steel in component parts of a homogeneous reactor. Two materials, titanium and tantalum, have showed excellent promise although their cross

DECLASSIFIED X-29-53

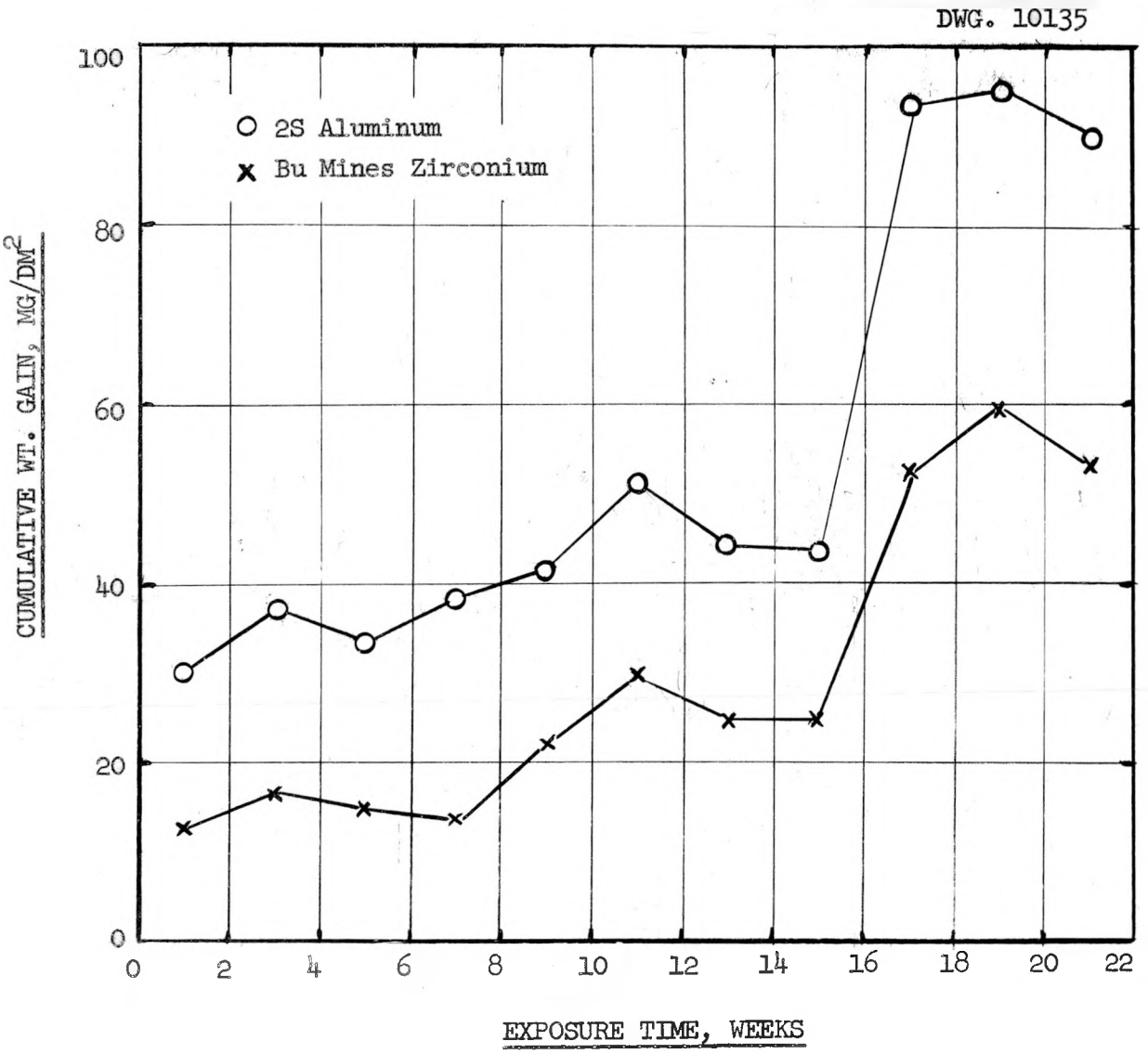

Figure 57. The Galvanic Corrosion Behavior of Bureau of Mines Zirconium and 2S Aluminum in Distilled Water at 200°C

DECLASSIFIED X-29-54

sections are relatively high as compared to zirconium or even stainless steel. Tests with these two materials have been in operation for 19 weeks in 0.17 *M* uranyl sulfate at 250°C under stagnant conditions. The corrosion data are shown in Fig. 58. The weight increases were greater for the tantalum specimen than for the titanium specimen. A slight corrosion rate for the titanium specimen was noted between the seventh and eighth week of exposure; this rate was 0.02 mil/year. After 13 weeks of the test, both samples tended to show leveling off to a constant weight gain for the ensuing six weeks. A tabulation of the weight-change rates for both materials is shown below.

EXPOSURE (weeks)	WEIGHT CHANGE ($mg/dm^2/day$) Titanium	Tantalum
1	+0.26	+2.90
2	+1.31	+2.10
3	+0.52	+1.00
4	+0.32	+0.80
5	+0.31	+0.70
6	+0.30	+0.75
7	+0.78	+1.38
8	-0.07	+0.95
9	+0.14	+1.32
11	+0.12	+0.63
13	+0.22	+0.36
15	+0.14	+0.31
17	+0.12	+0.27
19	+0.12	+0.25

The titanium specimen showed a very uniform film with a purple cast and no signs of corrosion attack or precipitation of uranyl sulfate. The tantalum specimen was gray-brown in color and was also in excellent condition. These samples will be submitted to the Optical Microscopy Section to determine whether or not uranium oxides are deposited on the surfaces in a fashion similar to the deposition on stainless-steel surfaces. If the mechanism of uranyl sulfate reduction on stainless-steel surfaces is attributed to the migration of iron atoms to the surface, there would be no reason to expect uranyl sulfate reduction on pure tantalum or titanium surfaces unless it was due to an additional unknown phenomenon.

Durimet 20. Durimet 20, a high-strength machinable austenitic stainless steel of the chemical composition

DECLASSIFIED X-29-55

SECRET

DWG. NO. 10136

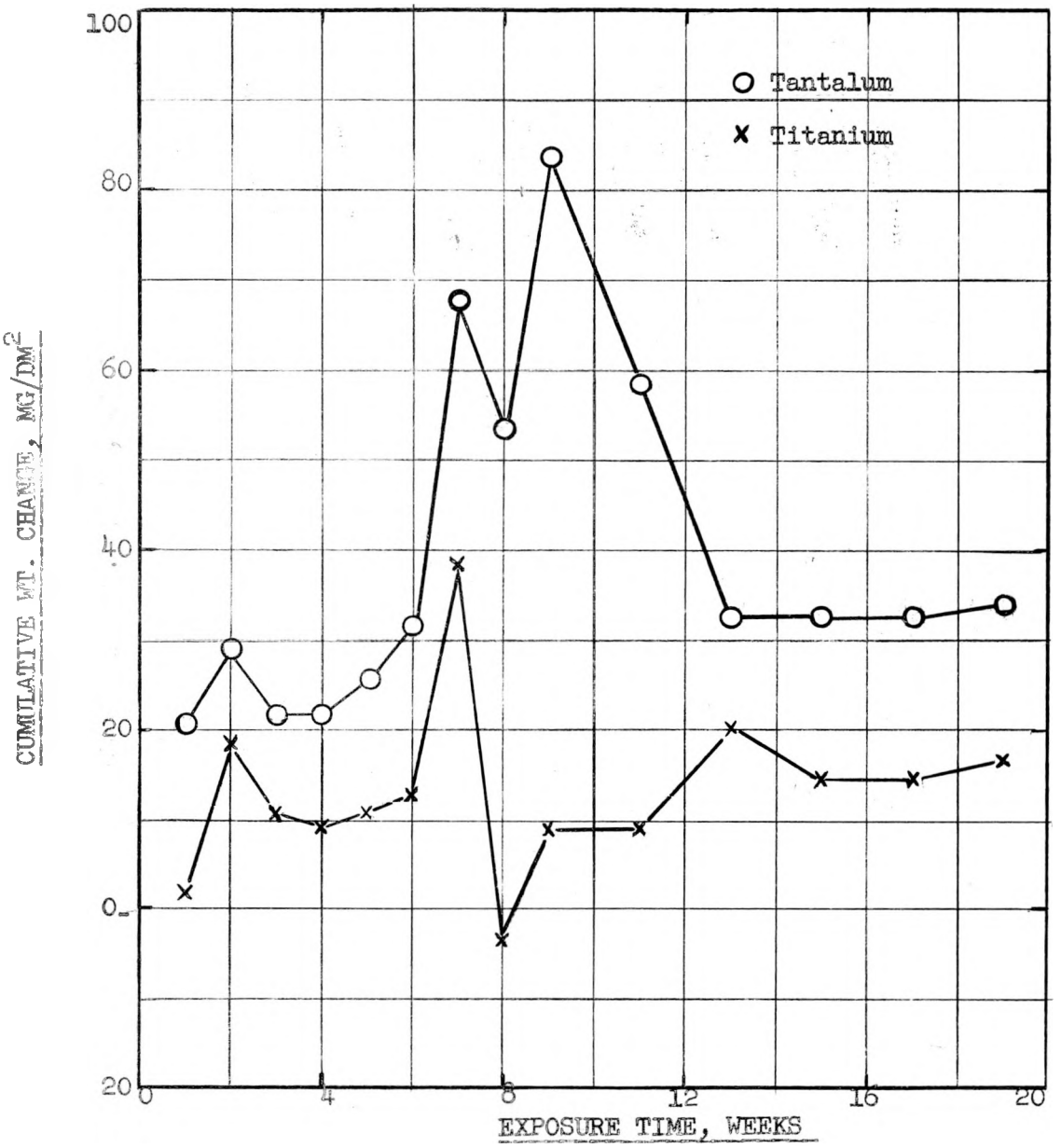

Figure 58. The Corrosion Behavior of Titanium and Tantalum in 0.17M Uranyl Sulfate at 250°C

DECLASSIFIED X-29-56

Nickel	29.0%	Copper	4.0
Chromium	19.0	Silicon	1.0
Molybdenum	3.0	Carbon	0.07 (max.)

was considered for intermediate-temperature operation, say 150°C, in uranyl sulfate solutions. A test was operated at 150°C in 0.17 *M* uranyl sulfate, changed weekly. Corrosion data appear in Fig. 59. The magnitude of corrosion attack on the specimen was slight, although a steady increase in weight loss started after the third week of exposure. The corrosion rate at the end of 12 weeks was 0.06 mil/year, and the sample retained a bright metallic luster during this time. The use of Durimet 20 at 150°C would offer a distinct advantage over stainless steels, since at this temperature the latter alloys in a non-pretreated condition are subject to fairly significant corrosion attack. The presence of 4% copper in the Durimet alloy greatly enchances the corrosion resistance of the material to sulfuric acid solutions. Durimet 20 is available in wrought and cast forms.

Durhy and Carboloy 44A. Two materials, Durhy and Carboloy 44A, were considered for use as possible bearing materials for the totally enclosed Westinghouse pump. Durhy is an extremely hard thermal-shock-resistant material used in the construction of turbine blades. It contains 36 to 44% silicon carbide, 44 to 55% silicon, and 6.4 to 8.9% carbon. Later information disclosed that where close tolerances are required, fabrication of the Durhy becomes extremely difficult. Carboloy 44A is a sintered metal carbide, essentially tungsten carbide bonded with cobalt, used for cutting tools. Tests were conducted in 0.17 *M* uranyl sulfate at 150°C. The Carboloy 44A alloy was found completely unsuitable for use in this medium; a cumulative weight loss of 7825.0 mg/dm^2 was observed at the end of 10 weeks, and there were evidences of solution reduction as shown by uranium analyses. The Durhy exhibited a cumulative weight loss of 318.8 mg/dm^2 for a 12-week period. No solution reduction was apparent, and the sample remained unchanged in appearance.

Type 440C Stainless Steel. Type 440C stainless steel, containing 16 to 18% chromium and 0.95 to 1.10% carbon, was checked in uranyl sulfate systems for corrosion resistance. This alloy was considered because of its high hardenability, Rockwell C 60-62, which would make it a good choice for bearing material. The results of tests in 0.17 *M* uranyl sulfate at 100 and 250°C

DECLASSIFIED X-29-57

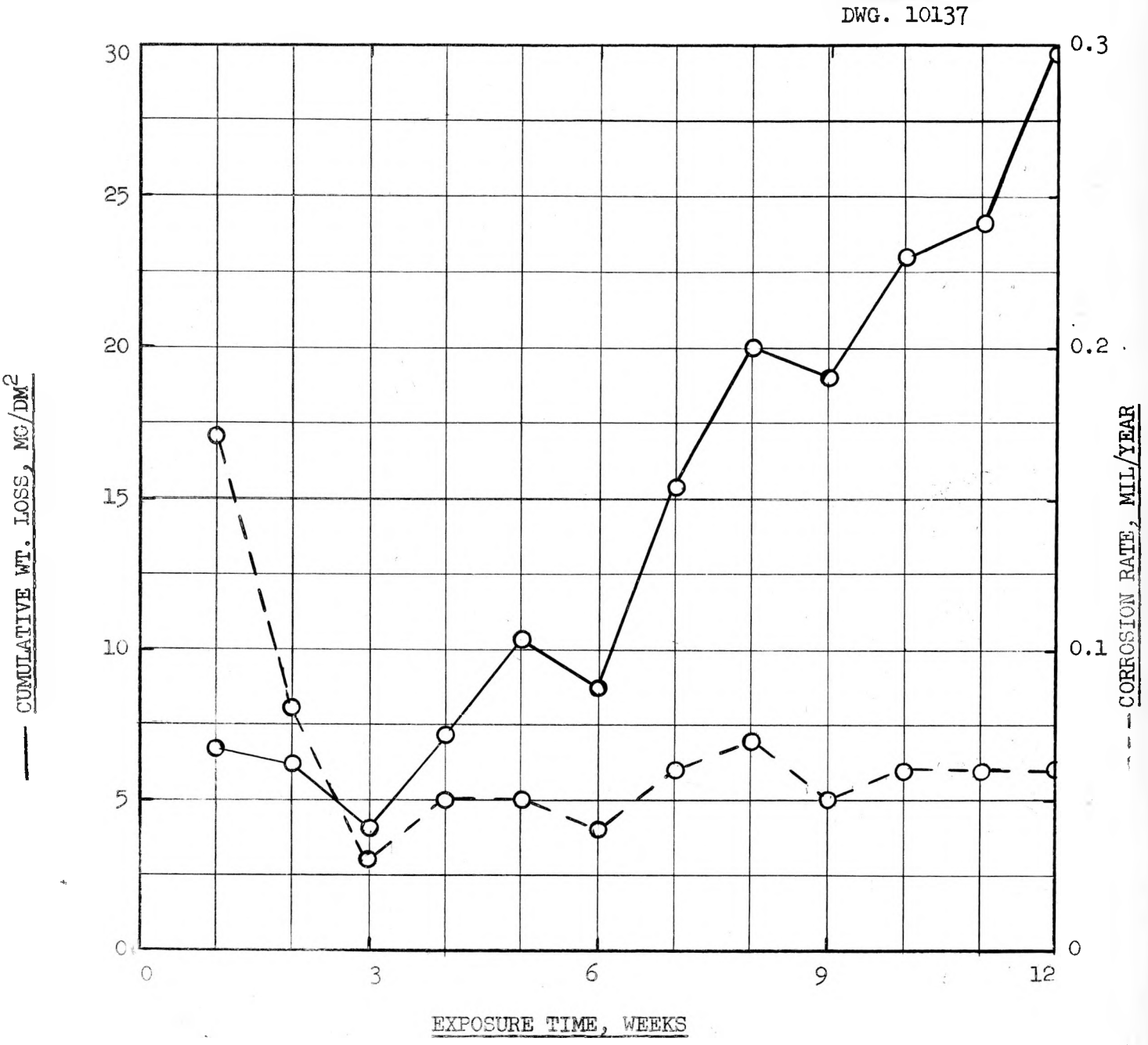

Figure 59. The Corrosion Behavior of Durimet 20 in 0.17M Uranyl Sulfate at 150°C

DECLASSIFIED X-29-58

were completely unsatisfactory. Severe corrosion rates, 135 mils/year, were encountered with all specimens, and complete solution reduction was observed and determined chemically in each case.

Uranyl Fluoride and Uranyl Nitrate Corrosion Studies

Preliminary corrosion studies have been initiated to determine the corrosion resistance of various materials in uranyl fluoride and uranyl nitrate systems. The major effort is being placed on the uranyl fluoride system at the present time.

Twenty metals and alloys, selected from a literature survey as having good resistance to fluoride solutions, are undergoing tests at temperatures of 100°C. Those materials which show promising corrosion resistance will then be exposed to temperatures of 150, 200, and 250°C in uranyl fluoride solution. One of the greatest problems in this investigation is to find a material sufficiently corrosion-resistant which may be used to fabricate a bomb or bomb liner to permit corrosion studies at the elevated temperatures.

Ten metals and alloys are undergoing tests in uranyl nitrate solutions containing 40 g of uranium per liter at 100°C. Metals showing good corrosion resistance will be exposed to higher temperatures. The maximum critical temperature for the uranyl nitrate—water system has been determined to be less than 200°C; at this temperature thermal decomposition occurs.

Several tests were run with uranyl nitrate solutions in stainless-steel bombs which had not been pretreated with nitric or chromic acid. The temperatures of these tests were 150 and 200°C. The tests were operated three to six days. In the 150°C test the uranium material balance was within the accuracy of the analytical uranium method, ±2%. The initial U(VI) concentration was 60 g/liter; the final total uranium content was 61.1 g/liter. The solution remained clear yellow in color throughout the test, but on the bottom of the test bomb there was observed a moderate mass of orange-colored crystals. These have been submitted to the Analytical Chemistry Division for chemical analysis. The uranyl nitrate solution exposed at 200°C in a stainless-steel bomb showed partial reduction; the initial uranium content was 60.0 g/liter, while the final uranium content was 34.5 g/liter. A light-green-colored precipitate was observed in the bottom of the test bomb; it has been submitted for identification.

DECLASSIFIED X-29-59

RADIATION STABILITY AND IN-PILE CORROSION

J. W. Boyle
F. J. Fitch
J. F. Manneschmidt
H. F. McDuffie
A. R. Olsen
D. M. Richardson
C. H. Secoy
M. D. Silverman
A. W. Smith
F. H. Sweeton

Summary

Twenty-two "in-pile" corrosion-irradiation tests of aqueous uranyl sulfate solutions in contact with only type 347 stainless-steel surfaces, carried out in the X-10 graphite pile during the past quarter, are discussed in this report. The stainless-steel surfaces had been either pretreated with 1% HNO_3, or with 2% CrO_3, or simply cleaned and etched prior to the experiments. Thirteen of the tests were classed as giving encouraging or successful results, seven as giving inconclusive results because of some abnormality during the run, and two as failures. Classification as being successful or having failed was on the basis of pressure-temperature-flux data recorded throughout the run; a successful run showed normal responses to temperature and flux changes and maintained appreciable pressures of hydrogen and oxygen in excess of steam pressure throughout the run; an unsuccessful run failed to maintain pressure in excess of steam pressure, suggesting that the uranium had been removed from solution. There is some evidence suggesting that the failures were associated with pile shutdowns. Available analytical data indicate that only very small amounts of tetravalent uranium and reduced sulfur are present at the end of a run.

Improvements in apparatus and technique during the past quarter now permit experiments to be carried out with greater safety and less loss of experimental data than previously. Additional facilities for radiation studies have been made available at hole 60 of the X-10 pile and placed in service.

In anticipation of the plans to do experiments at higher neutron flux in the MTR mock-up, a high-pressure testing area has been constructed. All experiments so far have been carried out at fluxes which, while not so high as those for which the HRE is designed, are considerably higher than those at which the HRE will operate until the system has been thoroughly tested. Thus, it is unlikely that deleterious radiation effects, the absence of which may be demonstrated in the present study, will be manifested at the low power levels which will characterize early operations of the HRE.

SECRET
UNCLASSIFIED X-29-60

Fundamental studies of films on stainless steel are underway, employing optical and electron microscopy. The results are reported in the section on Electron Microscopy.

Objectives

The major objectives of the group are to provide, in advance of the date of operation of the HRE, answers to the questions:

1. How long will the uranium remain in solution?
2. How long will the walls of the container remain protected from corrosion?

With the facilities available it is believed that solution corrosion data can best be obtained through experiments in stainless-steel bombs, made to withstand pressures encountered in the X-10 pile flux. Conditions as nearly as possible like those projected for the HRE are desired so as to minimize extrapolations, i.e., temperatures of 250 to 300°C are used, aqueous uranyl sulfate solutions containing 40 g of U^{235} per liter are placed in the bomb, type 347 stainless-steel surfaces are pretreated in accordance with techniques recommended by the Reactor Technology Divisions's corrosion group as being best for such solutions in the absence of radiation, and the highest possible neutron flux of the X-10 pile is used which is consistent with safety limits for the pressures in the bomb.

It is realized by the group, and should be made clear for the benefit of other workers, that these are essentially static experiments, whereas the HRE is to be a dynamic system. One very important factor in the dynamic system, the influence of flow upon corrosion, is being neglected. The study of this factor would probably require the HRE itself or an equally elaborate device for circulating hot uranium solutions inside the X-10 graphite pile.

Other objectives of the present study include determination of the effects of changes in pretreatment techniques, radiation intensity, concentration and enrichment of uranium, and temperature and type of uranium salt. Study of the causes of uranium precipitation and development of methods for preventing or reversing this effect are naturally of great interest, and all the information which is being gathered in the present study will be of value in these more fundamental efforts.

DECLASSIFIED X-29-61

Description of Experiments

General Technique. All experiments have been conducted by placing 5 to 8 ml of aqueous enriched uranyl sulfate solution inside a stainless-steel bomb, connecting the bomb to a Baldwin SR-4 pressure cell by means of a 20- to 30-ft length of small-diameter stainless steel tubing, placing the bomb inside a suitable furnace for temperature control, and exposing bomb and furnace to the neutron flux in the X-10 graphite pile. Pressure and temperature within the bomb are continuously recorded. Details of the bomb and fittings are given in Figs. 60 through 63.

Pile Facilities. During the past quarter experiments in hole 12 (a vertical hole) have continued. Three bombs may be exposed simultaneously in a single furnace in this hole. Hole 60 (a 4- by 4-in. horizontal hole terminating 1 ft from the pile core) has been made available and facilities have been constructed allowing a possible maximum of six bombs to be exposed simultaneously in this hole. One set of three experiments using three bombs was carried out in hole 11 (used by ANL and filled with water under pressure). Modifications of the ANL apparatus now in progress may facilitate use of this hole during the next quarter.

Experimental Information. As noted above, continuous records of the temperature and pressure are obtained throughout each run. The known position of the bomb in the pile, plus the record of the pile power, allows the flux to be calculated at all times during the run. Subtracting the steam pressure from the total pressure leaves a record of the pressure of hydrogen plus oxygen (plus inert gases) as a function of time, temperature, and pile power. Corrosion of the container is known to be accompanied by reduction of the uranium and precipitation as U_3O_8. Such precipitation would effectively prevent the formation of hydrogen and oxygen by preventing the fission fragments from traveling through the water. Accordingly, it may be inferred that, if the pressure within the bomb during an experiment falls to and remains at the value corresponding to steam pressure at the temperature of the solution, the uranium has been removed from the solution. Conversely, maintenance of a considerable pressure in excess of steam pressure is assumed to mean that the solution remains for the most part unaffected and in good condition.

DECLASSIFIED X-29-62

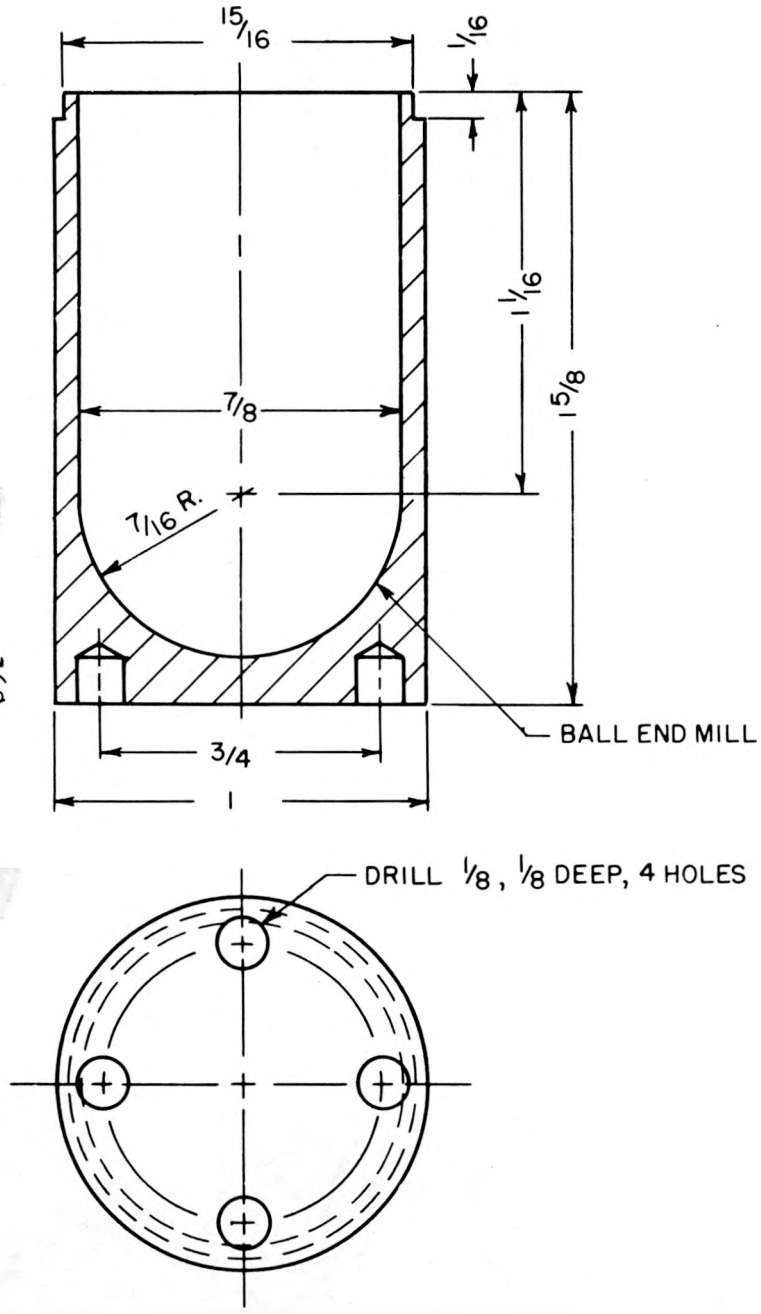

BOMB

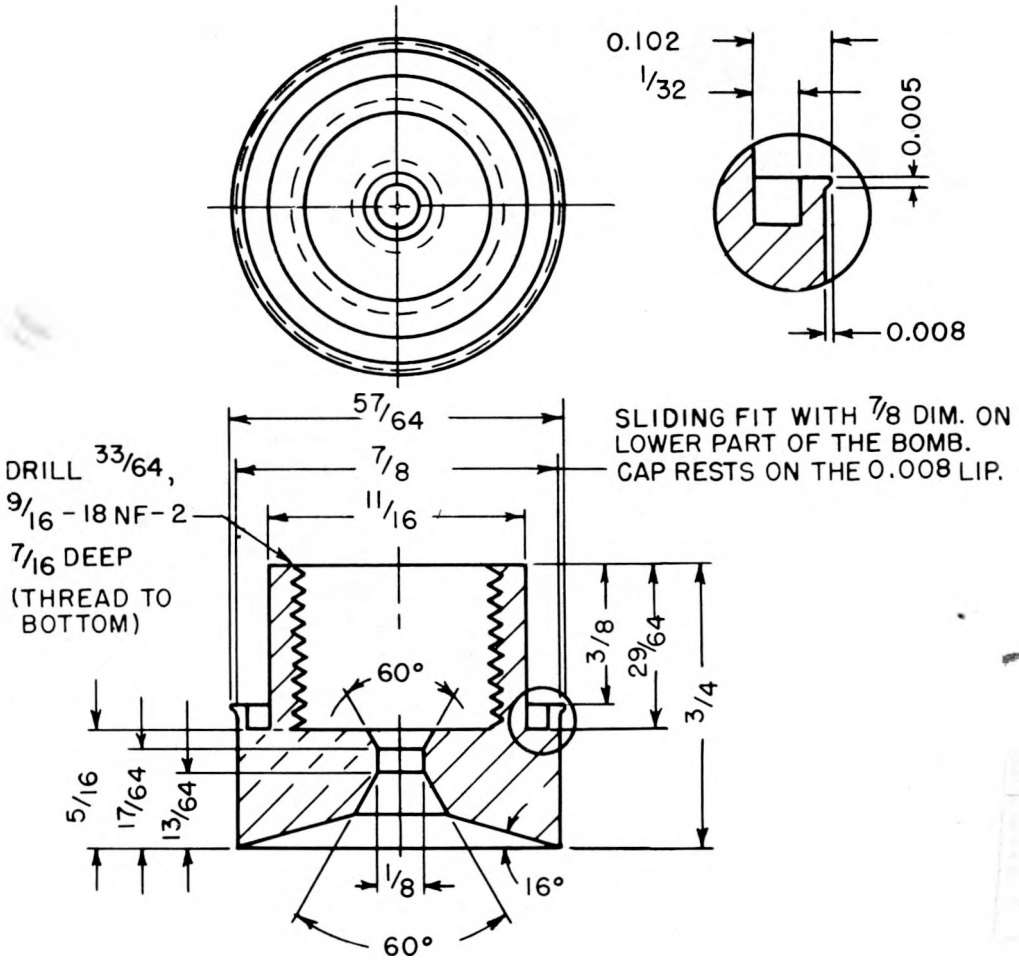

CAP

FIG. 60
HIGH PRESSURE BOMB

SCALE - 2" = 1" MATERIAL - STAINLESS STEEL #347

TOLERANCES UNLESS OTHERWISE SPECIFIED
DECIMAL ± 0.002 ANGLES ± 1/2
FRACTION ± 1/64

DWG. 10040

168

DECLASSIFIED
X-29-63

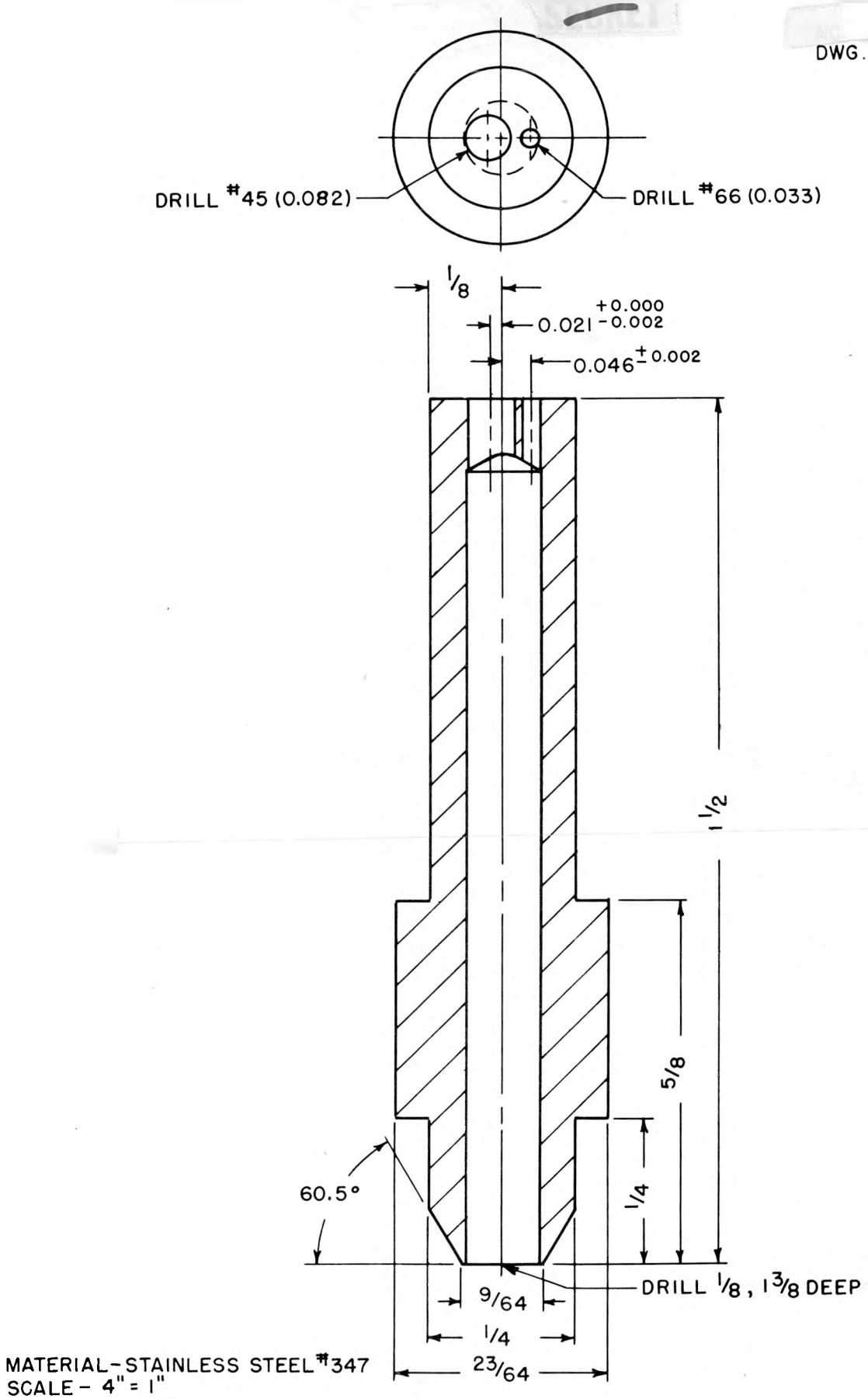

FIG. 61
HIGH PRESSURE BOMB FITTING
(VERTICAL INSERTION)

DECLASSIFIED X-29-64

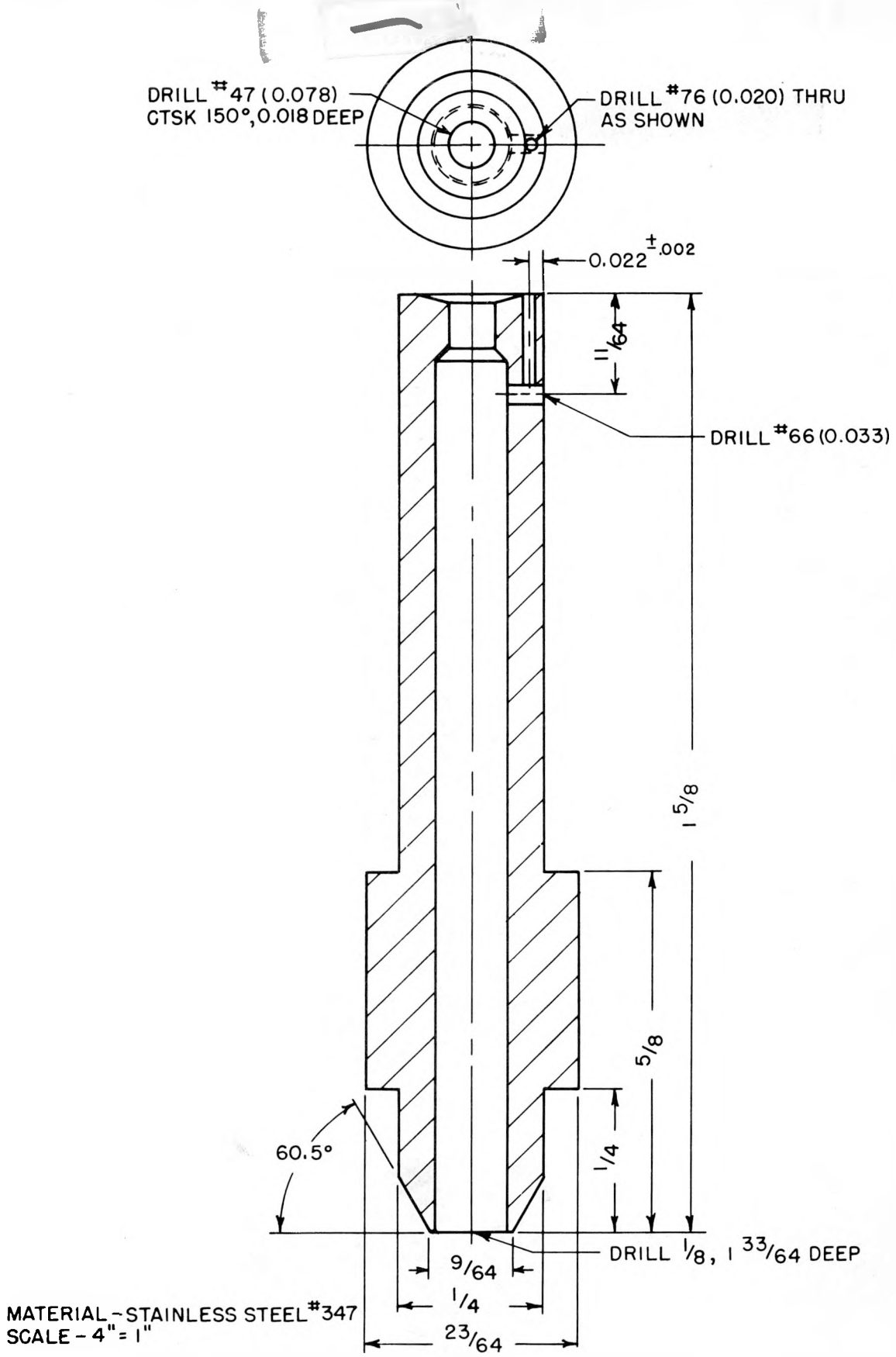

FIG. 62
HIGH PRESSURE BOMB FITTING
(HORIZONTAL INSERTION)

DWG. 10039

UNCLASSIFIED

DECLASSIFIED 4-29-65

DWG. 10038

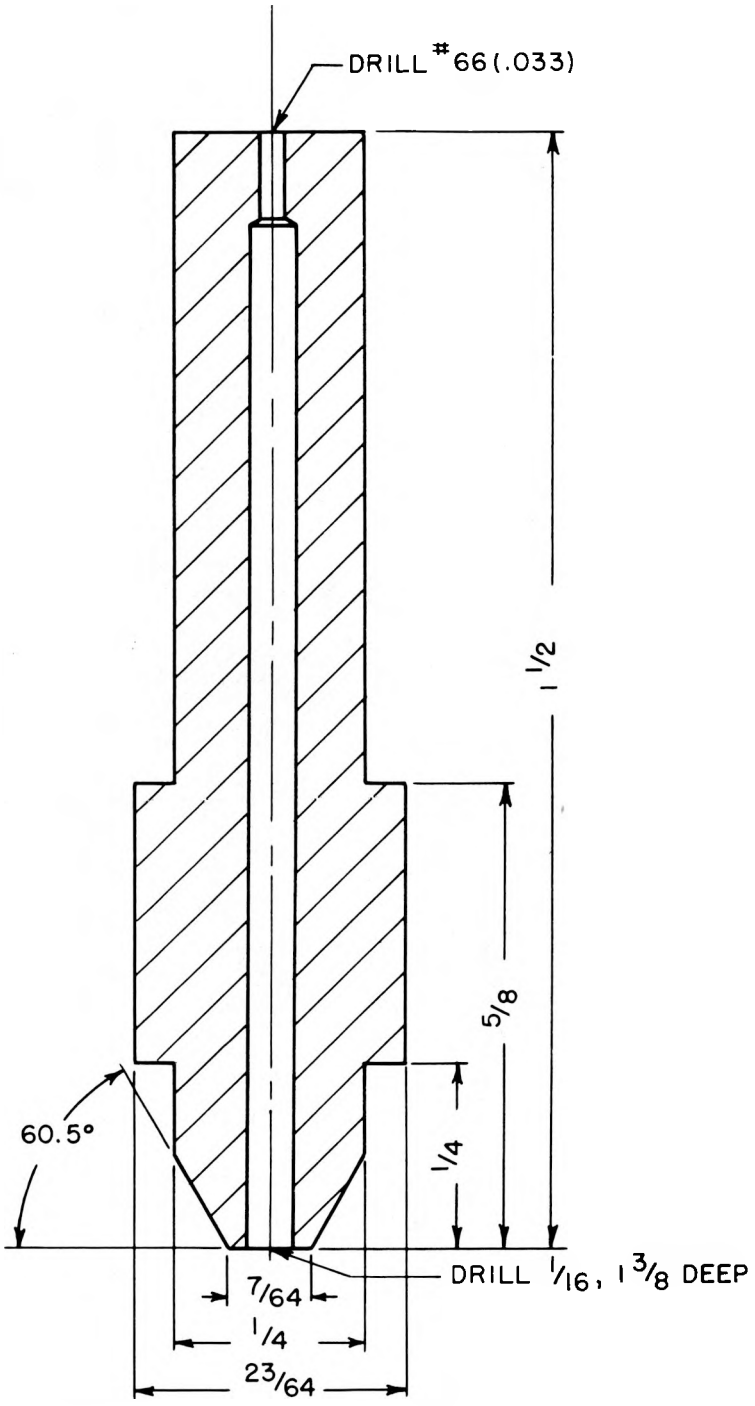

FIG. 63
HIGH PRESSURE CONNECTOR

MATERIAL – STAINLESS STEEL #347
SCALE – 4" = 1"

DECLASSIFIED X-29-66

At the conclusion of each experiment the residual gas over the solution is removed through a valve outside the pile at the pressure cell connection before the bomb is withdrawn from the pile. This gas is saved for subsequent analysis. After the bomb has been withdrawn from the pile and opened, analyses of the solution and/or sediment contained therein are carried out for comparison with similar analyses of unirradiated solutions. After the solution has been removed from the bomb, a small cylindrical corrosion specimen is removed for observation. The following analyses are made:

1. The gaseous material which is not condensable by liquid nitrogen when at a gas pressure of 100 μ Hg is analyzed for hydrogen, oxygen, and inerts.

2. The solution withdrawn from the bomb is analyzed for total uranium (mg/ml) to 1%, the U(IV)/U(VI) ratio, *p*H, Cl^-, Fe-Cr-Ni to 2 to 3%, and non-sulfate sulfur.

3. The solid residue is analyzed spectrographically for U, Fe, Cr, Ni, etc., after which the residue is dissolved and determinations of U, Fe, Cr, Ni, sulfate, and non-sulfate sulfur are carried out.

4. The appearance of the corrosion specimen and its weight change are determined in order to indicate the condition of the specimen.

Fabrication of Bombs and Fittings. All bombs used during the last quarter have been tested at 5000 psi pressure, and the heliarc welding around the top seam has been made slightly heavier. Bombs have consistently been free from recognized mechanical defects. It may be of interest to note that the mechanical construction of all bombs and thermocouple wells during the last two quarters has been essentially the same; thus the mechanical construction of all surfaces normally in contact with uranium solution has not changed.

Figures 60 through 63 show the bomb and the types of fittings used for the connections to the strain gauge. The width of the annulus around the thermocouple well at the cone seat has been increased during the past quarter from 0.005 to 0.021 in. in order to avoid collapse of the annular gas passageway at the time the fitting is forced into the conical seat. Before the thermocouple well is soldered in place, an area at the site of the proposed joint is mechanically cleaned of film or other surface contamination.

DECLASSIFIED X-29-67

Use of Small-diameter Pressure Tubing. The primary reasons for using small-diameter stainless-steel (type 347) tubing to connect the bomb with and transfer the pressure to the pressure cell (located 20 to 30 ft away, outside the pile) are (1) only a small mass of stainless steel is exposed to the pile flux, thus minimizing the radiation hazard on withdrawal of the apparatus, and (2) the small tubing is flexible, facilitating the necessary manipulations in a restricted space when charging or withdrawing the apparatus. The use of much larger or thicker stainless-steel high-pressure tubing would dictate slow withdrawal of apparatus at the conclusion of the experiment. Nevertheless some compromise between mass, flexibility, and ease of fabrication must be made which is consistent with safety. Originally the bombs were connected by means of 3-mil wall tubing (19 mils I.D. and 25 mils O.D.), but this tubing was found too easily broken by mechanical shocks. Beginning with run 301, the tubing used had a 7-mil wall (19 mils I.D. and 33 mils O.D.). This tubing appears to have much greater strength and toughness without contributing excessive radiation on withdrawal. The possibility of using tubing even as large as 1/16 in. O.D. is being investigated.

At first, joints involving the small tubing were made by means of silver solder and a hand torch (gas-oxygen), using a conventional hard-solder flux (Handy-Flux). This technique was open to objections because of the danger of overheating the tubing and because of the possibility of the presence of flux components which might have a deleterious effect on the protective character of the pretreated stainless-steel surface. Care was therefore exercised to avoid excessive heating, and the tubing and fitting were rinsed with a slow stream of distilled water for several hours to dissolve and remove flux components. Attempts have been made to use induction heating in a hydrogen atmosphere with silver solder to provide a fluxless weld of the thermocouple well and pressure tubing to the fitting in a single operation. Results to date have not been uniform; in some cases there has been excess heating, leading to excessive grain growth in the tube wall and intergranular penetration of the silver solder. Photomicrographs of typical sections are shown in the section on Optical and Electron Microscopy, Figs. 64 through 66. The development of couplings for small stainless-steel tubing is under investigation, in the expectation of being able to avoid all heating of the small tubing or the use of silver solder with such joints.

DECLASSIFIED X-29-68

High-pressure Testing. During the past quarter a cell for this purpose has been under construction in the basement of Building 205. Barricade walls of boiler plate separated by 1 ft of sand are used to provide the necessary protection, and all controls, together with the minimum amount of high-pressure tubing, are located outside the barricade. The compressor has been factory-tested at 22,000 psi. The gauge has a 20,000 psi range with a working pressure of 15,000 psi.

Safety Precautions. Operations involving uranium solutions containing fission products and a high level of activity at high pressures and high temperatures are extremely dangerous. Sudden rupture of a small tube might release a high pressure jet of fission-product solution which could penetrate the skin and create an emergency, possibly requiring immediate amputation. Consequently, precautions are taken that no person shall inadvertently approach parts of the system under pressure and that deliberate approaches shall be made only when the pressure is at the lowest possible value. Thus, after the pile is shut down and most of the recombination has taken place, the temperature of the bomb is dropped to below 100°C before the residual gases are withdrawn into a protected, evacuated glass bulb. After this operation there is no pressure on the solution, and the radiation and contamination hazards may be dealt with in the usual fashion. Moreover, experiments are always started with the tubing completely filled with distilled water; this prevents radioactive gases from diffusing to the outside of the pile and also acts as a buffer to prevent (by friction in the tube walls) the release of full pressure at the pile face.

Detailed Experimental Results

In order to facilitate detailed discussion of the twenty-two experiments, they are grouped according to pretreatment conditions and temperature of the irradiation into 10 groups designated by letters from *A* to *J*. Table 17 summarizes the experimental conditions for each of these groups and classifies each experiment as to the general conclusion.

Following pressure tests, the bombs were cleaned and etched for 3 min at room temperature with a saturated solution of ferric chloride in concentrated hydrochloric acid containing 2% nitric acid. Then they were flushed with

DECLASSIFIED X-29-69

TABLE 17

Summary of Irradiation Corrosion Experiments

GROUP	PRETREATMENT		IRRADIATION TEMPERATURE (°C)	RESULTS (Experiment Nos.)		
	ACID	TEMPERATURE (°C)		GOOD	INCONCLUSIVE	FAILED
A	1% HNO_3	250	250	290*a* 291*a* 306 307	297	
B	1% HNO_3	290	250	298 299		
C	2% CrO_3	250	250	292*a* 303 308		
D	2% CrO_3	290	250	309		300
E	None		250	304	302	
F	1% HNO_3	250	290		296 290*b* 291*b*	
G	1% HNO_3	290	290			305
H	2% CrO_3	250	290	292*b*	294 295	
I	2% CrO_3	290	290	301		
J	None		290			

DECLASSIFIED X-29-70

distilled water, rinsed with 10% sodium hydroxide solution, and again rinsed with distilled water. The pretreatment consisted in filling the cleaned bombs with either 1% nitric acid or 2% CrO_3 solution, submerging the filled bomb in a similar solution in an autoclave, and heating to either 250 or 290°C for 24 hr. After cooling, the bombs were rinsed again with distilled water and calibrated for volume. The uranyl sulfate solution was placed in the bomb from several hours to as much as one day prior to use. In the following discussion all pressures are given as total pressure after subtracting the steam pressure at the particular temperature involved.

Group A. Run 290*a* was one of a set of three (290*a*, 291*a*, and 292*a*) inserted in hole 11 in the circulating water of the ANL experiment. It was located approximately 4 ft from the vertical center plane of the pile. The run was terminated after 60 hr because of a leak in bomb 292*a* resulting in the contamination of the ANL facility. At the conclusion of the run the pressure in bomb 290*a* was 2200 psi, that in bomb 291*a* was approximately 1200 psi, and both were still rising. Analysis of the combined solutions from the three bombs indicated no loss of uranium from the solution within the experimental error of analysis.

Analysis of the uncondensable gas removed from bomb 291*a* at the end of the run gave the following results:

SAMPLE	H_2 (%)	O_2 (%)	INERTS BY DIFFERENCE (%)	H_2/O_2
1	57.8	28.7	13.5	2.01
2	57.3	28.7	14.0	2.00
3	57.9	29.0	13.1	2.00

The large percentage of inerts suggests that considerable air (nitrogen and oxygen) was included in the sample. If the hydrogen-to-oxygen ratios are calculated after correction for the oxygen that would be present if the inert gas is air, the values obtained are 2.30, 2.30, and 2.27.

The corrosion specimens from these three bombs were not examined at the conclusion of the runs. Instead, the bombs, fittings, and test specimens were

DECLASSIFIED X-29-71

refilled with fresh solution and returned to the pile after a cooling period of 18 days. This second series is designated runs 290*b*, 291*b*, and 292*b* and is discussed below under Groups *F* and *H*.

Run 297 was exposed for 185 hr in hole 12. A pressure peak of 3100 psi was reached at 30 hr, followed by a gradual fall to 1500 psi at 150 hr, after which a leak in the pressure tube allowed gaseous products (including steam) and perhaps some uranium to escape. A small quantity of yellow solution recovered from the bomb did not indicate that precipitation had occurred. Analysis showed 0.017 mg of U(IV) per milliliter, a very small amount of reduced uranium when compared with the U(IV) concentration of 0.043 mg/ml found in the unirradiated solution.

The corrosion-test sample showed a weight gain of 23.8 mdd (milligrams per square decimeter per day). Visual inspection showed the sample to be covered with a brown rust-colored scale, with only one small black patch of what looked like the pretreatment film remaining.

Runs 306 and 307 are, at the time of this report, in their fourth week in hole 12 without pressure-temperature evidence of uranium precipitation.

Group B. Bombs 298 and 299 were pretreated with nitric acid at 290°C and irradiated at 250°C. Run 298, exposed for 336 hr in hole 12, gave a pressure maximum of 4000 psi at 108 hr, followed by a fall to 1600 psi at the end of the run. The bomb was kept frozen at dry ice temperature from the time of removal from the pile until the time of chemical analysis (nine days) so as to try to preserve any easily oxidizable sulfur compounds present. When removed from the bomb, the solution was a clear yellow and quite viscous, indicating that a concentrating process had occurred by loss of water. It was diluted from 0.33 ml to 4.0 ml before any analyses were made. The reduced sulfur then amounted to 0.028 mg/ml as compared with 0.007 mg/ml for the starting solution. The volume at the start was 4.9 ml. The diluted sample also showed chromium present in the amount of 0.069 mg/ml and U(IV) present to the extent of 0.031 mg/ml compared with 0.043 mg/ml for the starting solution. These findings suggest that some corrosion of the surface and some reduction of the sulfate ion had taken place.

The weight change of the corrosion specimen was a gain of 3.7 mdd. Visual inspection indicated the best results to date. The entire surface had

DECLASSIFIED X-29-72

the same appearance as after pretreatment. However, there was a yellow- to orange-colored powder sprinkled over one end of the sample. Attempts to identify this powder will be made.

Run 299 was exposed for 280 hr in hole 12. A pressure peak of 4300 psi was reached at 20 hr and again at 140 hr, subsequently falling slightly to 3400 psi at the end of the run. Examination of the corrosion specimen and analysis of the solution have not been completed. Analysis of the gas gave a hydrogen-to-oxygen ratio of 2.07 ± 0.02 with only 0.4 ± 0.1% inert gas present.

Group C. This group includes runs 292*a*, 303, and 308, in which the pretreatment was done with 2% CrO_3 solution at 250°C and the irradiations were carried out at 250°C.

Run 292*a*, mentioned under Group A, was exposed for 60 hr in hole 11. This run was interrupted by a leak in the pressure tubing, first observed at 20 hr, after which the pressure appeared normal, building up to 2600 psi at 54 hr when another leak occurred. No evidence of precipitation of uranium from solution was obtained, either from pressure-temperature data or from chemical analysis of the solution removed from the bomb.

Run 303 was exposed for 336 hr in hole 12 along with runs 298 and 304. A pressure peak of 3000 psi was observed after 88 hr and again after 276 hr, falling to 2000 psi in between the peaks and to 2100 psi at the end of the run. The run was terminated by failure of the tubing when an attempt was made to change the position of the bomb to obtain a higher flux. Temperature-pressure data following this tubing break indicated that most or all of the water was lost as steam. Thus, analysis of the residue in the bomb may be encouraging if the uranium contained therein is water soluble, or inconclusive if otherwise. All the available evidence indicates that the solution was stable throughout the run with no substantial corrosion or precipitation of uranium. The corrosion specimen has not been examined yet.

Run 308, along with runs 306 and 307 in hole 12, is in its fourth week of testing without signs of precipitation of the uranium.

Group D. Run 300 was exposed for 280 hr in hole 12. A pressure peak of 2000 psi occurred at 100 hr followed by a smooth fall to 100 psi at the end of the run. Pressure-temperature data indicate that precipitation of the uranium

DECLASSIFIED X-29-73

may have been initiated by a 12-hr pile shutdown (162 to 174 hr). A few hours after the subsequent start-up the temperature was allowed to rise to 270°C and fall to 215°C over the course of 2 hr because of relay failure. However, it is believed that the pile shutdown rather than the temperature fluctuation was the event associated with the beginning of precipitation of uranium.

Run 309, in hole 60, is finishing its first week of testing with no abnormalities having been discovered. The pressure is being maintained at a considerably lower value than would otherwise be the case by the presence of a small piece of platinum foil wrapped around the thermocouple well above the liquid level. This simulates to some extent the action of a recombination unit for hydrogen and oxygen such as is contemplated for the HRE.

Group E. Bombs 302 and 304 were cleaned and etched in the usual manner but had no other chemical pretreatment. Run 302 was a 280-hr exposure in hole 12 along with bombs 299 and 300. The useful portion of this run was terminated after 40 hr by a rupture of the tubing leading to the pressure gauge. The bomb, in dry condition, was left in the hole for the remainder of the time so as not to disturb the other two bombs. Prior to rupture there was no evidence of precipitation of the uranium; the pressure rose normally, responded normally after a 3-hr pile shutdown, and fell normally after the furnace was raised to a position of lower flux at 23 hr. If the uranium is found to be water soluble when the bomb is opened, this will be called a successful run.

Bomb 304 was exposed for 336 hr in hole 12 along with bombs 298 and 303. A pressure peak of 1600 psi occurred at 52 hr, after which a very slow fall was observed. During the run the pressure followed changes in pile power, and was 300 psi at the end of the run with the pile at half power. The tubing ruptured when an attempt was made to change the position of the furnace to obtain higher flux, and the escape of steam left a dry bomb. As stated before, analysis of the residue in the bomb may be encouraging if the uranium content is water soluble or inconclusive if not soluble.

Group F. In runs 290*b* and 291*b*, the bombs used in 290*a* and 291*a* were rinsed with distilled water and refilled with fresh solution. No pressure (above steam pressure) was ever observed, indicating that the uranium was taken out of solution before the flux was applied or immediately thereafter. Probably the failure of these bombs can be attributed to the fact that they

DECLASSIFIED X-29-74

were allowed to remain exposed to the air for a period of 18 days between radiation exposures. The protective character of the pretreatment film is lost on prolonged exposure to air.

The corrosion specimen from runs 290*a* and 290*b* showed a weight loss of 24.0 mdd. It was brownish black in appearance and showed slight scaling.

The specimen from 291*a* and 291*b* showed a weight loss of 13.8 mdd and appeared to have a heavy black scale streaked with loose rust.

Bomb 296 was exposed for 320 hr in hole 12 along with bombs 294 and 295. The pressure failed to follow temperature changes at 60 hr and again at 95 hr, after a pile shutdown. Before the shutdown the pressure was about 500 psi. It is believed that the small tubing was clogged or restricted very near the bomb. The bomb has not yet been opened for examination.

Group G Bomb 305, in hole 60 and at 290°C, contained a large charge of uranium solution in order to maximize the ultimately available analytical sample. As a result of the low free volume (0.2 ml) at 290°C, pressure effects at start-up were exaggerated and accelerated. However, the run appeared normal with a pressure peak of 3600 psi at 9 hr, followed by a slow fall to 2350 psi at 95 hr when a pile shutdown occurred. Recombination of hydrogen and oxygen during the shutdown lowered the pressure almost to steam pressure. When the pile was started up again, the pressure not only failed to rise but even decreased to steam pressure. After 20 hr of no pressure with the pile up, the temperature was reduced to 250°C for an additional 8 hr with the pile up. At this time the heat was removed from the bomb and the temperature was allowed to fall toward pile ambient. Shortly thereafter the pile was shut down for about an hour, and at pile start-up the pressure in the bomb began to rise at a rate of approximately 300 psi per hour. After the pressure had risen to 5000 psi (including steam pressure at 190°C) the pile was shut down, the bomb was cooled, and the pressure was relieved by releasing some of the gas into an evacuated bulb. Following this, temperature control was re-established at 290°C with the bomb behaving normally for another 20 hr, at which time it was removed and frozen for subsequent examination.

Group H Run 292*b* was exposed for 132 hr in hole 12 along with 290*b* and 291*b*. For this run bomb 292*a* was reused after being rinsed with distilled water and refilled with fresh solution. The pressure was 900 psi at the end

DECLASSIFIED X-29-75

of the 132 hr period, and there was no evidence of precipitation of the uranium from pressure temperature data. Analytical data are not yet available. The corrosion specimen from 292*a* and *b* showed a weight loss of 14.2 mdd and appeared to be covered with a very flaky, reddish-black scale.

Bombs 294 and 295 were irradiated for 320 hr in hole 12. These experiments were marred by a temperature-control failure for 4 hr at 93 hr, which permitted the temperature to drop to some unknown value below 200°C. The pressure in run 294 failed to respond to temperature fluctuations after 250 hr. The bomb was found to be dry when opened although there was no evidence of leakage during the radiation. Some liquid leakage was noted through the severed pressure tubing after the assembly had been removed from the pile. Rinsing the bomb with water gave a slightly yellow solution indicating that at least some of the uranium had been deposited in a soluble form. The corrosion specimen lost 12.2 mdd. Visual inspection showed the entire surface to be covered with a very flaky, brownish rust-colored scale.

Bomb 295 gave a pressure peak of 1500 psi at 14 hr, followed by a fall to 400 psi at 93 hr. At this time the above-noted failure in temperature control occurred. When the temperature control was re-established, the pressure was 1900 psi, after which there was a rapid fall to 350 psi at 136 hr. At this point a pile shutdown occurred, and upon start-up there was no increase in pressure. In fact, the pressure continued to drop until, at 150 hr, the system showed no pressure above that of the steam.

Group I. Bomb 301 was irradiated for 670 hr (28 days) in hole 60 at a position which gave the highest neutron flux attainable in any experimental hole in the X-10 pile. This was also the first run using heavier walled tubing.

A pressure peak of 2300 psi at 24 hr was followed by a slow fall to 1200 psi at the end of four weeks. A temperature-control failure after eight days allowed the pressure to rise to 2700 psi, followed by a gradual return to the original pressure range over the next five days. Many pile shutdowns and changes in pile power occurred during this run, and the pressure responded normally in all instances. The length of time, temperature, and position in the highest flux of the X-10 pile without pressure temperature evidences of any substantial precipitation of uranium combine to make this a very encouraging experiment.

DECLASSIFIED X-29-76

Group J. No runs have been made under the conditions specified for Group J because of the decision to concentrate on bombs which have undergone some type of pretreatment.

Association of Pile Shutdowns with Uranium Precipitation. All the failures, as indicated by a loss of pressure, appear to be possibly related to the discontinuation of neutron flux accompanying pile shutdowns. Runs 290*b* and 291*b* were heated to operating temperature for 1.5 hr before being moved into a neutron flux, at which time they appeared to have no uranium in solution. Run 305 behaved normally from November 2 until a 20-hr shutdown on November 6. After the shutdown, during which most of the hydrogen-oxygen gas mixture had recombined, no increase in pressure was observed, indicating that by the time the pile started up again the uranium had precipitated completely from the solution. In run 300 most of the permanent gas pressure was lost over a four-day period starting at about the time of a 12-hr shutdown.

Plans for Next Quarter

Irradiations in the X-10 Pile. Expansion of the use of hole 60 will be carried as far as instrumentation will permit. A total of six bombs at one time is the ultimate possibility. Continuation of the work in hole 12 using three bombs at one time is contemplated. Consideration has been given to the possibility of sharing hole 11 with experimenters from ANL. This will depend on the availability of facilities at that hole and the relative difficulty of sharing facilities as compared with utilizing other holes to better advantage.

Irradiations in the MTR Mock-up. Plans are being made for the use of two sites in the MTR mock-up beginning in December or January. These are the vertical holes which are normally utilized for shim rods and the horizontal thimble holes which are normally intended for experimental use. The horizontal holes are to be utilized for radiation studies in much the same manner as the present experiments in hole 60 of the graphite pile, with the proper scaling up of shielding for the higher fluxes and beams anticipated. Until flooring and shelter are available at the site of the horizontal holes it is planned to make use of the vertical holes; this will require less in the way of special equipment since the unpressurized water tank of the mock-up may be used for shielding. Moreover, it is expected that these exposures will allow better

DECLASSIFIED X-29-77

estimation of the effects to be expected when the horizontal holes are used. Particular points for which information is needed and on which experiments are now in progress in the laboratory are the magnitude of the heat transfer problem and the magnitude of the pressure produced at the higher fluxes.

Uranium Peroxide Investigation. Ampoule experiments are underway in which the effects of different levels of uranium concentration, *p*H, temperature, and neutron flux upon the precipitation of uranium peroxide are being studied. This work is considered to be of interest in connection with problems of start-up and shutdown of the homogeneous reactor as well as the prevention of precipitation during operation at a steady level.

Joining Small-diameter Tubing. Metallurgical studies are underway in cooperation with T.E. Willmarth and members of the Metallurgy Division to study the effects of various welding procedures upon the small tubing in an effort to develop procedures which will minimize loss of experimental information as a result of mechanical failures.

Catalytic Recombination of Hydrogen and Oxygen. In cooperation with members of the Y-12 chemistry group who have been studying the subject in the absence of pile irradiation, experiments will be extended to study catalysts suitable for use in the HRE in a radiation environment.

Regeneration of Solutions. Experiments are underway to study the possibilities of reversing the corrosion-precipitation of uranium solutions in such a way as to bring the uranium back into solution without removing the solution from the bomb or the pile. Development of such a technique would have interesting implications for operation of the homogeneous reactor.

DECLASSIFIED X-29-78

OPTICAL AND ELECTRON MICROSCOPY

T. E. Willmarth F. D. McNeer
B. I. Gary

In this section are included the pictorial results of the work done on induction methods of soldering and the study of various samples of pretreated and corrosion-tested stainless steel. Pertinent information is included with each photograph.

DECLASSIFIED X-29-79

Fig. 64. Microstructure of 347 stainless steel before and after induction brazing (small-tube assembly).

1. Structure of parent metal
2. Structure 11.5 mm from heat zone
3. Structure 6 mm from heat zone
4. Structure in heat-affected zone
5. Silver solder as deposited
6. Structure of small tube in heat-affected zone
7. Diffusion of silver solder at grain boundaries
8. Polarized-light view of No. 7 (white lines and mass are silver solder

X-29-80

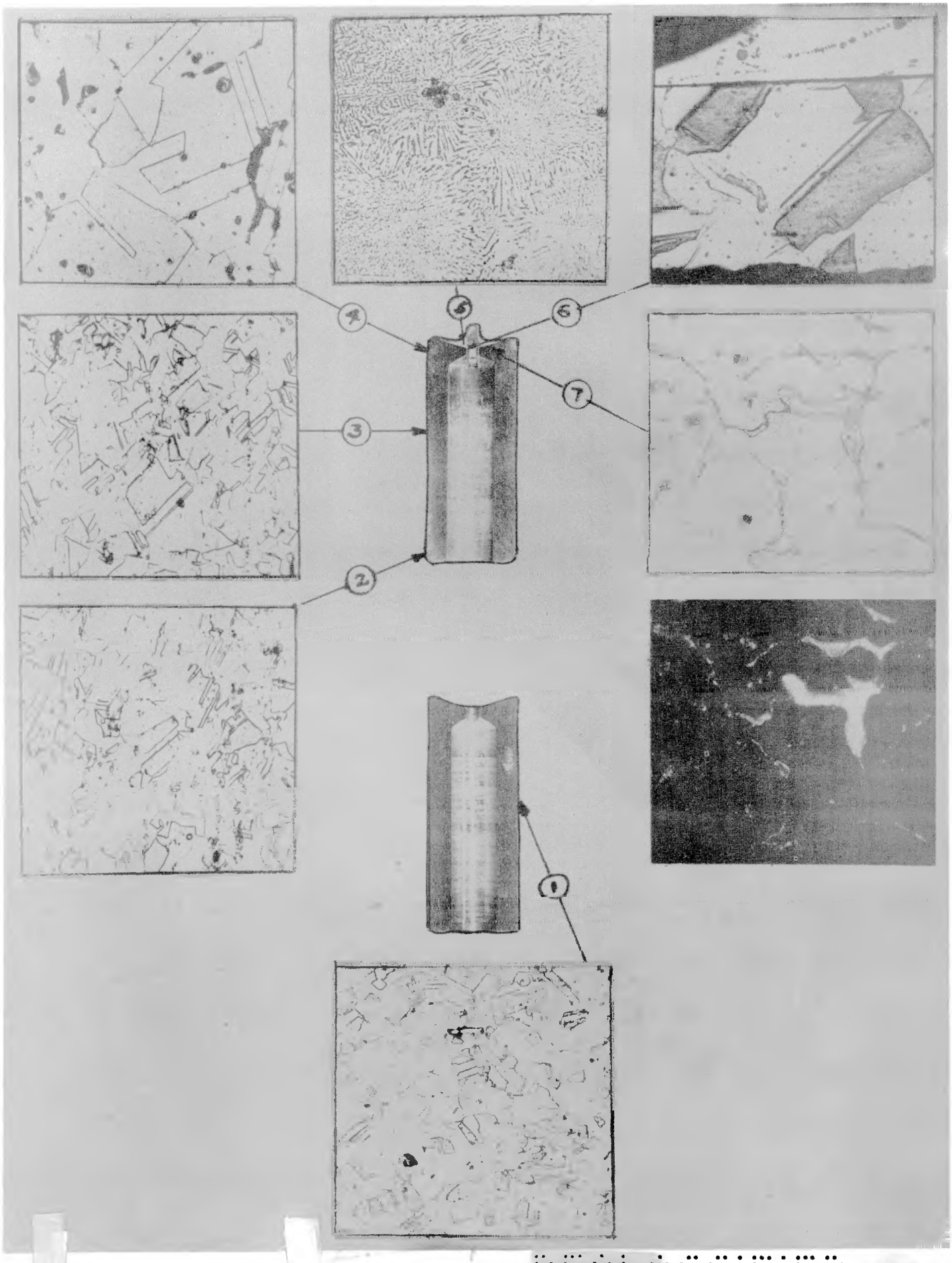

DECLASSIFIED

Fig. 65. Microstructure of 347 stainless steel before and after induction brazing (thermocouple assembly).

1. Structure of parent metal
2. Structure 11.5 mm from heat zone
3. Structure 6 mm from heat zone
4. Structure in heat-affected zone

Note: The large tube showed same gradation of structure. No diffusion of solder was observed in tube or fitting.

X-29-8212

C-154-5

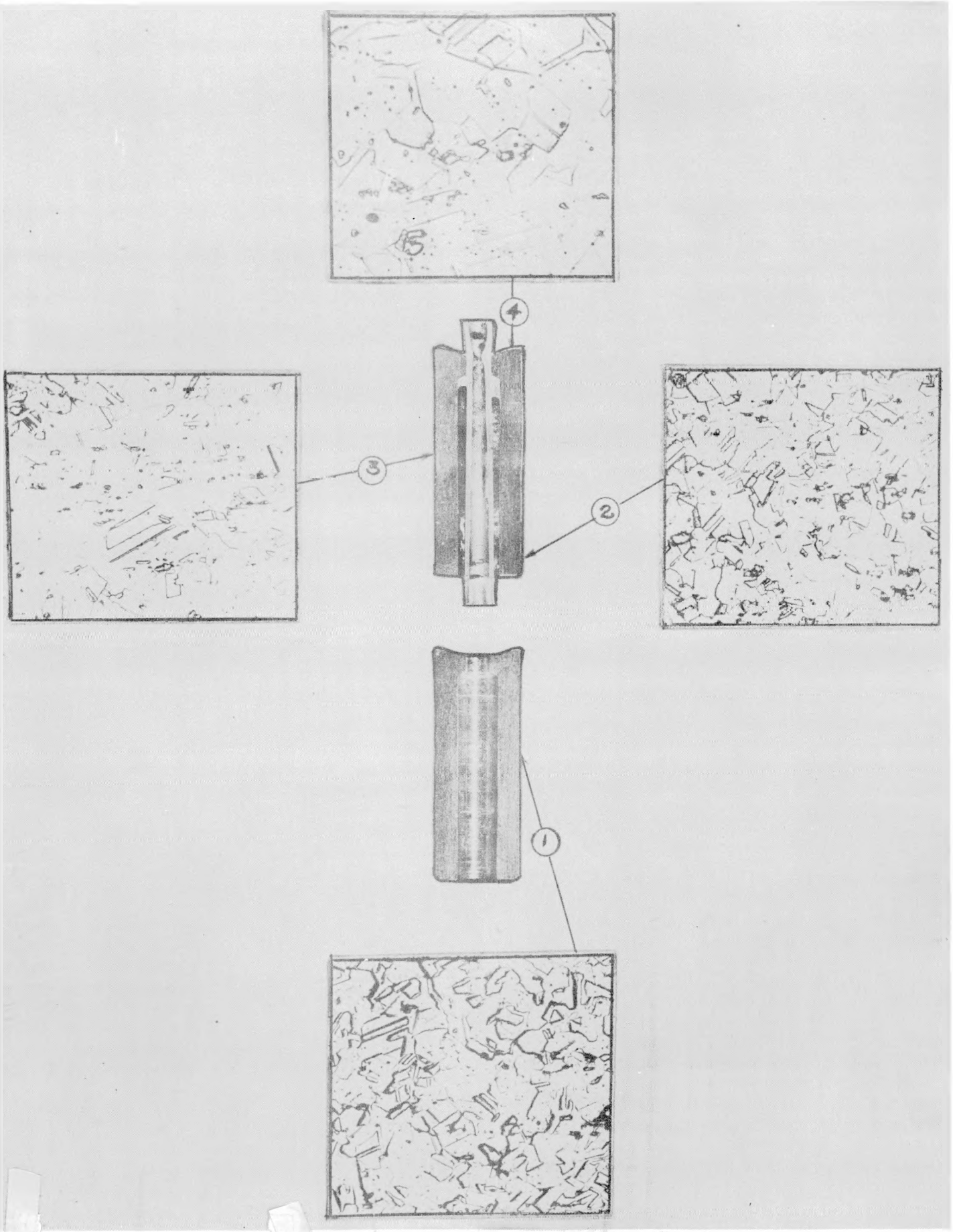

DECLASSIFIED
X-29-83

Fig. 66. Silver-Copper diffusion at grain boundary. 5000×.

X-29-84

NEG. #E-870-3

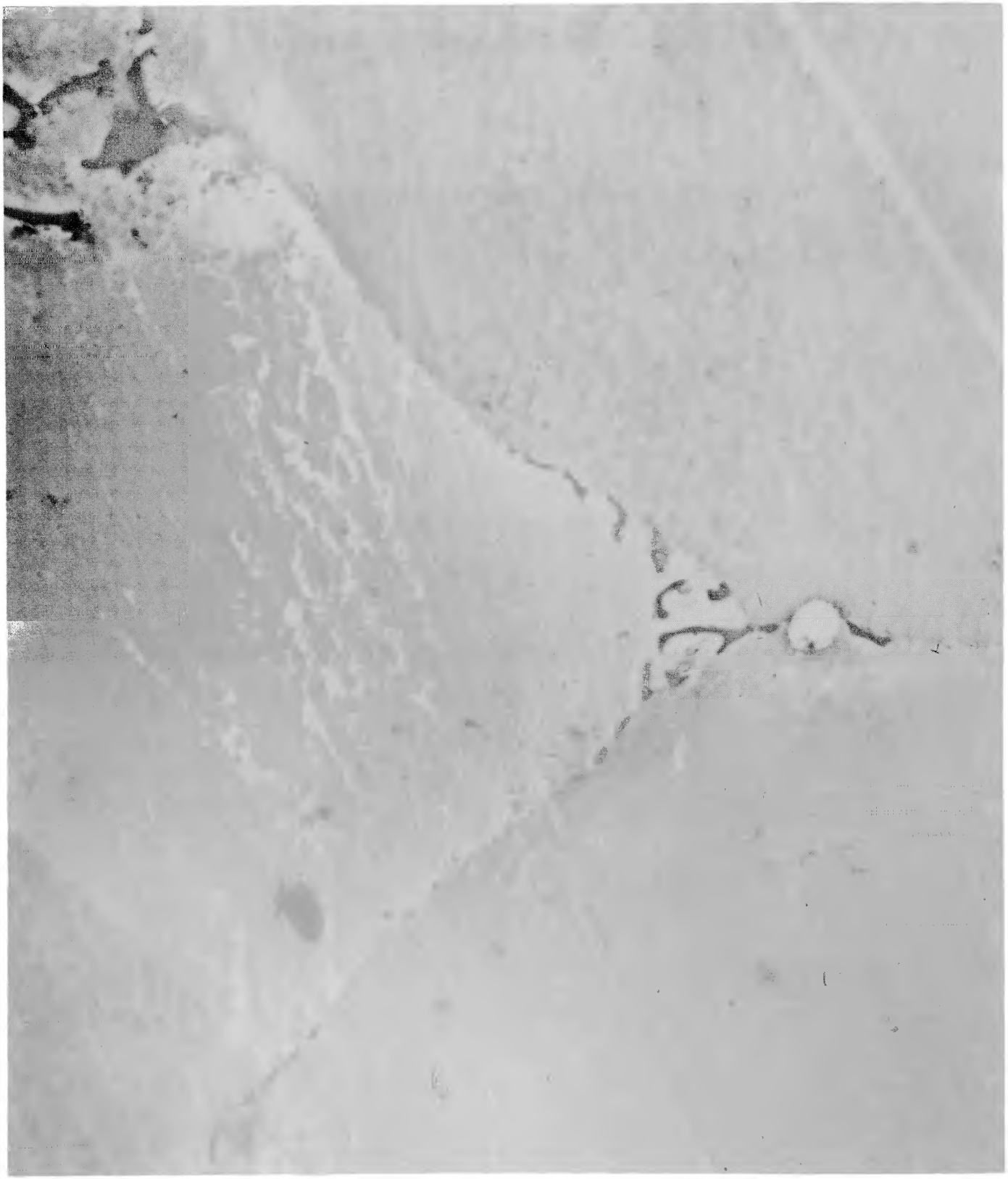

DECLASSIFIED X-29-85

Fig. 67. Silver-Copper diffusion at grain boundary. 5000×.

X-29-86

NEG. #E-871-1

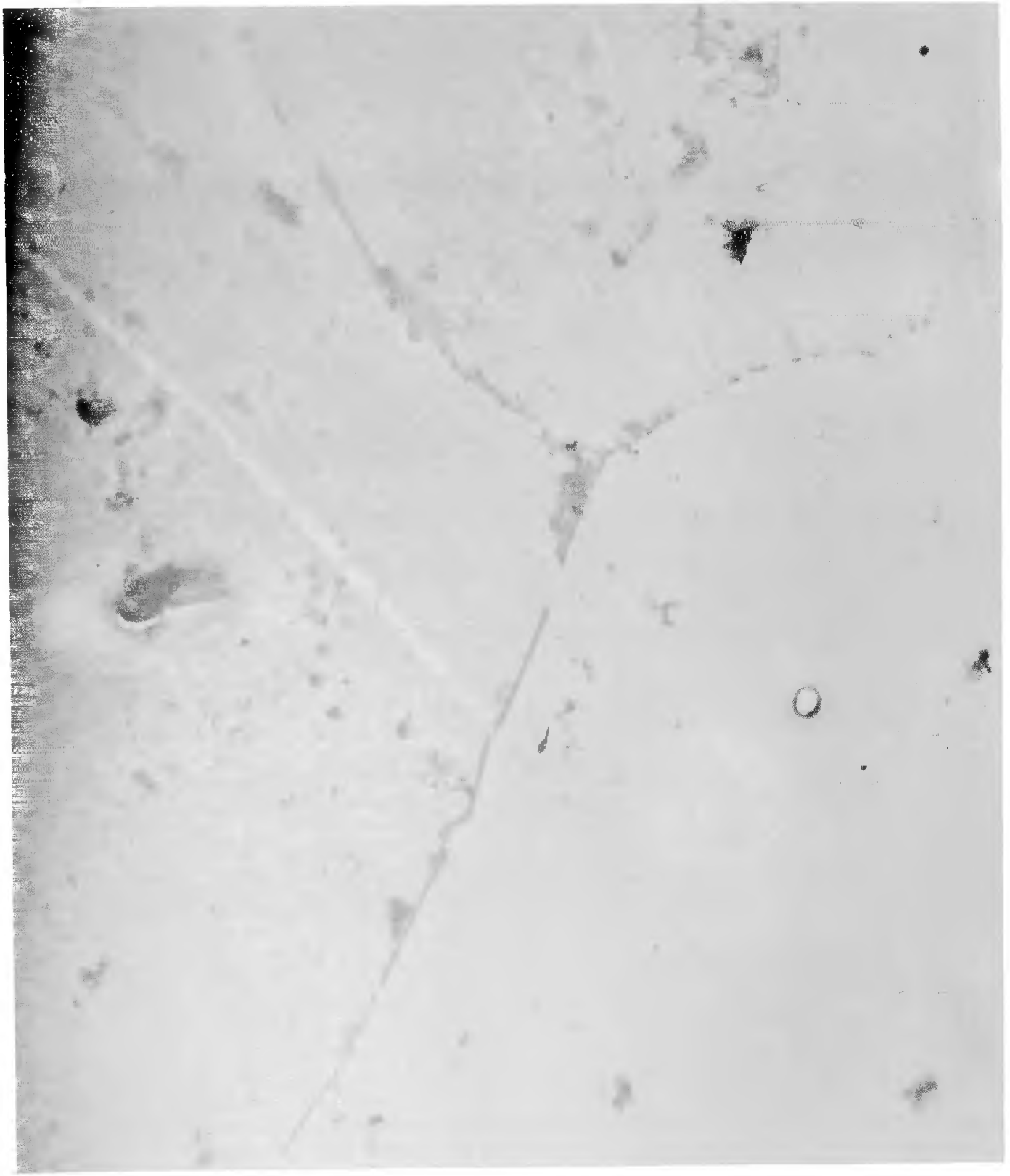

DECLASSIFIED X-29-87

Fig. 68. Silver-Copper eutectic appearing within grain of stainless-steel alloy. 5000×.

X-29-88 DECLASSIFIED

NEG. #E-870-4

DECLASSIFIED X-29-89

Fig. 69. Segments of two-layer film produced by heating iron in 1% HNO_3 at 100°C. Substrate layer is probably α Fe_2O_3; top layer is possibly α Fe_2O_3. Approximately 1000×.

DECLASSIFIED X-29-110

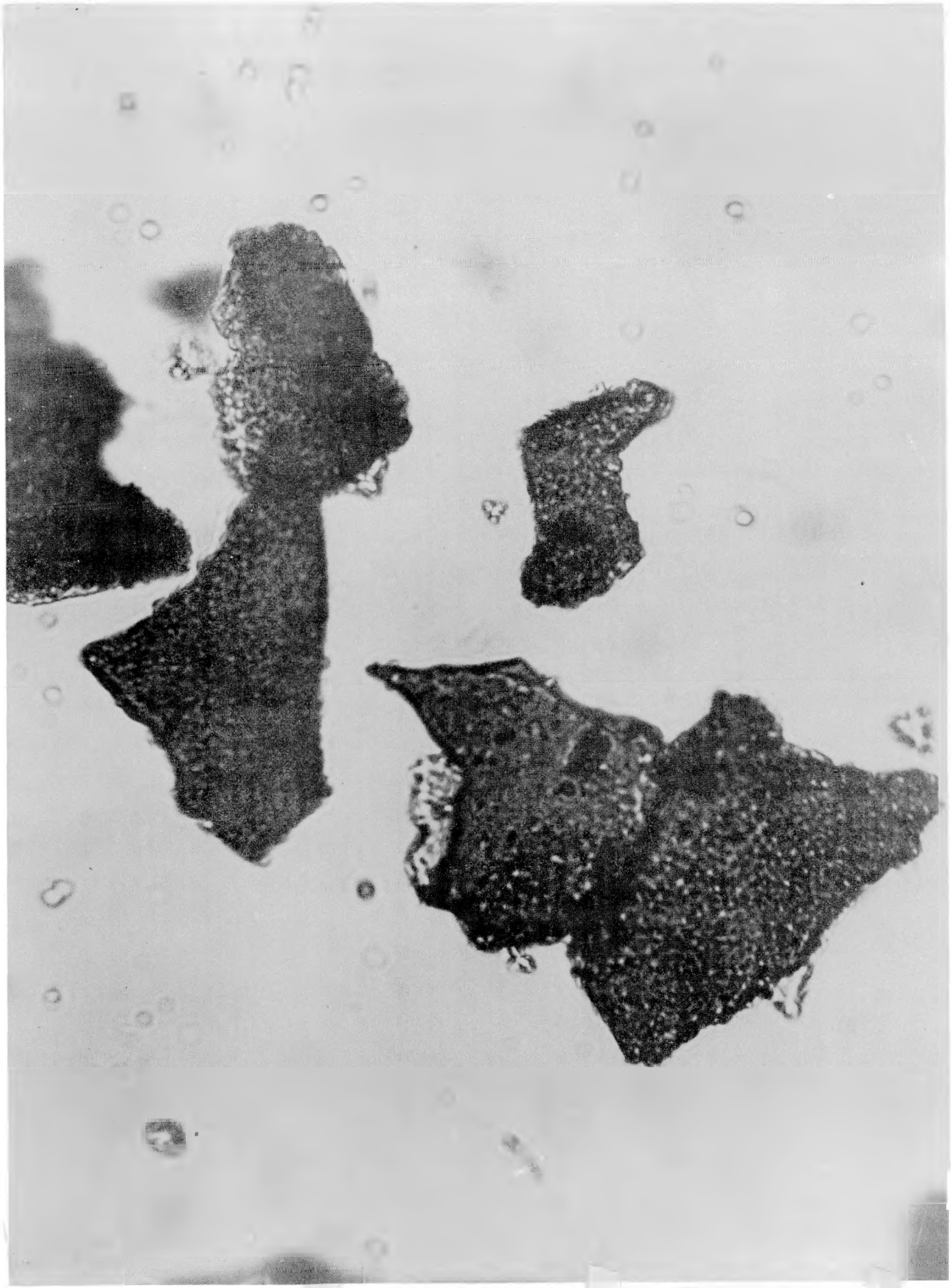

Fig. 70. Segment of film produced by heating Cr in 1% HNO_3 at 100°C. Electron diffraction pattern was too diffuse for accurate measuring. Small crystals are possibly $Cr(OH)_2$; large ones, Cr_2O_3. Approximately 1000×.

DECLASSIFIED X-29-108

NEG. #M-582

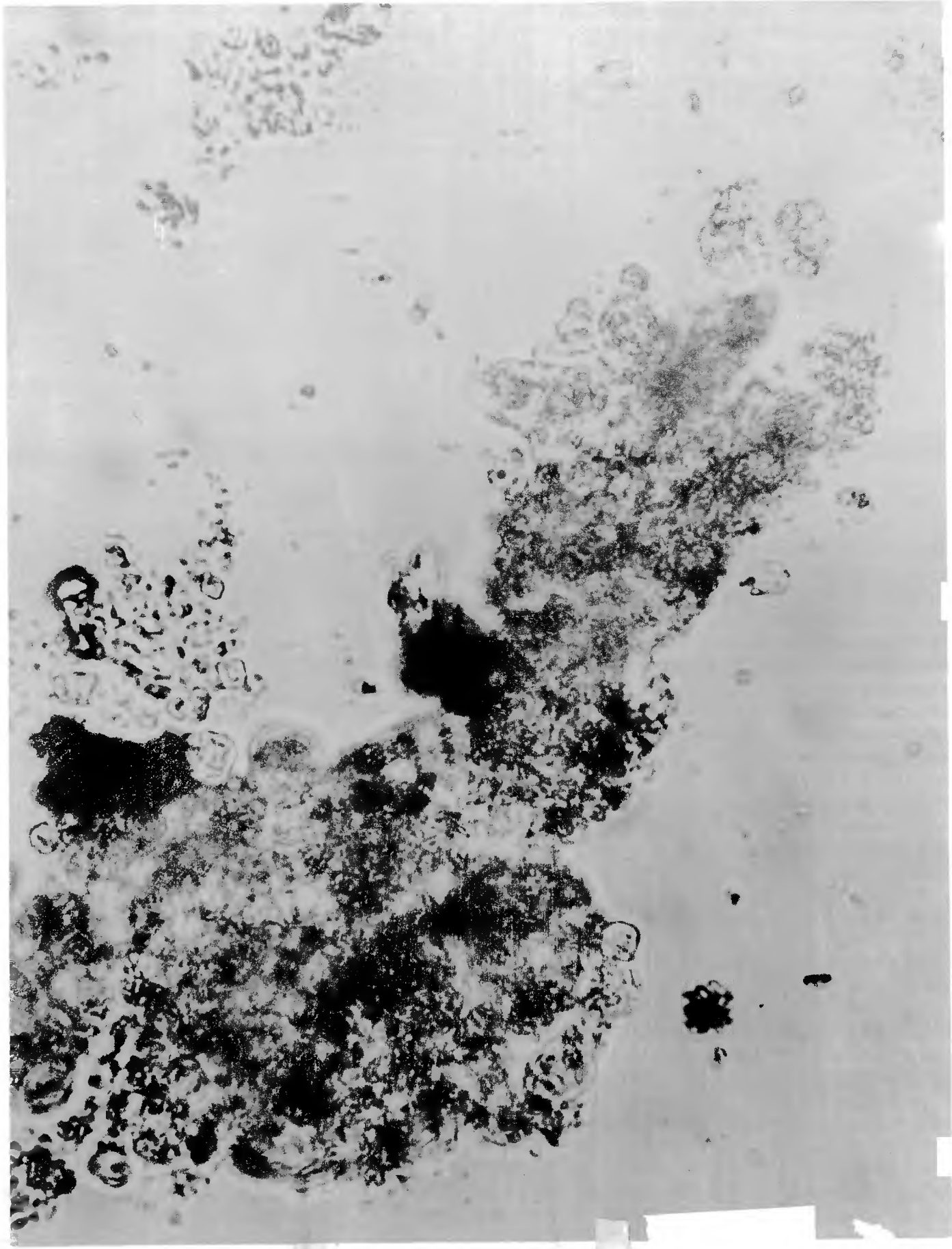

X-29-107

Fig. 71. Segment of film removed from type 347 stainless steel after immersion in 0.17 *M* uranyl sulfate containing 0.1 *M* HNO_3 for 3200 hr. This photomicrograph shows the presence of what appears to be three separate layers, indicated in the photograph by the following numbers: (1) the substrate layer, (2) the middle layer, and (3) a deposited layer. The substrate layer, labeled (1), appears to be a very thin pale-brown semitransparent film by transmitted light. This is probably the protective layer. The middle layer, labeled (2), appears reddish brown to deep amber by transmitted light and is much thicker than the substrate. This material is similar to that observed as the top layer in Fig. 69. The deposited layer, labeled (3), is black and resembles material deposited on wales of corrosion-test bombs during earliest tests and identified by X-ray studies as U_3O_8. 1000×.

DECLASSIFIED X-29-106

NEG. #ME-645

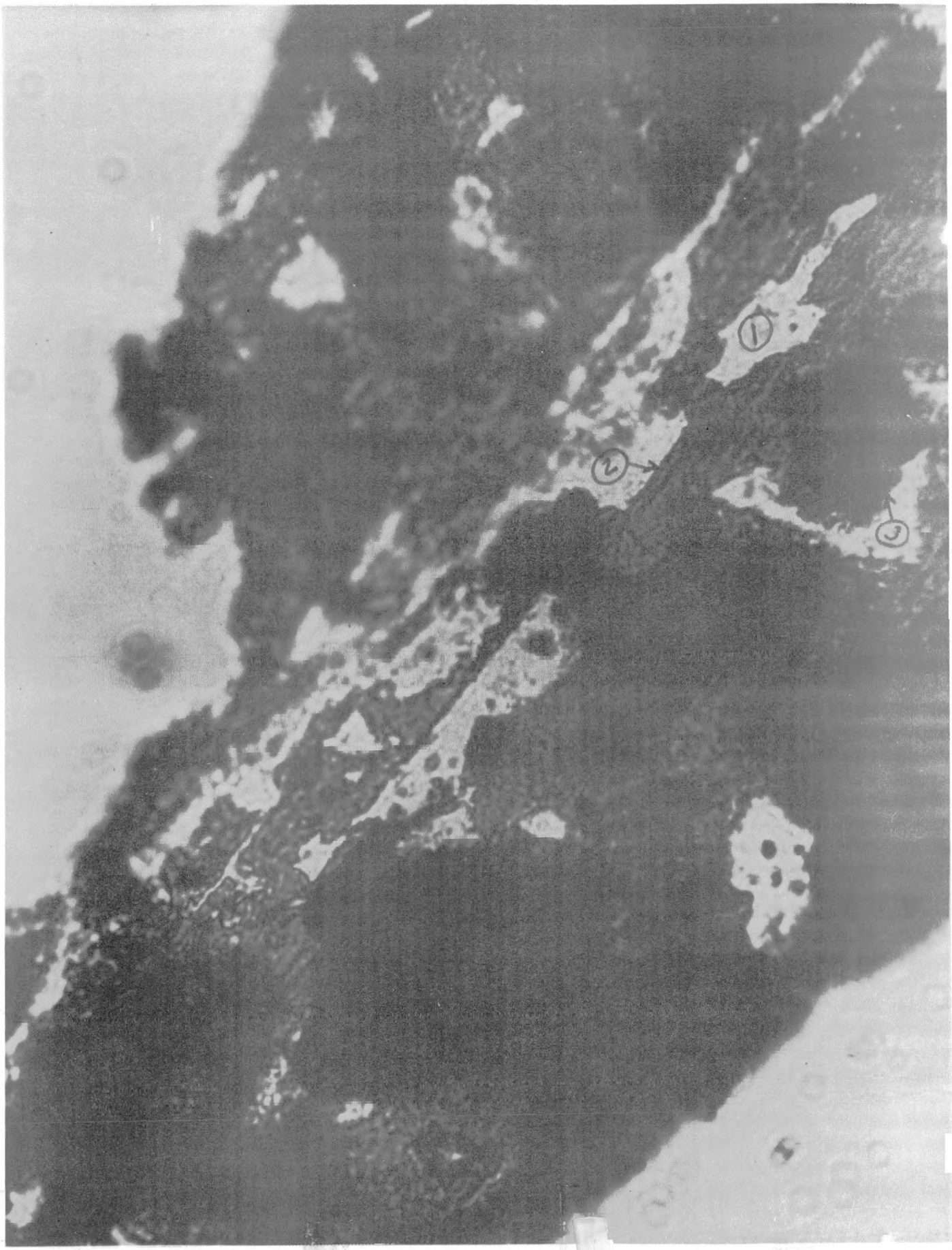

X-29-105

031912MJ30 200

Fig. 72. Greatly enlarged photomicrograph of area (1) in Fig. 71, showing the existence of a film structure just beyond the resolving power of the optical microscope. Approximately 4000×.

DECLASSIFIED X-29-104

Neg. No. ME-646

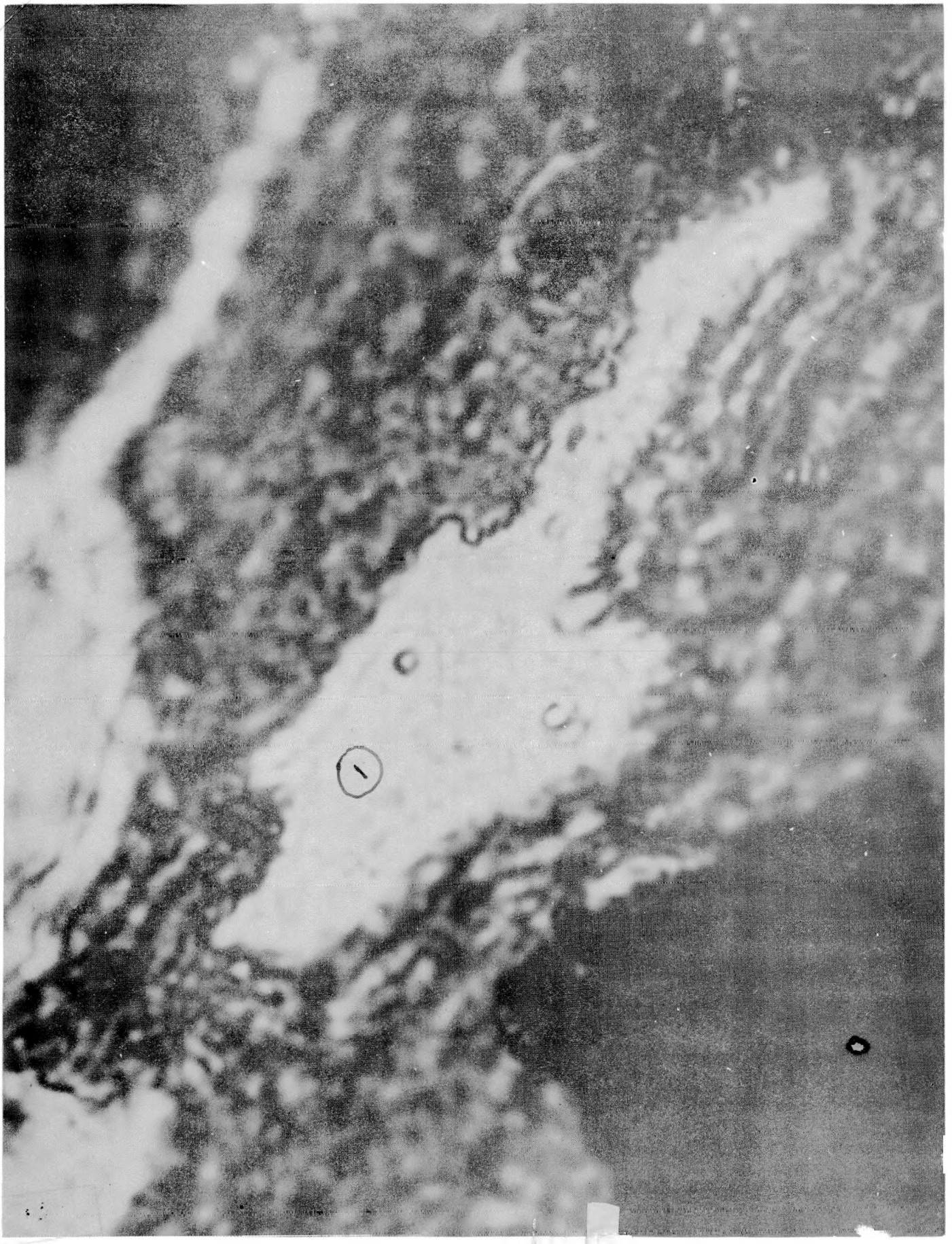

X-29-1

Fig. 73. Replica surface study of type 347 stainless steel pretreated with 2% chromic acid, showing that the surface of the material is extremely irregular and is composed of projections or hills of crystallites or aggregated crystallites. The color was reddish brown to amber by transmitted light. 200×

DECLASSIFIED X-29-102

Neg. No. ME-683

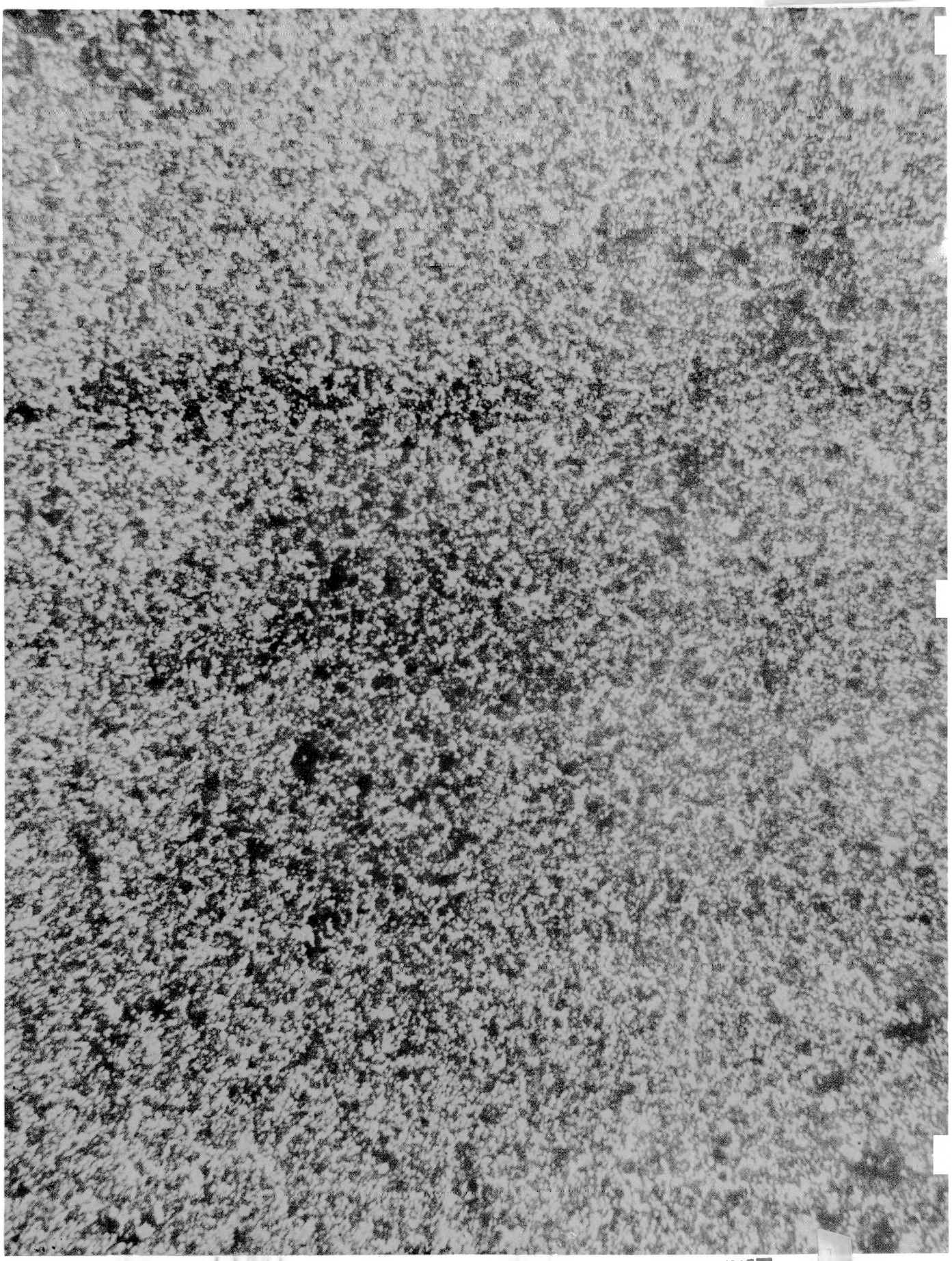

X-29-10

SECRET

Fig. 74. Surface study of type 347 stainless steel pretreated with 1% HNO_3. The surface layer here appears much tighter and more regular than that observed with chromic acid–pretreated type 347 stainless steel. The color was reddish brown to dark red by transmitted light. 200×.

DECLASSIFIED X-29-100

Neg. No. ME-682

X-29-9

SECRET

Fig. 75. Surface study of specimen after immersion for 3200 hr at 250°C in corrosion bath of 0.17 *M* uranyl sulfate containing 0.1 *M* HNO_3. The surface material here appears more regular and unbroken than that in Fig. 74 and has a more "crusty" appearance, with frequent overlapping. Striation markings following the machining marks of the base metal are less in evidence than in Fig. 74. The heavy scratch through the center was made in connection with thickness measurements. Thickness measurements of this surface material, segments of which are shown in Figs. 71 and 72, showed the distance from the top of the outermost layer to the top of the metal to be approximately 7 to 10 μ. By reflected light the material was black. 200×.

ORNL-RSIC X-29-98

Neg. No. ME-636

X-29-9

208

SECRET

Fig. 76. Replica of surface of type 347 stainless steel pretreated with 1% HNO_3. The surface appears to be made up of very small particles, approximately 0.1 μ in size. In this compact mass are much larger particles, 0.3 to 1 μ in size, which appear to be imperfect crystallites, possibly hexagonal in form. Within the temperature range at which this stainless steel was pretreated, i.e., 250°C, one would expect to find α Fe_2O_3, which is hexagonal. (At 225°C γ Fe_2O_3, a cubic spinel type of oxide, transforms to α Fe_2O_3, the hexagonal form.) X-ray spectrometer results on this sample were inconclusive. 9000×.

DECLASSIFIED X-29-96

E-872-3

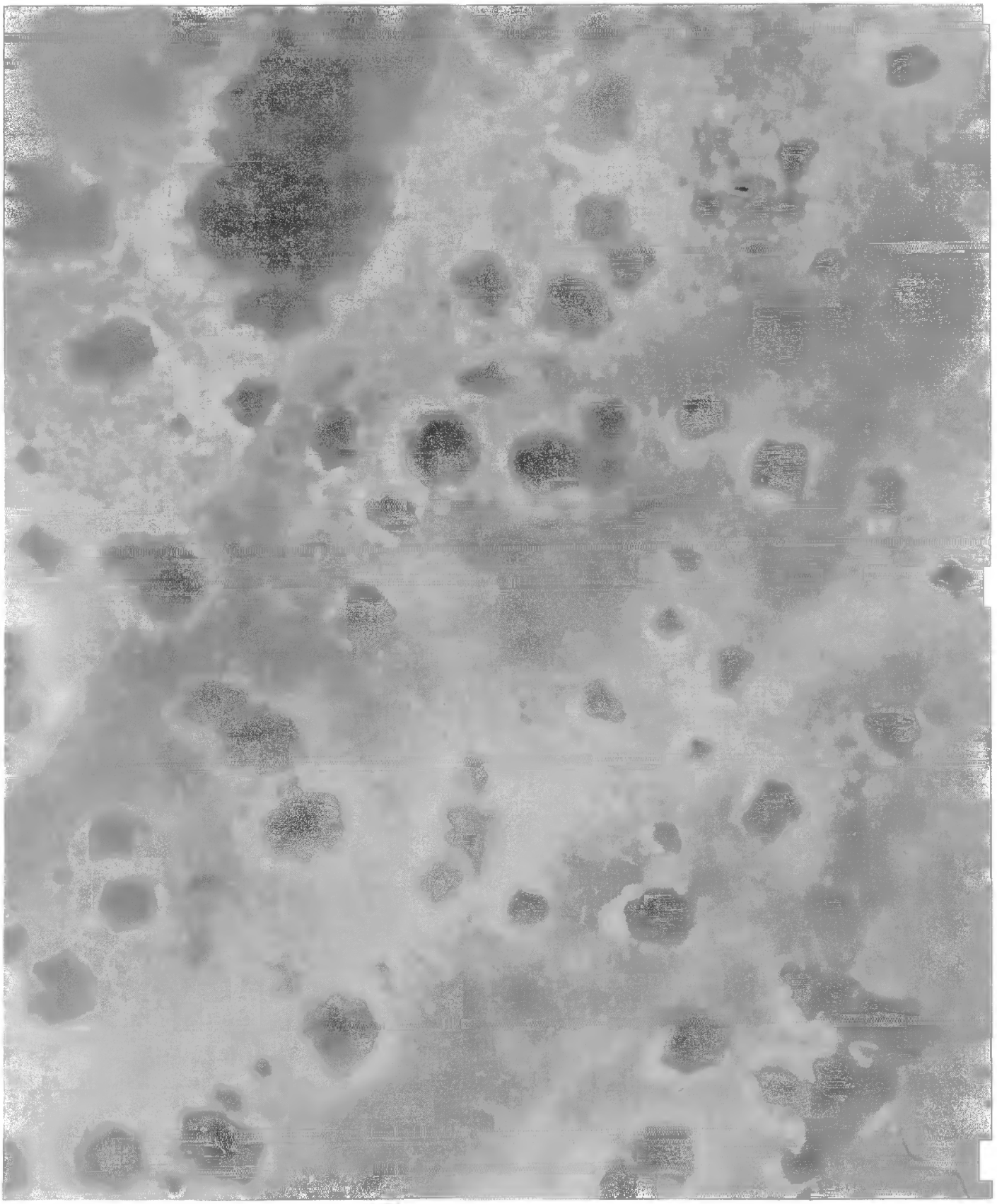

X-29-95

Fig. 77. Replica of surface of type 347 stainless steel pretreated with 1% HNO_3. This is a greatly enlarged view of the smaller particles observed in Fig. 76. 45,000×.

DECLASSIFIED X-29-94

E-876-1

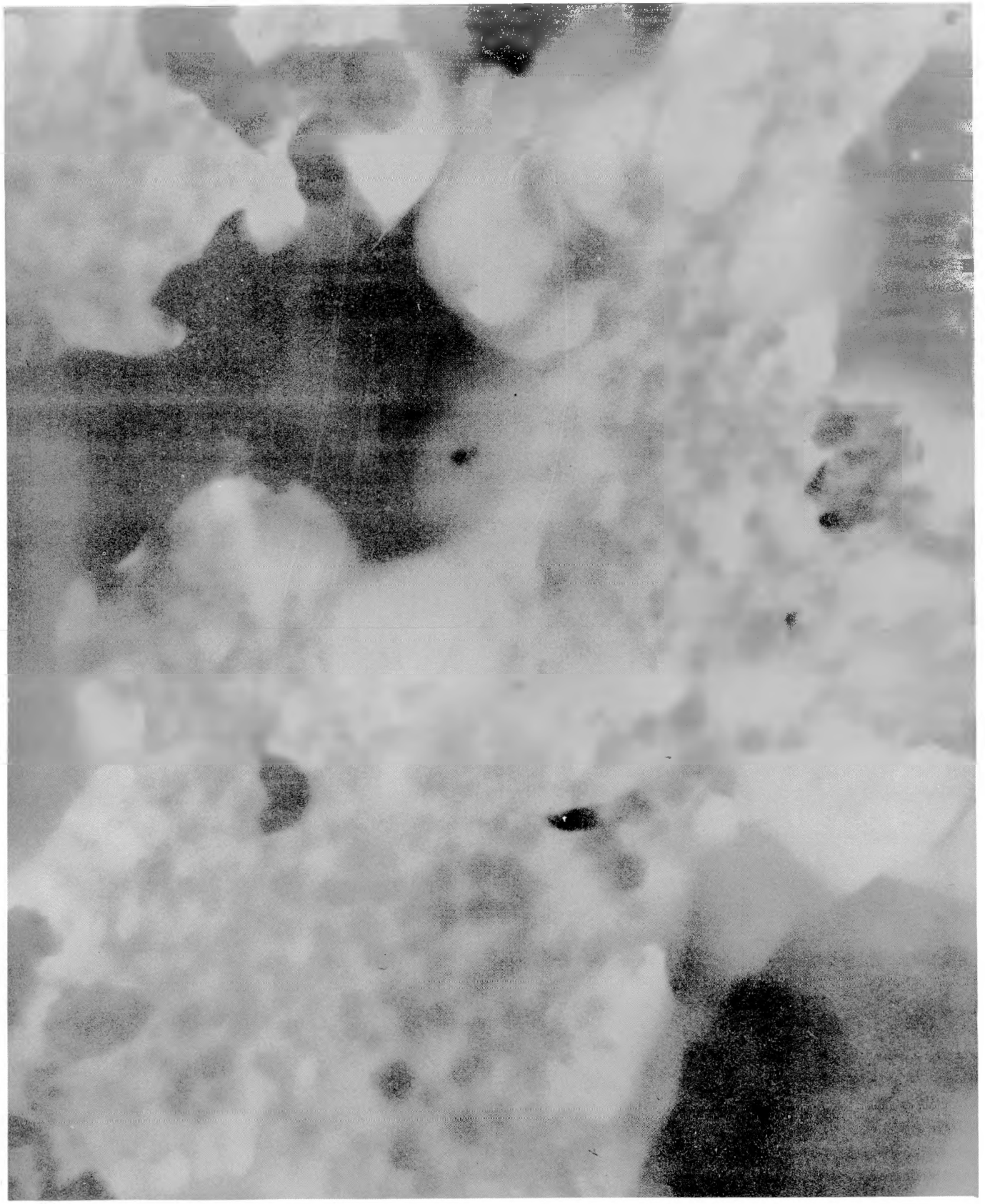

X-29-93

CONFIDENTIAL

Fig. 78. Replica of surface of type 347 stainless steel pretreated in 2% chromic acid at 250°C. The electron micrograph shows a subsurface apparently not so compact as that seen in Fig. 76 and seemingly different in nature. Small rod-shaped crystallites can be observed in the background. In the foreground can be seen again the large imperfectly shaped crystallites mentioned in Fig. 76, together with a few large rods. It can be assumed that the loss of sharp definition of the larger crystallites is caused partly by the greater distance between the top of the large crystals and the substrate. This is in accord with observations made of the structure of this same material at lower power in Fig. 73 (see description of surface). X-ray data on the sample were inconclusive. 9000×.

DECLASSIFIED X-29-92

E-872-4

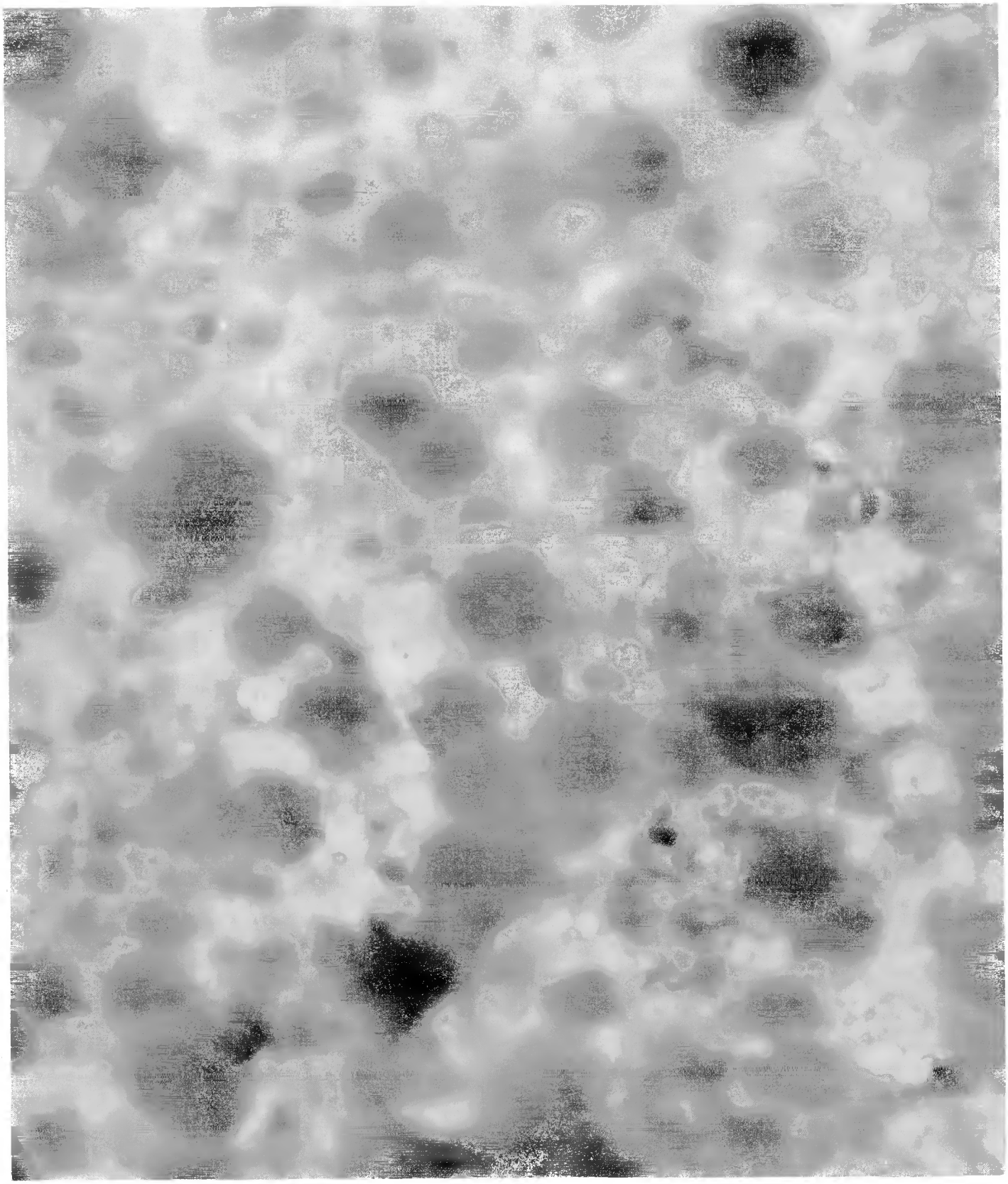

X-29-91

Fig. 79. Replica of surface of type 347 stainless steel pretreated in 2% chromic acid at 250°C. This picture shows more clearly the nature of the crystallites observed in the background in Fig. 78. Note the rodlike shape. 45,000×.

DECLASSIFIED X-29-90

E-875-2

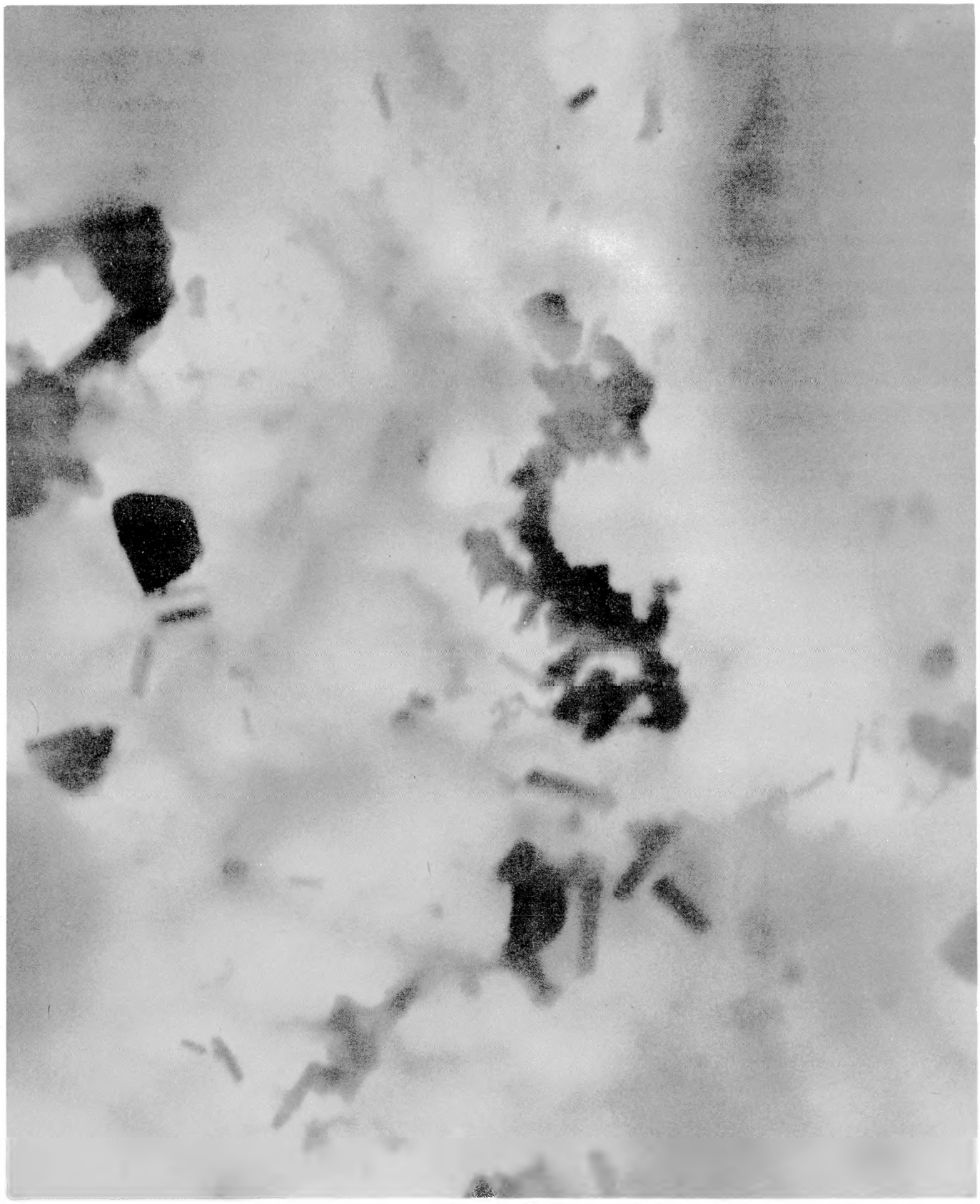

DECLASSIFIED X-29-111

The following four photographs are electron micrographs of replicas of type 347 stainless steel immersed in 0.17 *M* uranyl sulfate containing 0.1 *M* HNO_3 for 3200 hr at 250°C.

DECLASSIFIED X-29-112

Fig. 80. Electron micrograph illustrating the type of overall surface observed on this sample. It is composed of a dense mass of small particles which give it a crustlike appearance. There are some portions which overlap, labeled (1), and in other fields can be seen open areas, labeled (2). (Compare with Fig. 75.) The black dots in the background appear to be exceedingly small particles deposited on the outer surface of the crust. These could well be submicro crystallites of U_3O_8. X-ray examination of this sample showed the presence of α Fe_2O_3 or Cr_2O_3, and there was one line which could be associated with U_3O_8. 9000×.

X-29-113

E-840-3

UNCLASSIFIED X-29-114

Fig. 81. In this view of the sample are shown more closely the shape and compacting of the particles making up the surface. Cracks in the upper half of the picture are breaks in the replica film and should be disregarded. 9000×.

X-29-115 A31712A1030

E-840-1

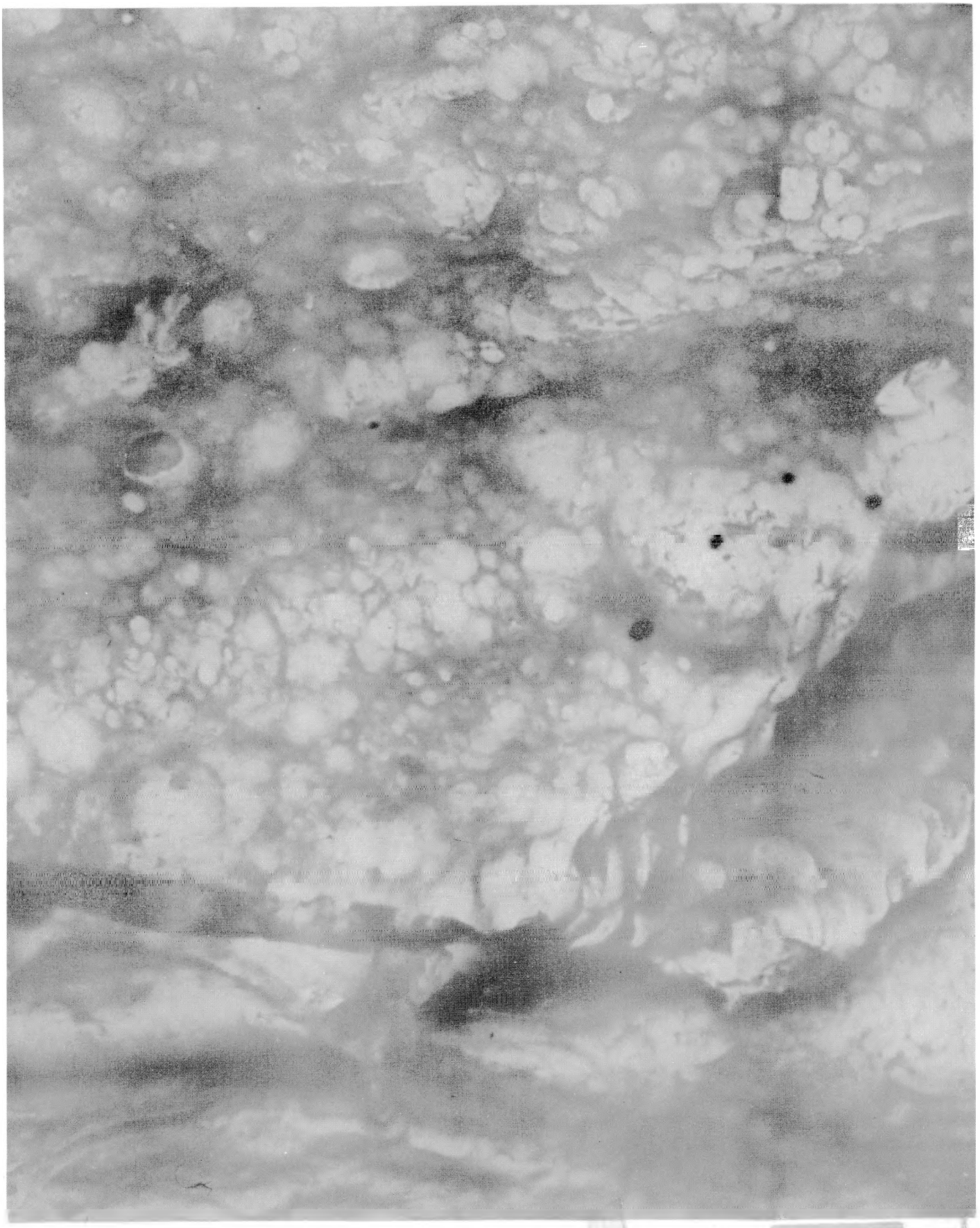

UNCLASSIFIED X-29-116

Fig. 82. This electron micrograph of the sample illustrates that, although the surface is seemingly tight at lower magnifications, openings between particles and rows of particles do exist. This suggests that the upper layer is permeable. 45,000×.

X-29-117

E-841-3

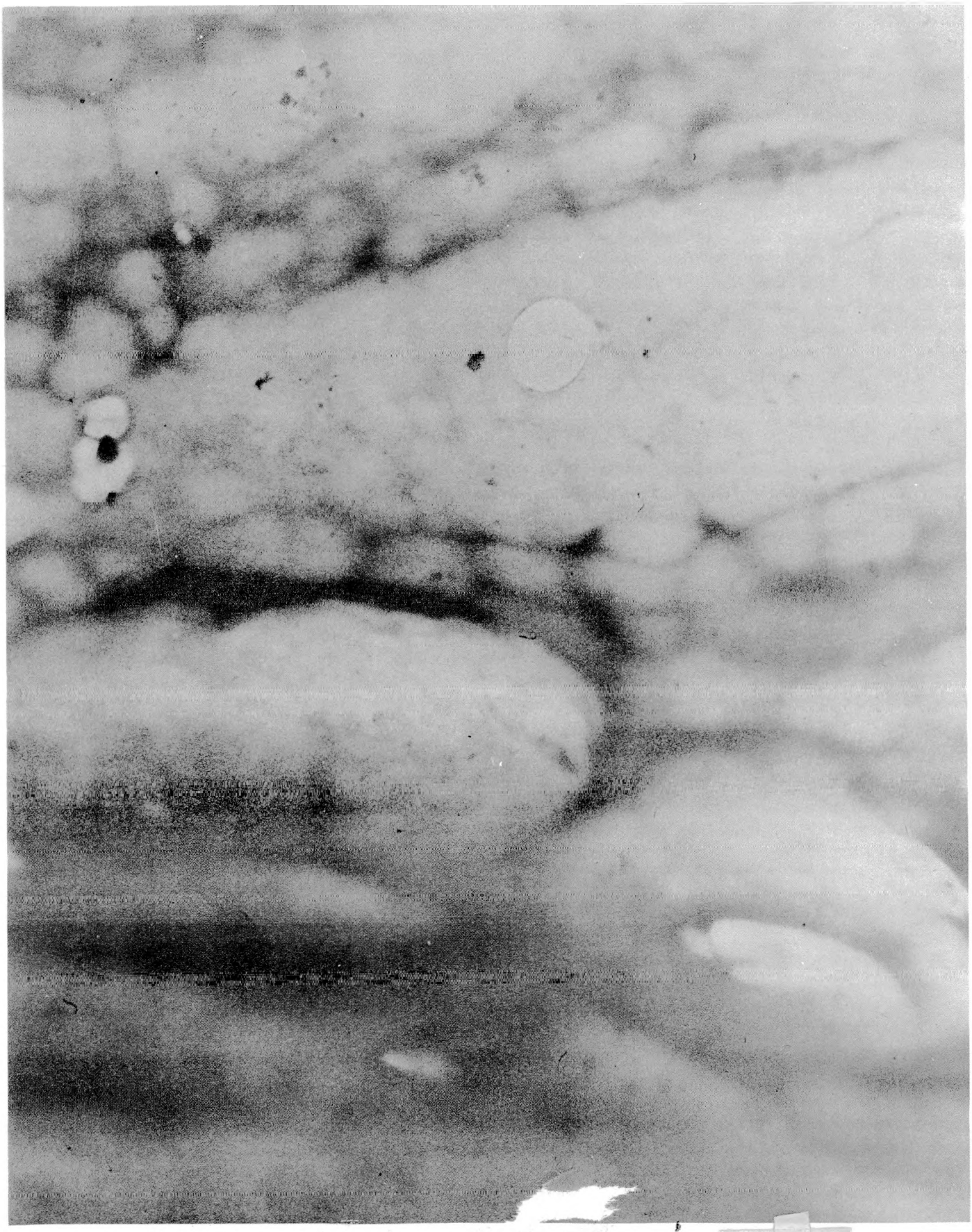

UNCLASSIFIED X-29-118

Fig. 83. Another area of the sample, showing well-formed crystals very similar to those observed in Fig. 76. It is believed that the area pictured here may be representative of the material lying immediately below the outer crust, possibly at such an opening in the outer surface as seen at (2) in Fig. 78. 45,000×.

X-29-11

E-841-5

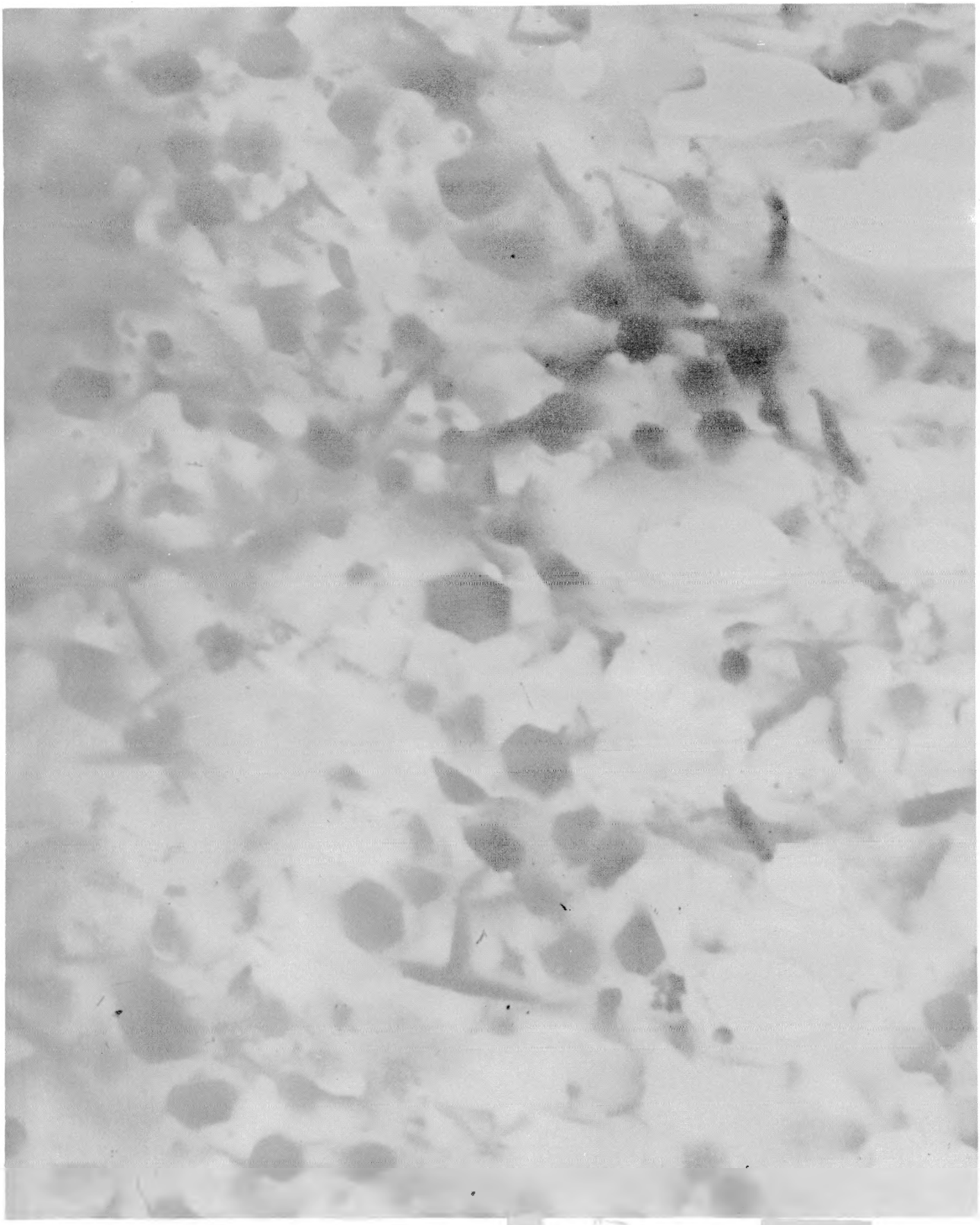

DECLASSIFIED X-29-120

Work Done in Relation to the HRE Project

Microscopic studies of the structure of crystal bar and Bureau of Mines zirconium.

1. Relationship of structure to previous treatment, i.e., heat-treatment, annealing, cold-working, hot-working, extrusion, etc.
2. Attempted identification of inclusions other than the carbide and nitride.

Microscopic studies of the structure and surface of Bureau of Mines zirconium after corrosion tests, i.e., immersion in uranyl sulfate solution.

1. Deposition of uranium oxide (U_3O_8) on surface and intergranularly observed on corroded specimens.
2. The observation and identification of the corrosion product as the monoclinic variation of zirconium oxide.
3. Studies which attempted to show the relationship between carbide inclusions and passivity of Bureau of Mines zirconium, e.g., electron microscopy of areas adjacent to carbide inclusions before and after corrosion tests.

Metallographic studies of stainless steel in relation to its use in the HRE.

1. Cross sections of various types and sizes of stainless-steel tubing and fittings prior to use.
2. Cross sections of stainless-steel tubing and fittings that had failed.
3. Cross-section studies of 347-stainless-steel fittings and tubing prepared by induction brazing and blanks of the same material to show microstructure and intergranular diffusion of silver solder after treatment.
4. Studies of the microstructure of stainless steel after corrosion tests.
5. Optical and electron microscope studies of the corroded surface, and material stripped from this surface of stainless steel 347 after corrosion tests.
    a. Layer thickness measurements.
    b. X-ray examination.

DECLASSIFIED X-29-121

6. Studies of the surface films or layers on type 347 stainless steel induced by pretreatment with 1% nitric acid and 2% chromic acid.
   a. Layer thickness measurements.
   b. X-ray examination.

Work Proposed in Relation to the HRE Project

Surface examination of hot samples at low power for pits, cracks, and buckling in protective layers.

Studies to determine any changes in protective layers of pretreated samples (HNO_3 and chromic acid) as a function of time before use and changes induced by being kept in an as-wet state (H_2O) or dry (room temperature and humidity).

Further studies of corroded stainless-steel surfaces by electron microscopy using replica techniques.

Investigation of the possibilities of using replica techniques with hot samples of stainless steel so that earlier studies can be made of possible radiation damage to protective layers.

Continuation of previous work on induction brazing of stainless steel in an attempt to further a reproducible method of producing assemblies that will stand up under working conditions.

Cooperation with personnel about to embark on electrochemical studies.

Continued work on zirconium corrosion problems.

Conclusions

Brazing of Stainless Steel by Induction Methods. Studies to date, results of which are shown in the microphotographs included in this report, suggest that a closer time and temperature control should be established on the process. Other expedients, which might lead to a refined grain size and a stronger structure, should possibly be tried, including (1) introduction of small amounts of nitrogen with the hydrogen gas, and (2) more rapid cooling of the assembly after fusion has taken place.

DECLASSIFIED X-29-122

From the standpoint of corrosion, the introduction of hydrogen at the elevated temperatures used in the past would appear to be injurious. Possibly some method to stop the flow of hydrogen, when the flow point of the solder is reached, could be worked out.

Studies of Films and Layers Formed on Passivation-treated 347 Stainless Steel and on Stainless Steel Immersed in 0.17 *M* Uranyl Sulfate Containing 0.1 *M* Nitric Acid for 3200 hr at 250°C. The observations made on the samples included in this report, while not conclusive, suggest the following:

1. Pretreatment methods, while establishing a seemingly protective film, also induce the growth of a crystalline layer on the surface of the substrate film which may act as a focus for formation of U_3O_8 which adheres to it.

2. Whereas so-called "protective films" are reported as being in the region of about 100 to 300 A in thickness, all pretreated material received so far has had an overall layer thickness of the order of 5 to 7 μ.

3. The layers formed above the substrate during corrosion tests are not protective in nature, inasmuch as they appear to be extremely porous.

4. From the electron microphotographs there appears to be some difference in the nature of the material formed at the surface of the stainless steel when chromic acid or nitric acid is used for pretreatment. The effect of this has not been determined.

5. X-ray results, while negative in the case of the pretreated samples, do show that the principal constituent of the outer built-up layer on the corrosion-test specimen is either Cr_2O_3 or α Fe_2O_3.

UNCLASSIFIED ORNL-29-123

V. RECOMBINATION OF HYDROGEN AND OXYGEN

DECLASSIFIED

INTRODUCTION

During the past quarter emphasis has been placed on study of catalytic recombination of hydrogen and oxygen to provide a basis for the design of catalytic recombiners for the reflector system as well as for use as supporting units in the fuel system. The study of explosion limits has been extended to lower temperatures and pressures and to include more complex gas mixtures. The feasibility demonstration of the combustion type recombiner has been virtually concluded, and preliminary testing of a catalytic secondary recombiner has been satisfactorily completed.

LABORATORY-SCALE STUDIES

W. R. Grimes
D. W. Kuhn
F. L. Daley
A. D. Ryon
A. A. Palko
K. O. Johnsson

Composition Limits for Explosions in Hydrogen-Oxygen Mixtures. The investigation of explosion limits in hydrogen-oxygen-steam mixtures as previously reported (ORNL-826) has been continued with a larger bomb of improved design. The explosion limit determined with this larger bomb (1050 ml volume, 3¾ in. I.D.) is, as shown in Table 18, lower than that observed in the earlier work (65-ml bomb, 1 in. I.D.). This is not surprising since it is known that in tubes of small diameter the observed explosion limit is a function of the diameter of the tube used for flame propagation. In tubes 2 in. in diameter and smaller the observed explosion limit increases as the tube diameter decreases. However, for tubes larger than 2 in. in diameter the observed explosion limit is virtually independent of tube diameter.

Explosion limits were also determined in this same apparatus for hydrogen-oxygen-helium-steam mixtures. Here again the gas mixture was in contact with liquid water in the bomb, so that the partial pressure of steam was determined by the temperature of the experiment. The pertinent data are shown in Table 19.

In all the explosion limit studies previously reported, the hydrogen-oxygen mixture was in the stoichiometric ratio of 2 moles of hydrogen to 1 mole of oxygen. Work has just been begun on determining how the explosion limit is

DECLASSIFIED

TABLE 18

Explosion Limits in H_2-O_2-Steam Mixtures

TEMPERATURE (°C)	TOTAL PRESSURE (psia)	PARTIAL PRESSURE (psia)			EXPLOSION LIMIT (% H_2 + O_2)
		H_2	O_2	STEAM	
100	19.06	2.83	1.42	14.81	22
113	29.3	4.3	2.2	22.8	22
147	85.0	14.3	7.1	63.6	25
170	158	29	14	115	27
180	199	36	18	145	27
192	262	47	23	192	27
242	661	105	52	504	24

TABLE 19

Explosion Limits in H_2-O_2-He-Steam Mixtures

TEMPERATURE (°C)	TOTAL PRESSURE (psia)	PARTIAL PRESSURE (psia)				EXPLOSION LIMIT		
		H_2	O_2	He	STEAM	% H_2 + O_2	% He	% H_2O
140	952	92	46	761	53	15	80	5
172	965	97	48	699	121	15	72	13
194	950	95	47	611	197	15	64	21
245	1018	128	64	292	534	19	29	52

DECLASSIFIED

affected if hydrogen, for example, is present in excess of the stoichiometric ratio. The data in Table 20 are probably typical of what may be expected.

TABLE 20

Explosion Limits in H_2-O_2-Steam Mixtures with Excess H_2

TEMPERATURE (°C)	TOTAL PRESSURE (psia)	PARTIAL PRESSURE (psia)			EXPLOSION LIMIT		
		H_2	O_2	H_2O	% H_2 + O_2	% H_2	% O_2
100	19.06	2.83	1.42	14.81	22	14.7	7.3
101	22.76	5.90	1.35	15.51	32	26	6.0

In the second mixture the composition of the dry gases is 81% hydrogen and 19% oxygen. The explosion limit in this case is probably dependent upon a sufficient percentage of oxygen in the gas-steam mixture.

Catalytic Recombination of Hydrogen and Oxygen. The use of "Product 43" (1% platinum on charcoal) as a catalyst for the recombination of hydrogen and oxygen mixed with steam has been investigated over a wide range of conditions. The catalyst has been found to give excellent conversions even at high flow rates, its principal limitation being that at temperatures above 350°C oxidation of the charcoal begins, as shown by the evolution of CO_2. For this reason experiments with other catalysts and catalyst supports are now in progress. One catalyst, prepared by depositing platinum on activated Al_2O_3, has been found to be as effective as Product 43.

Most of the testing of Product 43 has been carried out in a ¾-in. stainless-steel pipe (0.82 in. I.D.), and the length of the catalyst bed has been varied from 2 to 17 in. The composition of the hydrogen-oxygen-steam mixture has been varied from 0.2% electrolytic gas + 99.8% steam to 56% electrolytic gas + 44% steam. It must be pointed out that 56% electrolytic gas is far in excess of the allowable concentration of electrolytic gas when the reaction is carried out in a relatively massive bed such as a packed tube, since with rich mixtures the catalyst temperature exceeds 500°C and excessive burning of the charcoal results. It has been found that if the composition is maintained

DECLASSIFIED

at not more than 5% electrolytic gas, the catalyst temperature will not exceed 350°C, all the heat of reaction being transferred to the steam passing through the catalyst bed. Flow rates have been varied from 2 to 88 liters per minute. Space velocity, defined as the number of volumes per hour of electrolytic gas-steam mixture (calculated at 0°C and 1 atm) passing through unit volume of catalyst, has been varied from 600 hr^{-1} to 130,000 hr^{-1}.

The data in Table 21 were obtained with Product 43 catalyst in ¾-in. pipe, the length of catalyst bed being either 2 or 4 in., as indicated. As shown in Fig. 84, the efficiency of the catalytic conversion is, in certain limiting cases, dependent on temperature. This may be observed only at high space velocities, such as the 120,000 hr^{-1} cited in Fig. 84, curve *B*. At space velocities of the order of 30,000 hr^{-1} (curve *A*), the reaction is at least 99% complete even at temperatures less than 200°C. Figure 85 illustrates the same fact in showing the effect of composition on percent conversion. The richer mixtures on curve *B* of Fig. 85, show a higher conversion because the catalyst temperature increases as the proportion of electrolytic gas increases. In curve *A*, however, the space velocity is low enough (28,000 hr^{-1}) so that even in dilute mixtures, where the maximum catalyst temperature is as low as 182°C, the conversion is essentially 100% complete.

On the basis of these observations it is recommended that, when using Product 43 catalyst, the temperature of the catalyst not be allowed to exceed 350°C and that space velocities be not more than 35,000 hr^{-1}.

Pressure Drop Across Catalyst Mass. Since such data were necessary for engineering calculations relating to design of catalytic recombiners, the pressure drop across Product 43 masses in tubes of various sizes and at various gas flow rates was measured. For these measurements the Product 43 was packed in stainless-steel pipe. The gas used was air with the pressure drop measured by means of a draft gauge or U-tube manometer while the flow rate was measured with a wet-test meter or calibrated rotameter. The data obtained are shown in Table 22.

Poisoning of Product 43. It was stated in a previous report (ORNL-826) that Product 43 was not poisoned by moderate quantities of iodine. In those experiments apparatus was fabricated from stainless steel, when the apparatus was dismantled it was observed that severe corrosion of the steel had occurred,

DECLASSIFIED

TABLE 21

Catalytic Conversion of H_2-O_2 Mixtures to Water, Platinum-on-charcoal Catalyst

FEED TEMPERATURE (°C)	MAXIMUM CATALYST TEMPERATURE (°C)	TEMPERATURE RISE (°C)	COMPOSITION (% electrolytic gas)	STEAM FLOW RATE (liters/min at 100°C)	SPACE VELOCITY (hr^{-1})	EFFICIENCY OF CONVERSION REACTION (%)
140	170	30	0.85	87	120,000	86.0
160	195	35	0.85	87	120,000	94.8
185	215	30	0.85	87	120,000	97.9
215	240	25	0.85	87	120,000	98.9
150	175	25	0.43	87	120,000	96.7
150	190	40	0.85	87	120,000	97.6
150	225	75	1.7	87	120,000	99.0
185	205	20	0.43	87	120,000	98.2
185	220	35	0.85	87	120,000	98.8
185	250	65	1.7	87	120,000	99.2
125	145	20	0.93	40	55,000	90.0
125	180	55	1.8	40	55,000	96.2
125	215	90	2.7	40	55,000	98.4
125	250	125	3.6	40	55,000	99.2
125	182	57	1.8	20	28,000	99.98
125	237	112	3.6	20	28,000	99.95
125	302	177	5.3	20	28,000	99.83
125	360	235	7.0	20	28,000	*
150	260	110	3.6	10	31,000**	98.7
150	400	250	7.0	10	31,000**	99.13

* Some burning of charcoal occurred owing to high temperature. Formation of CO_2 interfered with usual determination of efficiency.

** In these two cases catalyst bed length was 2 in.; all others had a 4-in. bed length in ¾-in. pipe (0.82 in. I.D.).

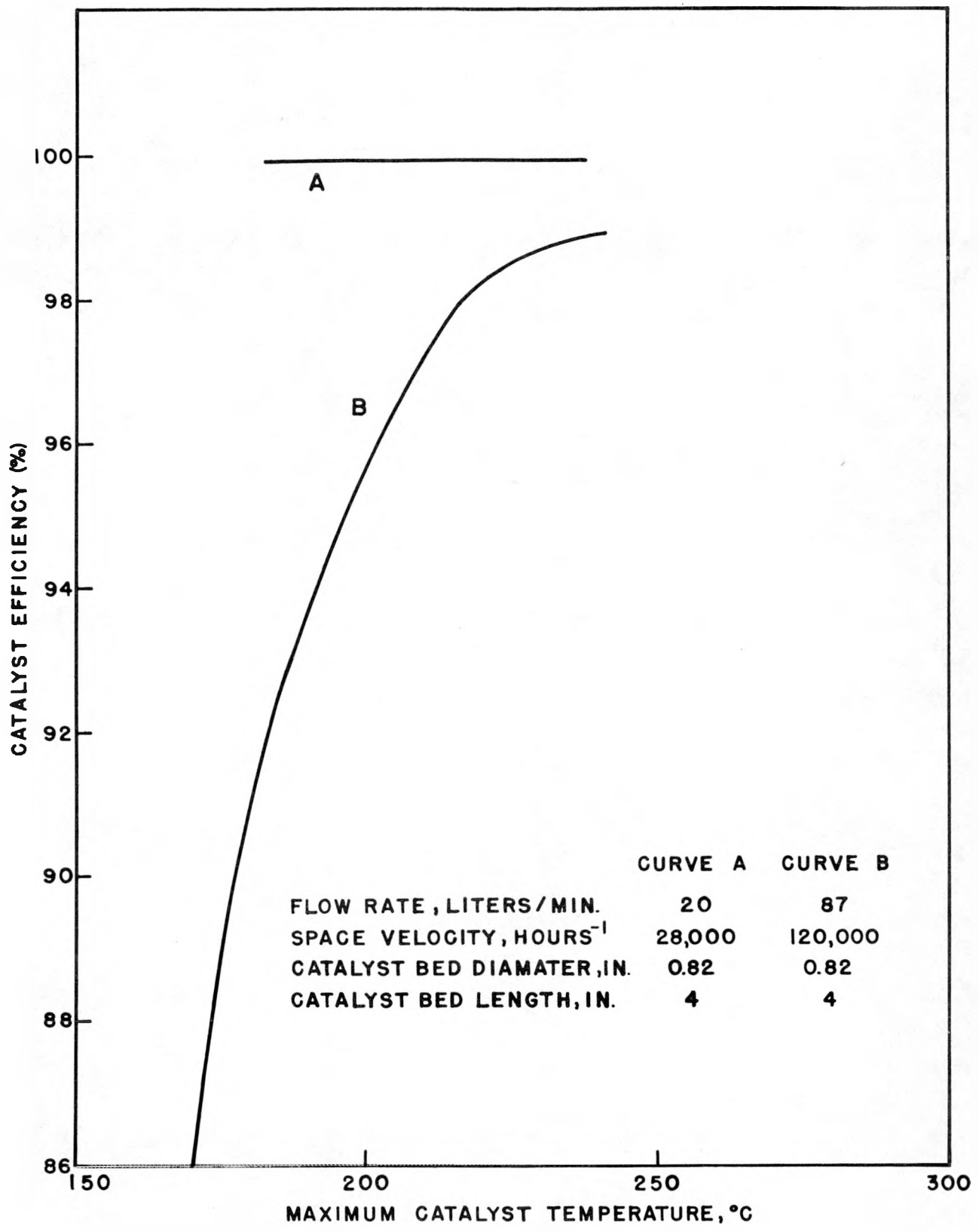

FIGURE 84 VARIATION OF CATALYST EFFICIENCY WITH TEMPERATURE

DECLASSIFIED

DWG. 10117

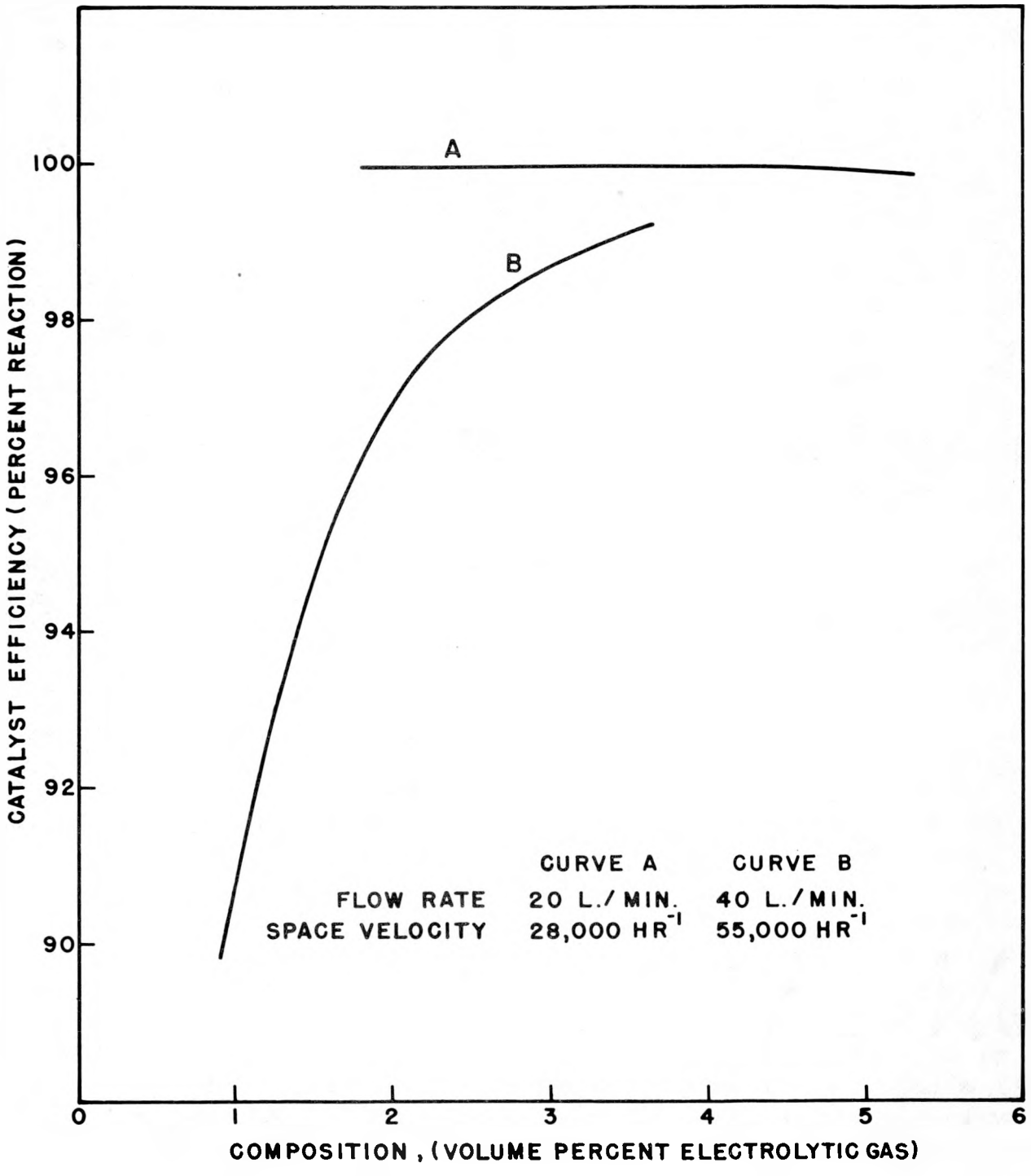

FIGURE 85 EFFECT OF GAS COMPOSITION AND FLOW RATE ON CATALYST EFFICIENCY

DECLASSIFIED

TABLE 22

Pressure Drop Across Packed Tubes of Product 43

3/4-IN. PIPE			1¼-IN. PIPE			2-IN. PIPE		
FLOW RATE		Δ P/IN. OF BED	FLOW RATE		Δ P/IN. OF BED	FLOW RATE		Δ P/IN. OF BED
liters/min	cfm	(in. of H_2O/in.)	liters/min	cfm	(in. of H_2O in.)	liters/min	cfm	(in. of H_2O in.)
4.2	0.15	0.083	2.8	0.10	0.01	51	1.8	0.20
6.8	0.24	0.17	5.4	0.19	0.022	76	2.7	0.40
8.8	0.31	0.25	8.8	0.31	0.042	93	3.3	0.60
10.5	0.37	0.33	14.7	0.52	0.080	108	3.8	0.80
11.9	0.42	0.42	16.7	0.59	0.10	119	4.2	1.0
16.4	0.58	0.67	22.7	0.80	0.16	130	4.6	1.2
20.7	0.73	1.00	25.5	0.90	0.20	147	5.2	1.6
			45	1.6	0.40	161	5.7	2.0

and it seemed likely that no iodine had reached the catalyst. More recent experiments with all-glass systems, to ensure that iodine is actually available to the catalyst, have shown that some poisoning does occur.

When 25 g of Product 43 was exposed to a flow of 33 mg per hour of iodine for 50 hr and then exposed for 18 hr to a flow of 9 liters per hour of steam, the efficiency of the catalyst was found to be 44, 83, and 94% of its initial value at temperatures of 180, 300, and 408°C, respectively. It appears that the efficiency of the poisoned catalyst is strongly dependent upon the reaction temperature.

In other tests the efficiency of fresh portions of catalyst was measured and subsequently checked at intervals following addition of known quantities of iodine vapor to the gas stream. In most of these studies 20-g portions of catalyst were exposed to 9 liters per minute of steam with 200 ml per minute of electrolytic gas and 47 mg per hour of iodine. While the efficiency of each portion tested has decreased with increasing exposure, there has been considerable variation in the amount of poisoning in the various tests. Analysis of the materials is not yet complete, but it appears that considerably more iodine is absorbed by the catalyst at low temperatures and that the poisoning is therefore more rapid and severe at the lower temperature. Elevation of the temperature serves to remove some but not all of the effect.

Since the amount of iodine fed per gram of catalyst is very much higher in these experiments than in the anticipated recombiner, it seems safe to say that poisoning by iodine should not be a major difficulty in actual operation. Studies designed to better evaluate poisoning by iodine and other materials are currently in progress.

The deleterious effect of uranium, as from entrained spray, on the catalyst bed has been approximated by dipping the catalyst in a 5% uranyl sulfate solution, drying the material, and testing its catalytic activity. After one dip the efficiency of the catalyst had dropped to about 75% and after two dips to about 50% of its original value. Analysis indicated that the material had picked up uranium equivalent to 4% of its weight. It is apparent, however, that if the catalyst were to serve as the primary recombiner, it would be necessary to guard against its exposure to entrained spray.

DECLASSIFIED

Preparation for In-pile Testing of Catalysts. Actual exposure of catalysts to hydrogen and oxygen produced during in-pile irradiation of uranium sulfate solutions has seemed very desirable as a method of simulating poisoning of the catalyst by gaseous fission products and uranyl sulfate spray. In preliminary tests without irradiation Product 43 has been supported on a stainless-steel gauge in a small bomb containing water at 250°C and has successfully recombined hydrogen and oxygen from an external source. The bomb assembly for in-pile study has been chosen and is now under test without irradiation. Irradiation of this specimen is scheduled to begin in the very near future.

PILOT-SCALE TESTS OF RECOMBINERS

W. R. Grimes T. S. Mackey
H. M. McLeod Don Phillips

A previous report (ORNL-826) has described the essential features of, as well as some preliminary operations with, a burner type recombiner for the fuel circuit. During the past quarter continued operation of this apparatus has demonstrated the feasibility of this equipment. A satisfactory system for quenching flash backs has been designed and tested. In addition, preliminary pilot-scale testing of a catalytic secondary recombiner has been satisfactorily completed.

Testing of the Burner System. Preliminary tests previously described provided necessary data for the selection of the most suitable burner orifice for the expected gas-flow range and optimum steam-flow values for prevention of flash backs at the lower gas-flow rates. This information provided the basis for the design of the pilot plant.

Description of Assembly. The pilot-plant installation consisted of a burner chamber, a condensate pot, and a condensate receiver, all contained within a sandbag barrier as a protection in the event of an explosion, together with equipment for metering hydrogen, oxygen, and steam, and for measuring and recording temperatures and pressures at various points in the system. The desired quantities of mixtures of $H_2 + \frac{1}{2}O_2$ and steam passed through preheaters to prevent condensation of the steam and entered the burner chamber through the burner orifice, where they were burned in contact with a spark. The water-cooled burner chamber (designed to condense up to about 30 lb of

DECLASSIFIED

steam per hour) was placed in a vertical position and connected to the condensate pot by means of a 2-in. pipe which extended 2 in. above the bottom of the burner chamber to maintain a constant level of condensate at that point as a protection for the bottom. The condensate pot contained an overflow outlet 4 in. above the bottom and was provided with means for heating or cooling as desired. Condensate and unrecombined gases overflowed into a receiver from which the water was siphoned at intervals for measuring. Unrecombined gases left the receiver through a cooler, where most of the water vapor was removed, and were conducted outside the sand barrier, where they were passed through a wet-test meter for measuring their volume or were discharged under about 6 in. of water to the atmosphere.

Operating Procedure. To demonstrate the feasibility of the flame recombiner as well as to obtain additional data on the performance of burner orifices, three pilot-plant runs, each lasting 5 to 6 hr, were made employing a flow rate of about 17 cfm with each of three different orifices; runs lasting 2 hr were also made with each orifice employing a gas flow rate of from 0.21 to 0.26 cfm with a steam flow rate of about 0.5 cfm. The orifices employed in these runs consisted of: (1) a hollow cylinder formed from a 3/4-in. standard copper pipe plug with approximately 1/8-in.-thick plate containing sixty-five 1/32-in.-diameter holes, (2) a solid type 316 stainless-steel cylinder about 9/16 in. thick, threaded to fit a standard 3/4-in. pipe tap, and containing sixty-five 1/32-in.-diameter holes, and (3) a solid copper cylinder which otherwise was the same as No. 2 except that its thickness was 1/16 in. less. Runs 1M and 1L were carried out employing burner orifice No. 1, runs 2M and 2L employing No. 2, and runs 3M and 3L employing No. 3. The burner-chamber cover plate, which contained the burner hood and orifice, was cooled by steam in run 1M and by water in all other runs.

Prior to starting a run at high gas flow rates (M series), cooling water was turned into the burner-chamber shell, cover plate, and condensate pot, and steam for heating the gases was turned into the heat exchanger. The system was purged with nitrogen, after which the flow of oxygen was started at a rate of about 1 cfm and that of metered steam at about 0.75 cfm. As soon as the temperature of the gases leaving the heat exchanger reached 300°F, the ignition system was turned on, the flow rate of oxygen was reduced to about 1/3 cfm, and that of hydrogen started at about 2/3 cfm. Burning of the gases was indicated by a pyrometer connected to a thermocouple located in the burner hood adjacent

DECLASSIFIED

to the flame. As soon as this temperature reached equilibrium, usually at about 350°F, the flow of combined gases was increased to the desired value while that of steam was shut off. The procedure for starting a run at low gas flow rates (L series) was essentially the same except that the steam flow rate was maintained constant at about 0.5 cfm and the gas was ignited at a combined gas flow rate of about 0.25 cfm and then adjusted downward to the rate below which combustion was not self-sustaining. At 15-min intervals the product water was siphoned from the receiver for measurement and the volume of unrecombined gases leaving the burner chamber was recorded. The results of the tests are given in Table 23.

Conclusions. For the runs with gas flow rates of about 17 cfm, the results show that the water produced in the recombination averaged about 31.8 lb per hour, which was slightly in excess of the 30 lb per hour equivalent of the maximum rate of gas formation at a power level of 1000 kw. The maximum deviation from the average in the hourly measurements of the product water was only 2.16%, indicating that steady flow rates were maintained rather closely during the runs. The average volume of unrecombined gases was 0.252 cfm during run 1M and 0.085 cfm during run 3M, largely because of unbalanced flow rates due to frequent changing from empty to full hydrogen and oxygen cylinder banks. However, during intervals between changes it was observed that the off-gas rate was as low as 0.083 cfm during run 2M and 0.033 cfm during run 3M. (Facilities were not available for measuring unrecombined gases during run 1M.) It was concluded that recombination in a closed system was feasible with combined gas flow rates of about 17 cfm and that the recombination was essentially complete.

For the runs with gas flow rates of 0.26 cfm or less, the results show that sustained combustion was maintained over a 2-hr period with combined gas flow rates as low as 0.21 cfm and a steam flow rate equivalent to about 0.46 cfm in runs 1L and 2L (31% gas) and 0.26 cfm of combined gas with about 0.46 cfm of steam in run 3L(36% gas). Combustion was not sustained for periods longer than 30 min below those gas flow rates. The volume of unrecombined gas leaving the burner chamber was negligible, indicating that recombination was essentially complete. The lowest gas flow rate that would sustain combustion in run 3L was 0.26 cfm as compared to 0.21 cfm in runs 1L and 2L; this may have been due to partial condensation of steam in the orifice openings. A water balance shows an excess for runs 1L, 2L, and 3L, amounting to 4.2, 8.2,

DECLASSIFIED

TABLE 23

Data from Pilot-plant Runs at Both High and Low Gas Flow Rates

RUN NO.	DURATION (hr)	BURNER ORIFICE NO.	PRODUCT WATER			OFF-GAS			COMBINED GAS FLOW RATES	
			TOTAL (lb)	AVERAGE (lb/hr)	MAXIMUM HOURLY DEVIATION (%)	TOTAL OFF-GAS (cu ft)	cfm at 70°F, 1 atm		$H_2 + \frac{1}{2}O_2$ (cfm at 70°F, 1 atm)	EQUIVALENT WATER (lb/hr)
							AVERAGE	LOWEST OVER 15-MIN PERIOD		
1M	6	1-H	191.5	31.9	-2.18	Not measured	Not measured	Not measured	17.1	31.84
2M	5	2-T	159.4	31.8	+2.14	75.65	0.252	0.083	17.1	31.84
3M	6	3-T	190.5	31.75	-1.6	30.5	0.085	0.033	17.0	31.65
1L	2	1-H	3.35	1.675		1.1	0.005		0.21	0.39
2L	2	2-T	3.79	1.89		0.095	0.0008		0.21	0.39
3L	2	3-T	3.62	1.81		None			0.26	0.48

and 0.6%, respectively, of the water that should have resulted from recombination and from steam condensation. Inasmuch as the close control of steam flow at these low flow rates is rather difficult, the errors indicated by measurements of total water produced are not regarded as serious. In general, the results of the runs at low gas flow rates were consistent with those obtained previously in the burner tests, and it was concluded that, by using a burner orifice similar to the orifices used in the pilot runs, the entire range of gas flow rates could be recombined if a small catalytic recombiner were installed to follow up the flame recombiner.

Automatic Quenching of Flash Backs. During operation of the pilot plant, considerable difficulty was experienced with flash backs. Although rearrangement of the piping resulted in minimizing the time lost due to flash backs, it was recognized that a recombination system should be developed with the viewpoint that flash backs were to be expected and that the necessary provisions for automatically quenching flash backs should be incorporated in the system. It appeared that the most promising method was that of maintaining a noncombustible mixture of gas and steam (about 25% gas) from the core up to a point near the burner chamber, at which point most of the diluting steam would be condensed and removed from the gas stream, leaving a mixture saturated with water vapor at the temperature and pressure of the system at the condenser exit.

The equipment for testing this possibility consisted of a vertically positioned tubular condenser, 4 in. in diameter and 5 ft long, containing seventeen ¼-in. pipes of 316 stainless steel around which the coolant water circulated, an electrically heated condensate pot operated as a reboiler, and a fitting which contained the burner orifice. A spark plug for igniting the gas behind the orifice burner was introduced to produce the flash backs. The gas and steam mixture was heated to about 250°F and passed into the bottom of the condenser, where most of the steam was condensed, and then passed upward and out to the burner orifice, where combustion was maintained by contact with a spark generated by a test coil.

Preliminary tests showed that flash-back quenching was not achieved when the condenser was operated as a total condenser (cold) with no steam in the inlet gas stream. With a 50% gas-steam mixture entering the condenser at a rate of about 2.3 cfm and with an exist gas temperature of about 155°F, flash

DECLASSIFIED

backs were repeatedly quenched in the condenser assembly, and in every case the gas readily relighted at the burner orifice. The conditions at the inlet and outlet of the condenser over a 15-min test period are given in Table 24.

TABLE 24

Conditions at the Condenser Inlet and Outlet During Flash-backs Quenching Tests

(Data obtained over a 15-min period)

	TEMPERATURE (°F)	FLOW RATES		COMPOSITION OF "STEAM"	
		GAS (cfm)	STEAM (cfm)	GAS (%)	STEAM (%)
Inlet	212	1.1	1.2	47.8	52.2
Outlet	156	1.1	0.23*	82.7	17.3

* Water vapor.

The results show that, under the conditions of the test, flash backs were quenched in the condenser without flashing back to the point of admixture of hydrogen and oxygen. Also, after every flash back the gas was relighted readily by the external spark. It should be emphasized that lack of quenching in the preliminary tests may have been due to lack of depth in the noncombustible zone caused by operating the condenser cold so that the shock wave resulting from the flash back either penetrated the zone or dispersed it to permit propagation of the flame front back to the point of mixing hydrogen and oxygen.

Testing of Catalytic Recombiner. The pilot-plant tests showed that a flame recombiner was suitable for recombining stoichiometric mixtures of hydrogen and oxygen at flow rates ranging from about 0.25 cfm of gas up to the maximum flow of about 17 cfm and that sustained combustion could not be maintained at flow rates much lower than 0.25 cfm. Tests conducted by another group indicated that recombination of electrolytic gas in the presence of a catalyst (Pt on charcoal) was complete provided the gas was diluted with steam to give an approximately 5% gas mixture and that the maximum catalyst bed temperature was not in excess of 750°F. Consequently tests were conducted to

DECLASSIFIED

determine: (1) the difference in catalyst bed temperature at various points in the bed at constant flow of steam and gas; and (2) the recombination efficiency, with the maximum bed temperature maintained at about 750°F.

The catalyst chamber consisted of an 8-in.-long section of standard 2-in. pipe of 316 stainless steel in which the 4.5-in.-long catalyst bed was maintained between two screens. Temperature along the length of the bed and that of the inlet gas stream were determined by moving a thermocouple in the thermowell, which extended completely through the bed. The combined gases were heated to above 212°F in a heat exchanger, after which they were mixed with steam and then passed into the catalyst chamber where the gases were reacted. The steam and unrecombined gases were then passed first into a condenser, to condense out the steam, and then through a wet-test meter to the atmosphere.

The initial test, for the purpose of determining the temperature of the gas stream at various points in the catalyst bed with constant gas and steam flow, was carried out with a gas flow rate of about 0.55 cfm and with sufficient steam so that the inlet mixture contained about 9% gas. Prior to starting the run the thermocouple was positioned at about the midpoint of the bed, and as soon as the temperature at this point remained unchanged over a 15-min period, temperatures were measured at ½-in. intervals throughout the length of the bed. These measurements indicated that the temperature of the gas stream as it passed through the bed rapidly increased from 212°F at the inlet to a maximum of about 1015°F at a point 3 in. from the bed inlet, after which the temperature decreased to about 780°F at the exit end.

The second test consisted of a 2-hr run with the maximum bed temperature held at about 750°F; the flow rate was about 8.3 cfm and the combined gas and steam contained 6% gas. The results in Table 25 show that recombination was 95% complete. Since the flow of hydrogen and oxygen during the 2 hr was not completely stoichiometric, the actual recombination efficiency probably was somewhat higher. The off-gas sample for which the analysis is shown was collected over an interval during the second hour, and the 11.2% CO_2 content indicates that some reaction between hydrogen and oxygen and the carbon occurred. Although it is known that the plant steam contains some CO_2, calculations based on the maximum possible quantity of CO_2 available from breakdown of Na_2CO_3 do not account for more than a small portion of that found in the off-gas sample. It may be concluded that catalytic recombination appears promising although study of catalysts with more inert base materials is needed.

DECLASSIFIED

TABLE 25

Operating Data for Catalytic Recombiner

Combined gas and steam flow rate (cfm)	8.3	Off-gas:	
Gas flow rate (cfm)	0.5	Total volume (cu ft)	3.125
Gas (% by volume)	6.0	Flow rate (cfm)	0.026
Maximum temperature in catalyst bed (°F)	752	Analysis (% by volume)	
Water balance:		H_2	74.4
Total collected (ml)	22,290	O_2	13.2
From steam (ml)	21,220	CO_2	11.2
From gas recombination (ml)	910	Efficiency, based on H_2 (%)	95
Excess (ml)	160		
Excess (% of total)	0.7		

PLANS FOR HRE

Based on experimental evidence, as reported previously, a recombiner for the HRE has been designed (see Fig. 3). The design specifications are given in Table 26. Figure 86 is a flow sheet outlining the plans for the catalytic recombiners and charcoal traps.

TABLE 26

Flame Recombiner Design Data

1.	Gas delivered to burner nozzle at 1000-kw power level of reactor	
	Hydrogen	0.0553 lb/min
	Oxygen	0.4400 lb/min
2.	Volume of Stoichiometric mixture at STP	14.79 cfm
3.	Total heat liberated	59.3 kw
		203,000 Btu/hr
4.	The combustible gas mixture generated in the reactor will be delivered to the burner nozzle mixed with a controlled amount of steam. It is assumed that the minimum combustible mixture consists of 30% gas and 70% steam. Actually, the gas mixture delivered to the nozzle will be in the order of 70% gas and 30% steam. The total pressure of combustible gas mixture and steam at the nozzle inlet is to be held at 14 psia. The delivery of gas and vapor mixture varies with the ratio of partial pressure of the combustible gas mixture to total inlet pressure as follows:	

UNCLASSIFIED

RATIO $\frac{P_{H_2} + P_{O_2}}{14}$	SATURATION TEMPERATURE (°F)	GAS-VAPOR MIXTURE FLOW RATE	
		(cfm)	(lb/min)
0.30	192	67.5	2.24
0.40	185	51.0	1.63
0.50	177	40.0	1.25
0.60	167	33.0	1.00
0.70	155	27.5	0.82
0.80	139	23.5	0.68
0.90	113	20.0	0.58
1.00		16.8	0.50

5. Burner Nozzle:

Material	Type 347 stainless steel
No. of holes	Approximately 150
Diameter of holes	0.0312 in.
Pitch of holes	3/32 in.
Length of holes	9/16 in.

6. Pressure drops through nozzle for gas-vapor at 1000-kw operating level of reactor:

GAS MIXTURE (% of total volume)	PRESSURE DROP (psia)
55	5
60	3
70	1.8
80	1.25
90	0.90
100	0.60

DECLASSIFIED

7. Heat transfer data:

Heat transfer surface area	Approximately 9.2 sq ft
Heat flux	Approximately 22,000 Btu/ft^2-hr
Average temperature gradient over combustion chamber wall	Approximately 66.8°F

8. Cooling water data:

	CALCULATED	EXPERIMENT
Quantity	3.12 gpm	7 gpm
Entrance temperature	70°F	70°F
Exit temperature	200°F	140°F

9. Combustion-chamber-wall average temperature 202°F

10. Combustion-chamber pressure data:

Working pressure of 70% mixture	12.2 psia
Design pressure	912 psig
Test pressure	1375 psig

DECLASSIFIED

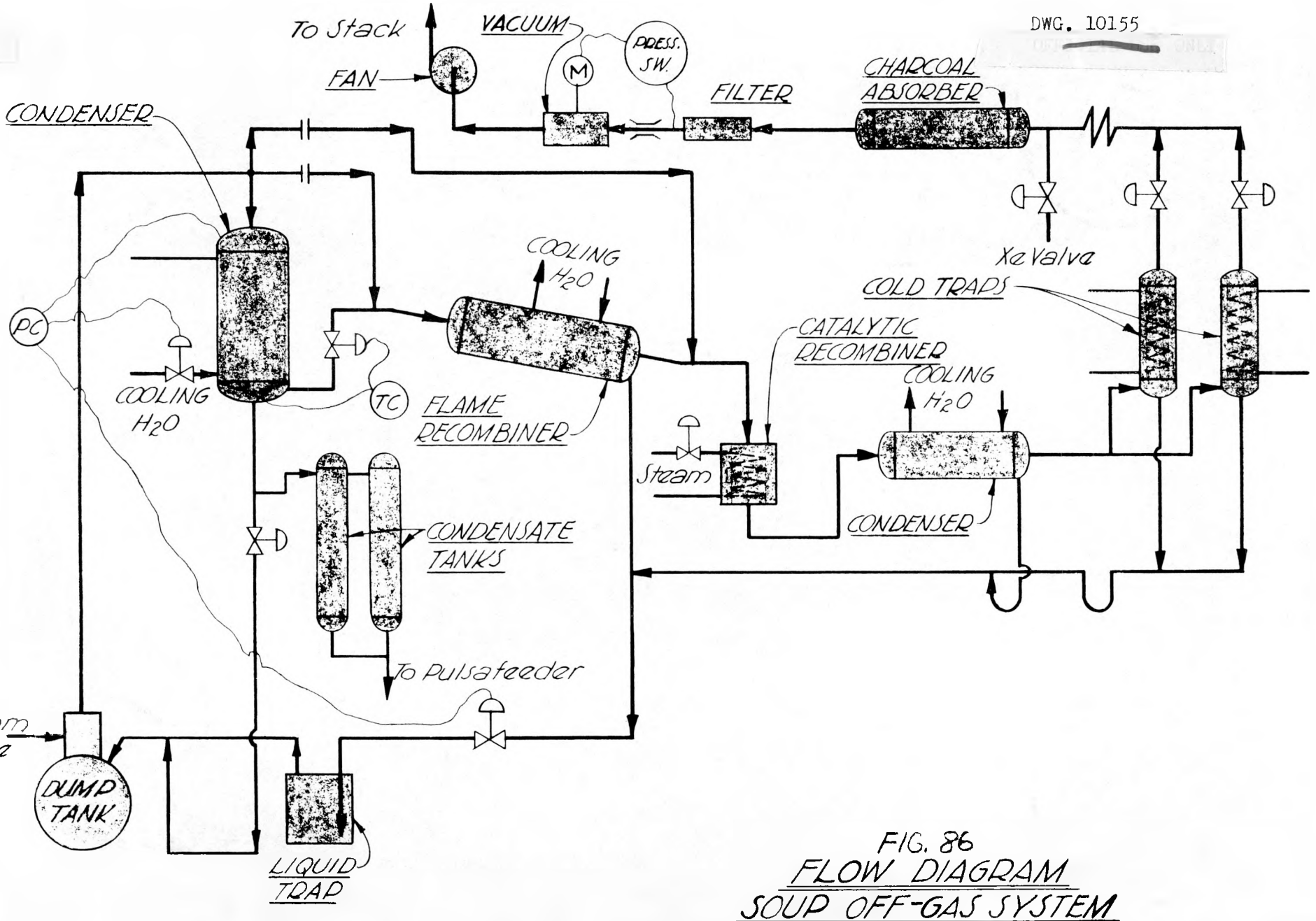

FIG. 86
FLOW DIAGRAM
SOUP OFF-GAS SYSTEM

This document contains information affecting the National Defense of the United States within the meaning of the Espionage Laws, Title 18, U.S.C., Sections 793 and 794. Its transmission or the revelation of its contents in any manner to an unauthorized person is prohibited by law.

219

VI. HRE CHEMICAL STUDIES

DECLASSIFIED

SOLUBILITY OF FISSION PRODUCT SULFATES AT HIGH TEMPERATURES AND PRESSURES

M. H. Lietzke and B. Zemel

This section describes measurements of the solubility of $La_2(SO_4)_3$, $CdSO_4$, and $ZnSO_4$ in water and in uranyl sulfate solution at elevated temperatures. The quartz-tube method described by Benrath[1,2] was used in all cases except for $La_2(SO_4)_3$ at 26°C. This method depends upon the visual observation of the appearance or disappearance of crystals in mixtures of known concentration. In the experiments described the tubes were heated in aluminum block furnaces which were mounted on rockers so that complete mixing could be accomplished. The temperatures were measured by iron-constantan thermocouples and recorded on a calibrated Brown recording potentiometer.

The scope of the measurements was limited by the ability to notice the first appearance of crystals in the tubes. With some salts the crystals were visible in much more dilute solutions than in the case of other salts. The solubility measurements of $La_2(SO_4)_3$ in UO_2SO_4 solution could be extended to 0.04% $La_2(SO_4)_3$ while the $CdSO_4$ and $ZnSO_4$ limits were much higher (2 to 3%). In all cases the measurements were extended to as dilute solutions as possible.

Lanthanum Sulfate. The solubility of $La_2(SO_4)_3$ in water and in a uranyl sulfate solution containing 30 g of uranium per liter (approximately the concentration to be used in the HRE) is shown in Table 27 and Fig. 87. Data at the lower temperatures from Seidel[3] are plotted on the same graph.

TABLE 27

$La_2(SO_4)_3$ Solubility

IN WATER		IN URANYL SULFATE SOLUTION CONTAINING 30 g OF U PER LITER	
TEMPERATURE (°C)	$La_2(SO_4)_3$ (%)	TEMPERATURE (°C)	$La_2(SO_4)_3$ (%)
26	2.04	97	2.04
108	0.61	105	1.74
113	0.46	120	0.87
115	0.37	145	0.29
117	0.31	169	0.15
		199	0.083
		215	0.042

(1) Benrath, A., Gjedebo, F., Schiffers, B., and Wunderlich, H., "Uber die Löslichkeit von Salzen und Salzgemischen in Wasser bei Temperaturen oberhalb 100°. I," *Z. anorg. allgem. Chem.* 231, 285 (1937).

(2) Benrath, A., "Uber die Löslichkeit von Salzen und Salzgemischen in Wasser bei Temperaturen oberhalb 100°. III," *Z. anorg. allgem. Chem.* 247, 147 (1941).

(3) Seidell, A., *Solubilities of Inorganic and Metal Organic Compounds*, vol. 1, p. 894, Van Nostrand, New York, 1940.

DECLASSIFIED

DWG. 9971

FIG. 87

SOLUBILITY CURVES OF LANTHANUM SULFATE

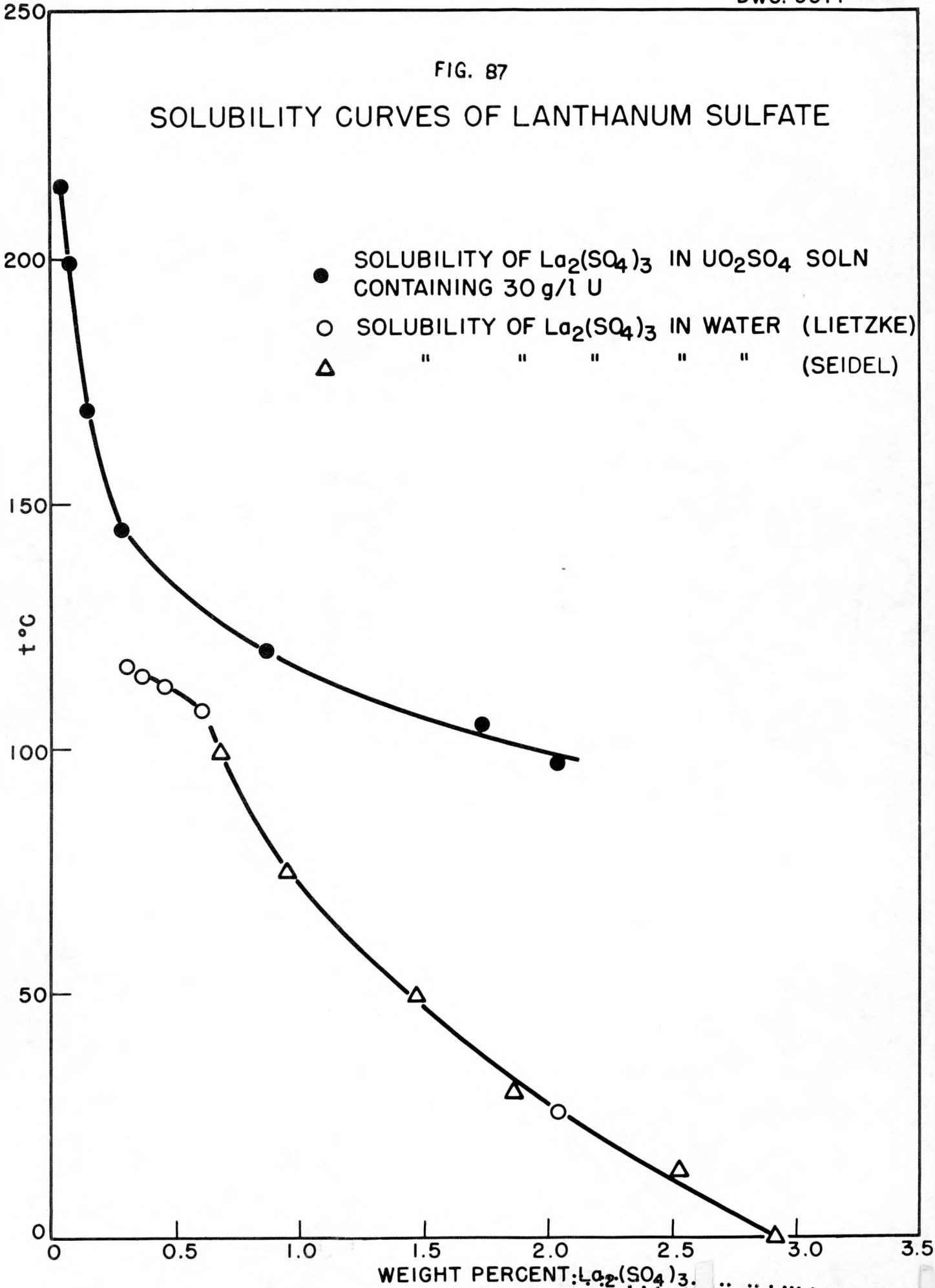

DECLASSIFIED

In both cases the solubility of $La_2(SO_4)_3$ shows a negative temperature coefficient. Since the $La_2(SO_4)_3$ solutions all showed a strong tendency to become supersaturated, it was necessary to heat them 50 to 70°C above the equilibrium solubility temperature before crystals appeared. The temperatures given in Table 27 represent the points at which the last crystals redissolved upon slow cooling. The $La_2(SO_4)_3$ crystals did not adhere to the sides of the tube.

Several of the $La_2(SO_4)_3$ solutions were heated to 300°C to check on the possible existence of double solubility points at a given concentration. No such points were observed. When the 0.31% $La_2(SO_4)_3$ solution was held at 260°C for 48 hr, there was no noticeable change either in the amount or in the type of crystals in the tube. The crystals redissolved easily at the expected temperature when the solution was cooled. Hence it appears that $La_2(SO_4)_3$ is stable at the temperatures investigated. To check on the stability of the $La_2(SO_4)_3$-UO_2SO_4 system in water at high temperatures, the tube containing 0.87% $La_2(SO_4)_3$ and 30 g of uranium per liter as uranyl sulfate was maintained at 250°C for 72 hr. There appeared to be no change either in the amount or in the form of the $La_2(SO_4)_3$ crystals in the tube. When the tube was cooled, the $La_2(SO_4)_3$ crystals redissolved at the expected temperature. The $La_2(SO_4)_3$-UO_2SO_4-water system therefore seemed to be stable at 250°C. The increased solubility of the $La_2(SO_4)_3$ in uranyl sulfate solution is probably due to strong sulfate complexing by the UO_2SO_4.

Cadmium Sulfate. The solubility of $CdSO_4$ in water and in a uranyl sulfate solution containing 30 g of uranium per liter was determined over a wide range of concentrations. Table 28 and Fig. 88 show the results obtained. Data obtained by Benrath[4] are plotted on the same graph.

TABLE 28

$CdSO_4$ Solubility

IN WATER		IN URANYL SULFATE SOLUTION CONTAINING 30 g OF U PER LITER	
TEMPERATURE (°C)	$CdSO_4$ (%)	TEMPERATURE (°C)	$CdSO_4$ (%)
124	29.6	175	28.5
160	14.8	200	14.2
182	7.4	219	7.1
190	3.0	251	2.8

(4) Benrath, *op. cit.* (1937).

DECLASSIFIED

DWG. 9972

FIG. 88

SOLUBILITY CURVES OF CADMIUM SULFATE

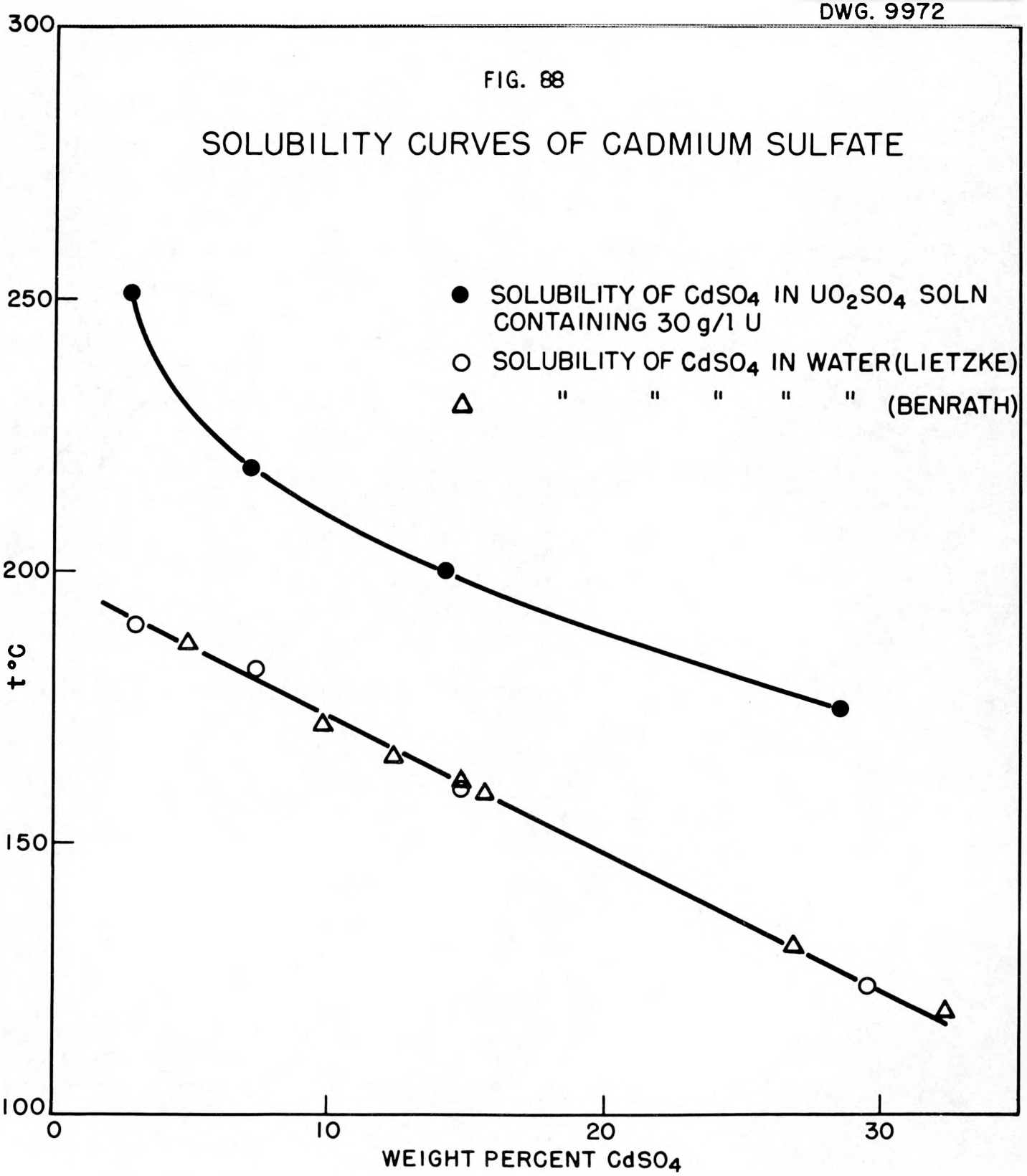

DECLASSIFIED

Like $La_2(SO_4)_3$, $CdSO_4$ showed a negative temperature coefficient of solubility, and the presence of uranyl sulfate in the solution increased the solubility of the $CdSO_4$ at a given temperature. The $CdSO_4$ solutions also showed a tendency to become supersaturated; hence the temperatures given represent the points at which the last crystals redissolved as the solutions were cooled. The crystals obtained at the higher temperatures (e.g., in the 3% solution) adhered to the walls of the tube, while the crystals from the more concentrated solutions were nonadherent. No double solubility points were found below 300°C at any given concentration. The $CdSO_4$-UO_2SO_4-water system did not appear to be as stable as the $La_2(SO_4)_3$-UO_2SO_4-water system. When the 2.8% $CdSO_4$ solution containing uranyl sulfate, in which crystals of $CdSO_4$ appeared at 251°C when the solution was heated steadily to this point, was held for 24 hr at 230°C or for 1 hr at 240°C, a brownish-orange precipitate appeared in the tube. The precipitate redissolved when the solution was cooled. Analysis showed that the precipitate did not contain any uranium. When the brownish crystals were dissolved in dilute H_2SO_4, a colorless solution resulted. When NaOH was added to the solution, a white precipitate of $Cd(OH)_2$ was obtained. The precipitate may have been cadmium oxide.

Zinc Sulfate. The solubility of zinc sulfate in water also decreased as the temperature increased. The data obtained are shown in Table 29 and in Fig. 89. Data obtained by Benrath[5] are plotted on the same graph, as indicated.

TABLE 29

Solubility of Zinc Sulfate in Water

TEMPERATURE (°C)	$ZnSO_4$ (%)
178	34.0
203	25.5
219	22.7
238	17.0
248	11.3
253	8.5
255	5.1
257	2.1

(5) Benrath, *op. cit.* (1941).

DECLASSIFIED

DWG. 9973

FIG. 89

SOLUBILITY CURVE OF ZINC SULFATE

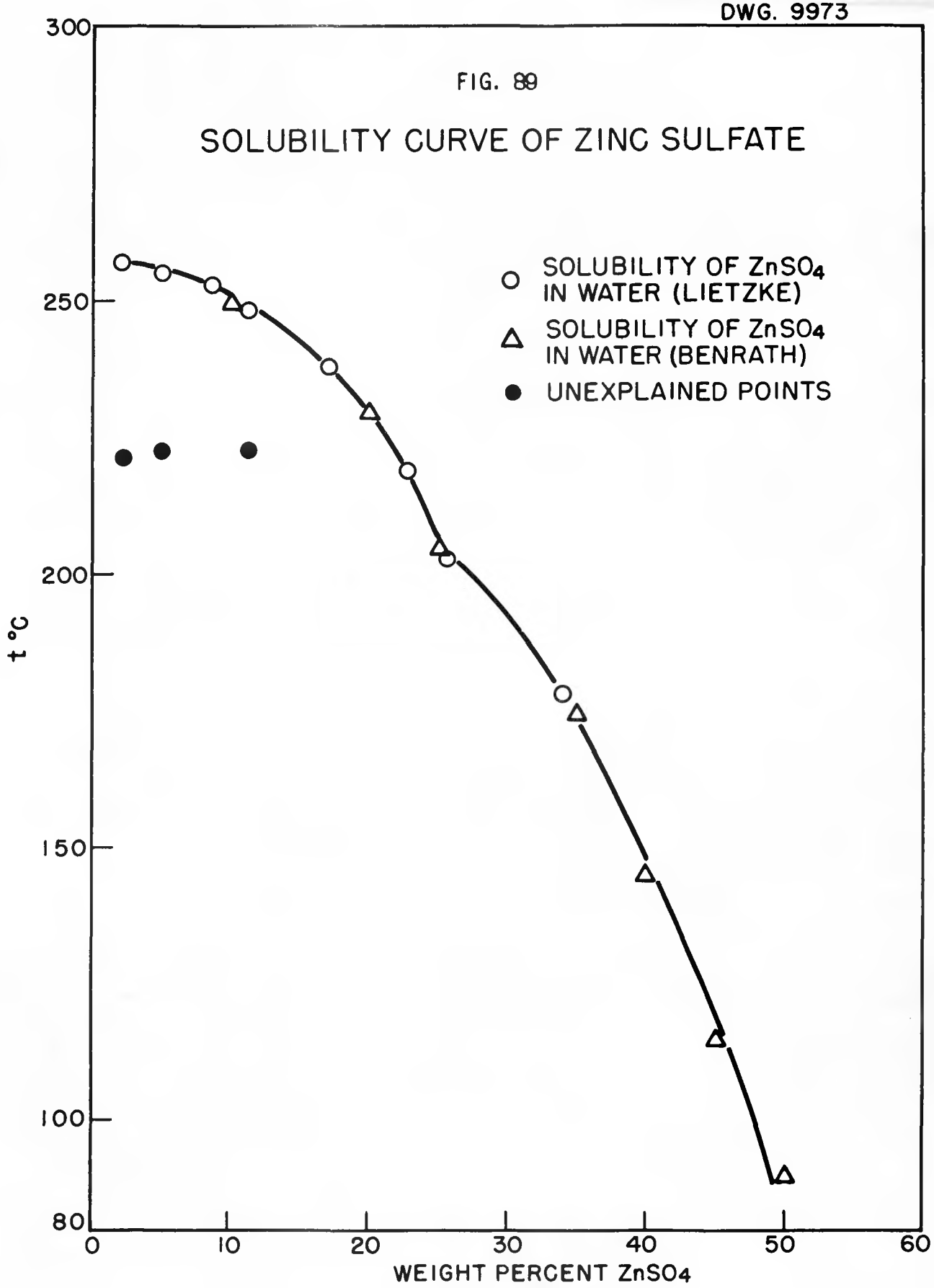

DECLASSIFIED

The zinc sulfate solutions, unlike the $La_2(SO_4)_3$ and $CdSO_4$ solutions, did not show a strong tendency to become supersaturated. No double solubility points at a given concentration were found below 300°C. The crystals of $ZnSO_4$ that appeared adhered to the walls of the tube.

Occasionally the zinc sulfate solutions behaved very peculiarly. For example, when the 2.1% solution was heated for the very first time, nonadherent crystals appeared in the solution at 225°C. The crystals redissolved on cooling. When the solution was heated again no crystals appeared at 225°C, but the "normal" adherent crystals were observed at 257°C. Several subsequent heatings failed to produce the nonadherent crystals in the tube again. This phenomenon was also observed in the 5.1% and in the 11.3% solutions. No explanation is given for this behavior although the points may indicate an extension of the lower half of the zinc sulfate solubility curve. The 2.1% zinc sulfate solution contained 0.39 mg of SiO_2 per milliliter after three heatings to 260°C, while a similar solution that had been heated only once contained only 0.03 mg of SiO_2 per milliliter.

When the 11.3% zinc sulfate solution was held at 250°C (2° above the point at which crystals appeared in the tube) for 24 hr a very large amount of crystalline material was deposited in the tube. X-ray analysis of these crystals showed them to be a mixture of $ZnSO_4 \cdot H_2O$ and $ZnSO_4$, which seems to preclude a hydrolytic reaction as the cause of the increased number of crystals. When the 17.0% zinc sulfate solution was held overnight at 210°C (28° below the point at which crystals normally appear) crystals appeared in the solution, and redissolved readily when the solution was cooled. Their composition has not yet been determined.

Future work will include measurements of the solubility of $Y_2(SO_4)_3$ and Cs_2SO_4 in both water and uranyl sulfate solutions.

Solubilities by Tracer Technique. The determination of the solubilities of the fission product sulfates by means of the radioactive tracer technique is continuing along the lines previously laid out (ORNL-826, pp. 78, 79).

The solubility of $SrSO_4$ in water has been determined over the temperature range of 129 to 320°C. The concentration of $SrSO_4$ in solution was determined from the ratio of the activity of the solution at any given temperature to that of a concentrated solution made up at room temperature and having a known specific activity.

DECLASSIFIED

Two different tracers in two different stock solutions were used, namely Sr^{89} (57 day) and Sr^{90} (25 year). The samples were evaporated on a 1 in. watch glass and mounted on an aluminum card. In order to avoid decay or other counter corrections an equivalent sample of the reference solution was counted in the same counter under the same conditions.

Sample runs, in bombs of 3 to 5 ml capacity at room temperature, lasted from 12 to 60 hr. At the end of each run the bomb and furnace were carefully and slowly upended at the equilibrium temperature; the bomb was then removed and cooled by plunging into cold water. In order to avoid the possibility of distillation from one part of the bomb to another, the bomb and furnace were inverted in several runs. The inversion was done periodically (after equilibrium was reached) for periods of several hours. However, no significant differences in solubility were noticed.

The resultant data are shown in Table 30 and plotted in Fig. 90. The triangles represent data obtained with Sr^{90} as a tracer, the circles represent those obtained with Sr^{89}, and the squares represent the data obtained by Booth and Bidwell.[6] Since the data of Booth and Bidwell were obtained as small differences in two large weights and since no attempt was made to check for solubility of the bomb material, it is felt that the lower results obtained by the tracer technique are the more valid.

TABLE 30

Solubility of $SrSO_4$ in Water

TEMPERATURE (°C)	TRACER	SOLUBILITY (mg/100 g of solvent)
124 ± 3	Sr^{89}	2.61
127 ± 3	Sr^{89}	2.64
163 ± 5	Sr^{89}	1.25, 1.35
168 ± 3	Sr^{89}	1.29, 1.37
186 ± 8	Sr^{89}	0.66
199 ± 5	Sr^{90}	0.8
220 ± 2	Sr^{89}	0.63
250 ± 4	Sr^{89}	0.248
260 ± 4	Sr^{90}	0.1, 0.096
273 ± 5	Sr^{89}	0.124
280 ± 2	Sr^{90}	0.123
319 ± 3	Sr^{89}	0.05

(6) Booth, H. S., and Bidwell, R. M., "Solubilities of Salts in Water at High Temperatures," *Am. Chem. Soc. J.* 72, 2567 (1950).

DECLASSIFIED

DWG 10171

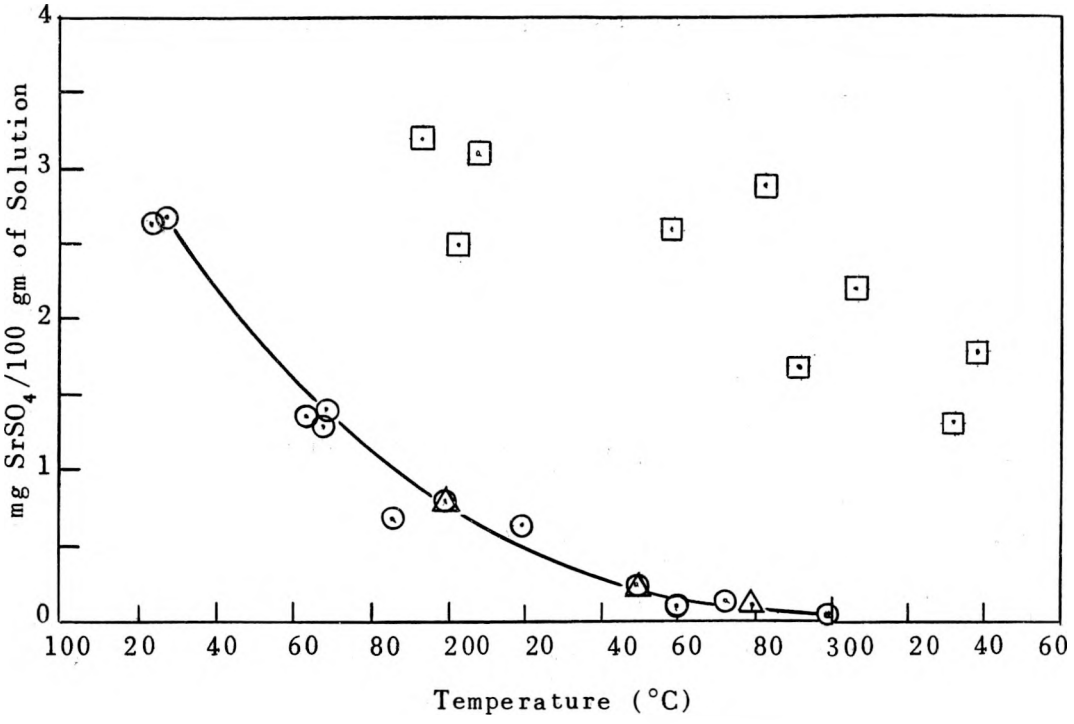

○ Data obtained with Sr^{89}

△ Data obtained with Sr^{90}

□ Data of Booth and Bidwell, *Am. Chem. Soc. J.* **72**, 2567 (1950)

Fig. 90. Solubility of Strontium-Sulfate in Water

DECLASSIFIED

An attempt was made to determine the solubility of $ZnSO_4$ by the tracer technique as a check against the work done by the quartz-tube method. The results obtained were, however, time-dependent in a manner which varied with temperature. The solutions obtained contained considerable amounts of iron, and the bombs showed a fair amount of etching. Apparently the $ZnSO_4$ solutions underwent hydrolysis and the resultant acid attacked the steel, thus driving the reaction to completion at a rate which increased with temperature. The stainless-steel bombs being used were apparently unsuitable for this type of compound, and the experiment was dropped.

Solubility studies are now being made on yttrium sulfate. $BaSO_4$ and $La_2(SO_4)_3$ tracer solutions have been prepared, and solubility studies will be undertaken on them shortly.

ANALYTICAL CHEMICAL CONTROL OF THE HOMOGENEOUS REACTOR SOLUTION

W. H. Davenport, Jr. and R. H. Powell

An investigation of methods for the analytical chemical control of the reactor solution has been reported.[7] The two most feasible methods appeared to be (1) the determination of density using an electromagnetic densitometer and (2) the determination of uranium concentration by its effect upon the Q of a suitable high-frequency coil (20-megacycle range). Accordingly work has been concentrated on the development of these methods.

Electromagnetic Densitometer. The principle of the electromagnetic densitometer and the high sensitivity which may be achieved under controlled conditions were reported in the previous HRE Quarterly Report.[8] The main problem in the adaptation of this method to the measurement of the reactor solution is in the fabrication of a unit which will withstand the conditions of the reactor and still retain the sensitivity that is desired for control of the soup. A unit has been partially completed, and to date no large sacrifices of sensitivity have been required. A schematic diagram of the unit is shown in Fig. 91.

(7) Davenport, W. H., Jr., and Powell, R. H., "Experimental Homogeneous Reactor Chemical Control," *Analytical Chemistry Division Quarterly Progress Report for Period Ending June 30, 1950,* ORNL-788, p. 51 (Oct. 4, 1950).

(8) "Experimental and Developmental—an Electromagnetic Densitometer," *Homogeneous Reactor Experiment Quarterly Progress Report for Period Ending August 31, 1950,* ORNL-826, p. 85 (Oct. 24, 1950).

DECLASSIFIED

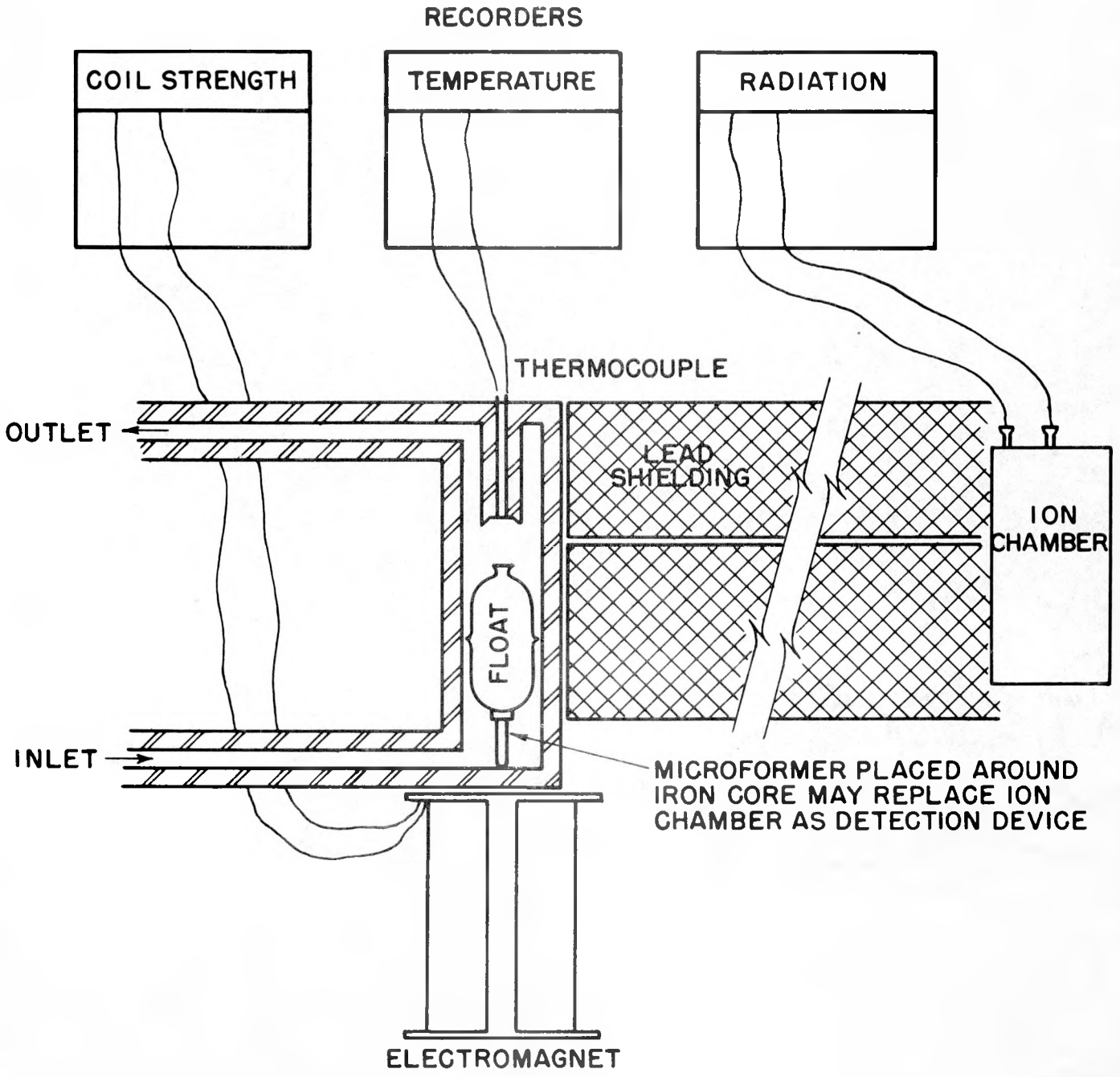

FIG. 91

ELECTROMAGNETIC DENSITOMETER

DECLASSIFIED

The component parts of the densitometer are float or sinker, magnetic coil, float detection device, temperature control, and electrical circuit.

1. Float or Sinker. A sinker (Fig. 92) has been constructed of type 309 stainless steel which is capable of withstanding hydraulic pressures up to 1700 psi. In the fabrication of the body, two dome-shaped cylinders were flanged at the base and heliarc-welded in an argon atmosphere at room temperature. The sinker body is 5/8 in. O.D. and 1-5/8 in. long, and has a 0.010-in. wall thickness. The collapsing pressure was determined by subjecting another sinker of the same dimensions to hydraulic pressures which started at 500 psi and increased in increments of 200 psi. At 1700 psi the sinker collapsed. The sinker may be equipped with a soft iron core and an Alnico magnet as shown in Fig. 92. The soft iron core makes possible the movement of the sinker by a magnetic field. Originally the Alnico magnet was added to operate a detection device which would determine the position of the sinker. Since it now appears that better methods of detecting the sinker position may be available, the Alnico magnet probably will not be used. In this case the sinker becomes a float in soup solutions with a density of 0.80 or higher.

2. Magnetic Coil. The float is moved by means of a magnetic coil placed at the bottom of the unit (Fig. 91). Placing the coil at the end of the pipe rather than around it has the advantages that better positioning of the float is obtained and the coil may be removed without disturbing the unit. In addition, the sides of the pipe are left available for thermostating or position-detecting devices. The distance over which the float is moved was arbitrarily set at ¼ in. Since the densitometer wall is ¼ in. also, the float must be moved from a point ½ in. away from the coil. The coil must pull a maximum mass of 2 g, which represents the difference between the mass of the float and the buoyancy of the soup at the highest density anticipated.

The specifications for a magnetic coil to meet these requirements were determined mainly by trial and error with the help of P. P. Williams of R. Toucey's Instrument Group. The final coil was wound by J. P. Leslie of the Electrical Shops, using 18-gauge single Vitrotex-covered copper wire and an Armco iron core of high purity. The core was 3/8 in. in diameter and 3 in. long. The outside diameter of the coil was 2½ in. and the number of turns 1520. The completed coil required about 1.5 amp current to move the float in the solution of density equal to 1.0.

DECLASSIFIED

PHOTO 6944

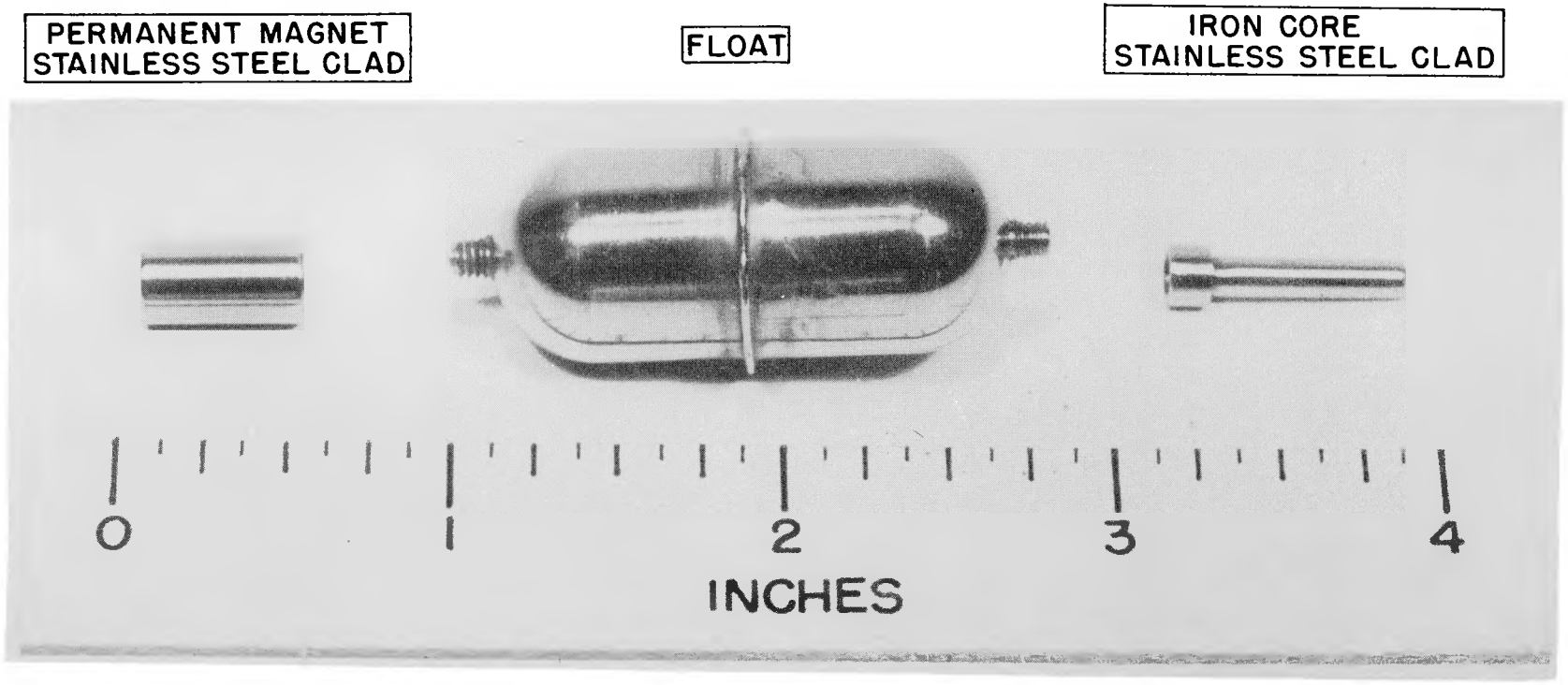

FIG. 92. SINKER

3. Position-detecting Device. Three methods of detecting the float position have been considered.

The first method is based on the response of a magnetic switch to the position of a permanent magnet attached to the sinker. A magnetic switch made by the Research Shops was tested and found to be fairly sensitive, but it lacked ruggedness and the fields of the magnetic switch, the Alnico magnet, and the magnetic coil overlapped. This overlapping could be lessened by changing the dimensions of the float, if necessary, if this method should be utilized. Further details of the operation of the magnetic switch are given in ORNL-867.[9]

A second method uses as a position indicator the change in radiation level at a given position in the pipe caused by displacement of the solution by the float. This change may be detected by means of an ionization chamber. The pipe would have to be completely shielded except for a slit at the detecting position level. A laboratory experiment was performed which indicated that the percentage change in radiation level produced by ¼ in. travel of the float would be sufficiently large to give a good indication of float position. In order not to contaminate the float, two test tubes were used in the experiment, one having an outside diameter of 5/8 in. to simulate the float and the other having an inside diameter of 15/16 in. to simulate the solution-containing pipe. Approximately 15 ml of a Zr-Nb solution, 1 millicurie/ml, was placed in the large test tube, with appropriate holdback carriers. Lead shielding was arranged so that a slit 1.8 by 0.2 cm was in a plane just below the bottom of the simulated float. When the test tube was lowered ¼ in. its maximum cross section was opposite the slit. Using a Geiger-Mueller probe from a "teacart" and 5 min counting time for counting rates of 12,000 to 19,000 c/m after correction for background and coincidence, the radiation level seen through the slit was determined for three positions: (1) maximum displacement of the solution, (2) partial displacement (moving float 1/8 in.), and (3) minimum displacement (moving float ¼ in.).

The results showed a 19% increase in counts for 1/8-in. movement and a 37% increase for ¼-in. movement. This percentage increase in radiation level was considered to be more than enough to give a good indication of float movement. Since changes in radiation level rather than absolute intensity are

(9) Davenport, W. H., Jr., and Powell, R. H., "Analytical Chemical Control of Homogeneous Reactor Solution," *Analytical Chemistry Division Quarterly Progress Report for Period Ending October 10, 1950*, ORNL-867, p. 71 (Dec. 28, 1950).

DECLASSIFIED

all that are necessary to indicate float movement, the accuracy of the ion chamber will not be important. At the high levels anticipated in the reactor solution the response of an ionization chamber should be very fast.

A third method of detecting float position might be that of using a microformer. The microformer is a three-winding differential transformer which would be located on the outside of the pipe. The position of the iron core of the float as it moves through the microformer determines the output voltage. The adaptation of a suitable microformer to the conditions of the reactor is now being investigated with the aid of W. Brand of the Instrument Department and R. Coyle of the NEPA project.

4. *Temperature Control.* At 250°C, the operating temperature of the reactor, the temperature coefficient of density is such that it has been estimated that temperature would have to be controlled or known to 0.1°C in order to measure uranium concentration in terms of density with an accuracy of 0.1 g of uranium per liter. If the solution could be cooled to the region of 100°C, much less rigid control of temperature would be required. In either case the temperature of the soup must be controlled either by thermostating or by measurement and compensation.

The disadvantage of thermostating is that the solution is constantly heating up internally, although the possibility of thermostating both a known solution and the unknown with the soup solution itself has been considered. In this way the effect of temperature or density measurement would be detected in the measurement of the standard solution.

The measurement of temperature is difficult but not impossible. With a carefully calibrated thermocouple the temperature might be followed with sufficient accuracy even at high temperatures.

5. *Electrical Circuit.* A Leeds and Northrup type K potentiometer has been obtained for measurement of the coil strength and for thermocouple measurement of the temperature on a laboratory scale. The coil strength will be measured in terms of the voltage drop across a standard resistor accurate to 1 part in 10,000.

For the laboratory investigation of the electromagnetic densitometer a stainless-steel pressure bomb has been fabricated by the Research Shops. The temperature of the bowl will be controlled with a resistance heater and

DECLASSIFIED

measured using a thermocouple placed in a high-pressure thermowell. The bomb is similar to the proposed densitometer (Fig. 91) except that the outlet and inlet tubes are replaced by a high-pressure removable cap at the top. The overall length of the bomb is 8 in., the inside diameter is 7/8 in., and the wall is 1/8 in. thick.

A commerical densitometer called the "Princo Densitrol" has been suggested by W. Brand of the Instrument Department as having possibilities for use in the reactor. This instrument uses a float also but differs from the electromagnetic densitometer in that no external force is placed on the float. The float acts as a hydrometer but its total travel is limited by a chain attached to the wall of the container and to the float. The weight added to the float by the chain varies with the movement of the float. The position of the float is indicated by a microformer. Mr. Brand is inquiring further into the possibilities of adapting an instrument of this type to the conditions of the reactor.

Q measurement. A major problem in the measurement of the Q of a high-frequency coil as affected by changes in uranium concentration is the introduction of an electrically insulated coil directly into the high-pressure high-temperature soup solution. The insulating material must combine ruggedness to withstand conditions of the reactor with low power loss. Increasing the wall thickness of the insulator in order to strengthen the unit results in a greater power loss. The reactor temperature of 250°C approaches and in some cases is higher than the softening temperatures of many of the common plastics, such as bakelite and Polythene. A higher melting plastic, Teflon, as well as these low-melting ones, has been reported "to deteriorate badly" under the maximum flux radiation of the Chalk River pile.[10] Several ceramics are being investigated. Commercial Lava and AlSiMag have low power loss and high mechanical strength. Favorable radiation stability is reported.[11,12] They are both porous, however, and a method for impregnating the pores or glazing the surface would be required before these insulators would be considered further.

(10) Averbach, B. L., Billington, D. S., Irvine, J. W., Jr., Johnson, W. E., Kaufman, A. R., Larson, A. W., Jr., Low, J. R., Untermyer, S., and Slater, J. C., "Survey of Effects of Radiation on Materials," AEC-500, p. 127 (no date).

(11) Coyle, Richard (NEPA), private communication to W. H. Davenport, Jr., Nov. 10, 1950.

(12) Sisman, O., private communication, Aug. 10, 1950.

DECLASSIFIED

Quartz shows possible applicability, but mechanical strength in the presence of high radiation has not been satisfactorily investigated. It is to be noted that fused quartz and crystalline quartz are being examined at Chalk River for changes in electrical insulating properties and dimensional stability as part of the general radiation damage studies. Plastics are also being examined.[13]

The results of these tests should be obtained as speedily as possible, since the Chalk River reactor is, at the present time, the nearest approximation to the highest flux of the proposed Homogeneous Reactor Experiment, and the flux, as well as total irradiation, is a factor to be considered in radiation damage.

A semiquantitative laboratory experiment gave indication that the change of Q with concentration should increase with increasing temperature. The test was not conclusive since the temperature was varied only from room temperature to 85°C.

Development of a Lava-insulated Platinum Coil for Q Measurement of Soup. Preliminary experiments with silicone No. 9971—treated baked lava, grade A, indicated that it was not possible to make the small pore spaces in the lava impenetrable to water at room temperature and atmospheric pressure conditions; furthermore, a chloride salt of the iron component of the lava formed to a slight extent. Introduction of any chloride ion into the stainless-steel piping system is to be avoided. Washing the ceramic did not remove this chloride satisfactorily.

Two cylinders 2 in. in diameter by 4 in. in length, with a 1-in.-diameter hollow core 3½ in. deep, were machined out of stock lava, grade A, and subsequently baked at 1850°F. One cylinder was silicone-treated as above, and the other was pressure-tested hydraulically for collapse and seepage of external water through the formed lava. At 3000 psi the cylinder was pressure stable, but a small amount of H_2O (about 20 ml) came through the lava walls in a 2-min pressure test. It is believed that a satisfactory glaze might be devised.

(13) Averbach, B. L. *et al.*, *op. cit.*

DECLASSIFIED

The above cylinders were tested for loss of power by measuring the Q of a copper coil (six turns of 18-gauge wire, 3/4-in. I.D. and 1 in. long) first in air and then inserted in the lava forms described above, using a Q meter type 160A (Boonton Radio Corp.) at 20 megacycles.

This particular coil had a Q of 230 in air and a Q of 227 within a 2- by 4-in. lava form, with ½ in. wall thickness separating the coil from the outside of the lava form; low power loss was therefore observed.

This copper coil within the lava insulator described above was surrounded by uranyl sulfate solution containing 28 mg of uranium per milliliter. A Q of 213 was observed at room temperature.

A solution lowers the Q of the coil insulator system. It is believed that the presence of an electrolyte solution is equivalent to inserting a resistance in the following electrical system when in resonance:

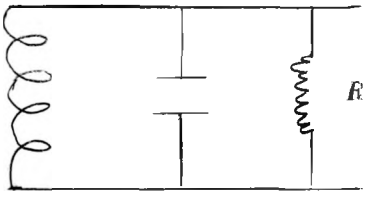

where R is the resistance of the solution.

A seemingly linear relationship between Q and concentration was observed in uranyl sulfate solutions over the concentration range 15 to 40 mg of uranium per milliliter by K. Klein of the Instrument Department when a 20-megacycle frequency was applied to such a system and the coil was glass-insulated within a test tube at room temperature and atmospheric pressure.

It is to be noted that if a method can be developed to glaze lava with a glaze stable under HRE conditions, if the lava wall thickness can be reduced to approximately a 1/8- to 1/4-in. insulation, and if lava can be successfully attached to a stainless steel surface, then such an insulated coil might be inserted directly into the high pressure external stream of the HRE to follow properties of the solution such as uranyl sulfate concentrations without sampling the soup. Such a development is being projected.

Preliminary experiments designed to measure the change of Q with temperature indicate that, over the limited range of temperature tested, Q measurement is a straight line function of Q with temperature changes, and that the increments increase with concentration of uranyl sulfate. Results of Q measurements are given in Table 31.

DECLASSIFIED

TABLE 31

TEMPERATURE (°C)	GLASS TEST TUBE (1/16 IN. WALL THICKNESS)		LAVA CYLINDER (½ IN. WALL THICKNESS)	
	21 mg/ml	28 mg/ml	21 mg/ml	28 mg/ml
30	188	183	212	210
60	178	164	205	202
85	170	152	*	*

*Measurement discontinued because of solution evaporation at high temperatures.

It is planned to obtain data up to 250°C with various concentrations of UO_2SO_4 at elevated pressures. A pressure bomb has been fabricated for this purpose by the Research Shops. Development of a suitable ceramic glaze is projected.

E. S. Cantrell and R. J. Fox of the Research Shop have embedded a platinum coil in powdered lava, grade A, with the hope that a satisfactory glaze may be developed to stand the HRE conditions. R. Steele and Dr. Max Bredig contributed to the joint enterprise by making stereoscopic X-ray examination of the position of the embedded platinum coil within the compressed lava molds as an aid to machining the molds, and viewing the position of the coil for electrical properties (Figs. 93, 94, and 95). Mr. Steele obtained a radioautograph (Fig. 96) of the molded ceramics after they had been machined by Mr. Cantrell.

The technique of Cantrell and Fox for embedding the platinum coils in the compressed lava grade A (Fig. 97) consists in putting the lava in a powdered form and then recompressing it with the coil in position. In making the coil it must be taken into account that the powdered lava is compressed about 260% at 60 tons.

A small coil on the same axis and wound in the same direction as the larger coil was made extending down the center lead. Both coils were made longer (Fig. 98) than the final desired dimension to allow for compression of the coil when compressed in the lava. The lava was compressed in a hardened steel die having a taper of 3/8 in. per foot. The lower plate of the die was provided with holes for leads of the coil to help position the coil in the billet.

DECLASSIFIED

Dwg. 9985

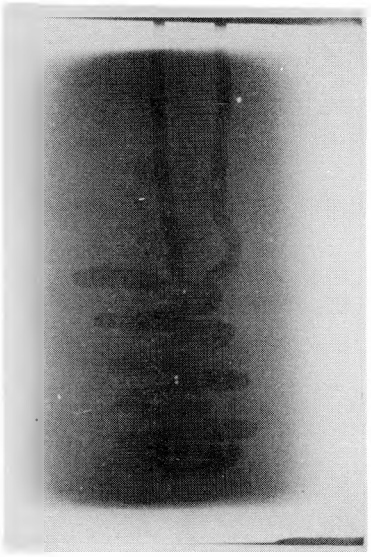

A-1 Position perpendicular to Pt. leads

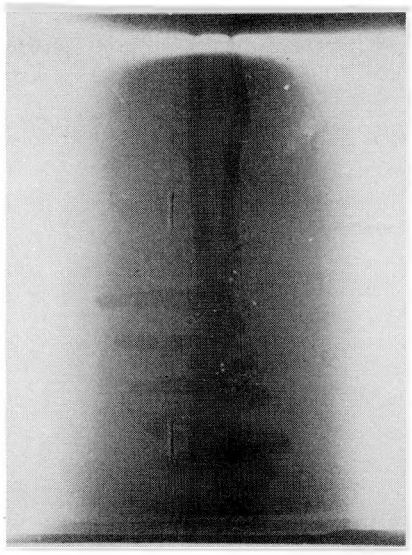

A-2 Position at 45° from position A-1

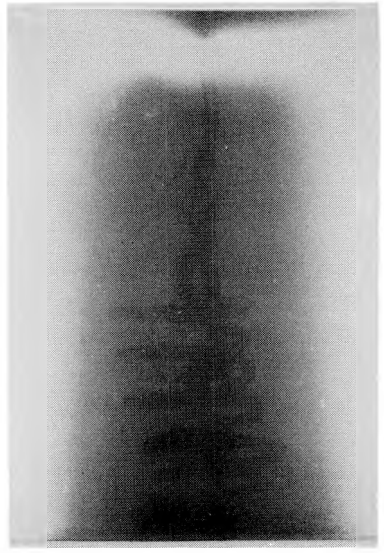

A-3 Position at 90° from position A-1

X-Ray Data
R1004 St
35 KV
6 ma.
20 secs.
Target Sample 12"
By R. M. Steele
Dr. M. Bredig

COMPRESSED LAVA CYLINDER "A"
(Side View)

FIG. 93

270

Dwg. 9986

B-1 Position perpendicular to Pt. leads

B-2 Position at 45° from position B-1

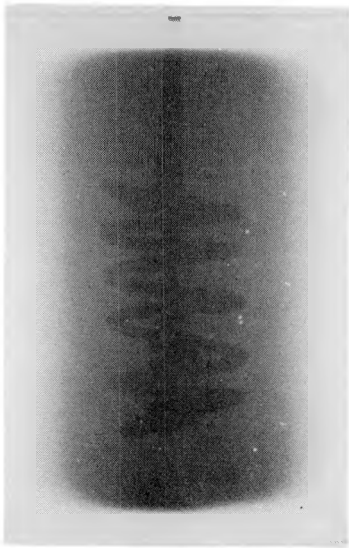

B-3 Position at 90° from position B-1

X-Ray Data
R1004 St
35 KV
6 ma.
20 secs.
Target Sample 12"
By R. M. Steele
Dr. M. Bredig

COMPRESSED LAVA CYLINDER "B"
(Side View)

FIG. 94

271

Dwg. 9987

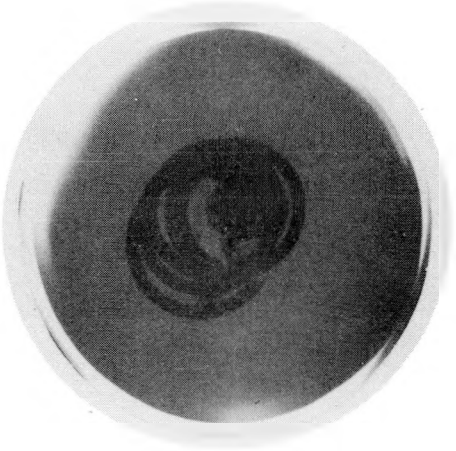

A - Top View

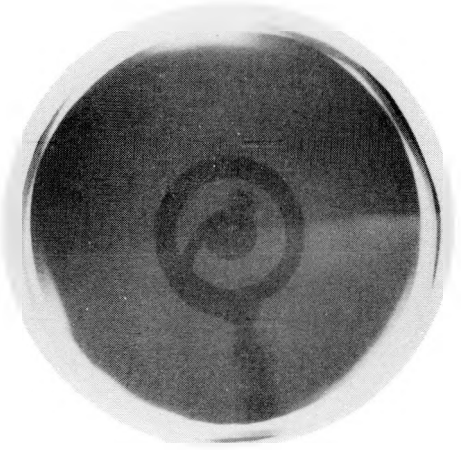

B - Top View

X- Ray Data
35 KV
6 ma.
120 secs.
Target Sample 12"
By R. M. Steele
Dr. M. Bredig

COMPRESSED LAVA CYLINDERS A AND B

FIG. 95

DECLASSIFIED

Dwg. 9988

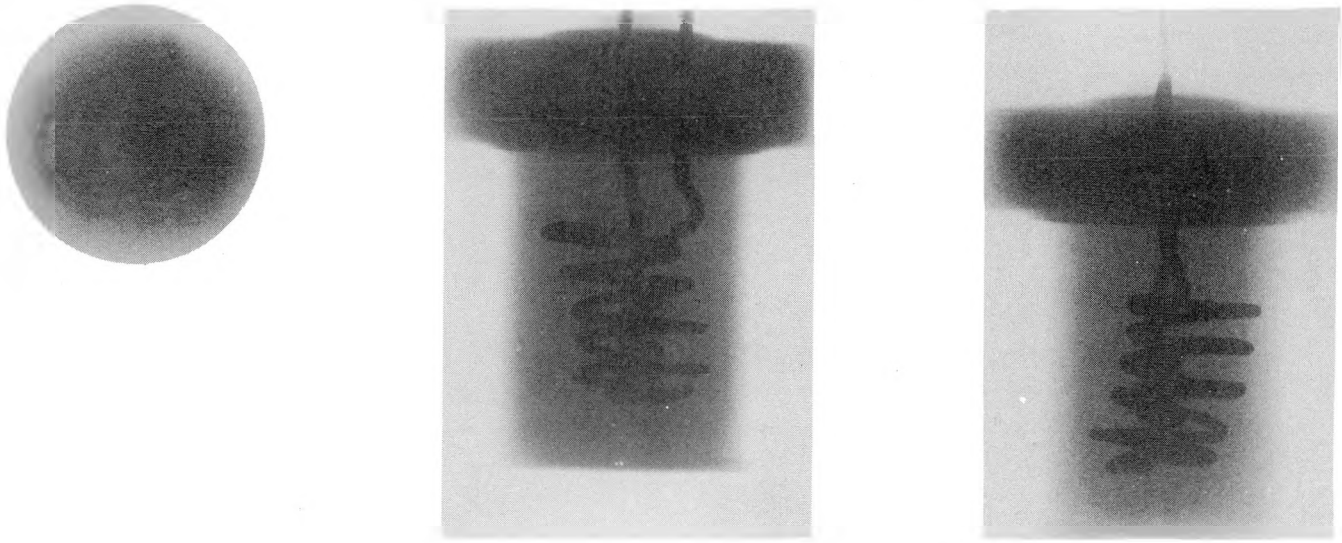

A - Top and Side Views

Exposure conditions same as X-ray
Position 90° to Pt. leads

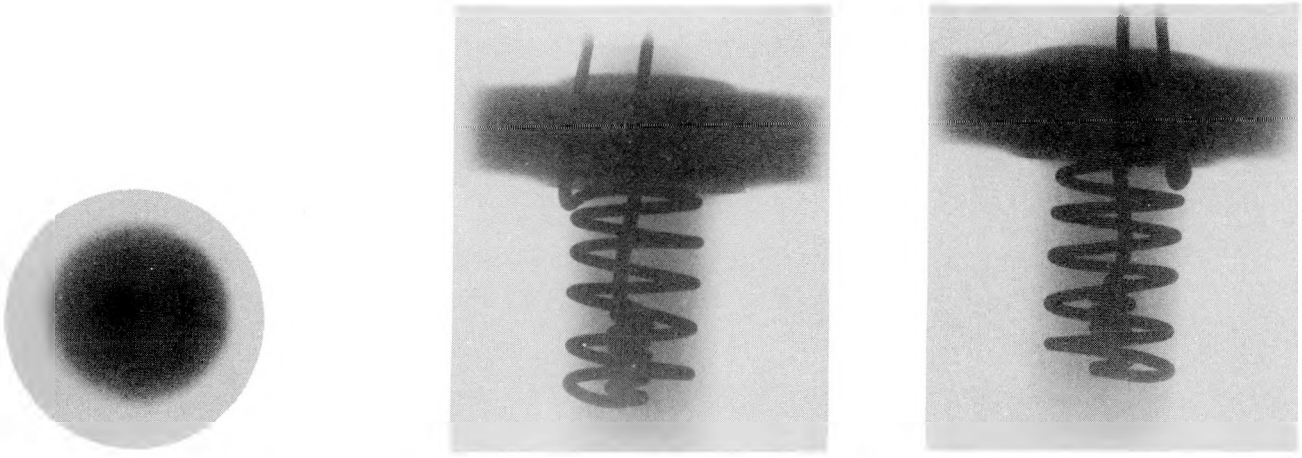

B - Top and Side Views

Exposure conditions same as X-ray
Position 110° to Pt. leads

COMPRESSED LAVA CYLINDERS A AND B AFTER MACHINING

FIG. 96

DECLASSIFIED

UNCLASSIFIED

DWG. 10276

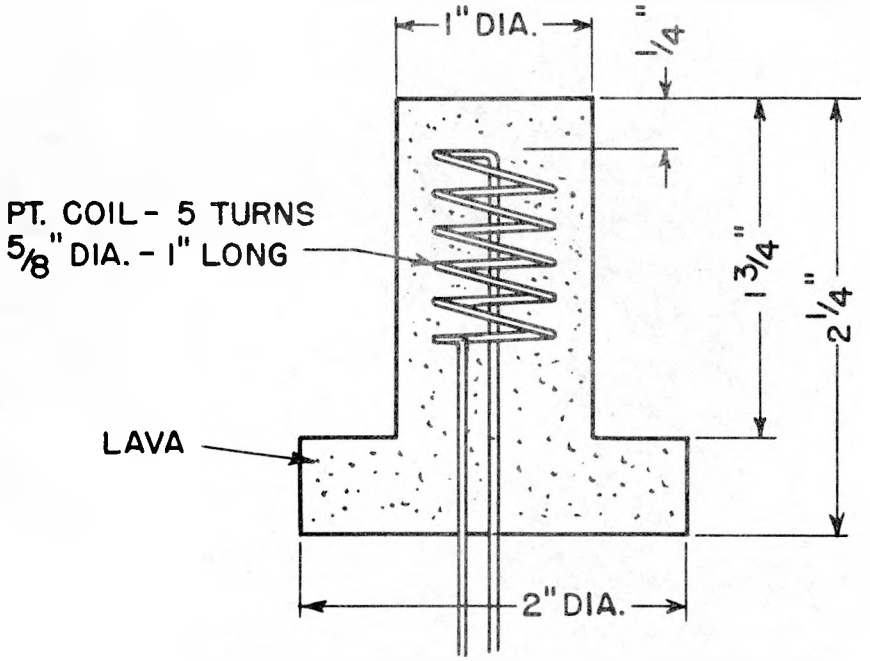

FIG. 97
COMPLETED Q COIL
PLATINUM EMBEDDED IN LAVA GRADE A

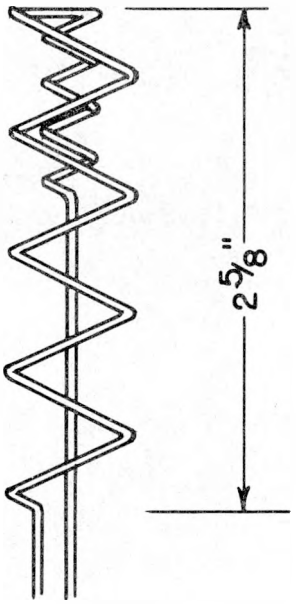

FIG. 98
PLATINUM COIL BEFORE COMPRESSION

DECLASSIFIED

Care must be taken, while loading the die with the powder, that a parting plane is not established. A small amount of tamping with a small rod will work a good portion of the air out of the powder, but partial compressing before all the powder is loaded will produce a parting plane and the billet will come apart at this point. All the powder must be compressed at the same time. The coil is positioned by weighing the quantity of powder required to reach the top of the coil, tamping with a small rod evenly around the coil, then loading the rest of the powder and compressing without tamping.

The billets were compressed at 60 tons (approximately 20 tons/sq in.), and it was noted that the billet expanded 0.020 in. in diameter when ejected from the die. (A study made after these billets were prepared indicates that lower pressures may be desirable.) They were fired over a 40-hr cycle at 1850°F maximum, a record of which is attached (Fig. 99). A great advantage of the recompressed billets is that they can be machined after firing by using carboloy tools, although even these tools do not stand up very long and require frequent resharpening. To date the Research Shop has not been successful in using carboloy tools on lava in its normal form after firing. The billets were turned to the desired sizes after firing. Another advantage of this technique is the fact that greater thicknesses can be fired without cracking.

Development of a Quartz Insulator for Platinum Coil for *Q* Measurement of Soup. A quartz thimble encasing either a copper coil or a platinum coil similar to that incorporated in the compressed lava, but wound in a suitable groove in a quartz rod, is being attempted in the Chemistry Division Glass Shop by Mr. Rustenbach. The quartz thimble and the quartz rod will be fused to make a seal against the soup. The quartz rod will be fused to a quartz base plate so that the base plate may be attached to a stainless-steel pipe by the "O" ring technique or by stainless-steel sylphon bellows. K. Klein is devising an automatic recording circuit for *Q* measurements.

One sample of a high-energy X- or gamma-ray absorbing glass containing tungsten phosphate, developed and patented by J. J. Rothermel, Kuan Han Sun, and Alexander Silverman has been obtained, and four samples of a slow-neutron absorbing glass, developed and patented by Leben Melnick, Hurd W. Safford, Kuan Han Sun, and Alexander Silverman has been received. An exploratory in-pile experiment is being conducted with one of the neutron-absorbing glasses at 250°C in the X-10 graphite pile for discoloration. If the preliminary experiment is successful, more detailed experiments are planned to test the glass in a slow-neutron flux.

DECLASSIFIED

DWG. 9989

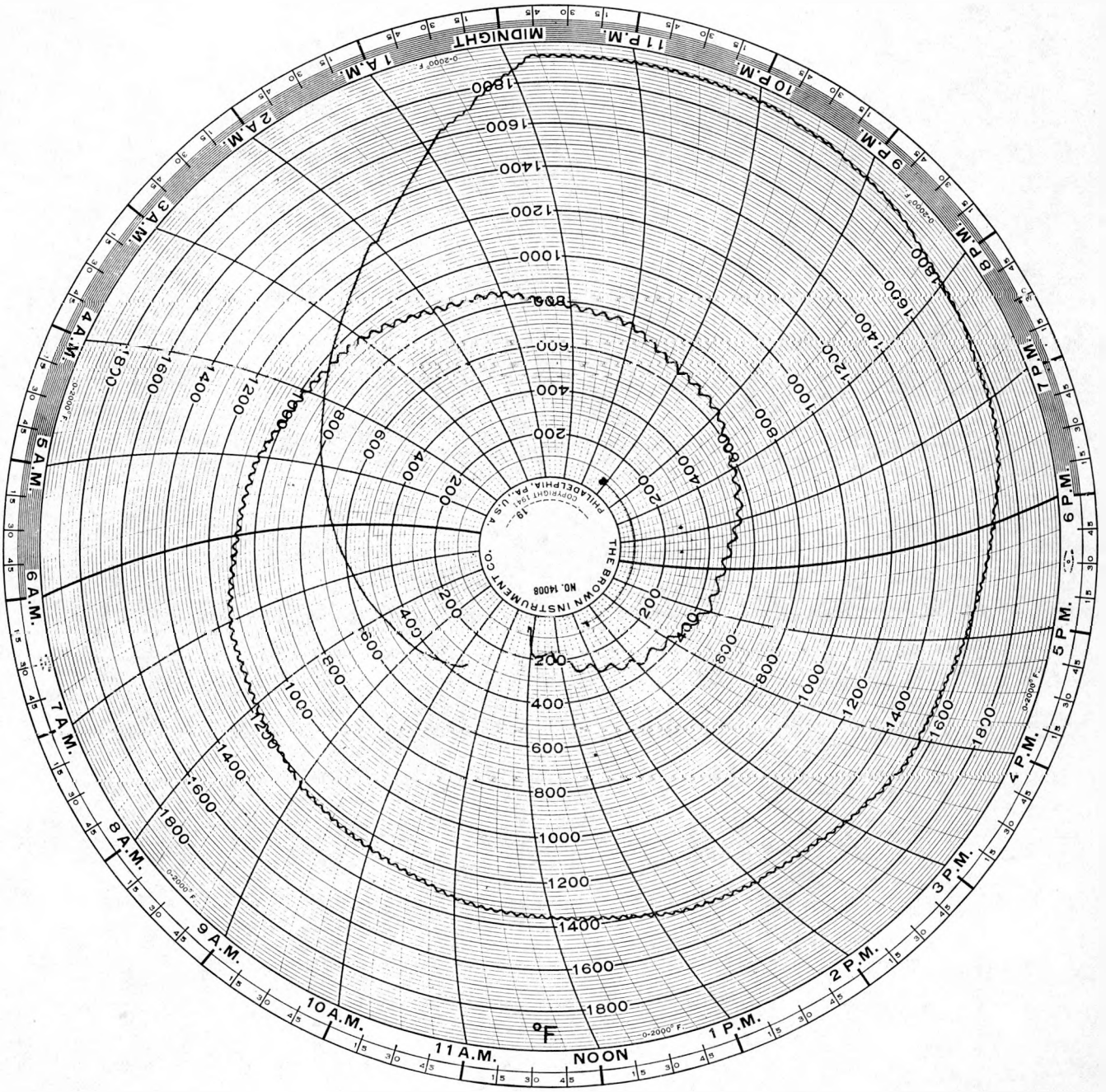

FIG. 98

TEMPERATURE CHART FOR FIRING OF CERAMIC A AND B

DECLASSIFIED

The in-pile radiation stability test on an Alnico magnet is continuing. Details of this test were previously reported in ORNL-867, *Analytical Chemistry Division Progress Report for Period Ending September 20, 1950.*

DECLASSIFIED

VII. LONG-RANGE CHEMISTRY

DECLASSIFIED

THE THORIUM NITRATE—WATER SYSTEM

W. L. Marshall J. S. Gill
C. H. Secoy

A study has been completed of the thorium nitrate—water system from room temperature to decomposition temperatures of the salt.

The only phase data in the literature are those of Misciatelli,[1] who gives comprehensive solubility data for the system from the freezing point of water to an ice eutectic at -43.5°C and 64 wt % salt, and the solubility curve of a hexahydrate determined from the eutectic point to 20°C. In our study this hexahydrate solubility curve was continued to a melting point at 110°C, from which temperature a solubility curve was determined for a tetrahydrate up to a melting point at 158°C. The solubility of another hydrate was then followed to 211°C. An initial hydrolytic decomposition temperature was determined between 115 and 130°C; above this temperature nitrogen oxides are liberated and basic thorium oxide is precipitated. However, in a closed system, the vapor phase appears to equilibrate with the liquid phase, and the system in this form does not show precipitation up to an experimentally determined curve, at which a solid phase appears even in the closed system.

Data which extend the density—weight percent relationship to greater salt concentrations than those previously studied were also determined, together with supercooling data, limiting-flow temperature estimates, and boiling points at atmospheric pressure up to saturation concentrations of aqueous thorium nitrate.

Experimental. Chemically pure thorium nitrate tetrahydrate obtained from the Maywood Chemical Company was used. Solubility data from room temperature to 140°C were obtained analytically by stirring the $Th(NO_3)_4$ solutions in the presence of excess salt for about 40 min in a 200-ml round-bottom flask set in a thermostat. (Preliminary sampling had shown that 10 to 15 min was sufficient for equilibration.) The stirrer was stopped the solid was allowed to settle, and duplicate samples of the clear solution were taken. These samples were weighed, evaporated to dryness, and ignited directly to ThO_2 at 900°C. Duplicate samples deviated approximately ±0.15%. Solid-phase samples were obtained by direct sampling of the solid, drying between filter papers, and ignition to ThO_2.

(1) Misciatelli, P., "The System Thorium Nitrate—Ether—Water Between 0 and 20°," *Gazz. chim. ital.* 60, 833 (1930).

DECLASSIFIED

Solubility and precipitation data above 125°C were obtained in 4- and 6-mm-I.D. quartz tubing by the synthetic method.[2,3] The rates of decomposition precipitation at the elevated temperatures were found to be relatively slow compared to the rates for attainment of solubility equilibrium. The latter can be checked directly by slowly raising the temperature of a solution of known concentration, but the former process either goes through an induction period or has a slow decomposition rate at the initial temperatures. Consequently, to obtain reliable decomposition data, solutions were rocked at various constant temperatures overnight; the decomposition temperatures determined are accurate within about ±4°C.

Supercooling and viscosity data were also obtained by this synthetic method.

Boiling points were determined by a modified micromethod[4] employing an inverted capillary tube inserted in a solution of the salt that was being stirred and refluxed. The temperature of the solution was lowered and the corrected boiling point was determined from the temperature at which bubbling from the capillary stopped.

Density was determined by direct measurement, in the tubes, of the volume for a given weight of solution, and by weighing volumetric aliquots from solutions.

Results and Discussion. The data are given in Tables 32 to 38 and are shown in Figs. 100 to 103. Table 32 gives our solubility-concentration-density data for the $Th(NO_3)_4$-H_2O systems. Tables 34, 35, and 36 give decomposition precipitation temperatures, supercooling, and viscosity estimations, which data are shown graphically in Fig. 100. The solubility data of Misciatelli[5] along the ice curve and up to 20°C are not shown, but a curve following his data is drawn. Line *AB* in Fig. 100 is the ice curve to the cryohydric eutectic point at -43.5°C and 64% salt. Line *BC* is the solubility curve for the hexahydrate. Solid phase analyses at 37.3 and 72.0°C verify Misciatelli's conclusion that the solid phase was the hexahydrate. The melting point of the

(2) Secoy, C. H., *The System Uranyl Sulfate—Water. II. Temperature-Concentration Relationships above 250°C*, ORNL-98 (July 7, 1948).

(3) "Phase Rule Studies," *Homogeneous Reactor Quarterly Progress Report for Period Ending August 31, 1950*, ORNL-826, p. 89 (Oct. 24, 1950).

(4) Siwoloboff, A., "Uber die Siedepunktbestimmung kleiner Mengen Flüssigkeiten," *Ber.*, 19, 795 (1886).

(5) Misciatelli, *op. cit.*

DECLASSIFIED

NOT CLASSIFIED

DWG. 9967

FIG. 100

THE THORIUM NITRATE – WATER SYSTEM

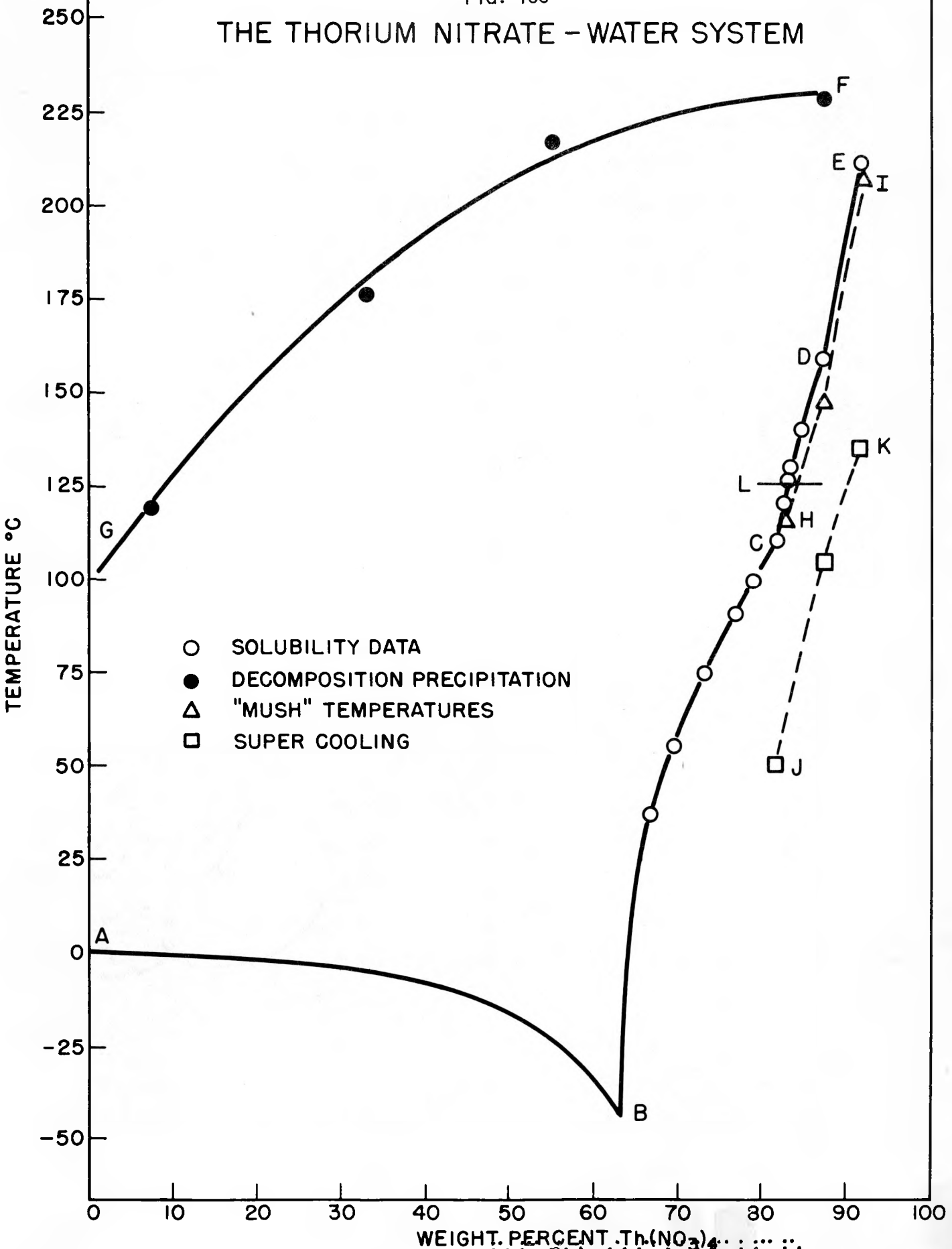

UNCLASSIFIED

DWG. 9968

FIG. 101

THE DENSITY OF AQUEOUS THORIUM NITRATE SOLUTIONS

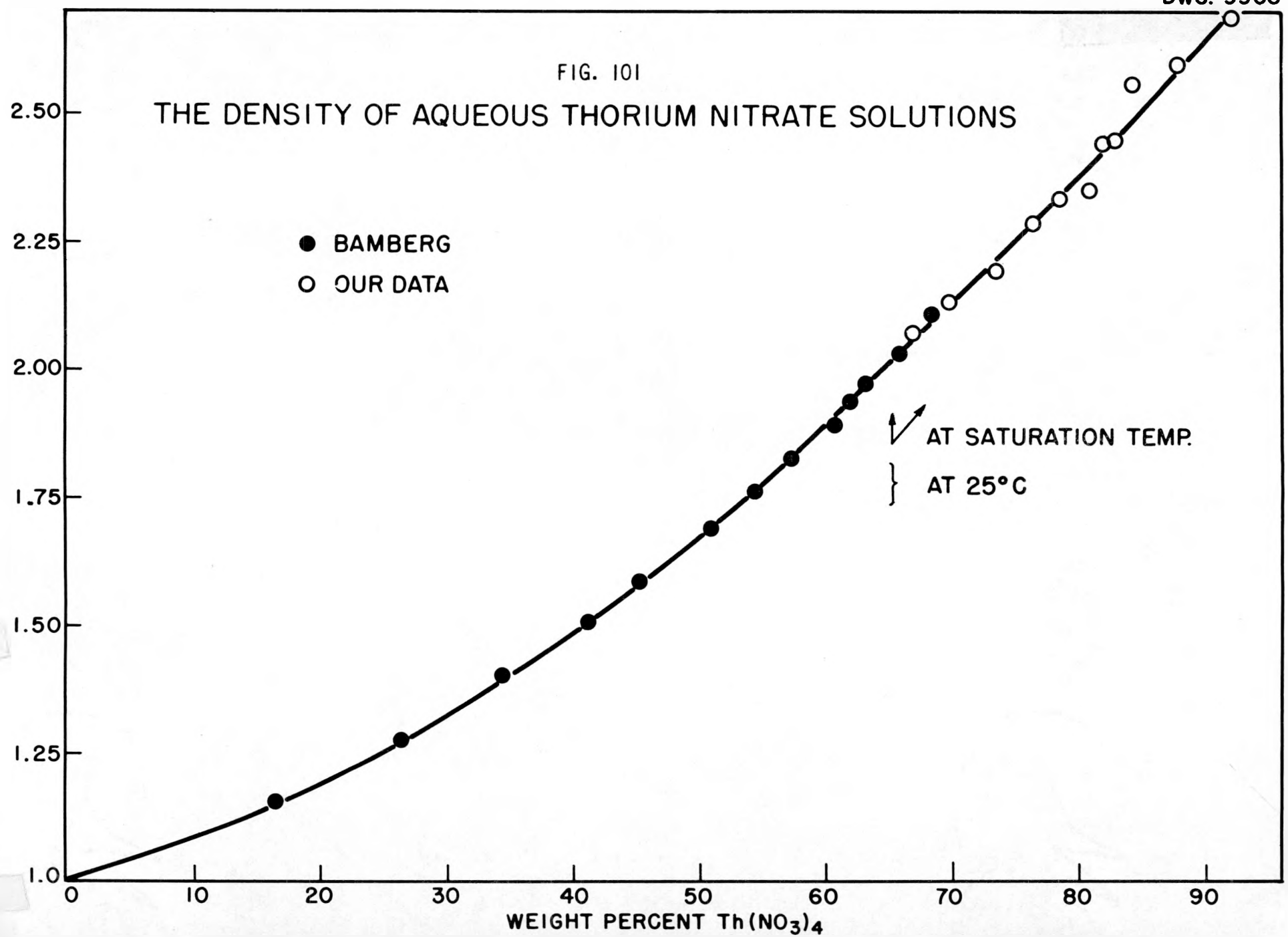

DWG. 9969

FIG. 102

GRAMS THORIUM/cc SOLUTION – TEMPERATURE; BOUNDARY REGION FOR COMPLETE SOLUTION, $Th(NO_3)_4$ – H_2O CLOSED SYSTEM

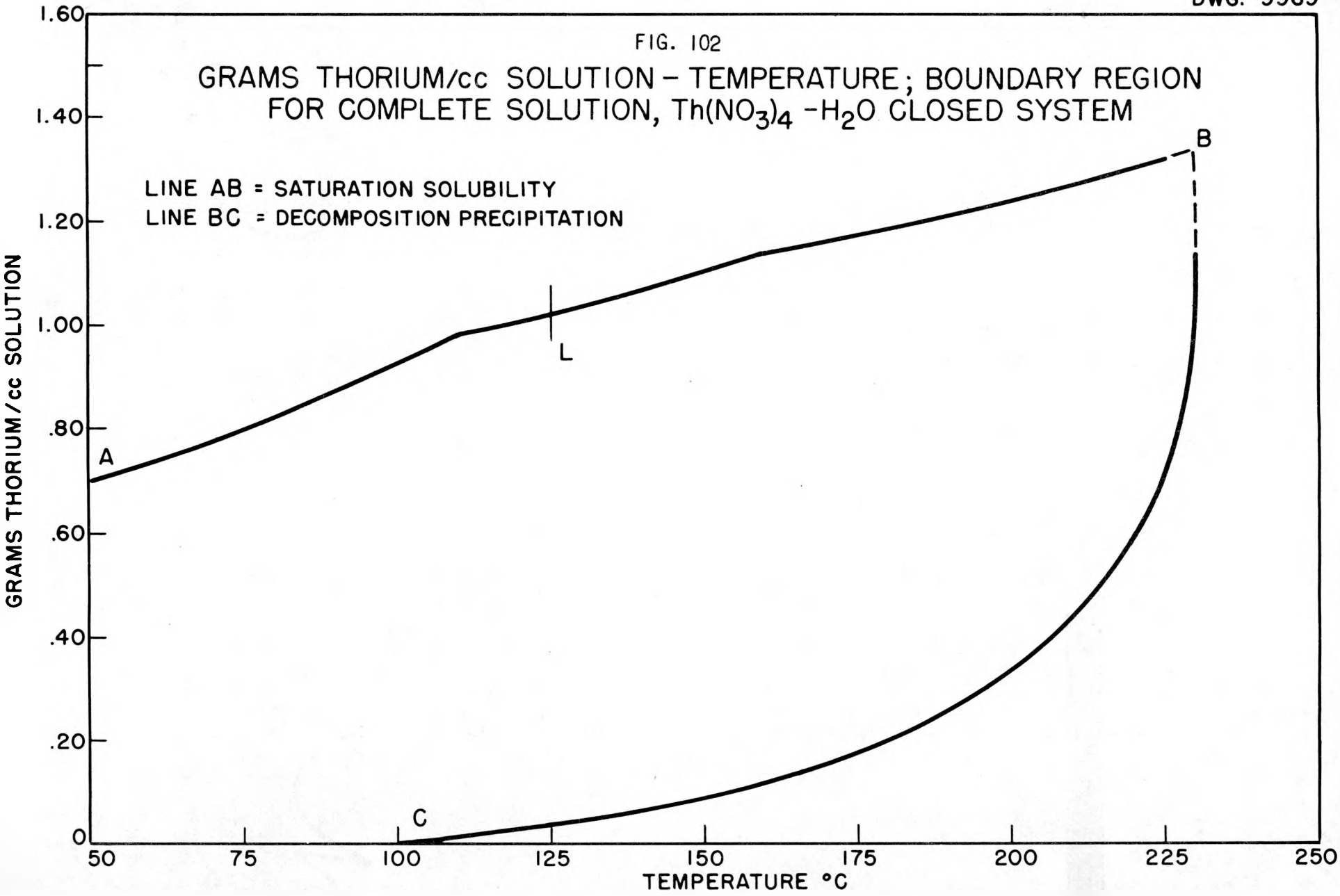

UNCLASSIFIED

DWG. 9970

FIG. 103

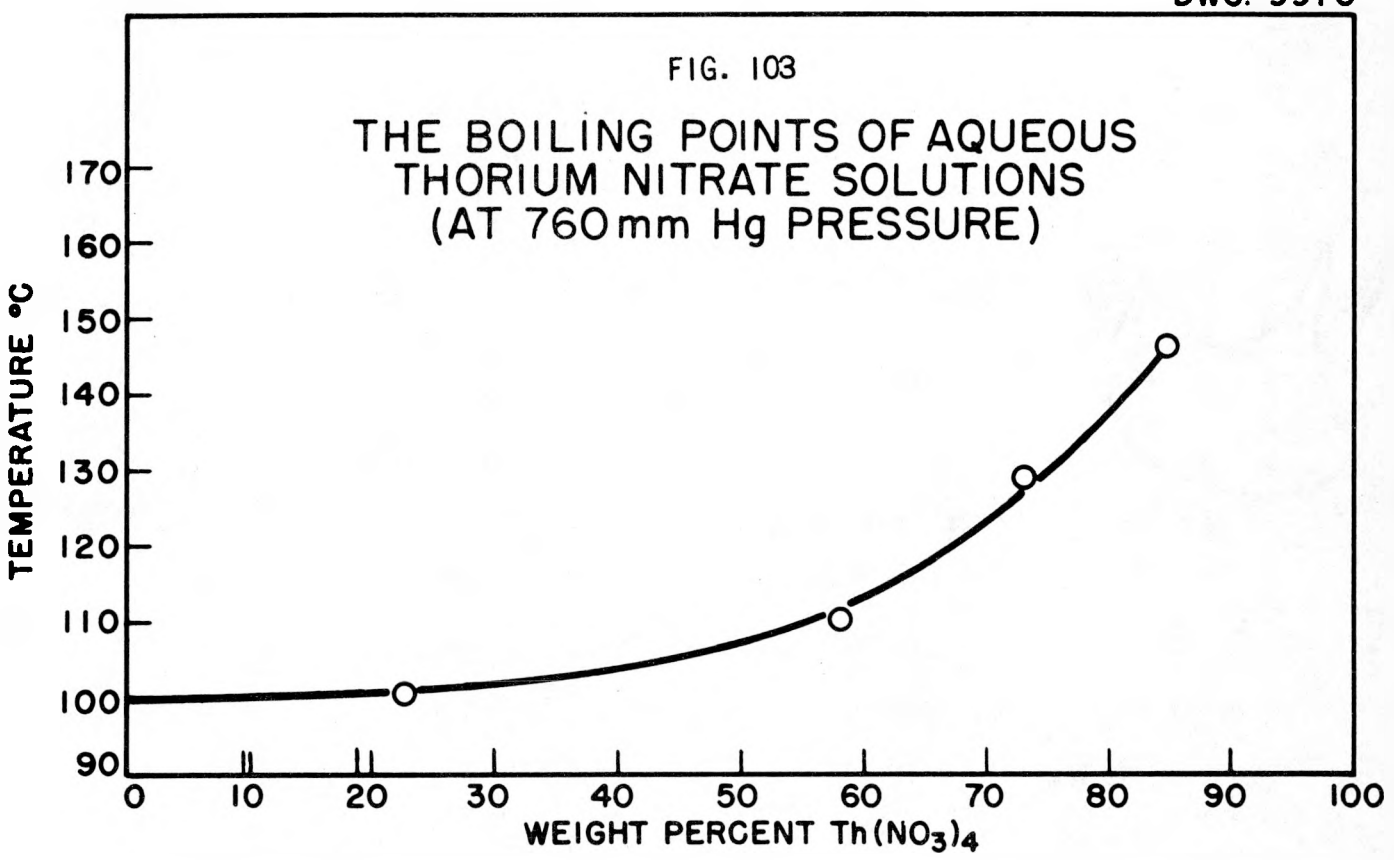

DECLASSIFIED

thorium nitrate hexahydrate is at 110°C (point *C*), at which temperature conversion to the tetrahydrate occurs, the solubility curve of this hydrate being shown by line *CD*. This conversion is indicated both by solid-phase analyses at 129.5°C and the break in the solubility curve at 110°C. Line *DE* is the solubility curve of an undetermined hydrate from the melting point of the tetrahydrate at *D*. Above 120 to 130°C, represented by line *L*, decomposition of the thorium nitrate occurs, giving nitrogen oxides and possibly basic thorium oxide; therefore, above this temperature most of the work was done in closed quartz tubes, as indicated in Table 32. Solubility data are given, however, for temperatures above 125°C on the assumption that decomposition was not extensive enough in a closed system to appreciably alter solubility values up to about 200°C.

Temperatures at which a solid + solution mush type mixture will actually flow to some extent in a 4-mm-I.D. tube are represented by line *HI*, accurate to about ±3°C. The extent of supercooling of a given concentration of solution is indicated by curve *JK*. It may be seen in Table 36 that flow of supercooled solution still occurs at much lower temperatures than flow of solid + solution mixtures.

Upper Limit, Decomposition precipitation Temperatures. By means of a series of $Th(NO_3)_4$-H_2O solution runs in closed tubes we have established a maximum solution line above which irreversible precipitation of a white substance occurs, presumably hydrated thorium oxide. It has been concluded that, while decomposition occurs below line *GF* (and above line *L* in the concentrated regions of Fig. 100), the following type of equilibrium, which is coupled with the usual nitrogen oxides—nitric acid—water equilibria, exists:

$$Th(NO_3)_4\ (aq) \rightleftharpoons ThO_2\ (aq) + 4NO_2 + O_2$$

Realizing that vapor-to-liquid ratio changes of the system will change the effective solution equilibria, all our ratios have been set at approximately 1:1.

Density-concentration data are given in Tables 32 and 33 and in Fig. 101. Density data at dilute concentrations have been reported elsewhere.[6] The

(6) Koppel, I., and Holtkamp, H., "Beiträge zur Theorie der Fabrikation von Thoriumsalzen," *Z. anorg. Chem.* 67, 266 (1910).

UNCLASSIFIED

data in the intermediate concentration range at 25°C (Table 33) are those of J. L. Bamberg of the Chemical Technology Division, presented in this report by his permission. Our data in the more concentrated region were obtained at the saturated-solution temperature.

Making use of the solubility-density-concentration relationships given in Tables 32 and 33 we have determined solubility data in terms of grams of thorium per milliliter of solution. The calculated data are given in Table 37 and are shown in Fig. 102 as line *AB*; they indicate the amount of thorium that might be expected in solution at a given saturation concentration. Line *L* of Fig. 102 corresponds to line *L* of Fig. 100 and represents the temperature at which decomposition starts.

Similarly, from density-temperature variations of water, we have estimated the density-concentration-temperature relationship of thorium nitrate solutions along the precipitation line *GF* of Fig. 100. For this estimation we have neglected temperature expansion coefficients of thorium nitrate in solution and have considered only the expansion due to the weight fraction of water in solution. Using these data we have determined the grams of thorium per milliliter of solution along the precipitation curve *GF* of Fig. 100; the data are given in Table 37. The variation as a function of temperature is shown along line *CB* of Fig. 102. Therefore the area between curves *AB* and *CB* of Fig. 102 represents a region in which no precipitation of a solid occurs in a closed thorium nitrate—water system of approximately 1:1 vapor-to-liquid ratio.

Boiling point data for aqueous thorium nitrate solutions at standard pressure are given in Table 37 and Fig. 103.

Breeder Pile Application. It is thus seen in Fig. 102 that it is possible to obtain 1 g of thorium as the metal per milliliter of saturated solution at 118°C. The boiling point at atmospheric pressure of a solution containing this concentration of thorium would then be approximately 142°C.

The decomposition precipitate in the concentrated solutions at higher temperatures is gelatinous and tends to remain suspended in the solution until the 275 to 300°C temperature range is reached. The precipitate then settles immediately. This precipitation could probably be avoided entirely and consequently higher temperatures might be used if some free nitric acid was added to the solution. All work given here is with reference to thermal stability and has no bearing whatsoever on radiation stability.

DECLASSIFIED

Summary. 1. A study of the system thorium nitrate—water has been extended from 20°C to decomposition temperaturesof the solution.

2. Density-concentration and boiling point data are given.

3. The experimental data indicate that a solution containing 1 g of thorium per milliliter can be attained in an aqueous solution of thorium nitrate at and above 118°C. Such a solution appears to be satisfactory, in so far as chemical stability is concerned, as a breeder blanket. Of course, N^{15}-enriched nitrate would be required in order to minimize neutron losses.

TABLE 32

The Solubility and Saturation Density of Aqueous Thorium Nitrate

TEMPERATURE (°C)	DENSITY (g/ml)	$Th(NO_3)_4$ (wt %)	METHOD OF ANALYSIS	SOLID PHASE	
				$Th(NO_3)_4$ (wt %)	COMPOSITION
37.3	2.09	67.07	Analytical	81.18 (theoretical for $Th(NO_3)_4 \cdot 6H_2O$, 81.62)	$Th(NO_3)_4 \cdot 6H_2O$
54.5	2.17	69.78	Analytical		$Th(NO_3)_4 \cdot 6H_2O$
72.0	2.23	73.39	Analytical	80.82 (theoretical for $Th(NO_3)_4 \cdot 6H_2O$, 81.62)	$Th(NO_3)_4 \cdot 6H_2O$
90.2	2.37	76.39	Analytical		$Th(NO_3)_4 \cdot 6H_2O$
99.7	2.41	78.56	Analytical		$Th(NO_3)_4 \cdot 6H_2O$
110.4	2.44	81.11	Analytical		$Th(NO_3)_4 \cdot 6H_2O$ + $Th(NO_3)_4 \cdot 4H_2O$
110.9	2.45	81.50	Analytical		$Th(NO_3)_4 \cdot 4H_2O$
120.2	2.57				$Th(NO_3)_4 \cdot 4H_2O$
120.6	2.54	82.01	Analytical		$Th(NO_3)_4 \cdot 4H_2O$
128		82.41	Synthetic		$Th(NO_3)_4 \cdot 4H_2O$
129.5	2.59			85.84 (theoretical for $Th(NO_3)_4 \cdot 4H_2O$, 86.95)	$Th(NO_3)_4 \cdot 4H_2O$
130.5	2.53	82.85	Analytical		$Th(NO_3)_4 \cdot 4H_2O$
139.5	2.70	84.27	Analytical		$Th(NO_3)_4 \cdot 4H_2O$
159	2.75	87.41	Synthetic		$Th(NO_3)_4 \cdot 4H_2O$
211	2.86	91.82	Synthetic		(?)

DECLASSIFIED

TABLE 33

The Density of Aqueous $Th(NO_3)_4$ at 25°C*

$Th(NO_3)_4$ (wt %)	DENSITY (g/ml)	$Th(NO_3)_4$ (wt %)	DENSITY (g/ml)
16.54	1.161	57.63	1.833
26.28	1.279	60.84	1.894
34.30	1.400	61.94	1.938
41.39	1.508	63.34	1.971
45.41	1.586	66.06	2.035
51.02	1.694	68.26	2.110
54.41	1.765		

*Original data of J. L. Bamberg of the Chemical Technology Division.

TABLE 34

Decomposition—Precipitation Temperatures of $Th(NO_3)_4$-H_2O Solutions

$Th(NO_3)_4$ (wt %)	TEMPERATURE, UPPER LIMIT BEFORE PRECIPITATION (°C)
87.41	229
55.23	217
32.94	~176
7.41	~113

DECLASSIFIED

TABLE 35

Initial Flow Temperatures (Solid-Liquid Mush) of $Th(NO_3)_4$-H_2O System

$Th(NO_3)_4$ (wt %)	TEMPERATURE (°C)	FLOW IN 4-mm TUBING
82.41	116	Medium to none
87.41	148	Medium to none
91.82	208	Medium to none

TABLE 36

Supercooling Flow Temperatures, $Th(NO_3)_4$-H_2O System

$Th(NO_3)_4$ (wt %)	TEMPERATURE (°C)	FLOW IN 4-mm TUBING
82.41	>65	Medium to fast
82.41	65	Slow to none
82.41	<50 (crystallization)	
87.41	>115	Medium to fast
87.41	115	Slow to none
87.41	104 (crystallization)	
91.82	>150	Medium to fast
91.82	150	Slow to none
91.82	135 (crystallization)	

DECLASSIFIED

TABLE 37

Boundary Curve Data

(Calculated from Density-Temperature-Solubility-Precipitation Data)

TEMPERATURE (°C)	SOLUBILITY OF THORIUM NITRATE (g Th/ml)	CONCENTRATION OF SOLUTION AT DECOMPOSITION-PRECIPITATION TEMPERATURE (g Th/ml)
50	0.704	
60	0.735	
70	0.779	
80	0.825	
90	0.872	
100	0.922	
110	0.979	
120	1.007	
130	1.026	0.040
140	1.059	0.060
150	1.099	0.084
160	1.144	0.115
180	1.195	0.200
200	1.240	0.335
210	1.281	0.440
220	1.302	0.600
225	1.32	0.715
230	1.34	1.14
232	1.35	1.35

TABLE 38

The Boiling Points of Aqueous Thorium Nitrate Solutions at 760 mm Hg Pressure

$Th(NO_3)_4$ (wt %)	TEMPERATURE (°C)
22.3	101
58.0	110
72.3	130
85.3	147

DECLASSIFIED

URANIUM SLURRY STUDIES

L. E. Morse

Summary. During the past quarter the preparation of slurries suitable for use in the homogeneous reactor was further investigated. These slurries contain 40 g of uranium as a solid per liter, and they should be stable with respect to sedimentation upon shutdown of the slurry-circulating pumps. The operating conditions are 250°C and 1000 psi pressure.

It has been shown that slurries prepared from anhydrous UO_3 in water, although stable at room temperatures, break and settle very rapidly after being heated at 250°C for 1 hr. Further work indicated that these slurries could be stabilized by the addition of bentonite, a naturally occurring colloidal alumino-silicate clay having cation-exchange properties.

Studies on bentonite showed that the clay was best utilized when present in particle sizes below 25 mμ. The clay was fractionated to separate the smaller particles in a Sharples centrifuge. It was found necessary to remove from the bentonite all the exchangeable cations such as iron, magnesium, calcium, sodium, and potassium since the presence of these positively charged ions adversely affected the stability of the bentonite colloids. By means of electrodialysis the exchangeable cations were removed, producing a hydrogen bentonite.

Thermal Stability of Uranium Trioxide–Bentonite Slurries. The thermal stability of a slurry prepared from anhydrous UO_3 and a suspension of bentonite heated at 250°C in a stainless-steel bomb (Table 39) was studied at intervals up to 526 hr. This slurry showed good stability at the end of 330 hr of heating but settled with fairly hard caking on standing at room temperature after being heated for 526 hr. There were indications of the presence of colloidal ferric hydroxide. Analyses made at various time intervals showed that the iron content of these slurries increased as the heating period lengthened. These analyses also showed that iron had been introduced into the slurries during their preparation in the colloid mill. This will necessitate changes in the method of preparation.

It is not known whether the iron introduced during the heating is due to either corrosion or erosion of the stainless-steel-bomb surfaces or both. It may be possible to protect the steel against corrosion by passivation. However, if there is appreciable erosion, it will necessitate the addition of phosphates, which previous work has indicated to be effective in complexing the iron.

DECLASSIFIED

TABLE 39

Sedimentation Behavior of Slurries over Long Heating Periods

Slurry composition: uranium, 40 g as anhydrous UO_3; bentonite, 1000 ml of suspension containing 12 to 15 g of electrodialyzed bentonite solids of average particle size below 25 mμ

Heating conditions: 250°C in stainless-steel bomb

Heating time (hr)	4	66	100	189	330	526
Sedimentation time (days)	5	1.5	0.75	3.6	1.8	1*
Sampling level**	Uranium concentration (g/liter)					
1	14.1	17.8	10.3	8.8	1.2	10.0
2	30.1	33.5	39.3	36.3	1.6	6.7
3	32.8	35.7	39.3	39.2	40.0	21.8
4	32.8	34.0	40.0	40.7	50.7	54.8
5	34.0	35.0	40.0	41.9	52.7	58.0
6	37.0	38.0	41.3	44.2	55.7	61.7
Volume ratio of settled solids to total solids	0.90	0.88	0.90	0.88	0.69	0.60

*On longer standing, sedimentation continued until all the solids had settled out and packed fairly hard.

**Successive 3-ml samples were removed until the entire volume was sampled.

DECLASSIFIED

One other possible approach is conversion of the hydrogen bentonite to another suitable bentonite, for example, a beryllium bentonite. This probably would show less sensitivity to the presence of foreign cations.

Colloidal Silicic Acid as a Slurry Stabilizer. An investigation was made of colloidal silicic acid (H_2SiO_3) as a possible slurry stabilizer in place of bentonite. It was prepared by passing Na_2SiO_3 through a cation-exchange resin in the hydrogen form and aging the resulting clear solution until it became colloidal.

The results of several tests using various concentrations of H_2SiO_3 indicated that for a heating period of 22 hr at 250°C in a stainless-steel bomb colloidal H_2SiO_3 was not as effective a stabilizer as bentonite under the same conditions (Table 40).

It appears from qualitative observations on the degree of settling that over 4% SiO_2 (40 g per 1000 ml) as colloidal silicic acid would be necessary to achieve a satisfactory suspension of UO_3.

Further experiments will be carried out using mixtures of colloidal silicic acid and colloidal aluminum hydroxide in an attempt to prepare aluminosilicate systems with satisfactory stabilizing properties.

Uranium Dioxide as an Alternate Reactor Fuel. Inasmuch as cations affect the stability of the bentonite colloids unfavorably, and anhydrous UO_3 is hydrolyzed by water to yield water-soluble uranium, slurries were prepared substituting UO_2 for UO_3 as the fuel material. The brown oxide UO_2 is known to be unreactive, although there is no information available concerning its behavior with water at 250°C.

To avoid iron contamination the slurries were prepared by hand grinding in a mullite mortar. Analyses of several slurry samples indicated that a fairly uniform dispersion was achieved.

The composition of the slurry was 40 g of uranium as UO_2 (obtained from K-25) plus 1000 ml of a bentonite suspension containing 15 g of electrodialyzed bentonite solids of average particle size below 25 mμ. This slurry was heated in a sealed quartz tube for 138 hr at 250°C. After standing 24 hr at room temperature, analyses for uranium distribution showed that almost all the uranium had settled out.

DECLASSIFIED

TABLE 40

Colloidal Silicic Acid as a Slurry Stabilizer

Slurry composition: uranium, 40 g as anhydrous UO_3; H_2SiO_3, 1000 ml of suspension

Heating conditions: 250°C for 22 hr in stainless-steel bomb

Sedimentation time: 24 hr

SILICIC ACID CONCENTRATION (g SiO_2/1000 ml)	CONDITION OF SILICIC ACID	VOLUME RATIO OF SETTLED SOLIDS TO TOTAL SOLIDS
20	Freshly prepared	0.35
20	Colloidal suspension	0.32
30	Gel	0.46
40	Gel	0.57

DECLASSIFIED

On the possibility that the UO_2 might have contained some water-soluble impurities, another sample of the brown oxide was ground in a ball mill and then heated with 6 *N* H_2SO_4 for 1 hr. The undissolved oxide was separated, washed until the filtrate was colorless, and then ignited for 1 hr at 900 to 1000°C. On cooling it was made into a slurry and heated in the previously described manner. The analysis for uranium distribution again showed that all the uranium had settled out after 24 hr of standing.

Judging from previous results the amount of iron in these slurries would not be sufficient to account for the observed settling of the solids; therefore it would seem that sufficient U(IV) ion has been produced from the UO_2 to flocculate the bentonite and render it useless as a stabilizer. Since U(IV) is a very highly charged ion, only small amounts of it would be required to bring about the flocculation of the bentonite.

As a comparison, it is interesting to note that a slurry using uranium phosphate, $U_3(PO_4)_4$, in place of UO_2 was much more stable under the same conditions.

THORIUM SLURRIES FOR BREEDER PILE

T. C. Runion

In the production of 23 from the neutron irradiation of thorium, certain advantages in neutron economy and in engineering features of pile design are offered by a system containing the thorium in the form of a suitable slurry. The immediate objective is the production of such a slurry with the following physical and chemical characteristics:

1. A thorium concentration exceeding 1000 g/liter.
2. Stability to intensive heat and radiation; i.e., the thorium should not floc or pack for relatively long periods of operation or during temporary shutdown.
3. Stability to the products of equilibrium pile operation, e.g., peroxide and fission products.
4. High fluidity to permit efficient pumping and circulation; if gelling properties are in evidence the slurry must have a high degree of thixotropy.
5. The slurry must not be excessively erosive or corrosive.

UNCLASSIFIED

Present Status of Work. Using ThO_2 of approximately 0.5-μ particle size, thixotropic gels containing about 1000 g of thorium per liter have been prepared which are very stable at room temperature. Starting with the production of fused ThO_2 at 1000°C from $Th(OH)_4$, $Th(NO_3)_4$, or $ThOCO_3$, slurries were stabilized with 3.5% bentonite by the procedures used in the preparation of oil-well drilling muds. Such slurries have a high degree of fluidity under increasing rates of shear, and they set to a plastic gel at rest. After one month of syneresis the solids still occupied more than 95% of the original volume. Demonstration of the stability at higher temperatures and pressures is awaiting the arrival of a suitable autoclave. However, the success of L. E. Morse of the Chemical Technology Division with uranium slurries along these lines holds some promise for this approach with thorium.

Future Program. *1. Synthesis of Bentonite.* It is planned to attempt the laboratory synthesis of a bentonite with the idea of obtaining a product of more consistent properties than the natural product. Using this form of bentonite the stability of thorium slurries under heat and radiation will be investigated.

2. *Breeder Blankets Utilizing "Fluidized ThO_2."* Anhydrous ThO_2 in the particle size range of 0.1 to 1.0 μ has a high degree of fluidity, even at very high temperatures. This property may be further increased by the incorporation of an inert diluent of low cross section. It is planned to investigate the behavior of such a system from an engineering point of view.

3. Separation of Thorium, Uranium, and Protactinium. No major difficulty is anticipated with this operation. Since ThO_2 is highly insoluble in dilute nitric acid, it is believed that a leaching process will selectively remove the uranium after an appropriate decay period for protactinium. Alternatively, the entire system would be dissolved, using HF as a catalyst, and processed by the 23 process that has already received pilot-plant-scale demonstration.

DECLASSIFIED

CONTINUOUS FUEL PROCESSING

I. R. Higgins and W. E. Shockley

Summary. For continuous removal of fission products from uranium solutions in homogeneous reactors selective adsorption methods have been emphasized since they approach the ideal process requirements in simplicity and exhibit high specificity for fission product ions in uranyl sulfate solution. By using a combination of adsorbers, selective removal of all the major fission products and plutonium has been demonstrated. The organic cation exchangers have a preferential affinity for plutonium, the rare earths, barium, strontium, yttrium, and cesium; the organic anion exchangers for molybdenum, iodine, tellurium, niobium, and ruthenium; and Super Filtrol inorganic adsorber for cesium, niobium, zirconium, and plutonium.

All the adsorbers hold up some uranium temporarily, which must be completely and selectively removed from the adsorbed fission ions. Uranium is eluted from the organic cation exchangers with 0.25 *M* sulfuric acid and from Super Filtrol with $(NH_4)_2SO_4$ at the same molarity and *p*H as the fuel solution. The selective desorption of uranium from the anion exchangers has not been successfully accomplished.

Only preliminary tests have been made using electrolytic methods. Indications are that molybdenum, iodine, and tellurium are most readily deposited with negligible uranium loss. It is considered fortunate that the activities removed by this method overlap those removed by the anion exchangers from which uranium is removed with difficulty.

In a sulfate fuel system barium will be expected to precipitate out after one week or less of production in the HRE. Zirconium has also been precipitated by hydrolysis of Zr(IV) in uranyl sulfate. Quite likely there are other precipitations, of which advantage should be taken by filtration.

Successful application of the above-mentioned methods could almost be assured if there was nothing to fear from radiation damage. Dowex 50, chosen to remove the rare earth activities especially, is an organic polymer, and experiments using a Co^{60} gamma source have shown a definite loss in capacity of the resin from radiation damage. Some loss in capacity is not alarming since only a few grams of fission products is involved, and the decontamination factor, K_D, for rare earth activities in UO_2SO_4 is high. Also, any

DECLASSIFIED

loss in capacity is beneficial as far as uranium holdup is concerned. Since there is definitely a capacity loss with radiation, the processing cycle must be adjusted to allow the maximum permissible build-up of fission products in the reactor and the maximum practical increase in fuel inventory to allow for decay.

In general, a processing cycle for the HRE is visualized as follows: One complete fuel batch, 70 liters, is cycled every 21 days, allowing a 1% accumulation of fission products. One day's cooling is allowed to reduce radiation energy, which increases the fuel inventory by about 5%. The processing methods of electrodeposition and Super Filtrol adsorption, which are not subject to radiation damage, are introduced first to relieve the radiation load on the organic adsorber Dowex 50. From this processing cycle and the Co^{60} gamma radiation studies on resins, 1 kg of Dowex 50 is calculated to lose 90% of its capacity in about two days. At this point the resin bed could be removed, the uranium eluted with 0.25 *M* H_2SO_4, and the resin discarded or processed for plutonium. It is undesirable to use a material even slightly sensitive to radiation, but no other method has yet been found as efficient for rare earth removal as the organic cation resins.

Cation-exchange Studies. The only major fission products in solution in UO_2SO_4 solution with well-defined cationic properties are plutonium, the rare earths, strontium, and cesium. These four are representative of four different valence states, Pu^{4+}, RE^{3+}, Sr^{++}, and Cs^{+}, and they behave accordingly (Fig. 104). The relatively low affinity of Dowex 50 for UO_2^{++} may be realized by noting the preferential adsorption of monovalent cesium. Figure 105 indicates the degree of shift from equilibrium caused by using a coarser mesh resin and faster flow rates. Figure 106 indicates the influence of a greatly increased UO_2^{++} ion concentration. Figures 104, 105, and 106 indicate the high selectivity and capacity for the particular activities mentioned.

Figure 107 indicates the capacity loss thus far from the 300-curie Co^{60} gamma source. The energy absorbed by water from this source was determined to be 0.01 calorie/g/min. Assuming the same energy absorption by Dowex 50 resin and a 1% fission product build-up, 21 g, in the HRE reactor with a one-day cooling period, the fission-product energy build-up on the adsorber indicates that 1 kg of Dowex 50 resin would lose nearly all its capacity in 1½ days. Table 41 shows the effect on resin life and fuel inventory with longer cooling periods. Figures 108 through 111 indicate how the breakthrough of Nb, Pu,

DECLASSIFIED

DRAWING 10246

FIG. 104

DOWEX 50 CAPACITY TEST

for Fission Activity

from Uranyl Sulfate- 30g. U/l.

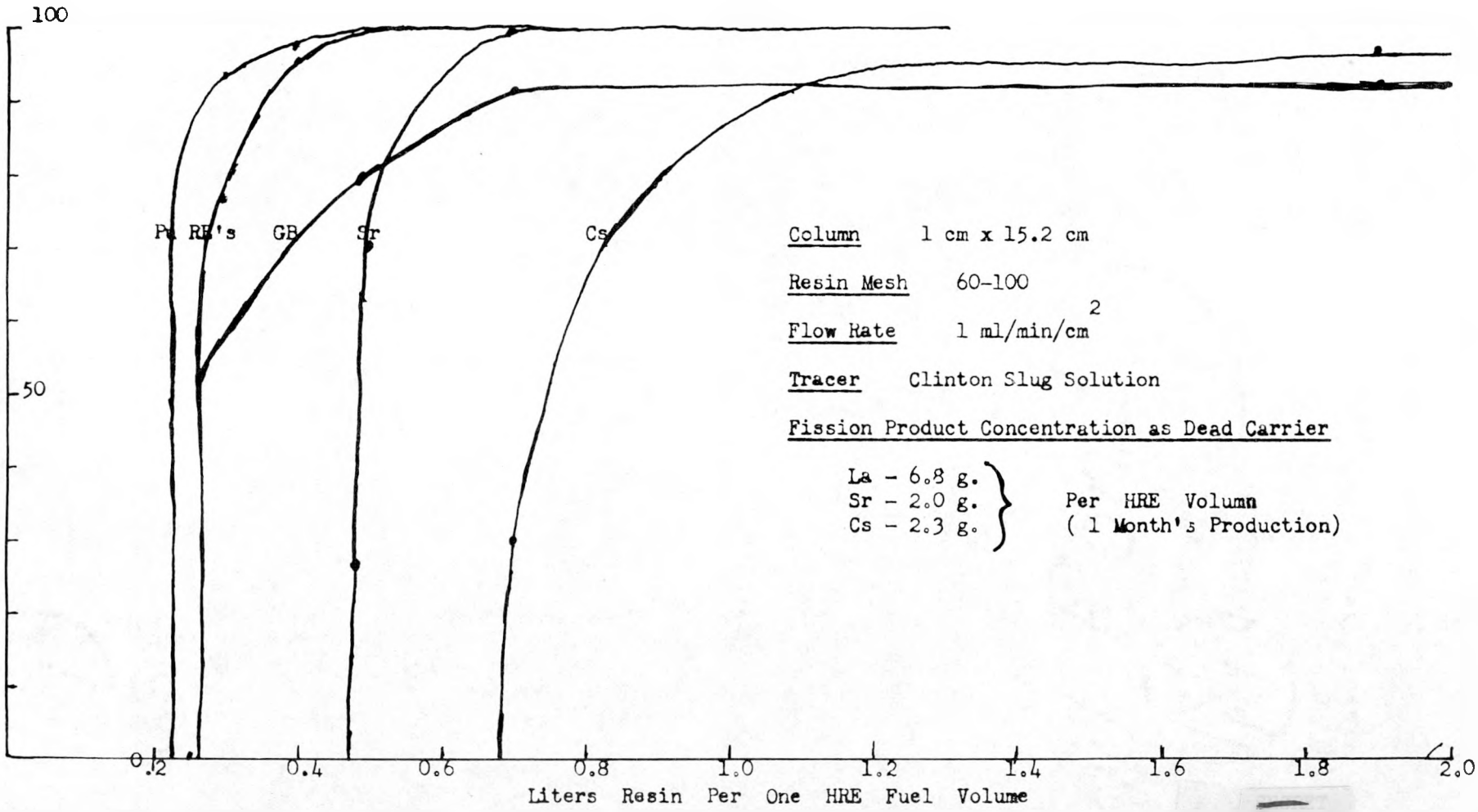

CLASSIFIED

DRAWING 10247

FIG. 105

DOWEX 50 CAPACITY TEST

for Fission Activity

from Uranyl Sulfate - 30g/l U

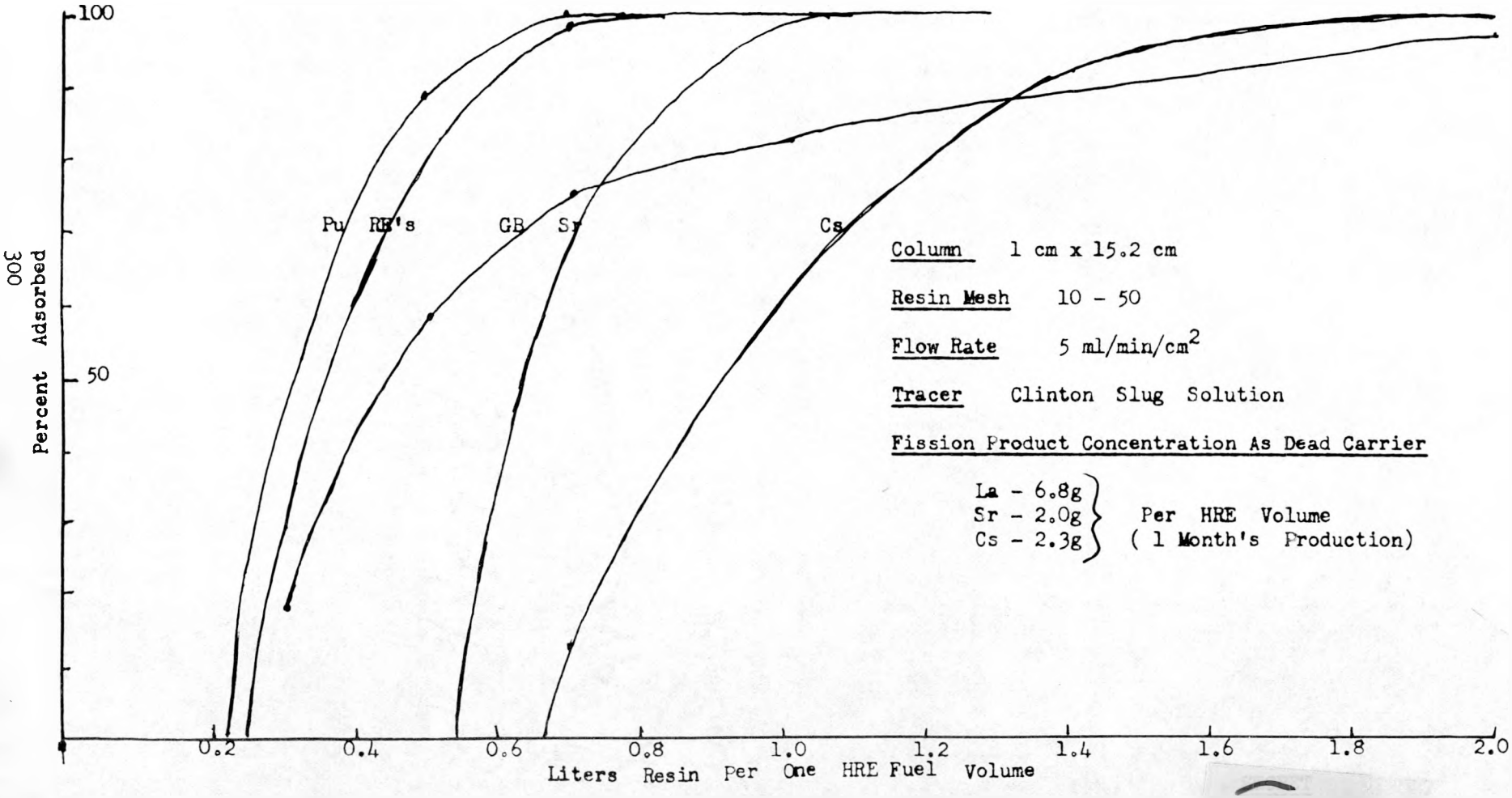

DRAWING 10248

FIG. 106

Dowex 50 Capacity Test

for Fission Activity

from Uranyl Sulfate - 200g. U/l

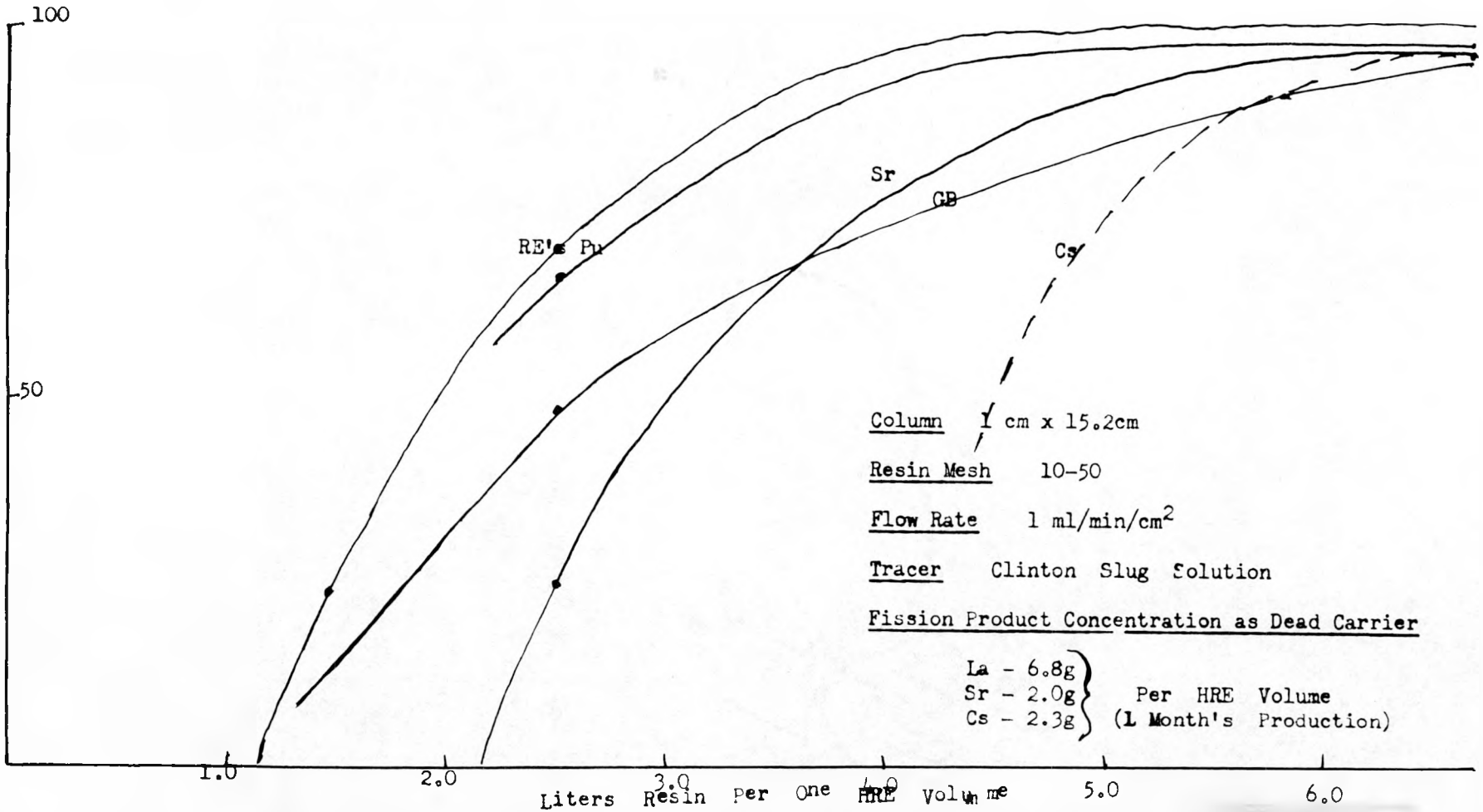

301

DRAWING 10249

FIG. 107

DOWEX 50 CAPACITY LOSS FROM IRRADIATION

from a 300 Curie Co^{60} Gamma Source

(Energy absorption assumed to be the same as for water

Or 0.7 Watt-Hours Per Gram Per 1000 Hours)

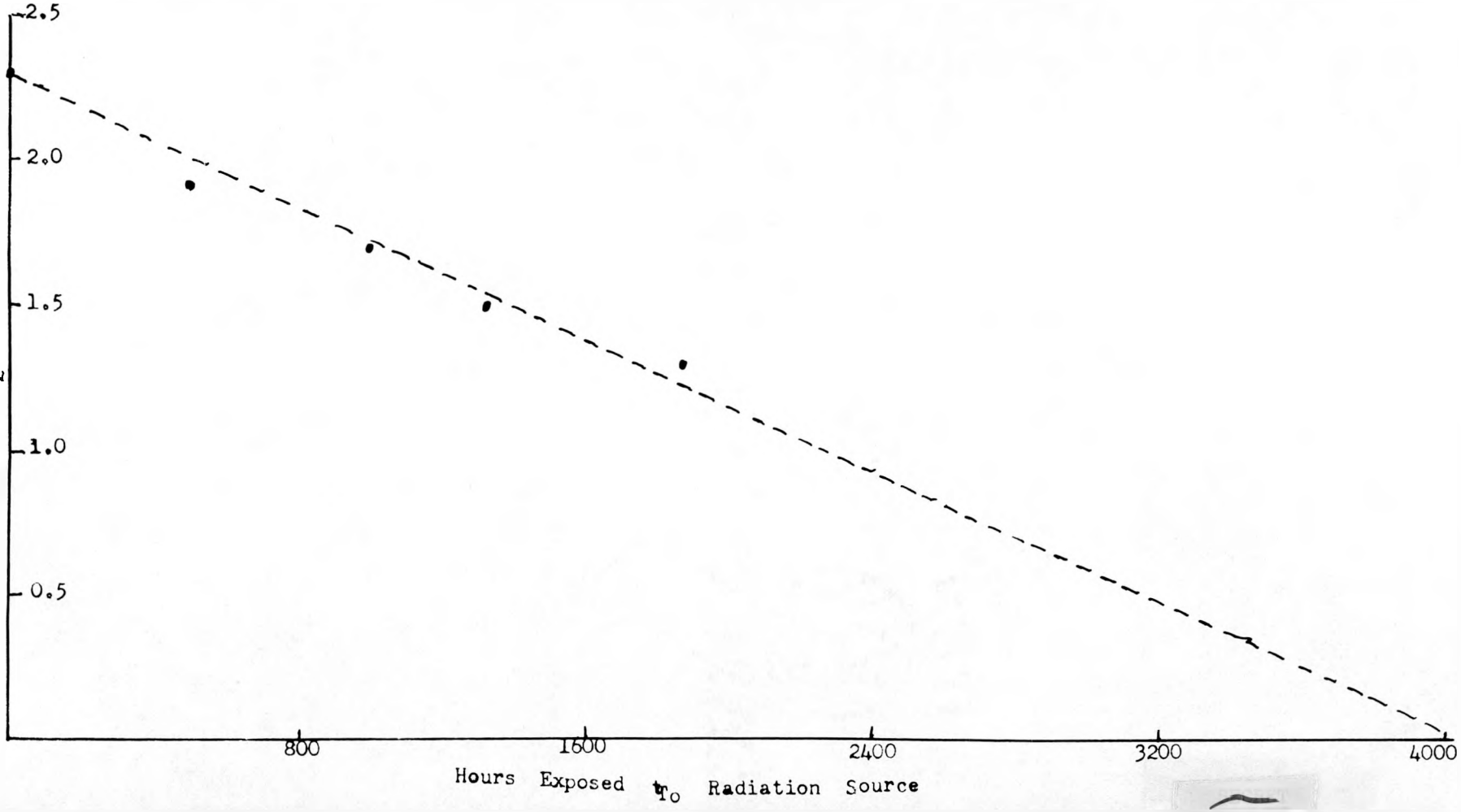

202

DRAWING 10250

FIG. 108

STRONTIUM BREAKTHRU on IRRADIATED DOWEX 50 RESIN

Solution Uranyl Sulfate 30g. U/l

Column 0.3 cm x 5.4 cm

Flow Rate 2 ml/min/cm^2

Activity Clinton Slug Solution (Tracer Only)

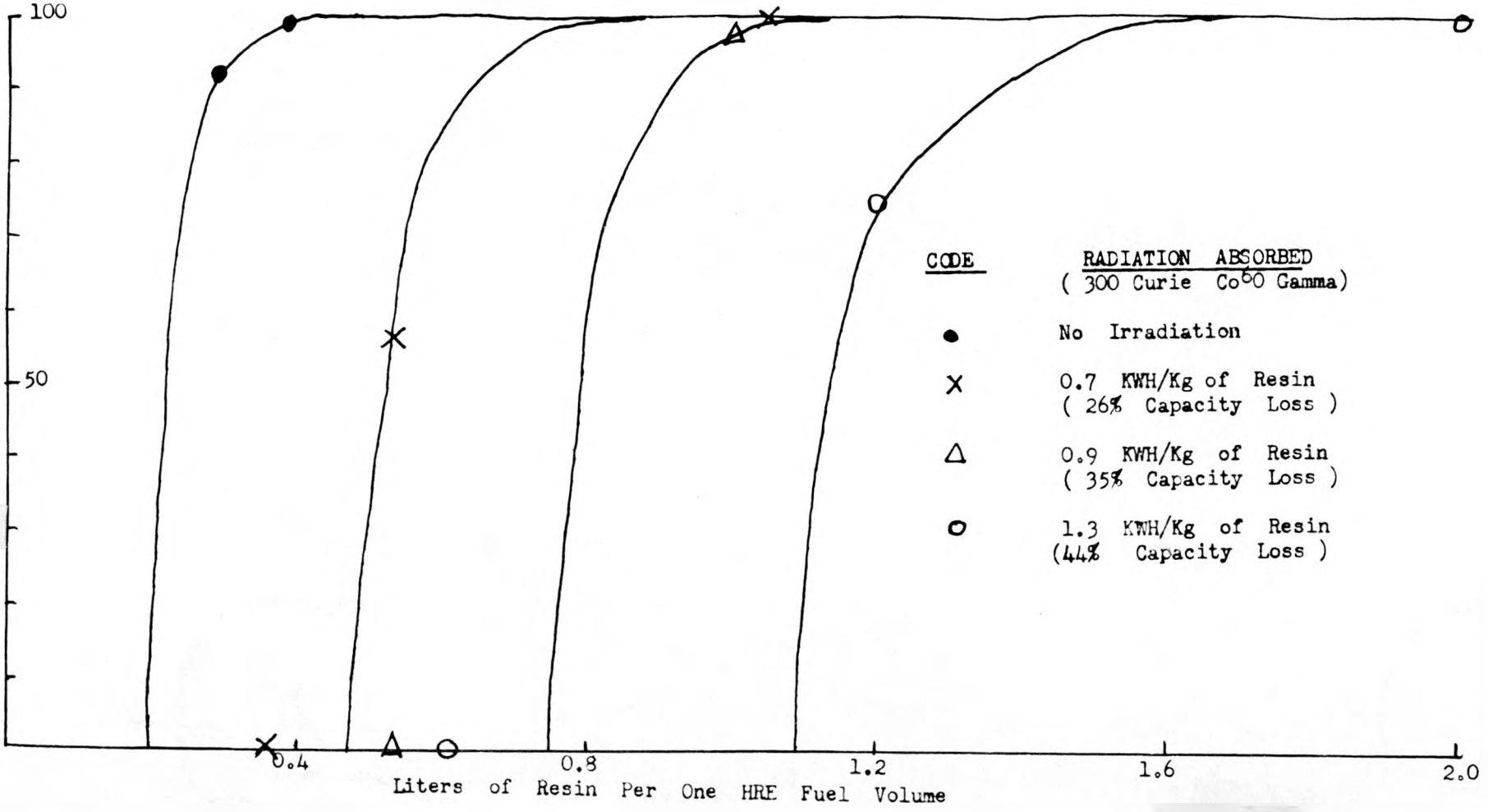

CLASSIFIED

DRAWING 10251

FIG. 109

CESIUM BREAKTHRU on IRRADIATED DOWEX 50 RESIN

Solution Uranyl Sulfate 30g. U/l

Column 0.3 cm x 5.4 cm

Flow Rate 2 ml/min/cm^2

Activity Clinton Slug Solution (Tracer Only)

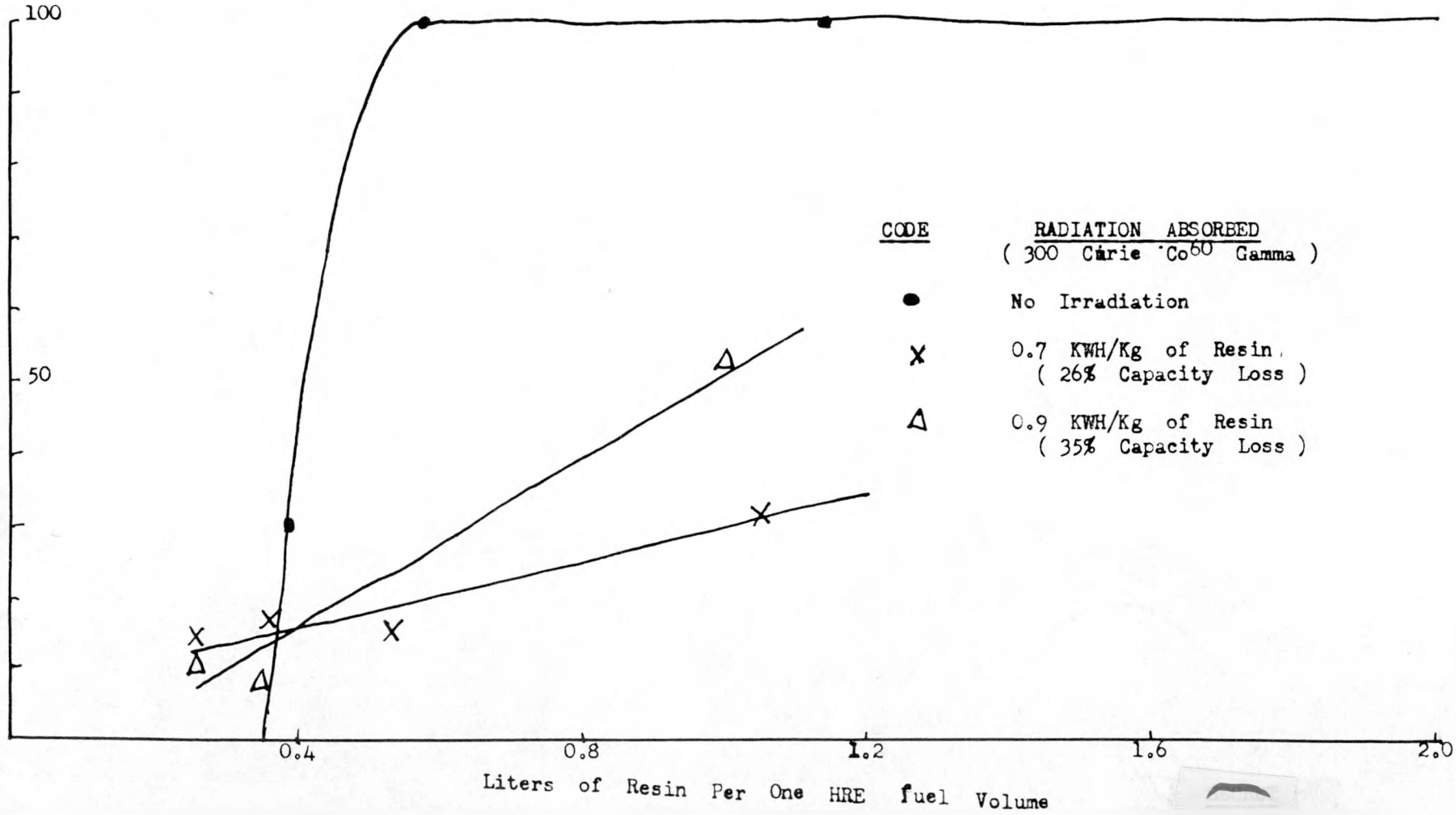

304

DRAWING 10252

FIG. 110

NIOBIUM BREAKTHRU on IRRADIATED DOWEX 50 RESIN

Solution Uranyl Sulfate 30g. U/l

Column 0.3 cm x 5.4 cm

Flow Rate 2 ml/min/cm^2

Activity Clinton Slug Solution (Tracer Only)

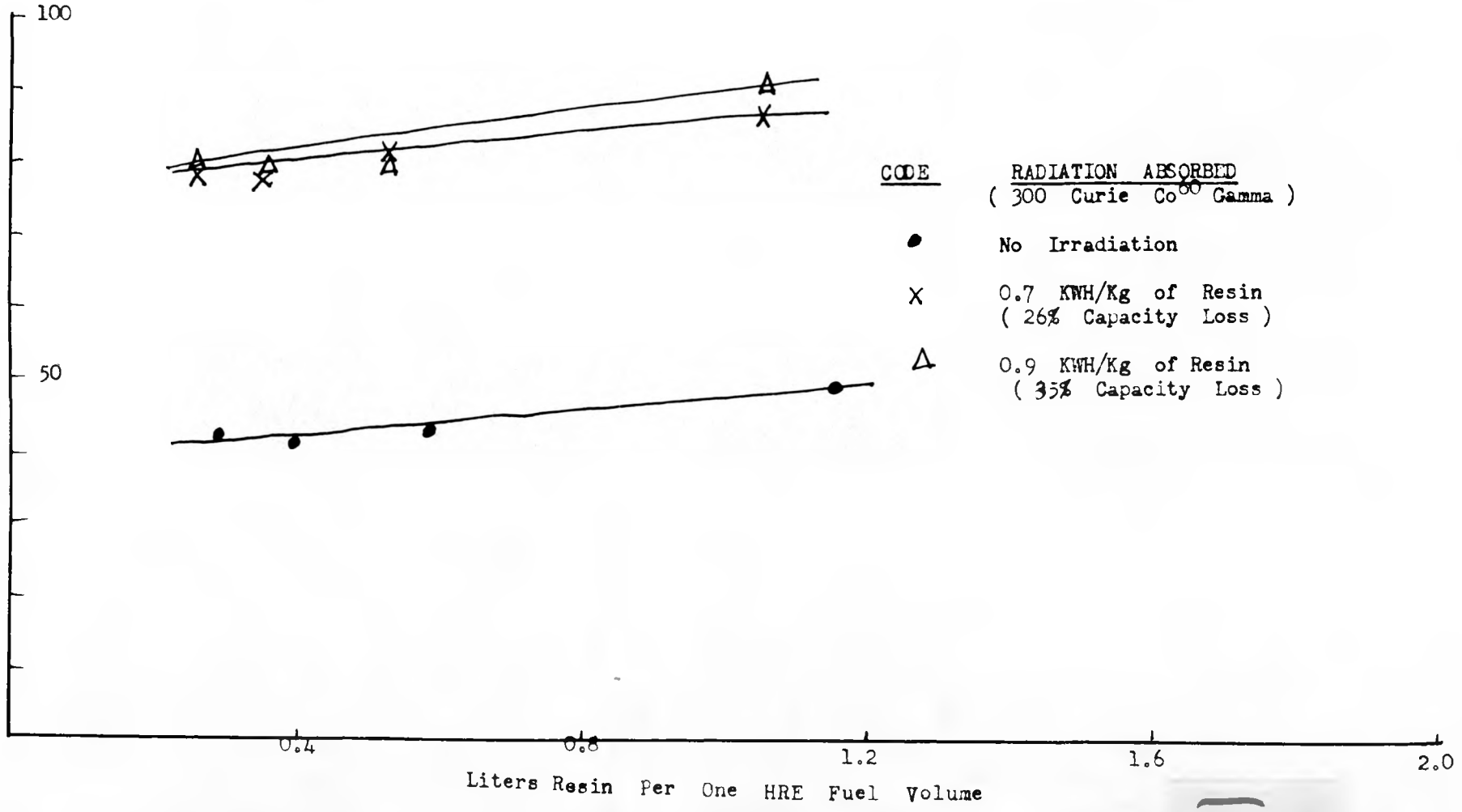

DRAWING 10253

FIG. 111

PLUTONIUM and RARE EARTH BREAKTHRU on IRRADIATED DOWEX 50 RESIN

——— Plutonium

——— Rare Earth's

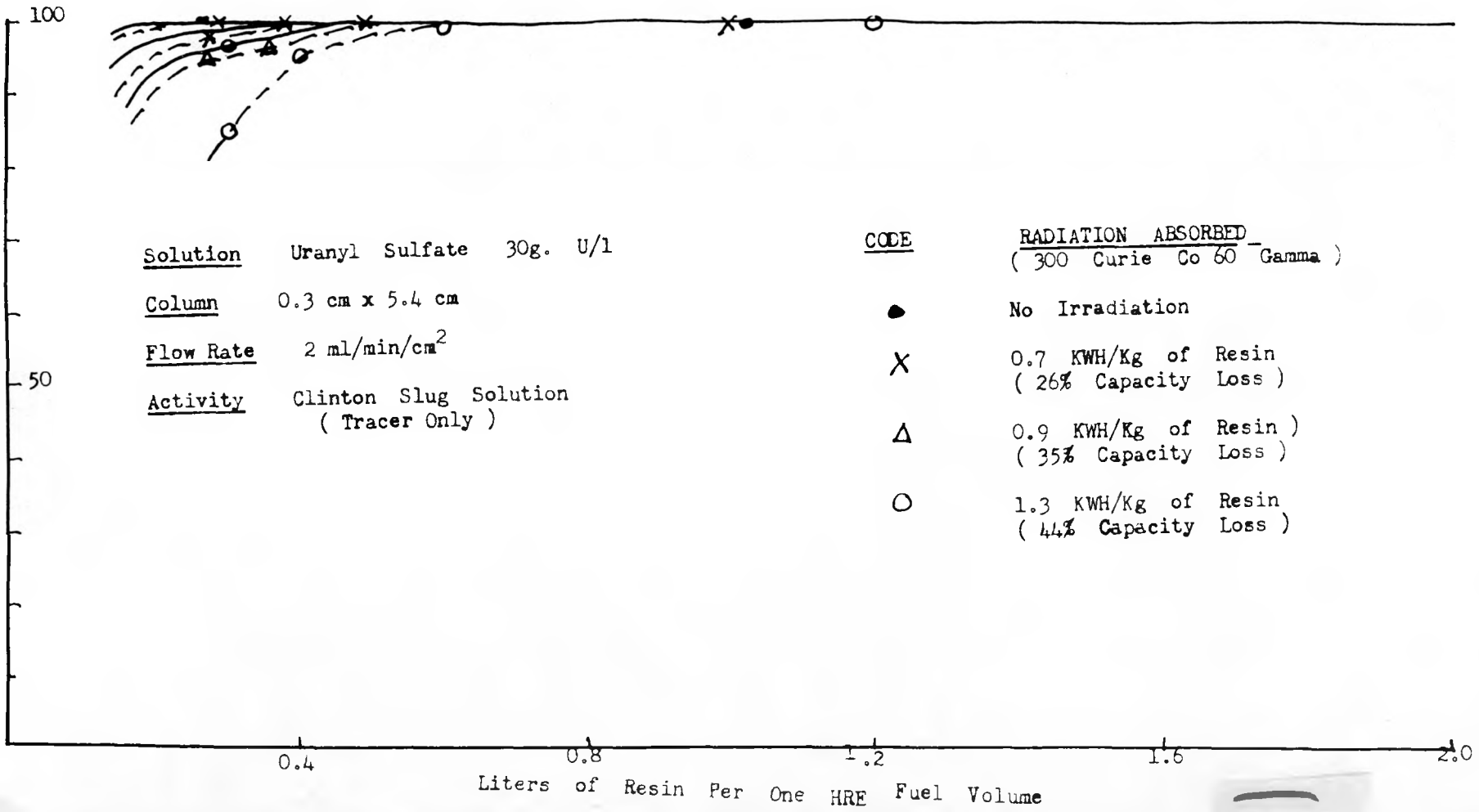

306

tracer rare earths, Sr, and Cs changes in radiated resin used in a column. A quicker breakthrough would be expected because of loss in capacity, but the abnormal increase of niobium adsorption in unexplained. Apparently the resin polymer is altered in such a way that it forms an active center with an affinity for niobium. The nature of cesium adsorption seems to change also.

All exchange groups not filled with fission products are occupied by UO_2^{++}. It will never be possible to load the capacity to 100% with fission products because of radiation effects. Therefore the uranium must be selectively desorbed without disturbing other adsorbed ions. Uranium has some complexing affinity for sulfate and is selectively desorbed with dilute sulfuric acid. The efficiency of Dowex 50 and the effect of particle size and flow rates are shown in Fig. 112.

Anion-exchange Studies. The highly basic anion organic exchangers, Dowex A-1 and A-2 and IRA-400, exhibit a highly selective adsorption for certain anionic fission products in the presence of the uranyl sulfate fuel. The affinity for molybdenum seems to be particularly high, followed by iodine and tellurium, as indicated in Fig. 113. Also, considerable portions of the "bad actors" niobium and ruthenium are adsorbed. However, uranium is held up, probably as a sulfate complex, on all active centers not occupied by fission products. The removal of this uranium has not been accomplished to the degree desired without removing the adsorbed activity also. The application of anion resins cannot be considered unless this problem is overcome. Radiation effects on anion resins have not been studied.

Inorganic Adsorbers. These adsorbers were of interest because they are less sensitive to radiation and often exhibit unusual affinity for certain ions; for example, Super Filtrol has a very high affinity for cesium, is good for niobium, zirconium, and plutonium, but has almost no affinity for rare earths. In general they do not have the high capacity of the organic ion exchangers, are more sensitive to *p*H, and do not always yield all adsorbed material with vigorous chemical treatment. The uranium holdup of Super Filtrol is about 5 g per kilogram of adsorber. It can be removed by various eluting agents but selectively only by using a sulfate salt of the same *p*H and ion concentration as the uranyl sulfate fuel.

The inorganic adsorbers activated charcoal, activated alumina, Super Filtrol, silica gel, and bentonite were tested to determine their selective adsorption of fission products activities from uranyl sulfate. Super Filtrol and activated alumina showed most promise.

DECLASSIFIED

DRAWING 10254

FIG. 112

URANIUM ELUTION from DOWEX 50

WITH 0.25M SULFURIC ACID

Column 1 cm x 15.2 cm

Resin Form UO_2R

Resin Volume 10.8 ml

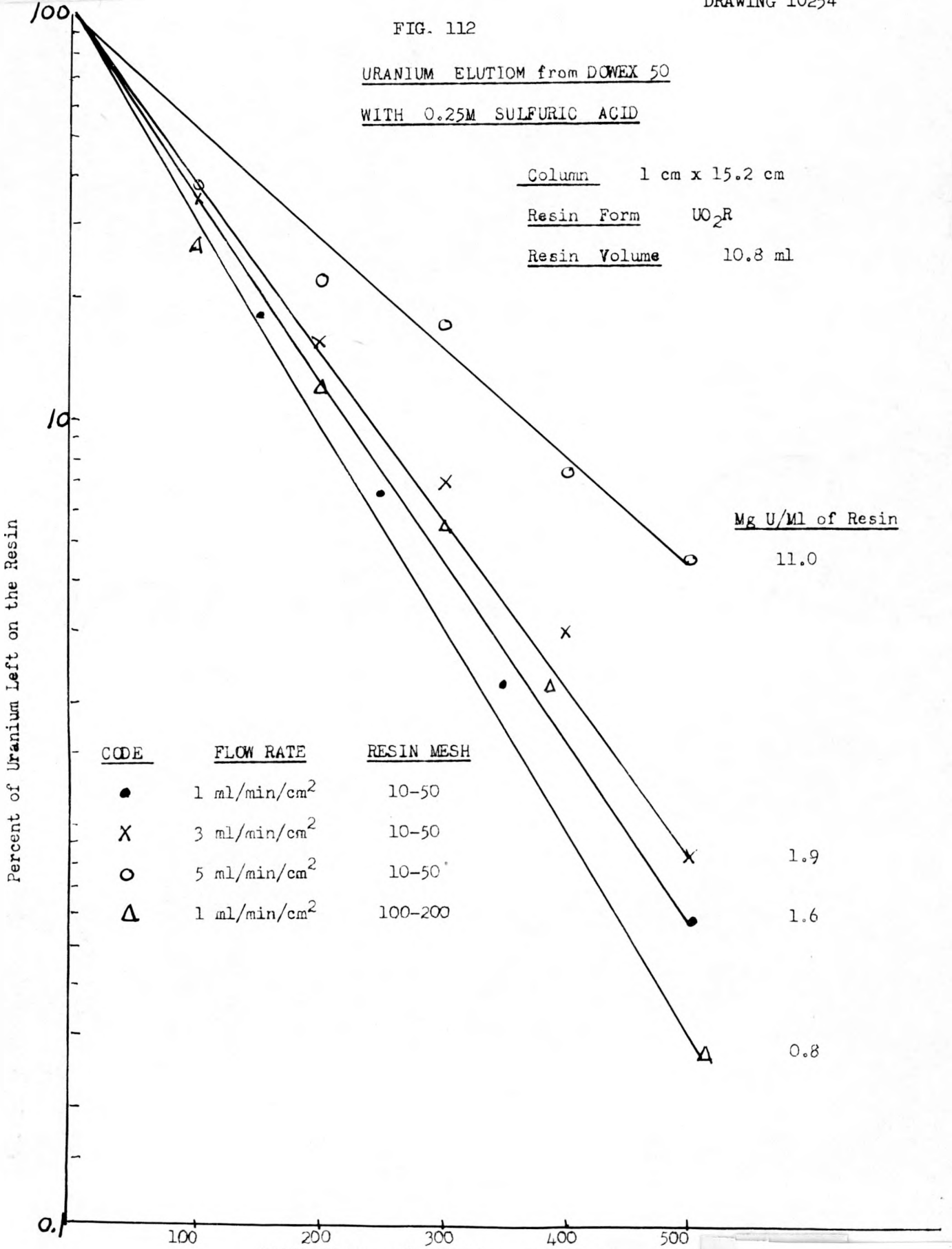

CONFIDENTIAL
DECLASSIFIED

DRAWING 10255

FIG. 113

DOWEX A-1 AFFINITY TEST for FISSION ACTIVITY

Solution Uranyl Sulfate 30g. U/l

Column 1 cm x 5.1 cm

Flow Rate 1 ml/min/cm^2

Activity UO_2SO_4 "Rabbit" (Tracer Only)

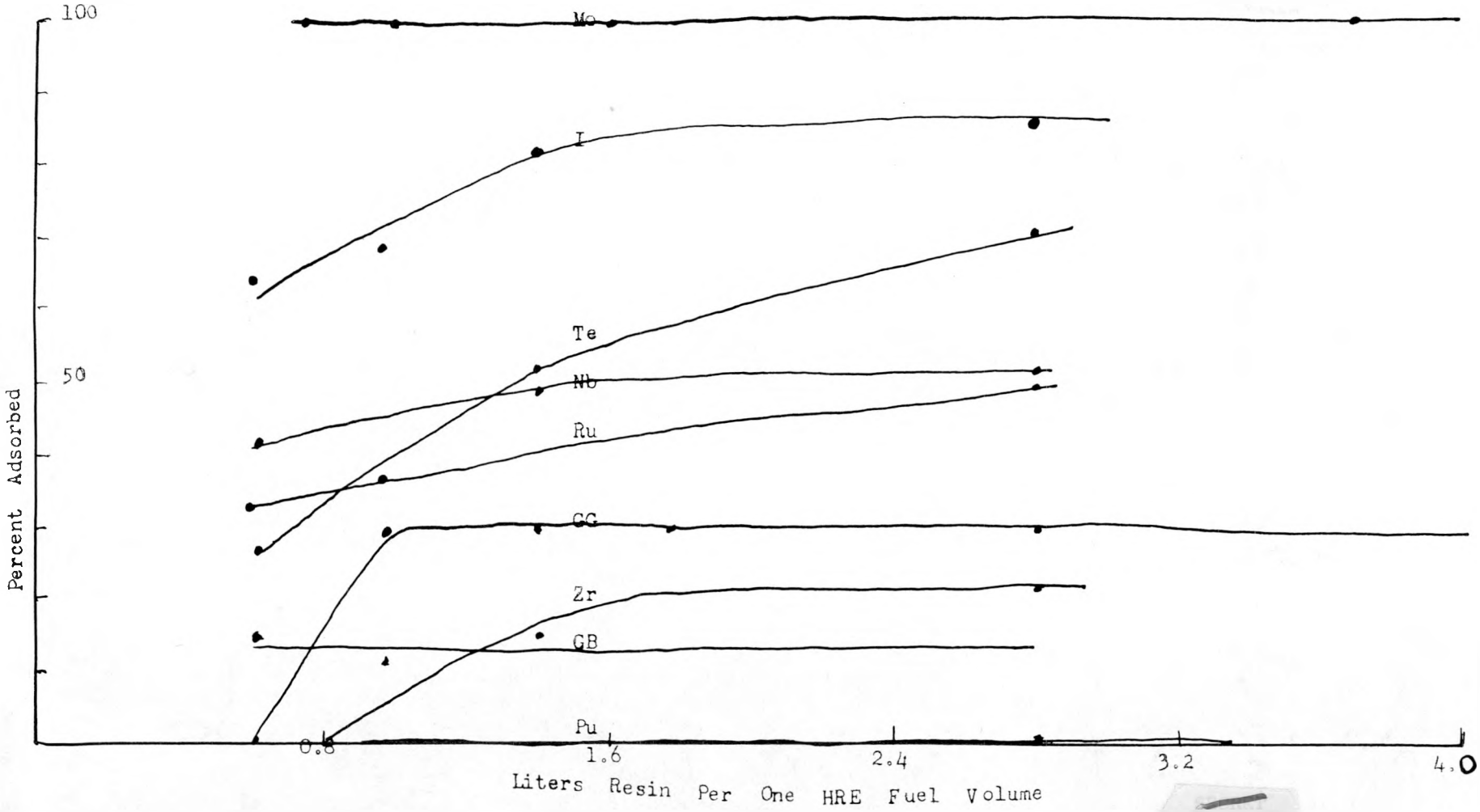

declassified

Electrolytic Methods. Very little work has been done using electrolysis, but the method looks very attractive since no radiation effects are expected. Few, if any, chemicals have to be added, and uranium losses are expected to be very low. Using a copper cathode, a lead anode, and a trace of cupric ion in solution, molybdenum has been plated almost quantitatively on the cathode, and iodine, tellurium, and ruthenium from 10 to 50% on the anode. Using 0.2 amp, uranium losses have been of the order of 5 mg per 100 sq cm of cathode and less than 1 mg per 100 sq cm of anode for a 1-hr run.

TABLE 41

Life of Dowex 50 Resin with Various Cooling Periods, Assuming About 90% Capacity Loss Due to Radiation from the HRE

Fission Product Accumulation in the Reactor, 21 g (1%)
Fission Product Removal Rate, 1 g/day

TIME OF COOLING	FUEL HOLDUP (%)	LIFE OF 1 kg OF RESIN (days)	FISSION PRODUCTS ADSORBED PER kg OF RESIN (g)
1 hr	0.2	0.62	0.07
1 day	4.8	1.6	1.66
2 days	9.5	2.1	2.22
3	14.3	2.5	2.50
4	19.1	3.1	3.07
5	23.9	3.4	3.44
10	47.7	5.0	5.0
21	100.0	9.1	9.1

DECLASSIFIED

PERSONNEL

Project Engineer — **C. E. Winters**

Assistant Project Engineer — **C. H. Secoy**

ENGINEERING AND REACTOR PHYSICS

Design

W. R. Gall

W. E. Sholl
C. L. Segaser
T. H. Thomas
C. M. Wetzel* (On loan from ORSORT and Bureau of Ships)
F. C. Zapp
C. W. Day

D. T. Jones (On loan from Engineering Department)

G. B. Berry
W. L. Carter
W. L. DeRieux
R. W. French
A. G. Grindell
M. C. Lawrence
R. N. Mason
W. Terry
A. E. Zulliger
R. L. Cauble
R. H. Chapman
A. E. Strauchman

Development

C. B. Graham

I. Spiewak
J. O. Bradfute
J. S. Culver
R. Wilson
W. L. Ross
C. G. Heisig
B. T. Resnick* (On loan from ORSORT and U. S. Naval Shipyard)
C. Savage
G. Letz* (On loan from ORSORT and Electric Boat Company)
C. D. Zerby
W. K. Stair (ORINS Research Participant)
R. Van Winkle
C. M. Burchell
W. B. Krick
R. Smith, Jr.

DECLASSIFIED

Corrosion

J. L. English

A. R. Olsen
S. H. Wheeler

H. L. Barker
L. L. Fairchild
J. M. Brown

Control and Instrumentation

J. R. Quarles

C. A. Mossman (On loan from Instrument Department)
B. P. White (On loan from Instrument Department)
J. Owens* (On loan from Instrument Department)
L. Inglis (On loan from Instrument Department)
W. P. Walker

Reactor Physics

J. M. Stein (On loan from Westinghouse)

J. M. Burnham (On loan from ORSORT and Electric Boat Company)
H. L. F. Enlund (On loan from ORSORT and Gibbs and Cox, Inc.)
P. R. Kasten

CHEMISTRY

Radiation Studies

C. H. Secoy (Group Leader)* (Chemistry Division)

J. W. Boyle, Jr.
F. J. Fitch
J. F. Manneschmidt
H. F. McDuffie
D. M. Richardson
M. D. Silverman
A. W. Smith
F. H. Sweeton

Recombiner Studies

W. R. Grimes (Group Leader)* (Materials Chemistry Division)

D. W. Kuhn
A. D. Ryon
F. L. Daley
A. A. Palko
K. O. Johnsson*
H. M. McLeod*
T. S. Mackey
Don Phillips

DECLASSIFIED

C NFIDENTIAL

Chemical Analytical Controls

W. H. Davenport (Chemistry Division)
R. H. Powell

Solubility of Fission Product Sulfates

H. M. Lietzke (Chemistry Division)
B. Zemel

Phase Rule Studies

C. H. Secoy (Group Leader) (Chemistry Division)

W. L. Marshall
J. S. Gill

Slurries

T. C. Runion* (Chemical Technology)
L. E. Morse

Continuous Fuel Processing

I. R. Higgins* (Chemical Technology)

Analytical Service Group

P. F. Thomason (Group Leader)* (Analytical Chemistry)

A. D. Horton*
F. J. Miller*

Optical and Electron Microscopy Service Group

T. E. Willmarth (Group Leader)* (Analytical Chemistry)

F. D. McNeer* B. I. Gary*

LONG RANGE STUDY GROUP

R. C. Briant
R. B. Briggs
George Garrett
C. B. Graham
J. A. Lane
N. F. Lansing
L. C. Noderer
L. R. Quarles
C. H. Secoy
J. M. Stein
R. W. Stoughton
J. A. Swartout
A. M. Weinberg
C. E. Winters

HOMOGENEOUS REACTOR STEERING COMMITTEE

G. H. Clewett
W. R. Gall
C. B. Graham
J. A. Lane
C. E. Larson
S. C. Lind
E. J. Murphy
L. R. Quarles
C. H. Secoy
J. M. Stein
J. A. Swartout
E. H. Taylor
A. M. Weinberg
C. E. Winters

* Part time.

DECLASSIFIED